Variation in Dental Morphology and Bite Force Along the Tooth Row in Anthropoids

by

Lynn Lucas

A Dissertation Presented in Partial Fulfillment
of the Requirements for the Degree
Doctor of Philosophy

Approved May 2012 by the
Graduate Supervisory Committee:

Mark Spencer, Chair
Gary Schwartz
William Kimbel

ARIZONA STATE UNIVERSITY

August 2012

ABSTRACT

Modern primate diet is well-studied because of its considerable influence on multiple aspects of morphology, including the shape of the facial skeleton and teeth. It is well-established that differences in craniofacial form influence feeding abilities by altering the nature of bite force production. Tooth morphology, likewise, has been shown to vary with diet across primates, particularly in the details of occlusal form. It has also been suggested that tooth form (e.g., tooth root size and shape and crown size) reflects, in part, the demands of resisting the stresses generated during feeding. However, while they are central to our efforts to infer diet in past species, the relationships between bite force production, craniofacial morphology and tooth form are not well-established.

The current study is separated into two parts. In Part I, the hypothesis that crown size and root surface area are adapted to resist masticatory stress is evaluated by testing whether these features show correlated variation along the tooth row in a taxonomically diverse sample of primates. To further explore the adaptive nature of this correlation, pair-wise comparisons between primates with mechanically resistant diets and closely-related species consuming less resistant foods are performed. If crown size and root surface area covary along the tooth row, past research suggests they may be related to bite force. To test this hypothesis, Part II examines the variation of these dental characteristics in comparison to theoretically-derived bite force patterns along the tooth row.

Results suggest that patterns of maximum bite force magnitude along the tooth row are variable both within and between species, underscoring the

importance of individual craniofacial variation on masticatory force production. Furthermore, it is suggested that some adaptations traditionally associated with high bite force production (i.e., facial orthognathy) may increase anterior biting force at the expense of posterior biting force. Taken together, results from the current study reveal that both tooth root and crown size vary in conjunction with the mechanical properties of diet and with bite force patterns along the tooth row in anthropoids.

DEDICATION

For my dad, Dr. Michael Lucas, who has taught me to take nothing for granted and to attack every challenge, especially the unexpected ones, with gusto.

ACKNOWLEDGMENTS

This dissertation could not have been completed without the help and support of numerous people. First and foremost, I would like to extend my thanks to my committee members Gary Schwartz and Bill Kimbel and especially to my committee chair, Mark Spencer. Thank you for teaching me and challenging me to ***think***.

The process of collecting the primate µCT scans central to my dissertation was long and arduous—much more so than I ever would have imagined before I began this project. My thanks to the many people at Harvard University who made data collection possible. Thank you Judy Chupasko and Mark Omura of the Museum of Comparative Zoology, who generously let me wheel a cart full of monkey skulls across the street to the Center for Nanoscale Systems (CNS) every day (sometimes multiple times a day) for 5 weeks during the summer of 2010. Thanks also to Michele Morgan from the Peabody Museum of Archaeology and Ethnology for granting access to their chimpanzee collection. Finally, thank you to Fettah Kosar, who runs the µCT scanner at CNS, for not only teaching me how to use the scanner, but also for granting 24-hour a day 7-day a week access to it, which, it turns out, was not overkill at all, but exactly what was needed to collect all of the data that form the basis of this dissertation.

Funding for this project was provided by Sigma Xi Grants-In-Aid of Research, a SHESC Special Research Grant, a GPSA Dissertation Grant, and an ASU Dean's Writing Fellowship; thanks to Tae O'Connor, Heidi Scheier, Jodi Guyot, and Mena Bell for helping me secure and spend every cent.

My sincerest thanks to all of my fellow graduate students, past and present, who have collectively provided hours of stimulating scientific discussion and commiseration when appropriate; thank you Caley Orr, Jeremiah Scott, Kristi Lewton, Thierra Nalley, Stephanie Meredith, Heather Smith, Laura Stroik, Amy Shapiro, Sam Russak, Kierstin Catlett, Terry Ritzman, and Halszka Glowacka.

To my motley crew of undergraduate research assistants, thank you for spending hours erasing pixels, organizing files, and tolerating the lab computer! Without your help, I would still be sorting through it all: thank you, Angie Gutierrez, Brittany Tullinen, Erik Thunberg, Morgan Texeira, Courtney Bruce, Scott Hamilton, and Lawrence Fatica.

Thanks go to Rebecca Fisher, my unofficial mentor, who is easily one of the best teachers I've ever had in my entire academic career. Thank you for your expertise and support both in and out of the classroom. Thanks also go to my latest office-mate, Hallie Edmonds, for letting me draw scores of triangles on my sciencing board and talk about them at length without fleeing or even fidgeting too much. To my friend, Joyful Scientist Lynn Copes, thank you for sciencing with me for the last 5 years. You are an inspiration.

Thanks to my mother and sister, Patty and Jessica Lucas, and to my dad and stepmom, Michael Lucas and Kay Hampshire, for their constant love and support. Finally, to my husband Emory, thank you for everything you do. There are no words to convey the depth of my love for you and gratitude for your presence in my life.

TABLE OF CONTENTS

Page

CHAPTER Page

LIST OF TABLES

Table Page

LIST OF FIGURES

Figure Page

Figure Page

CHAPTER 1

INTRODUCTION

Modern primate diet is well-studied because of its considerable influence on multiple aspects of primate morphology, including the shape of the facial skeleton and teeth. It is well-established that differences in the form of the facial skeleton influence feeding abilities by altering the nature of bite force production. Tooth morphology, likewise, has been shown to vary with diet across primates, particularly in the details of occlusal form. It has also been suggested that tooth form (e.g., crown size, enamel thickness and microstructure, occlusal topography, tooth root size and shape) reflects, in part, the demands of resisting the stresses generated during feeding (Kay, 1975, Lucas et al., 1986, 2008a,b). However, while they are central to our efforts to infer diet in past species, the relationships between bite force production, craniofacial morphology and tooth form are not well established.

Our current understanding of masticatory adaptation derives from the interplay of predictions from mechanical models and rigorous testing of those predictions via experimental and comparative studies. The forces that break down food are a function of both the occlusal topography of a particular tooth and of the ability of the masticatory system to generate bite force on that tooth; therefore, both are expected to be related to habitual feeding behaviors. This study evaluates data on tooth morphology in conjunction with models of feeding mechanics to test specific hypotheses about how the primate masticatory system has responded to dietary pressure over time.

Both experimental and theoretical studies suggest that bite forces change along the tooth row (in lizards: Anderson et al., 2008; in hyenas: Binder and Van Valkenburgh, 2000; in opossums: Thompson et al., 2003; in bats, Dumont and Herrel, 2003; in monkeys: Oyen and Tsay 1991; in humans: Mansour and Reynik, 1975; Pruim et al., 1980; van Eijden et al., 1988; van Eijden, 1991; Iwase, 1998; Spencer, 1998; Throckmorton and Ellis, 2001; Ferrario et al., 2004). Such variation in force production along the tooth row can be predicted to reflect or influence tooth morphology. Despite this logical connection, studies that explicitly test hypotheses regarding dental adaptations to stress resistance are rare (e.g. enamel thickness, Dumont, 1995; periodontal ligament morphology, Asundi and Kishen, 2000; tooth root size, Spencer, 2003). Furthermore, there is no consensus concerning *patterns* of bite forces along the tooth row. While some studies find that bite force steadily increases posteriorly (in monkeys, Oyen and Tsay 1991; in humans, Mansour and Reynik, 1975; van Eijden, 1991; Iwase, 1998), others find that bite forces remain static or decrease posteriorly (in humans, Pruim et al., 1980; Spencer, 1998; Ferrario et al., 2004).

Using micro-computed tomography (μCT) scans of skulls from a broad taxonomic array of primates, this study examines whether the assumed relationship between root and crown size and bite force is supported across a large variety of taxa, and also within individuals. In other words, are the largest teeth located where the highest bite forces are produced in the mouth? By determining how tooth morphology and bite force covary along the tooth row, this study tests the assumed link between them and provides a solid foundation for a more

complete understanding of how tooth roots and crowns have evolved in response to masticatory force.

Although tooth roots and crowns are structurally and functionally connected, they are different structures evolving under differing selection pressures. Roots are genetically distinct from crowns, develop after crown development has ceased, and are attached to their sockets by the periodontal ligament (discussed in Chapter 2). In contrast, crowns develop first and are put to use even before the root has finished developing; furthermore, crowns come into direct contact with food being chewed and thus experience wear. Despite their shared role in food processing, it is clear that tooth roots and crowns evolve in distinct local environments.

Research suggests that taxa that eat harder foods have bigger tooth roots and crowns; however, there is no work that directly links root size to bite force production. The current study tests the hypothesis that bite force is related to tooth (root and crown) size by estimating bite force at each tooth along the tooth row and comparing the pattern of bite force magnitude to the pattern of tooth size. The largest teeth should be the ones to which the highest bite forces are applied, while the smallest teeth should be located where estimated bite forces are lowest.

It is important to directly link root size to bite force because roots are surrounded by tissue on all sides; that is, roots do not come into direct contact with food. Therefore, some variables that influence crown size (i.e., food particle size) may be irrelevant to the evolution of root form. However, the force with which food is processed must travel through both the crown and root, suggesting

that both have evolved in response to mechanical loading. Linking root size to bite force allows us to understand tooth morphology as it relates to force production alone, rather than the combined pressures of force production and particle size and whether the particle is sticky or gritty, all of which may impact crown morphology (Lucas et al., 1984; Lucas, 2004).

This dissertation is divided into seven chapters. The vast literature pertaining to the form and function of the dentition and craniofacial skeleton is synthesized and presented in Chapter 2. This chapter includes descriptions of the models of feeding mechanics which are the basis for estimations of bite force in the current study and which inform the interpretations of study results. Chapter 3 outlines the materials and methods used to carry out the current research, including all of the equations used in bite force estimation. Results and discussion of scaling analyses are presented in Chapter 4. Chapters 5 and 6 discuss and describe the results of the tests of hypotheses concerning dental form along the tooth row and the relationship between dental form and bite force, respectively. Chapter 6 also describes patterns of bite force along the tooth row across sample taxa. Chapter 7 summarizes the important results within the current study and discusses possibilities for future research.

CHAPTER 2

BACKGROUND

Multiple lines of research suggest that different components of tooth form (e.g., root and crown size and shape, enamel microstructure) have been shaped primarily in response to selection pressures from food material properties.

Studies have suggested a link between tooth morphology and bite force but have rarely tested the nature of this link (but see Spencer, 2003). This study examines whether predicted maximum bite force magnitudes match quantified variation in root and crown form along the tooth row in a diverse sample of primate taxa, and also the extent to which root size and crown size, both of which have been proposed to be related to stress resistance, are correlated.

The current study is divided into two separate but logically connected parts. Part I of the study focuses on variation in tooth root and crown size within and among a set of diverse species of primates. The first portion of this chapter will evaluate the current state of knowledge relating to the variation of tooth root and crown size, including reviews of tooth anatomy and development, comparative and functional morphology, and what is known to be related to dental morphological variation in primates.

Part II of the study compares variation in tooth morphology along the tooth row with variation in bite force along the tooth row. Thus, the second portion of this chapter will review our current understanding of craniofacial biomechanics, including the models used to estimate bite forces and their predictions, and comparative and experimental work in validating said models. Finally, the third portion of this chapter outlines hypotheses and rejection criteria.

TOOTH FUNCTION AND MORPHOLOGY

Tooth Anatomy and Development

A typical mammalian tooth consists of four components (Figure 2.1). The innermost component, the pulp, contains blood vessels, lymph, and nerve fibers necessary for the upkeep of living tissue. The pulp is surrounded by dentin, the mineralized hard tissue that makes up most of the volume of the tooth. The dentin of the crown is covered and protected by an even harder mineralized tissue called enamel, while the dentin of the root is covered by the mineralized connective tissue, cementum. The periodontal ligament (PDL) consists mainly of collagen fiber bundles that insert into the cementum and attach the root to the surrounding alveolar bone. The PDL is discussed in greater detail below.

Tooth development begins at six weeks in utero, when the epithelium over the mandible thickens to become the dental lamina. During the lamina stage (Figure 2.2), Meckel's cartilage provides support for developing tissues, and blood vessels are already present (Schroeder, 1991). From the lamina stage, development continues through a bud stage to the cap stage, where the tooth bud assumes the shape of a dome in response to pressure from the surrounding blood vessels. At this time, mesenchymal cells condense to form the dental papilla, from which pulp and dentin derive, and the dental follicle (Bernick and Grant, 1982). Additionally, the enamel organ is formed from cells from the epithelial cap and eventually produces tooth enamel (Schroeder, 1991). Together, the dental papilla and enamel organ make up the tooth germ. During the bell stage, the tooth germ grows larger and the cells begin to differentiate. Stellate

reticulum, a substance of star-shaped cells pushed apart by fluid pressure, separates the inner and outer enamel epithelium.

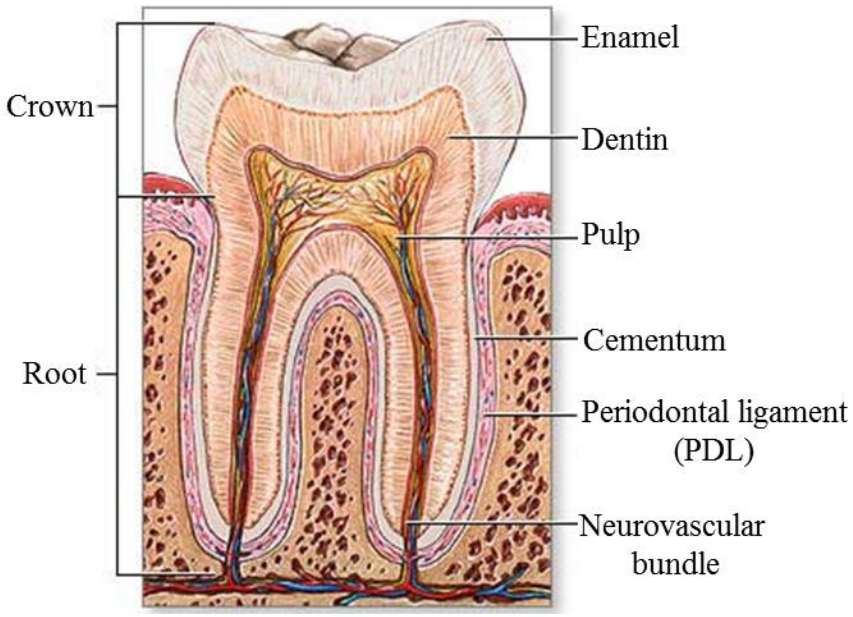

Fig. 2.1. Major components of tooth structure. Figure adapted from www.nlm.nih.gov.

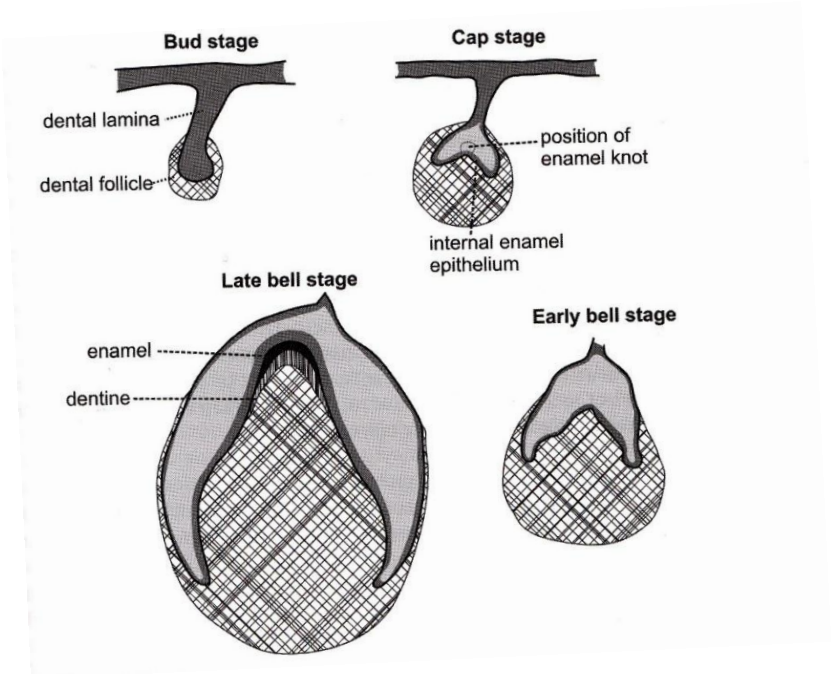

Fig. 2.2. Tooth crown development. From Hillson (1986, 2005).

The juncture of the inner/outer epithelium is called the cervical loop. At the end of the bell stage, the developing tooth pinches off from the dental lamina. At this point, the inner enamel epithelium has folded to create the shape of the enamel-dentine junction (EDJ). Cells of the inner epithelium elongate to form ameloblasts, which move to form the tooth enamel. Neighboring cells in the dental papilla form ondontoblasts, specialized connective tissue cells that build and maintain dentin by moving toward the center of the papilla, leaving thin tubes of dentin behind (Schroeder, 1991; Park et al., 2007).

After the crown is fully developed, root formation begins (Figure 2.3). An extension of the cervical loop forms a collar of cells called Hertwig's epithelial root sheath (HERS) (Schroeder, 1991; Park et al., 2007), which is responsible for signaling the formation of ondontoblasts that create the dentin of

the tooth root (Park et al., 2007). HERS is largely responsible for the size, shape and number of roots for each tooth. For multi-rooted teeth (e.g., postcanine teeth like those examined in this study), HERS extends and bends sharply inward, forming the epithelial diaphragm at the apical boundary of the papilla (Schroeder, 1991). Processes arise from the cervical loop across the apical end of the papilla and meet in the center of the future furcation of the roots; here, they fuse to allow for the formation of separate epithelial sheaths that will guide future root formation (Kovacs, 1971; Schroeder, 1991).

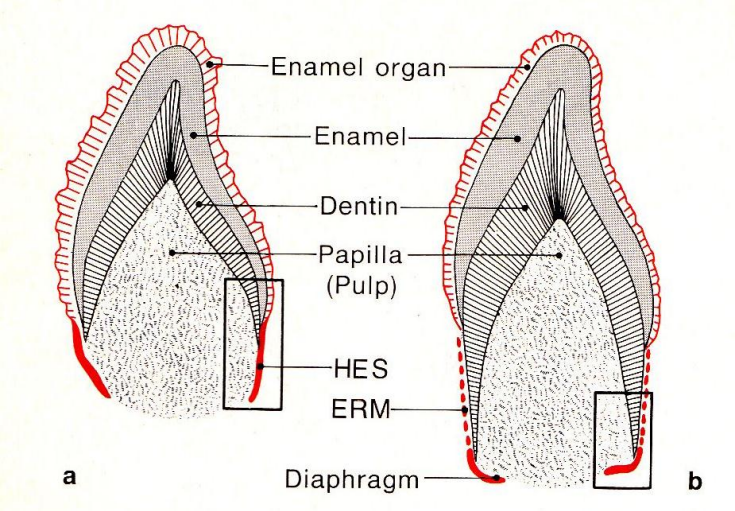

Fig. 2.3. Schematic of tooth root development in (a) a 2.5 month-old infant and (b) an 8 month-old infant. HES = Hertwig's epithelial root sheath (Figure from Schroeder, 1991).

Kovacs (1971) divided root formation into two stages, the eruptive phase and the penetrative phase. The eruptive phase begins with initial root formation and continues until the tooth crown comes into functional occlusion. At this point, the root is about 2/3 of its total length. During the eruptive phase, the

epithelial diaphragm retains its position within the dental canal, and the tooth moves superiorly. The penetrative phase of root development begins when the tooth crowns are in occlusion. At this point, the epithelial diaphragm pushes down into the alveolar bone, elongating the dental canal as root growth is completed (Kovacs, 1971).

The periodontal ligament

The periodontal ligament composed primarily of collagen fiber bundles that have a complex, three-dimensional overlapping arrangement, which connect the tooth root to the alveolar bone (Pearson, 1982). The collagen fiber bundles, along with the blood vessels and nerve endings that supply the tooth, are embedded in a gel-like ground substance, which is composed of water, hyaluronic acid, proteoglycans, and glycoproteins (Pearson, 1982; Linden, 1990). Together, the collagen fibers, neurovascular structures, and the ground substance comprise the PDL. Aside from anchoring the tooth to the jaw, the PDL functions as a hydrodynamic damping mechanism that absorbs and distributes occlusal forces into alveolar bone (van Driel et al., 2000) and also provides sensory feedback used in the neural control of chewing (Linden, 1990). Each of these functions is discussed separately below.

PDL biomechanics

It is now well-established that the PDL responds to force in a viscoelastic manner (Embery, 1990; Luke, 1998; Dorrow et al., 2002, 2003; Natali et al., 2004; Komatsu, 2010; Fill et al., 2011), meaning the PDL has properties of both viscous and elastic material. Elastic materials deform immediately when stressed,

and then return to their original form once the stress is removed (Meyers and Chawla, 2009). Liquids have a biomechanical property known as viscosity, a liquid's resistance to movement, which results in frictional energy loss over time (Meyers and Chawla, 2009). Low-viscosity liquids, like water, move more quickly and easily, and lose less energy than high-viscosity liquids, like molasses. Orthodontic research has revealed that if a force is applied to a tooth, once the force is removed the tooth recovers its original position, an elastic property; but it also takes *time* to recover the original position, a viscous property; thus, the PDL is viscoelastic (Luke, 1998; Dorrow et al., 2002, 2003; Natali et al., 2004; Meyers and Chawla, 2009).

The viscoelastic nature of the PDL is most likely due to the elastic nature of the collagen fibers coupled with the viscous nature of the ground substance and other fluids in the periodontal space (Dorrow et al., 2002, 2003). Collagen fibers of the PDL have a wavy, crimped structure when not loaded (Gathercole and Keller, 1982); when force is applied to a tooth, these fibers first straighten before being loaded in tension (Gathercole and Keller, 1982; Dorrow et al., 2003). Thus, initial responses to stress in the PDL are hypothesized to be governed by the ground substance, which is joined later by straightened collagen fibers loaded in tension (Dorrow et al., 2003). However, it should be noted that, while supported with indirect evidence, the hypothesis that stress in the PDL is first encountered by the ground substance followed by the collagen fibers requires direct testing. A complete understanding of the biomechanical properties of the PDL is unknown at this time (Natali et al., 2004; Fill et al., 2010).

Although the exact details of the biomechanical behavior of the PDL are currently unresolved, research clearly indicates that the PDL plays an important role in stress resistance. Experimental and photoelastic stress analyses indicate that the strain profile in a loaded tooth changes at different positions on the tooth root (in rodents: Chiba et al., 1990; Komatsu et al., 1998; Yamazaki et al., 2001; in humans: Deines et al., 1993, Asundi and Kishen, 2000) such that maximum strain and shear stress are highest in the cervical portion of the root and diminish apically when loaded axially (Mandel et al., 1986; Asundi and Kishen, 2000). Furthermore, the PDL varies in strength and thickness along the tooth root in conjunction with masticatory stress patterns; that is, portions of the tooth root that experience more stress show a relative increase in the organization and attachment of the PDL to the bone and cementum (in rodents: Chiba et al., 1990; Komatsu et al., 1998; Yamazaki et al., 2001; in humans: Sloan, 1982; Mandel et al., 1986; Deines et al., 1993; Asundi and Kishen, 2000).

In a recent finite element modeling (FEM) study, Panagiotopoulou and colleagues (2011) constructed several FE models with the PDL modeled variably in thickness and elasticity that they validated against an experimental protocol. They found that strain across the mandible was not affected by changes modeled in the PDL material properties; instead, the PDL affected only the local environment around the stressed tooth, the alveolar bone adjacent to the tooth socket. Taken together, research indicates that the PDL plays an important role in managing the strain environment of a loaded tooth by damping occlusal forces as they move through the tooth to the surrounding alveolar bone.

Sensory feedback

The PDL is innervated by two types of nerve groups: somatic sensory and autonomic. The autonomic nerves regulate the smooth muscle cells of blood vessels, controlling patterns of blood flow around each tooth, while the sensory nerves allow the PDL two types of sensation, pain and pressure (Hannam, 1982). Among the sensory cells are periodontal mechanoreceptors (PMRs), nerve endings that contain receptor molecules that respond to pressure created when the tooth is loaded. When activated, these mechanoreceptors cause reflex activity in the jaw musculature (Hannam, 1982; Morimoto et al., 1989; Linden, 1990; Hidaka et al., 1997; Trulsson and Gunne, 1998; Türker and Jenkins, 2000; Johnsen and Trulsson, 2003, 2005).

Experimental work on rabbits has shown that when sensory feedback from PMRs is removed using local anesthesia, masseter muscle force during chewing is greatly decreased relative to non-anesthetized chewing (Lavigne et al., 1987; Morimoto et al., 1989). Additionally, Haraldson (1983) found that bite forces in human subjects with no teeth (who were using dentures) were greatly decreased relative to subjects with natural teeth. In the same study, Haraldson also found that while bite-to-bite muscle activity is highly variable in people with natural teeth, people wearing dentures do not exhibit variation; in other words, denture-wearers do not modify muscle activity as they chew. Experiments in humans that measured voluntary maximum bite force both before and after local anesthesia of teeth also showed a drastic decrease in bite force after anesthesia was administered, unless the subject was given reassurance or visual feedback of bite

force level. Once subjects were certain that they were not going to break their teeth, they were able to bite harder by exerting a conscious effort to do so (Lund and Lamarre, 1973; Orchardson and MacFarland, 1980; Linden, 1990).

Consensus is that PMRs are responsible for a major part of jaw closing muscle activity during mastication. When a tooth is loaded and the force gradually increases, PMRs excite jaw closing muscular activity; conversely, when force on a tooth rapidly increases, PMRs inhibit jaw closure (Lavigne et al., 1987; Dessem et al., 1988; Morimoto et al., 1989; Lund, 1990). Additionally, Turker and Jenkins (2000) found that when there is a sudden yield of resistance on the tooth (when the tooth is rapidly unloaded), PMRs act to inhibit jaw closure.

It is important to note here that the fundamental rhythmic pattern of mastication is controlled by a central pattern generator (CPG) located in the brain stem (Dellow and Lund, 1971). The output of the CPG is modified by input from the motor cortex, which initiates and stops mastication, and by peripheral sensory feedback from PMRs, which gives information about food hardness (Linden, 1990; Agrawal et al., 1998; Foster et al., 2006; Lund and Kolta, 2006; Mistry and Hamdy, 2008). Sensory feedback is not necessary to generate the basic masticatory rhythm, but does play a major role in reflex muscle activity during chewing (Haraldson et al., 1979, Orchardson and MacFarland, 1980; Haraldson, 1983; Lavigne et al., 1987; Dessem et al., 1988; Morimoto et al., 1989; Linden, 1990; Hidaka et al., 1997; Trulsson and Gunne, 1998; Turker and Jenkins, 2000; Lund and Kolta, 2006; Mistry and Hamdy, 2008).

Taken together, these studies indicate that the PDL and its mechanoreceptors can dramatically impact force profiles over a chewing cycle. Furthermore, PMRs can enhance or inhibit jaw-closing muscle activity and contribute to the control of bite forces (Haraldson, 1983; Morimoto et al., 1989; Linden, 1990; Agrawal et al., 1998; Türker and Jenkins, 2000; Türker, 2002; Johnsen and Trulsson, 2003, 2005).

Tooth root comparative and functional morphology

Theoretical and comparative studies suggest that teeth with more attachment sites for the PDL (i.e., teeth with more root surface area), are better able to resist masticatory stress compared with teeth with less root surface area (Deines et al., 1993; Spencer, 2003). Comparative studies reveal that among species with diets of differing mechanical properties, root surface areas are larger in those that process a resistant diet (platyrrhines: Spencer, 2003; cercopithecoids and carnivores: Kupzcik, 2003; anthropoids: Kupzcik et al., 2009).

Variation in tooth root size both among species and along the tooth row has been observed for primates in general (Kovacs, 1971; Abbott, 1984; Kupzcik, 2003), although traditionally the explanations for the source of this variation have been developmentally based, rather than functional in nature. Furthermore, within the field of paleoanthropology, variation in tooth root number has been used to assess taxonomic affinity of fossil specimens (Abbott, 1984; Wood et al., 1988; Tobias, 1995).

Early studies of tooth root variation that concentrated on developmental mechanisms that influence root length found that, in humans, for teeth with

deciduous predecessors, early extraction of deciduous dentition adversely affects permanent tooth root length (Brin and Koyoumdjisky-Kaye, 1981; Brin et al., 1991). Furthermore, early experimental research suggests a correlation between facial protrusion and root size such that animals with shorter faces also tend to have shorter tooth roots (in rats: Riesenfeld, 1970; in dogs: Riesenfeld and Siegel, 1970; in baboons: Siegel 1971, 1972; in humans: Garn et al., 1980; Spencer and Demes, 1993). Siegel (1972) found that the highest correlation between root and facial length was present in teeth located near growth sites in the jaw: the canine near the premaxillary-maxillary suture, M^1 at the maxillary-palatine suture, and M_3 near the mandibular ramus. This evidence supports suggestions that tooth root length is affected by developmental processes.

Finding a developmental link between facial protrusion and root length does not preclude the possibility that either or both of these variables are influenced by selection for the generation of specific bite forces. In fact, facial length is known to play a very important role in masticatory force production (discussed in detail below) (Greaves, 1978; Spencer, 1999). Furthermore, root length may not be equivalent to root surface area. In other words, a tooth with a relatively long root may not have a higher surface area than a tooth with relatively shorter roots, depending on how the root is shaped and whether it is single- or multi-rooted (Kupczik, 2003; Kupczik et al., 2005). Kupczik and colleagues (2005) explored the relationship between root surface area and the number of roots for individual teeth, but found no relationship between the two. They suggested that the number of tooth roots in a given tooth is a genetic

polymorphism, rather than an adaptation for increasing root surface area (Kupczik et al., 2005).

Wood et al. (1988) set out to systematically describe postcanine tooth root morphology in hominin specimens, with an emphasis on using variation in root morphology to assess taxonomic affiliation. They found that premolar form is indeed helpful in distinguishing between eastern African robust australopiths and members of the genus *Homo*. However it should be noted that the adaptive strategy of each group is distinct. Members of the genus *Homo* generally have smaller, less robust tooth roots than robust australopiths; however the mechanical demands of the diet of the latter have been hypothesized to be linked to their larger teeth (Robinson, 1956; Wood et al., 1988; and many more). Additionally, Wood et al. (1988) found no consistent interspecific variation in molar root form among their hominin sample, suggesting that while some postcanine teeth (i.e., premolars) may provide important taxonomic information, molar root morphology varies independently of taxonomic affiliation.

Current research suggests that tooth root surface area correlates with a tooth's ability to withstand masticatory loads such that teeth with more root surface area can withstand high magnitude and/or repeated occlusal forces. Studies that examine the variation of root form along the tooth row show that proxies for root surface area, like root length and root number, may not accurately reflect the size of the area of attachment for the PDL (Kupczik et al., 2005). The current study uses measurements of tooth root surface area to evaluate the

hypothesis that large tooth roots correlate with high bite forces and large tooth crowns.

Tooth root and crown independence

Because tooth roots and crowns are physically and functionally connected, it is important to assess the degree of independence between them. While teeth with larger crowns generally have larger roots, the proportion of root to crown size is not consistent among taxa, suggesting that crown and root size may vary independently (Kovacs, 1971; Abbott, 1984; Wood et al., 1988; Kupczik, 2003; Spencer, 2003; Kupzcik et al., 2009). This conclusion is supported by experimental studies that show that mice with a mutation in the *Nfic* gene (a gene known to be associated with tooth root development) develop molars with normal crowns, but that lack roots entirely (Steele-Perkins et al., 2003).

Crown size

In the past, it has been suggested that variation in tooth crown size is linked to differences in energy requirements (Pilbeam and Gould 1974; Gould, 1975), sexual dimorphism (Lucas et al., 1986; Cochran, 1986; Hlusko et al., 2006), and body size (Kay, 1975, 1978; Goldstein et al., 1978; Gingerich and Smith, 1985; Lucas et al., 1986) in addition to variation in the mechanical properties of food (and, consequently, bite force) (Kay, 1975, 1978; Hylander, 1985; Lucas, 1986; Demes and Creel, 1988; Dumont, 1997; Cuozo and Sauther, 2006). Additionally, studies have shown that different aspects of crown morphology, including overall size, may be affected by changes in developmental

factors (Jernvall et al., 2000; Jernvall and Jung, 2000; Kangas et al., 2004; Kavanaugh et al., 2007).

Crown size and metabolic rate

Gould (1975) famously reasoned that tooth size (specifically, molar size) is related to the total intake of food an animal needs to satisfy its baseline energy requirements, which are in turn governed by body size and metabolic rate. According to Gould's "metabolic scaling" hypothesis, tooth size should be proportional to body mass raised to the 0.75 power, since body mass scales to metabolic rate at the 0.75 power. This is significant because it is a different relationship than would be expected based on a hypothesis of geometric scaling or isometry, which predicts that tooth size (an area) should scale with body mass (a volume) with a scaling coefficient of two-thirds or 0.67 (For a more detailed discussion of scaling, see Chapter 3).

Gould's (1975) hypothesis has been challenged and tested in myriad different ways, and with a variety of (often conflicting) results (Kay 1975, 1978; Wood, 1979; Gingerich and Smith 1985; Lucas et al., 1986b; Vinyard and Hanna, 2005; Copes and Schwartz, 2010). While some studies indicate that primate postcanine tooth size scales isometrically with body mass (Wood, 1979; Gingerich et al., 1982), others suggested negatively (Kay, 1975) or positively (Gingerich and Smith, 1985; Vinyard and Hanna, 2005) allometric relationships. While the exact relationship between primate body mass and postcanine tooth size remains unclear, no study found support for the hypothesis that postcanine tooth size scales with metabolic rate.

Crown size and sexual dimorphism

In the studies reviewed above, body size was used as a proxy for metabolic rate. This can be problematic, however, since many (although not all) primates have large body size dimorphism. In such cases, it is necessary to examine males and females separately, since the relationship between tooth size and body size may differ between the sexes. Current research indicates that size dimorphism varies in magnitude and pattern along the tooth row, and while many studies conclude that postcanine tooth dimorphism is low (Oxnard et al., 1985; Lucas et al., 1986a; Plavcan, 2002), it is well-documented that among primates with substantial body and/or canine size dimorphism, there is greater variation in the magnitude of dimorphism for all features (O'Higgins et al., 2001), including postcanine tooth size (Masterson and Hartwig, 1998; Uchida, 1998; Plavcan, 2002). However, these patterns of variation appear to differ across species (Uchida, 1998; Plavcan, 2002).

In studies that have focused specifically on postcanine tooth size and body size dimorphism, it has been found that, despite the expectation that males (with a larger body mass) would have proportionally large dentition, female primates actually have relatively larger postcanine teeth than their male counterparts (Lucas et al. 1986a; Cochard, 1987). Researchers have tried to explain these results by observing that female metabolic requirements during pregnancy and lactation exceed those of males (Cochard, 1987). However, this explanation is unsatisfactory given that in primates with size monomorphism, postcanine tooth size is the same in males and females (Lucas et al., 1986a,b; Cochard, 1987;

Lucas, 2004), despite the females' added metabolic burden associated with pregnancy and lactation.

After years of investigation, the exact relationship between body size and postcanine tooth size is not clear. In fact, Lucas (2004) concludes that "there is no critical relationship between postcanine tooth size and body size" (166). Recently, it has been suggested that postcanine tooth size, rather than scaling with body mass, is more closely influenced by overall facial size (Scott, 2011). Scott found that among 29 species of anthropoids, primates with longer faces also tended to have larger postcanine teeth. Furthermore, when facial size was held constant, the correlation between postcanine tooth size and body mass was not significant (Scott, 2011). These findings suggest that facial size (which may vary in response to the mechanical challenges of diet, discussed below), rather than overall body mass, may explain much of the variation present in primate postcanine tooth size.

Crown size and diet

It has long been suggested that tooth crown size is directly related to diet, such that relatively large tooth crowns are associated with difficult-to-process foods. Within the context of primate dietary research, foods that are difficult to process may be described as "hard" or "tough", depending on their specific mechanical properties (discussed in detail below). While the material properties of many primate foods are unknown, there is research containing these data for some taxa (pitheciins: Kinzey and Norconk, 1990, 1993; primate faunivores: Strait and Vincent, 1998; strepsirrhines: Yamashita, 1998, 2003; *M. fuscata*: Hill

and Lucas, 1996; *G. berengei*: Elgart-Berry, 2004; mangabeys: Lambert et al., 2004; *Cebus*: Wright, 2005; hominoids; Taylor et al., 2008). The sample for this study includes species for which information about food material properties is available whenever possible. Despite the paucity of data on the exact material properties of primate foods, there is a rich literature linking variation in crown size to variation in the mechanical properties of diet. Studies that investigate dietary correlates of crown size always find that primates whose diets include hard and/or tough foods have larger tooth crowns that closely related primates with a softer diet (Robinson, 1954; Jolly, 1970; Kay, 1975, 1978, 1981; Lucas et al., 1986b; Demes and Creel, 1988; Kinzey and Norconk, 1990, 1992; Anapol and Lee, 1994; Cuozo and Sauther, 2006).

Food Material Properties

Teeth function to fragment and fracture solid food particles (Lucas and Teaford, 1994). The mechanical properties of food govern how easily a particle is fractured (i.e., crack initiation) and fragmented (i.e., crack propagation) and consequently the magnitude of bite force necessary to process specific foods. External physical properties of food, like size, volume, shape, and abrasiveness, all affect the probability of particle fracture. Changes in these external properties correspond to changes in the size of a tooth (Lucas et al., 1986; Teaford, 2002; Lucas, 2004). Thus, food with a large, rough outer shell (like nuts or some fruits) is best accommodated by large teeth that can more easily start a crack through the outer layer. Once the crack is begun, however, it must be propagated so that the food particle will fragment with further processing. Fragmentation is governed

by the internal properties of food, such as strength, toughness, and deformability (Lucas et al., 1986b; Lucas, 2004). These properties influence the shape of a tooth (Kay, 1975; Lucas and Luke, 1984; Lucas et al., 1986b; Teaford and Ungar, 2000; Teaford, 2002; Lucas, 2004). Because foods are variable in their internal and external mechanical properties, teeth are variable in size and shape.

When a force is applied to an object, that object is stressed. Stress always results in some amount of distortion (this is also called deformation or strain). If an object deforms enough, it cracks (fractures).

To understand the relationships among applied force, deformation, and fracture of an object, researchers look at the stress/strain ratio (Figure 2.4). Stress, σ, is measured as the amount of force divided by the area over which it is distributed. Strain, ε, is a dimensionless variable calculated by the change in the length of an object divided by the original length of the object. By plotting the stress/strain ratio for an object, it is possible to determine the amount of force an object can withstand before deforming permanently or fracturing. This is an object's stiffness or rigidity, and is called Young's modulus or the modulus of elasticity (*E*). Within the realm of food material properties, a food with a high value for *E* is considered hard (Lucas, 2004; Lucas et al., 2008). Once an object has been fractured or cracked, its internal properties govern how much work is needed to propagate the crack further. This is called toughness and is represented by the variable *R*. *R* is the measure of the work done to produce a unit area of crack (Lucas, 2004; Lucas et al., 2008).

Foods that are resistant to initial fracture (hard foods) require higher bite force magnitudes than those that fracture more easily (soft foods). Likewise, foods that resist fragmentation (tough foods) require more repeated forces or longer duration of force than those that fragment readily (brittle foods) (Lucas et al., 1986b; Lucas, 2004). Within the context of primate diet, hardness is usually used to characterize nuts and fruits, which may be difficult or easy to fracture depending on the stage of development, but once breached are generally easy to chew. Toughness characterizes leaves, which fracture very easily, but resist crack propagation due to their cellular structure. While both fruits and leaves can be tested for both hardness and toughness, these foods do not have high values for both properties (Lucas et al., 2008). The foods typically eaten by primates that are very tough are generally not very hard and vice versa.

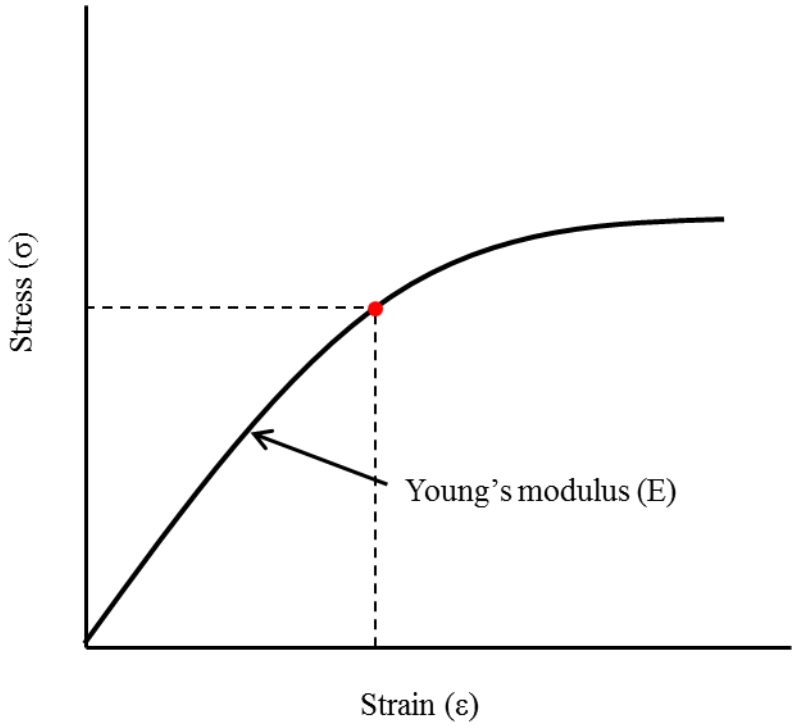

Fig. 2.4. Young's modulus. The red dot indicates the point at which the object under stress permanently deforms.

The current study examines the size (surface area) of tooth crowns and roots. According to Lucas (2004), the size of a tooth may be affected by food hardness, but not by its toughness. Instead, toughness exerts pressure on tooth shape. Complicating the matter is the fact that food consumed in the wild may also be covered with abrasive particles associated with nearby soil matrix. Consequently, a leaf, usually considered tough, may also exhibit characteristics associated with hard food due to its accompanying grit (Lucas et al., 1986b; Lucas, 2004). The result of this association is that assessing the differing selective pressures of hardness and toughness is difficult, if not impossible, to determine without experimental controls. In view of this difficulty, the current study combines hard and tough foods into one category, "resistant", such that primates with a mechanically resistant diet (eating hard and/or tough foods) are predicted to have dental morphology such as relatively large tooth roots (Spencer, 2003; Kupzcik, 2003) and crowns (Demes and Creel, 1988; Spencer, 2003; Lucas, 2004) that reflects evolution to resist high magnitude and/or high frequency loading force.

Patterns of molar crown size

There is variation in the pattern of postcanine tooth size along the tooth row among primates (Swindler, 1979, 2002; Gingerich and Schoeninger, 1979; Lucas et al., 1986b) such that, while some species show the pattern M1>M2>M3 (e.g., humans and cebids), others show M1<M2>M3 (e.g., *Alouatta* and *Pan*) or even M1<M2<M3 (e.g., *Mandrillus* and *Papio*). While this variation is often described, the explanation for differing patterns of postcanine crown size is still

unclear. Studies focusing on developmental factors suggest that M1 has the ability to inhibit the development of subsequent molar teeth (Sofaer, 1977; Kavanaugh et al., 2007). Kavanaugh and colleages (2007) suggest that by manipulating the balance of molecular signals that activate and inhibit tooth formation, M1 controls an "inhibitory cascade" that sequentially affects molars along the tooth row, potentially creating differing patterns of crown size among species. One consequence of this developmental mechanism is that M2 consistently makes up about one-third of the molar tooth row in rats (Kavanaugh et al., 2007). Lucas et al. (1986b) show that M2 is the least variable molar in the primate tooth row, which Kavanaugh et al. (2007) cite as support that the inhibitory cascade they observed in mice may apply across mammals.

In addition to concluding that M2 is not particularly variable among primates, Lucas et al. (1986b) used a ratio of M1 occlusal area to M3 occlusal area to determine whether patterns of crown size along the molar row are correlated with diet. They found that the M1/M3 ratio is inversely related to the percentage of leaves (and in some cases, leaves and seeds) consumed. In other words, primates that consumed large amounts of leaves had larger M3s relative to M1s, resulting in larger overall postcanine occlusal area for more folivorous primate species (Lucas et al., 1986b).

The production of phenotypic variation is constrained by functional, environmental, and developmental factors, none of which are mutually exclusive. Developmental mechanisms such as the inhibitory cascade are manifestations of how selection for functional features, like tooth size, may be implemented

(Kavanaugh et al., 2007). While it is obvious that changes in complex developmental interactions can affect the ultimate phenotype of a tooth (Steele-Perkins et al., 2003; Kavanaugh et al., 2007; Park et al., 2007), the fact that crown size correlates with the mechanical properties of food so consistently (Jolly, 1970; Kay, 1975, 1978, 1981; Lucas et al., 1986b; Demes and Creel, 1988; Kinzey and Norconk, 1990, 1992; Anapol and Lee, 1994; Cuozo and Sauther, 2006) suggests that the ultimate variable driving variation in tooth size is functional in nature.

Note about tooth enamel

Many studies suggest that dietary variation has been a major determinant of variation in enamel thickness. Regardless of size, animals that process hard diets have thicker enamel than their close relatives who process soft diets (primates and bats: Dumont, 1995, 1999; primates: Shellis et al., 1998; hominoids: Smith et al., 2005, Vogel et al., 2008). The current study was designed with the intention of comparing enamel thickness along the tooth row both within and between species to test the hypothesis that enamel thickness varies with bite force along the tooth row. However, the data necessary to assess this hypothesis cannot be collected from the current sample due to extreme wear on the tooth crowns and a paucity of juvenile specimens. Future investigations into the relationship between enamel thickness and bite force will require a sample that has been specially selected to include juveniles at each stage of dental development within a species, so that patterns of enamel thickness along the tooth row can be examined.

CRANIOFACIAL BIOMECHANICS

The upper and lower jaw work in concert with the dentition to process food; consequently, differences in craniofacial form are often interpreted in the context of dietary adaptation (DuBrul, 1974, 1977; Hylander, 1979a; Rak, 1986; Bouvier, 1986a,b; Demes and Creel, 1988; Spencer and Demes, 1993; Spencer, 1995, 1999; Wright, 2005; Constantino, 2007; Constantino and Wood, 2007; and many more). Craniofacial diversification can be seen in closely related lineages that utilize differing dietary strategies. For example, within cebids, *Cebus apella*, a hard object feeder, has larger temporalis muscles, wider zygomatic arches, and taller mandibular rami than its closest relatives (Constantino, 2007). Similarly, robust australopiths have flat, "dished" faces, hypermegadont dentition, and robust mandibular corpora compared to their gracile counterparts, and it has been suggested that they were hard object feeders and/or tough food specialists (DuBrul, 1974, 1977; Rak, 1986; Hylander, 1988).

The type of food an animal can consume is at least partially constrained by the maximum bite forces it can produce. Jaws capable of producing high magnitude bite forces may be advantageous for seed predators (e.g., pitheciines), while a more energy-efficient masticatory system may be better suited to primates who spend much of their time chewing tough leaves (e.g. colobines). By observing the relationships among the muscles of mastication and their relationship to the maxilla, mandible, temporomandibular joints (TMJs), and teeth, differences in force production capability among taxa can be compared. The primary selection pressures related to the production of masticatory force are

those that favor an increase in force magnitude or those that favor a decrease in the energetic cost of mastication (i.e., long duration/high frequency loading) (Spencer, 1995).

To understand systematically how bite forces are distributed along the jaw and how changes in face and jaw form affect feeding mechanics, mathematical models have been developed that treat the jaw as if it were a Class III lever (Gysi, 1921; Greaves, 1978; Smith, 1978; Spencer, 1995). These models of feeding mechanics are crucial to the study of the evolution of force production, but it is important to note that all models are simplifications and are therefore incomplete to some extent. While such simplifications may obscure the finer details of any mechanical structure, they are necessary in order to answer simple questions that would otherwise go unanswered due to complex interactions within the system. Ultimately, of course, these models must be validated against experimental and/or comparative data.

The models discussed below were formulated to facilitate the comparison of craniofacial structure among primates (rather than describe movement and muscle activity during mastication) and are therefore relatively simple. First and foremost, the concept of static equilibrium is key to these models. In a static analysis, it is assumed that no motion occurs, such that the sum total of all forces acting on a body cancel each other. This principle allows for the calculation of a force given the appropriate information of other forces in action, and is generally thought to be acceptable for most analyses of force production during feeding. Additionally, analyses of masticatory forces use vector mechanics, with the

complex forces at the occlusal surface, in the TMJ, and generated by masticatory muscles simplified using vectors, which can be manipulated mathematically or graphically. Commonly, the force vectors for each of the masticatory adductor muscles (temporalis, masseter, and medial pterygoid) are summed to produce a single muscle resultant force vector. Because these forces are complex, it is also common to analyze only components of the bite force, muscle resultant force, and joint reaction force within a defined reference framework (e.g. relative to the occlusal plane).

Simple lever model

The most basic model used to interpret the biomechanics of chewing is a simple lever model. In this model, the masticatory adductors (the temporalis, masseter, and medial pterygoid muscles) apply an upward force on the mandible, closing it, and this upward pull is resisted by downward reaction forces at the bite point and the TMJs. The muscle moment arm, or lever arm, is the perpendicular distance from the muscle force to the fulcrum (usually modeled at the TMJ). The resistance moment arm (here, the bite force moment arm) is the distance from the resistance force (the bite point) to the fulcrum (Figure 2.5).

Following the principle of static equilibrium, the basic equation for determining force magnitudes in this simple model is:

$$Bb + Jj + Mm = 0 \quad (1)$$

where B, J, and M are the magnitudes of the bite force, joint reaction force, and muscle resultant respectively, and b, j, and m are their respective moment arms.

Placing the fulcrum at the TMJ means that j equals zero in this equation because no torque is generated by J. Using this model, bite forces and joint reaction forces can be calculated for a given bite point (Gysi 1921; Bramble, 1978; Greaves, 1978; Smith 1978; Hylander, 1985; Spencer, 1995).

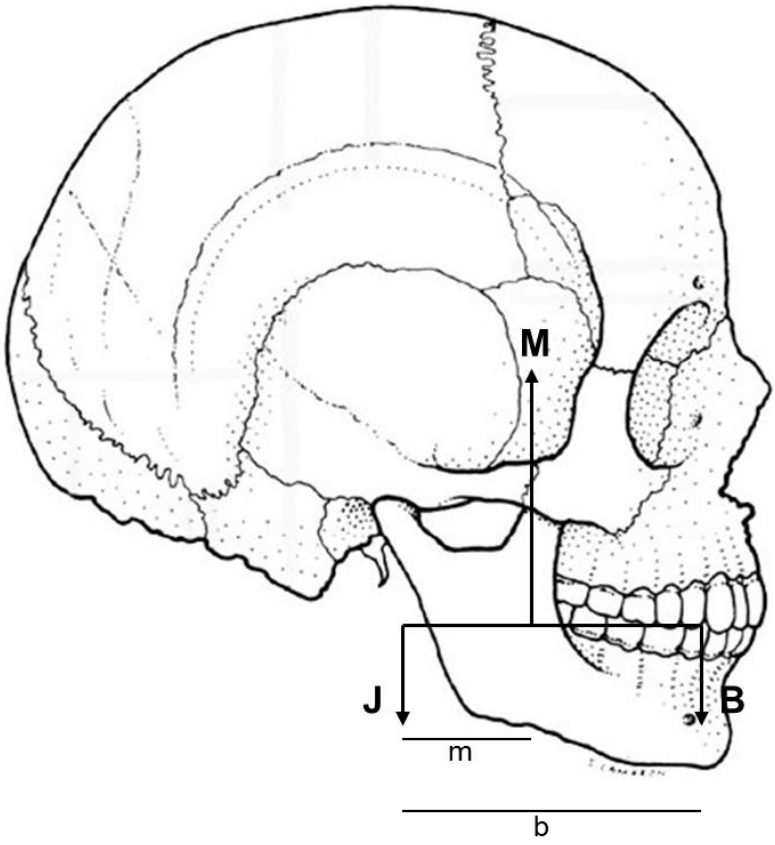

Fig. 2.5. Simple lever model. J = joint reaction force. M = muscle resultant. B = bite force magnitude. m = muscle moment arm (lever arm). b = bite force moment arm (load arm).

Using the simple lever model described above, researchers have found that when bite points are located in the anterior dental arcade, the working side (w-s) and balancing side (b-s) TMJs are compressed and resist most of the load; as the bite point moves posteriorly, it approaches the muscle resultant force and bears more of the load relative to the TMJs (Hylander, 1979b, 1985; Hylander and Bays, 1978, 1979). Bite points posterior to the muscle resultant can therefore result in tension at the TMJ as the condyle is pulled away from its articulation point (discussed in further detail below) (Maynard-Smith and Savage, 1959; DuBrul, 1974, 1977; Hylander 1975, 1978, 1985; Greaves, 1978; Smith, 1978; Demes and Creel, 1988; Spencer, 1995, 1999).

A longer bite force moment arm relative to the muscle moment arm results in less bite force for the amount of muscle force input and more condylar reaction force; conversely, a relatively short bite force moment arm reduces condylar reaction force and allows larger bite forces to be generated for a given amount of muscle force (Gysi, 1921; Bramble, 1978; Smith, 1978; Antón, 1994). The simple lever model predicts that an increase in bite force magnitude can be achieved temporarily by moving the bite point posteriorly along the tooth row or, permanently, by configurational changes in the masticatory system during evolution (Gysi 1921; Bramble, 1978; Greaves, 1978; Smith 1978; Hylander, 1985; Spencer, 1995, 1999; Wright, 2005; Constantino, 2007). These adaptations include anteroposterior shortening of the face, anterior repositioning of the masticatory muscles, and vertical deepening of the face and are seen in primates with resistant diets (e.g. *Cebus apella*). Each of these adaptations increases

mechanical advantage, the former two by increasing the lever/load arm ratio (Figure 2.6), described above (decreasing the distance between the masticatory muscles and the bite point) (DuBrul, 1977; Hylander, 1979a, Ravosa, 1990; Spencer and Demes, 1993; Antón, 1994) and the latter by raising the TMJ above the occlusal plane, which also increases leverage (Maynard-Smith and Savage, 1959; Ward and Molnar, 1980; Spencer, 1995), discussed below. In addition to these changes, force production can be increased without changing spatial relationships by increasing the size of the muscles of mastication.

Muscle resultant inclination and raising the TMJ in the simple lever model

The simple lever model assumes that the TMJ lies on the occlusal plane, and that the muscle resultant vector is perpendicular to the occlusal plane, two assumptions that are violated in primates (and most other mammals), which typically have TMJs situated high above the occlusal plane and an anterosuperiorly inclined muscle resultant (Spencer, 1995). Raising the TMJ in the simple lever model results in a reference line that changes with each bite point (Figure 2.7), resulting in the augmentation of the bite force moment arm for each bite point. Furthermore, reorienting the reference line for each bite point results in a change in the magnitude and direction of the normal and axial components of muscle resultant force, joint reaction force and bite force (Spencer, 1995). If the TMJ is raised while the muscle resultant vector is oriented vertically relative to the occlusal plane, the normal component of the muscle resultant force is decreased, and the bite force curve becomes flattened, especially distally (Spencer, 1995).

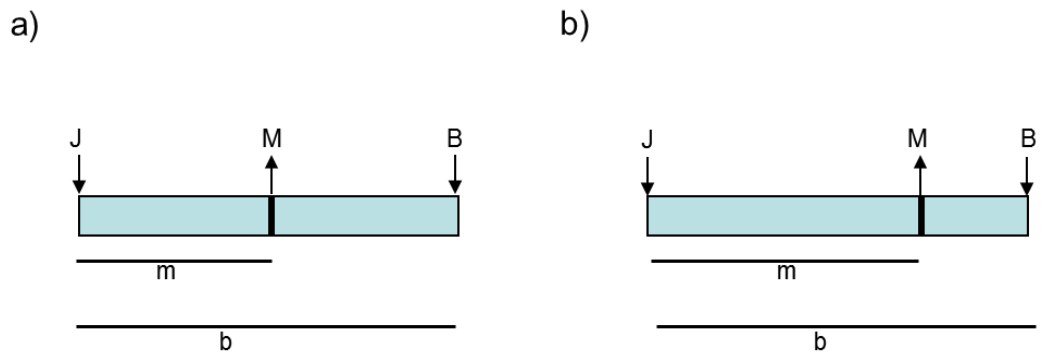

Fig. 2.6. Mechanical advantage. a) J = joint reaction force, M = muscle resultant force, B = bite force, m = lever arm, b = load arm. b) An anterior movement in muscle resultant, M, relative to the joint reaction force, J, results in an increased lever arm/load arm ratio (m/b), increasing the bite force.

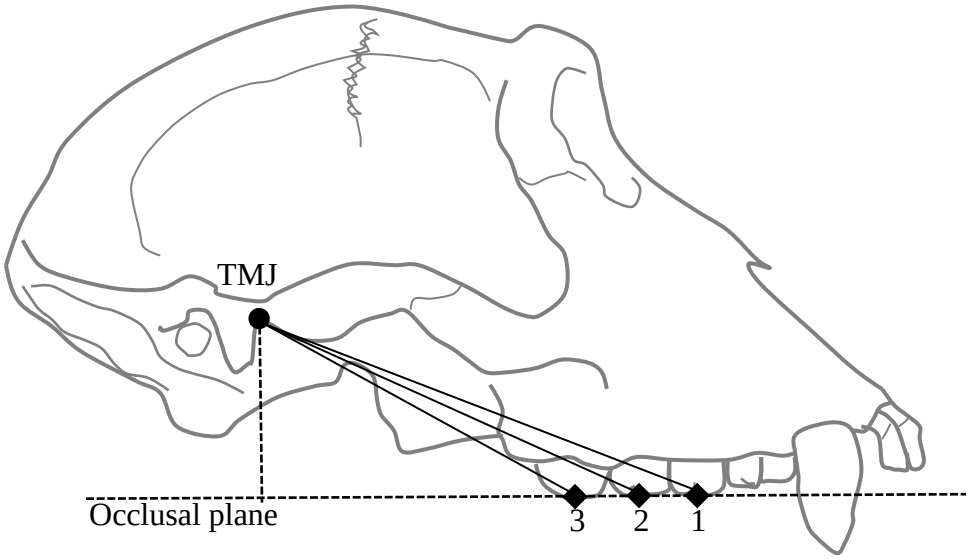

Fig. 2.7. Raising the TMJ above the occlusal plane. Note that the reference line changes with each bite point (1, 2, and 3).

The simple lever model only considers forces that are perpendicular (normal) to the reference line. However, this is unlikely to reflect reality given that the muscles of mastication are not oriented completely vertically relative to the occlusal plane. If the muscle force vector is angled (Figure 2.8), it can be broken down into its component parts, the vertical M_N and axial M_A, which together make up the total muscle force, *M*.

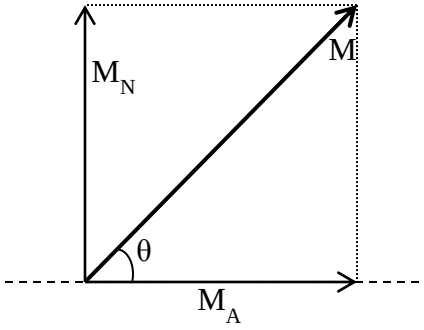

Fig. 2.8. Vectors of *M*.

The magnitude of M_N and M_A are determined by the angle of M at the reference line such that

$$M_N = M \sin \theta \quad (2)$$

$$M_A = M \cos \theta \quad (3)$$

When the TMJ is raised and the muscle resultant is inclined, the resulting changes in the relative magnitudes of M_N and M_A at each bite point and in the length of the muscle resultant moment arm impact the shape of the bite force curve. When the muscle resultant vector is perpendicular to the reference line, M_N has the highest magnitude and M_A is zero; as the changing bite point moves the reference line, M_N will decrease relative to M_A (Spencer, 1995). Furthermore, the muscle resultant moment arm, *m*, will be augmented. The combined result of raising the TMJ and inclining the muscle resultant in the simple lever model is a bite force curve in which bite force is increasing at all bite points, but the shape of the curve is relatively flattened. In other words, bite force magnitude continues to increase distally along the tooth row, but the change in force on adjacent teeth is relatively small.

Even when considering the effects of a raised TMJ and an anterosuperiorly inclined muscle resultant, the simple lever model predicts that bite forces will increase as the bite point moves posteriorly along the tooth row due to a decrease in the bite force moment arm relative to the muscle resultant moment arm. However, the simple model also predicts that the TMJ may be loaded in tension at posterior bites, which would result in joint dislocation

(discussed above). Most mammals are able to chew without dislocating the TMJ, suggesting that the simple lever model is incomplete.

Constrained lever model

The simple lever model predicts increasing bite forces as the bite point moves posteriorly along the tooth row. However, the TMJ may be dislocated (the mandibular condyle is pulled away from its articular surface) at posterior bite points (Maynard-Smith and Savage, 1959; DuBrul, 1974, 1977; Hylander 1975, 1978, 1985; Greaves, 1978; Smith, 1978; Demes and Creel, 1988; Spencer, 1995, 1998). Greaves (1978) argued that the ligaments of the TMJ are poorly suited to resist tensile forces and therefore constraints must exist in the masticatory system to avoid regular TMJ dislocation. He therefore proposed a modified model of masticatory biomechanics, often referred to as the constrained lever model. One way Greaves' (1978) constrained lever model differs from previous models is that it is oriented in the occlusal view.

The upward pull of the muscle resultant force is resisted at three points: the working side (w-s) TMJ, the balancing side (b-s) TMJ, and the bite point, making up what Greaves called the "triangle of support" (Figure 2.9). The muscle resultant lies on the midline because the muscles of mastication on both sides of the TMJ are assumed to be exerting maximum (and equal) force. When bite points are located in the anterior dental arcade, the w-s and b-s TMJ resist most of the load. As the bite point moves posteriorly, the area included within the triangle of support diminishes such that eventually the muscle resultant will fall outside its boundaries, at which point the mandibular condyle is prone to

dislocation. To prevent dislocation, it is hypothesized that at posterior bite points the muscle resultant is shifted from the midline toward the working side dentition by reducing muscle force on the balancing side (Figure 2.10) (Greaves, 1978). This action serves to maintain the muscle resultant within the triangle of support and protect the TMJ from dislocation by avoiding loading the joint in tension (Greaves, 1978; Spencer, 1995, 1999).

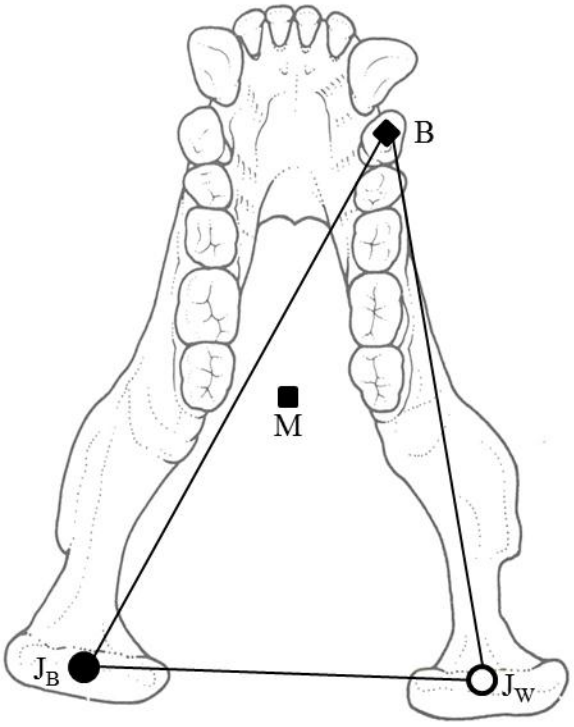

Fig. 2.9. The constrained lever model (Greaves, 1978). Viewing the mandible from the occlusal surface, it is possible to consider both anteroposterior and mediolateral relationships between the working- and balancing-side joint reaction forces (J_W and J_B, respectively), the muscle resultant (M) and the bite force (B). (mandible illustration from Aiello and Dean, 2002; figure modified after Spencer, 1995)

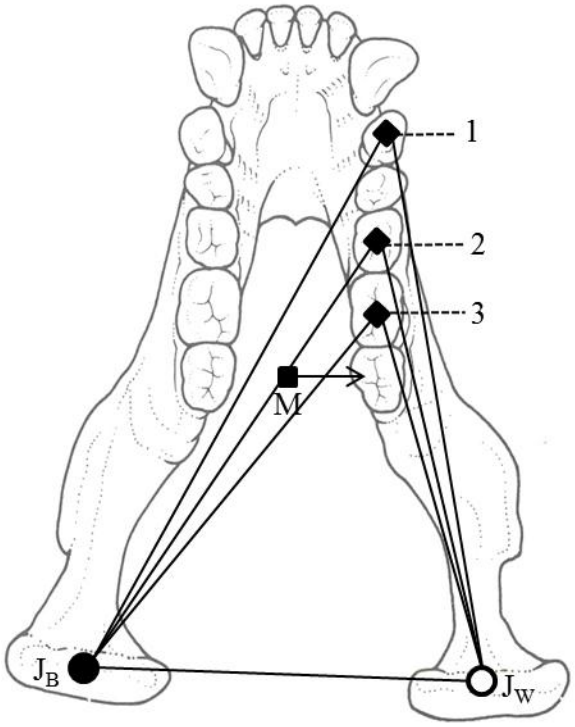

Fig. 2.10. Triangle of support. An anterior bite point (1) creates a triangle of support that encompasses a midline muscle resultant. Bite point 2 is the most posterior bite point possible while still maintaining a midline muscle resultant within the triangle. Bite point 3 creates a triangle of support in which a midline muscle resultant cannot fall. The muscle resultant must be moved laterally so that it is encompassed within the triangle of support by reducing muscle force on the balancing side. (mandible illustration from Aiello and Dean, 2002; modified after Spencer, 1995)

Building on Greaves (1978), Spencer and Demes (1993) proposed that the masticatory system can be divided into three regions, defined by how TMJ integrity is maintained in each (Figure 2.11). Region I is in the anterior portion of the mouth. Bite points located here produce a triangle of support that encloses a midline muscle resultant. Thus, bite points within Region I never require a shift in the muscle resultant to protect against jaw dislocation. Predictions for bite forces in Region I are identical for both the simple and the constrained lever model: as the bite point moves posteriorly in this region, maximum bite force increases.

Region II is posterior to Region I and requires that the muscle resultant be shifted laterally to maintain position within the triangle of support by reducing muscle force on the balancing side. Here, the predictions of the constrained model deviate from those of the simple model. While the simple lever model predicts an increase in bite forces as the bite point moves distally, the constrained model predicts that maximum bite force in Region II will remain constant due to the reduction of force necessary to maintain joint integrity as the bite point moves further distally. Greaves (1978) hypothesized that grinding dentition is located in Region II because this is the part of the mouth where the highest bite forces are predicted, and indeed among anthropoids premolar and molar teeth typically fall into Region II (Spencer, 1995). Region III is the most posterior region, where the muscle resultant will never fall into the triangle of support regardless of the amount of lateral shifting. For this reason, teeth are not expected to be located in Region III.

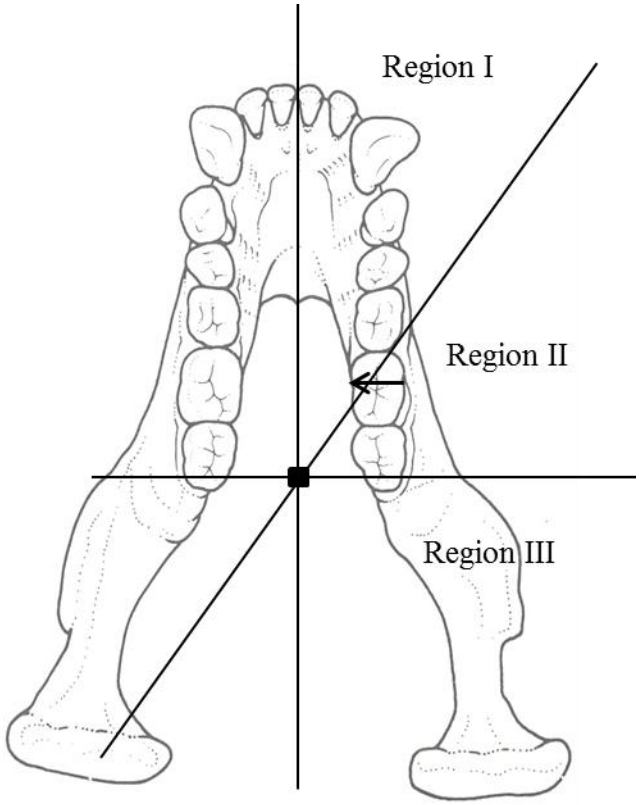

Fig. 2.11. Regions I, II, and III. Note that mediolateral changes in tooth position can shift the bite point from Region II to Region I, averting the need for differential shifts in muscle activity to maintain the integrity of the TMJ. (mandible illustration from Aiello and Dean, 2002; modified after Spencer, 1999).

Effect of configurational changes on bite force curves in Region II

Mediolateral changes in the bite point can alter constraints on muscle activity and bite force patterns (Spencer, 1995; Osborn, 1996). Primates with relatively narrow palates, like baboons, have increased their bite force capabilities by evolving dentition positioned more medially relative to the TMJs (Spencer, 1995). In Region II, bite forces increase with medial movement because less of a reduction in b-s muscle force is needed to shift the muscle resultant into this region. As teeth move medially (or as the TMJs move laterally), the triangle of support will encompass a midline muscle resultant at more posterior bite points. Therefore, lateral shifting of the muscle resultant is only needed at the most posterior bite points, shortening Region II. Conversely, moving the bite point laterally (or the TMJs medially) will effectively lengthen Region II, since a lateral shift of muscle resultant is needed relatively anteriorly in this configuration (Spencer, 1995).

Like the simple lever model discussed above, the constrained lever model assumes that the TMJ lies in the occlusal plane and that the muscle resultant vector is vertical, unlike the configuration in primates in which the TMJ is raised above the occlusal plane and the muscle resultant vector is inclined. Similar to the simple lever model, raising the TMJ in the constrained lever model results in a decrease in the normal component reaction force magnitudes, an effect that becomes more pronounced distally as the reference plane becomes more inclined (Spencer, 1995). Recall that in Greaves' (1978) constrained lever model, the bite force curve in Region II is predicted to be flat; thus, raising the TMJ above the

occlusal plane in the constrained lever model depresses an already-flat curve, resulting in a *decline* in distal bite forces (Spencer, 1995). Therefore, it has been hypothesized that the highest bite forces are produced at the *anterior* portion of Region II (Spencer, 1995), a departure from the simple lever model that predicts higher bite forces as the bite point moves posteriorly.

As with the simple lever model, the depression of bite forces that occurs when the TMJ is raised can be counteracted by inclining the muscle resultant vector. However, the combined increase in the height of the TMJ and inclination of the muscle resultant vector results in a change in the intersection point between the triangle of support and the muscle resultant vector, which results in changes in the length of the muscle resultant moment arm, *m*, and has major implications for the boundaries of Region II (Figure 2.12). The higher the TMJ, the more anteriorly an inclined muscle resultant intersects with the reference plane, increasing the length of the muscle resultant moment arm and shifting Region II anteriorly along the tooth row. Thus, b-s muscle force will decrease at more anterior bite points, resulting in the depression of calculated bite forces (Spencer, 1995). Together, raising the TMJ and inclining the muscle resultant in the constrained lever model can result in multiple patterns of bite force along the tooth row that are especially variable at distal bite points.

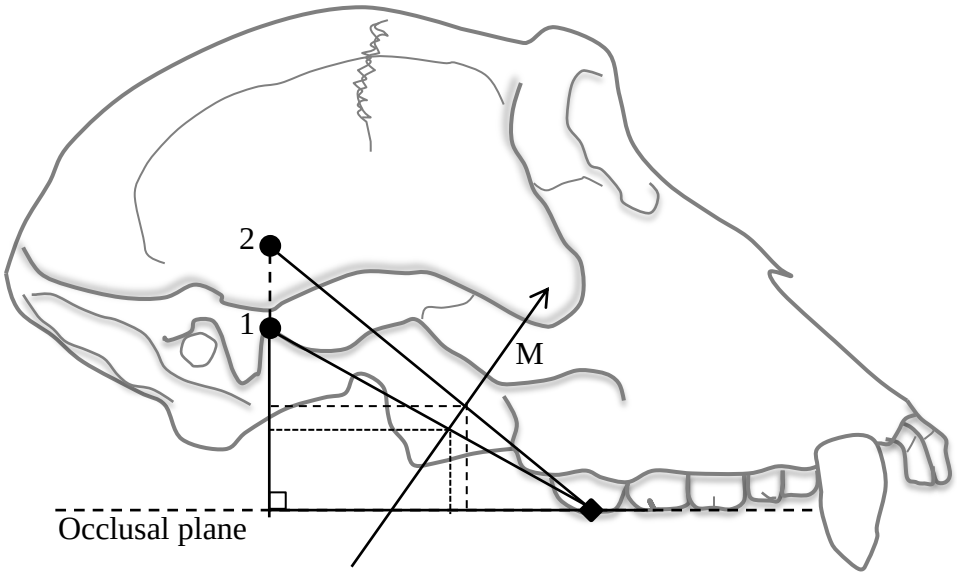

Fig. 2.12. Raising the TMJ and inclining the muscle resultant vector. Raising the TMJ from point 1 to point 2 changes the intersection point between the inclined muscle resultant vector and the reference plane, seen here in a lateral view. Region II will begin more anteriorly with the TMJ in postion 2.

The Buffer Zone

The constrained lever model predicts that at maximum bite force production in Region II, the muscle resultant will lie directly on the medial side of the triangle of support. This configuration allows the maximum amount of b-s muscle force without dislocation of the w-s TMJ. However, even slight variations in the position of the muscle resultant in this configuration can result either in its further inclusion within the triangle of support, or its exclusion. Since the mastication of food is a dynamic process, it is likely that such variations in muscle resultant position occur frequently, making Greaves' (1978) prediction of muscle resultant position open to frequent dislocation of the TMJ.

Spencer (1995, 1999) proposed that to reduce the probability of joint dislocation during maximum bite force production in Region II, the muscle resultant should lie further within the triangle of support, creating a "buffer zone" around its borders. Region II is defined as the region within the mouth where a lateral shift of the muscle resultant is required to maintain its position within the triangle of support; therefore, the introduction of a buffer zone effectively changes the predictions for the parameters of Region II. To fall within the triangle of support, complete with buffer zone, a muscle resultant must be shifted laterally at a more anterior bite point than in Greaves' (1978) original model (Figure 2.13).

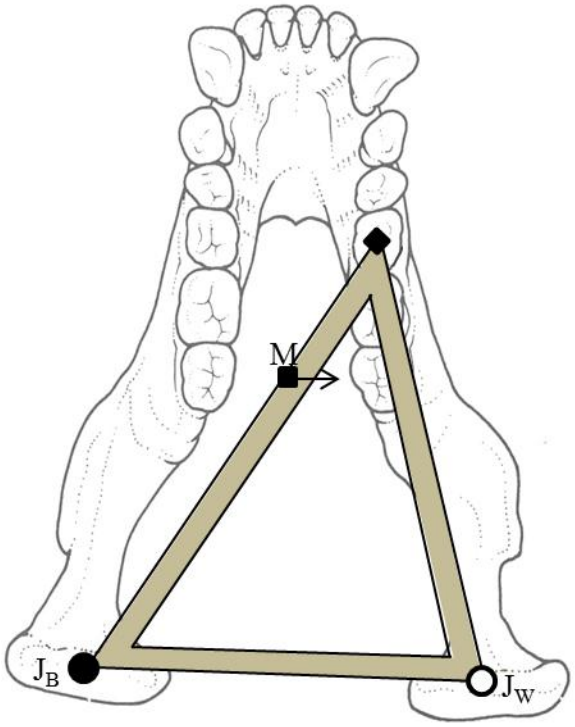

Fig 2.13. Buffer zone. The muscle resultant lies along the medial side of this triangle of support, but not within the triangle's buffer zone. To protect the TMJ, the muscle resultant should be shifted laterally so that it lies inside the buffer zone, out of danger of causing joint dislocation. (mandible illustration from Aiello and Dean, 2002; modified after Spencer, 1995).

Simple vs. Constrained lever model predictions

Both the simple lever model and the constrained lever model are useful for interpreting craniofacial form, but each model has different predictions due to the constraints incorporated into the latter. As discussed above, predictions for bite force, working-side muscle force, and balancing-side muscle force in Region I are virtually identical between the simple and constrained models, while predictions for bite force profiles in Region II differ significantly between the two due to the constrained model's assumption that muscle force will be decreased in this region to maintain joint integrity. Additionally, mediolateral changes in bite point position result in a change in the length of Region II, which affects where on the tooth row the highest magnitude bite forces can be produced. This has been supported by theoretical analysis of the human mandible (Osborn, 1996).

Interpretation of the selection pressures acting on the masticatory system may differ depending on which model is used. The simple lever model predicts that maximum bite force increases as the bite point approaches the TMJ. Therefore, any evolutionary change that results in more posterior bite points (e.g., facial shortening relative to the TMJ) would be interpreted as an adaptation to increased bite force. However, the constrained lever model (and the buffer corollary proposed by Spencer [1995]) suggests that such changes may leave the TMJ more vulnerable to dislocation, and therefore may only occur if the TMJ is adequately protected (e.g., b-s muscle force is decreased such that the muscle resultant is always located within the triangle of support). In addition to shortening the bite force moment arm relative to the muscle resultant moment

arm, facial shortening also results in a reorientation of Region II, a Region in which muscle force is continually decreasing. Thus, a short face may help to concentrate high bite forces at the anterior end of Region II (where muscle force is relatively high), but does not necessarily augment bite forces on all teeth.

Experimental Research

Theoretical models must be grounded in observable data to be useful in the interpretation of primate craniofacial configuration. While direct and explicit validation of a model through experimental work is not always possible, experimental tools can lend support to a model provided the data are interpreted correctly and carefully. Experimental studies have evaluated both the simple and constrained lever models with conflicting results. While some studies find that bite force increases posteriorly as predicted by simple lever models (in monkeys: Oyen and Tsay 1991; in humans: Mansour and Reynik, 1975; van Eijden et al., 1988; van Eijden, 1991; Iwase, 1998), others find that bite forces remain static or decrease posteriorly (in humans: Pruim et al., 1980; Spencer, 1998; Ferrario et al., 2004), conforming more closely to the constrained lever model.

The conflicting results of experimental studies on bite force may be due to limitations of methodology. Bite force can be directly measured *in vivo* using bite force transducers (Mansour and Reynik, 1975; Hylander, 1978; van Eijden at al., 1988; van Eijden, 1991; Dumont and Herrel, 2003; Ferrario et al., 2004; Kawata et al., 2007) or can be estimated via electromyography (EMG) (Møller, 1966; Pruim et al., 1980; Hylander, 1983; Ahlgren et al., 1985; Hylander et al., 1998, Spencer, 1998). However, both transducers and EMG have limitations.

Electromyography (EMG) measures the electrical activity of muscles and has been used in many studies examining muscle activity while biting (e.g., Møller, 1966; Pruim et al., 1980; Hylander, 1983; Ahlgren et al., 1985; Hylander et al., 1998). It has been demonstrated that masticatory muscle activity changes in accordance with differing bite forces such that an increase in bite force is accompanied by an increase in muscle activity (Lindauer et al., 1993; Proeschel and Morneburg, 2002), although it has been shown that EMG may overestimate bite force for isometric bites relative to chewing (Proeschel and Morneburg, 2002). While muscle activity is not equivalent to muscle force, the two have been shown to be highly correlated (Hylander and Johnson, 1989), and it is generally acceptable to use EMG data to estimate relative muscle force. Research shows that EMG patterns change as the bite point moves along the tooth row (Spencer, 1995), indicating differential muscle forces at different bite points. While changes in EMG patterns suggest changes in bite force patterns, these data are several steps removed from direct measurement of bite force magnitudes, which change based on bite position as well as muscle force magnitude and direction.

Bite force can be directly measured by using bite force transducers, and many studies have used this method (e.g., Mansour and Reynik, 1975; Hylander, 1978; van Eijden at al., 1988; van Eijden, 1991; Dumont and Herrel, 2003; Ferrario et al., 2004; Kawata et al., 2007). However, even with a direct measure of bite force, such studies are limited. Transducer studies cannot measure bite force during normal mastication since doing so would result in a severe modification of loading conditions that would result in data inappropriate to

evaluate normal feeding mechanics. Furthermore, to be useful in evaluating biomechanical models of force production, bite forces must be compared among teeth along the tooth row. Therefore, many studies that evaluate bite forces on one tooth only (e.g., Kawata et al., 2007) do not provide useful information for evolutionary questions.

The predictions of a simple lever model are inconsistent with the hypothesis that dental variation along the tooth row matches patterns of maximum bite force potential in most primate species. For all primates (and indeed mammals), this model predicts an increase in maximum bite force magnitudes as the bite point is moved posteriorly. If root and crown size are adapted to masticatory force production, tooth size gradients should match this pattern. However there is wide variation in the pattern of crown and root size among primates (Abbott, 1984; Swindler, 2002; Kupczik, 2003; Spencer, 2003). The constrained lever model combined with modifications laid out by Spencer (1995) to incorporate a raised TMJ, an anterosuperiorly inclined muscle resultant, and a buffer zone around the triangle of support (together referred to as the Spencer model throughout the remainder of this dissertation) predicts a wider range of possible bite force patterns depending on masticatory configuration, including patterns that match tooth size gradients observed in humans and some non-human primates (Spencer, 1995, 1998). Consequently, the Spencer model is the basis for the evaluation and interpretation of biomechanical data in this study.

Rigorous examination of the relationships among components of the masticatory system is necessary to understand past and present variation of primate craniodental anatomy. The current study examines the patterns of dental characteristics (root and crown size) along the tooth row to assess their relationship with one another and with bite force production. Additionally, these data are compared in primates that are closely related but have diets with differing mechanical properties to test the hypothesis that these relationships are functional in nature. While it is possible that some aspects of these morphologies are developmentally linked (Kavanaugh et al., 2007), studies have shown that both root and crown size vary independently (Abbott, 1984; Kupczik et al., 2003; Spencer, 2003; Steele-Perkins et al., 2003). Thus, it is reasonable to interpret variation in tooth and craniofacial morphology within a functional context as opposed to relying solely on allometric relationships or developmental processes to explain both inter- and intraspecific differences in craniodental morphology.

HYPOTHESES AND PREDICTIONS

The current study is separated into two parts. Part I assesses covariance between dental variables along the tooth row in an intraspecific analysis, wherein root and crown size patterns are analyzed within each species in the sample. Additionally, Part I examines whether variation in root and crown size can be explained by differences in function by conducting an interspecific analysis utilizing pair-wise comparisons of closely-related primates consuming diets of differing mechanical properties.

If crown size and root surface area covary along the tooth row, past research suggests they may be related to bite force. To test this hypothesis, Part II of the study examines the relationship between dental variation and variation in calculated bite force along the tooth row within each species.

Part I: Dental relationships

Hypothesis 1a: Root surface area and crown size will covary along the tooth row.

It has been proposed that root surface area (Spencer, 2003; Kupzcik, 2003) and crown size (Demes and Creel, 1988; Spencer, 2003; Lucas, 2004) should be greatest where bite forces are highest. If both of these aspects of tooth morphology are responding to selection for increased bite force production, then root and crown dimensions should covary along the tooth row. While size gradients may vary among species, these parameters are predicted to vary together in all taxa.

Hypothesis 1b: Root surface area and crown size are functionally related, and primates with mechanically resistant diets will have relatively higher values for these characteristics than closely-related primates with soft diets.

Rejection criteria: If root surface area and crown size do not covary along the tooth row, then Hypotheses 1a and b will be rejected. If root surface area and crown size covary, but primates with mechanically resistant diets do not show relatively higher values for these characteristics than their closely-related soft diet counterparts, the hypothesis that root surface area and crown size are functionally linked via dietary stress resistance will be rejected.

Part II: Dental features and bite force patterns

Hypothesis 2: Teeth that withstand high magnitude bite forces will have larger root surface areas relative to teeth that habitually experience lower magnitude loading.

This applies along the tooth row, where bite force magnitude is known to change with bite point (Mansour and Reynick, 1975; Pruim et al., 1980; van Eijden et al., 1988; van Eijden, 1991; Oyen and Tsay, 1991; Iwase, 1998; Spencer, 1998; Throckmorton and Ellis, 2001; Dumont and Herrell, 2003; Ferrario et al., 2004), and among species with diets of differing mechanical properties (Spencer, 2003).

Hypothesis 3: Teeth that withstand high magnitude bite forces will have larger crowns relative to teeth that habitually experience lower magnitude loading.

Previous researchers have suggested that crown size should be largest where bite forces are highest (Hylander, 1985; Demes and Creel, 1988; Spencer, 2003; Lucas, 2004). If the suggested relationship is accurate, the pattern of crown size should mirror the pattern of bite force magnitude along the tooth row within species. Furthermore, primates with mechanically resistant diets should have relatively larger crowns than closely-related primates with soft diets.

Rejection Criteria: If crown size and/or root surface area variation along the tooth row do not correlate with calculated bite force patterns, then Hypotheses 2 and/or 3 will be rejected accordingly.

CHAPTER 3

MATERIALS AND METHODS

The hypotheses for Part I of the current study center on dental morphological variation. Data on tooth root and crown surface area were taken from three-dimensional (3D) models generated from μCT scans of sample skulls. Root and crown surface area are compared within species to determine whether root and crown size covary along the tooth row. Additionally, root and crown surface area are compared between species using pair-wise comparisons to determine whether primates processing resistant diets have larger tooth roots and crowns than closely-related primates with softer diets. For Part II of the study, landmark data were collected from skulls using a digitizer and geometric morphometric software programs and used to calculate bite force curves for each individual sampled. Calculated bite forces are compared to both root and crown surface area along the tooth row to determine if root and/or crown surface area covary with bite force within species.

SAMPLE

The sample for this study comprises specimens within Harvard's Museum of Comparative Zoology (MCZ) and the Peabody Museum of Archaeology and Ethnology in Cambridge, MA. Care was taken to include species that encompass the vast geographical, taxonomic, and dietary variety within anthropoids. Additionally, species that are closely related but that have diets of differing mechanical properties have been included to facilitate the use of pair-wise comparisons for hypothesis testing. Adult females (determined by having a fully-

erupted M3) were preferentially scanned, but to increase sample sizes in species with a paucity of specimens, adult males were also included. Any specimen in which sex was not specified and could not be visually determined based on canine size was assumed to be female. Twenty-nine species from seven subfamilies are represented for a total of over 200 individuals (see Tables 3.1 and 3.2 for specimen list). Although the sample for the current study includes a broad selection of primate taxa, sample sizes for some species are quite small. Study protocols required that all individuals were scanned at the CNS, restricting the sample to individuals located on Harvard University campus. Every effort was made to maximize sample sizes for each taxa where possible.

TABLE 3.1. Specimen list for rank correlation analyses.

Subfamily	Species	N
Callithrichidae	[a]*Callithrix sp.*	M = 7 F = 7
	[a]*Saguinus sp.*	M = 5 F = 5
Cebinae	*Aotus trivirgatus*	M = 1 F = 7
	Cebus apella	M = 5 F = 9
	Cebus capucinus	M = 2 F = 7
	[a]*Saimiri sp.*	M = 4 F = 2
Pitheciinae	*Callicebus moloch*	M = 10 F = 0
	[a]*Pithecia sp.*	M = 3 F = 3
Atelinae	*Alouatta caraya*	M = 1 F = 3
	Alouatta palliata	M = 0 F = 10
	Ateles geoffroyi	M = 0 F = 17
Colobinae	*Presbytis hosei*	M = 1 F = 4
	Presbytis rubicunda	M = 4 F = 4
	Trachypithecus cristata	M = 0 F = 14
	Colobus polykomos	M = 1 F = 5
	Piliocolobus badius	M = 4 F = 5

(cont.)

[a]Specimens with no species designation are noted by their genus name followed by *sp.*

TABLE 3.1 (cont). Specimen list for rank correlation analyses

Subfamily	Species	N
	Macaca fascicularis	M = 1 F = 6
	Macaca fuscata	M = 1 F = 1
	Lophocebus albigena	M = 5 F = 1
	Cercocebus torquatus	M = 2 F = 1
	Papio anubis	M = 3 F = 2
	Mandrillus sp.	M = 5 F = 1
	Cercopithecus mitis	M = 0 F = 12
Cercopithecinae	*Erythrocebus patas*	M = 3 F = 1
	Pan paniscus	M = 0 F = 3
	Pan troglodytes	M = 0 F = 13
Hominidae	*Gorilla gorilla*	M = 0 F = 5
Total N:		216

[a]Specimens with no species designation are noted by their genus name followed by *sp*.

TABLE 3.2. Specimen list for comparative analyses.

Subfamily	Species	Diet group	N
Cebinae	*Aotus trivirgatus*	Soft	M = 4 F = 6
	Cebus apella	Resistant	M = 7 F = 9
	Cebus capucinus	Soft	M = 2 F = 8
	Saimiri sp.	Soft	M = 5 F = 5
Pitheciinae	*Callicebus moloch*	Soft	M = 10 F = 0
	Chiropotes satanas	Resistant	M = 0 F = 2
	Pithecia sp.	Resistant	M = 4 F = 3
Atelinae	*Alouatta caraya*	Resistant	M = 1 F = 3
	Alouatta palliata	Resistant	M = 0 F = 10
	Ateles geoffroyi	Soft	M = 0 F = 17

[a]Specimens with no species designation are noted by their genus name followed by *sp*.

TABLE 3.2 (cont). Specimen list for comparative analyses

Subfamily	Species	Diet group	N
Colobinae	*Colobus polykomos*	Resistant	M = 1 F = 5
	Piliocolobus badius	Soft	M = 4 F = 5
Cercopithecinae	*Macaca fascicularis*	Soft	M = 1 F = 8
	Macaca fuscata	Resistant	M = 1 F = 1
	Macaca sylvanus	Resistant	M = 1 F = 0
	Lophocebus albigena	Resistant	M = 5 F = 3
	Cercocebus torquatus	Soft	M = 2 F = 1
	Papio anubis	Soft	M = 4 F = 4
	Mandrillus sp.	Resistant	M = 5 F = 1
Hominidae	*Pan troglodytes*	Soft	M = 0 F = 13
	Gorilla gorilla	Resistant	M = 0 F = 5
Total N:			166

[a]Specimens with no species designation are noted by their genus name followed by *sp*.

Platyrrhines

Among New World monkeys, species from each subfamily are represented in the sample.

Callithrichinae

This group includes the genera *Callithrix* (marmosets) and *Saguinus* (tamarins). Marmosets have elongated lower incisors and a wide gape that have been suggested to be adaptations for gumnivory (Rosenberger, 1992; Garber et al., 1996; Vinyard et al., 2003), while tamarins only exploit gum opportunistically and rely mostly on fruit (Ferrari and Martins, 1992; Garber et al., 1996). While gum itself is not a resistant food, it has been suggested that the amount of masticatory force necessary to gouge through bark to get to the gum is considerable (Dumont, 1997, Spencer, 1999; Williams et al., 2000). However, a recent comparative study indicates that craniofacial from within tree-gouging primates is optimized for maximum gape, rather than maximum bite force (Vinyard et al., 2003). There is currently no *in vivo* data to indicate actual force production during gouging behavior; consequently, whether tree-gouging requires relatively high bite forces is unknown. It is clear that marmosets are more morphologically specialized for gouging behaviors than tamarins (Digby et al., 2007 and references therein), however, these morphological specializations have not been linked to increased bite forces. Therefore, there is no *a priori* reason to predict that callitrichids will differ from one another in postcanine tooth size. Consequently, both *Callithrix* and *Saguinus* are in the "Soft" diet food group, and were only used in intraspecific analyses.

Cebinae

Included in Cebinae are the genera *Cebus* and *Saimiri*. There has been long-standing debate over the place of *Aotus* within platyrrhine phylogeny and molecular studies have variably placed it within cebids (Porter et al., 1997), in its own separate family, Aotidae (Groves, 2001), and, most recently, as a sister taxon to callitrichids (Perelman et al., 2011). Although *Aotus* may be more closely related to callitrichids than to cebids, it lacks the morphological specializations related to gummivory that characterize tamarins and marmosets, and has not lost M3 as tamarins and marmosets have. Due to these major morphological differences, *Aotus* is included in Cebinae for the purposes of this study.

Both *Cebus* and *Saimiri* are generally frugivorous while also incorporating insects into their diet (Sussman, 2000; Campbell et al., 2007). *Saimiri* may spend up to 80% of its time foraging for insects, and during the dry season becomes completely insectivorous for up to a week at a time (Janson and Boinski, 1992). Additionally, *Saimiri* eats soft, ripe fruit that is typically softer and smaller than the fruit consumed by *Cebus* (Janson and Boinski, 1992). *Aotus* is a nocturnal primate, making it difficult for researchers to determine the exact composition of its diet; however, studies indicate that *Aotus* is primarily frugivorous (Fernandez – Duque, 2003; 2007). *Aotus* supplements its diet with young leaves, floral nectar, and insects (Sussman, 2000).

The genera *Aotus*, *Cebus*, and *Saimiri* are examined together in a Kruskall-Wallace analysis to determine whether tooth morphology differs among these groups. Based on dietary data reported in the literature (discussed above),

Aotus and *Saimiri* fall into the "Soft" food category, while *Cebus* is in the "Resistant" food category. Accordingly, it is predicted that *Cebus* will have relatively larger tooth roots and crowns than either *Aotus* or *Saimiri*.

Within *Cebus* it has been shown that *Cebus apella* regularly exploits foods that are more mechanically challenging to breach than other members of its genus (Kinzey, 1974; Rosenberger, 1992; Wright, 2005). Also, *Cebus* is known to shift dietary focus in response to seasonal food availability (Sussman, 2000). During the dry season, *C. apella* has been observed biting into extremely hard palm nuts that cannot be accessed by its close relative, *Cebus albifrons* (Sussman, 2000); furthermore, *C. apella* accesses these nuts using their canines and premolars rather than their molar teeth (Kinzey, 1974; Izawa, 1979). Due to the well-documented difference in the mechanical demands of its diet, *C. apella* (Resistant) is compared with *C. capucinus* (Soft). It is predicted that *C. apella* will have larger premolar root and crown surface area than *C. capucinus*, due to the emphasis the former places on the use of anterior premolars for hard food processing.

Pitheciinae

The pitheciins include the sakis (*Pithecia*) and bearded sakis (*Chiropotes*), and the titi monkey (*Callicebus*). Although *Callicebus* is morphologically distinct from *Pithecia* and *Chiropotes*, molecular analysis indicates that it forms a sister group with the sakis (Schneider and Rosenberger, 1996; Ray et al., 2005) and so is included in the comparative analysis of this group.

Both *Pithecia* and *Chiropotes* are seed predators and sclerocarpic foragers. Sclerocarpic foraging involves penetrating a fruit's hard outer pericarp with the anterior dentition, then masticating the relatively soft seeds with the postcanine dentition (Kinzey and Norconk, 1990). Both *Pithecia* and *Chiropotes* have been found to possess derived anterior dental morphology related to their mechanically challening diet (Kinzey, 1992; Anapol and Lee, 1994; Norconk et al., 1998; Martin et al., 2003). The fruit eaten by *Chiropotes* is very hard, exceeding the hardness of fruits exploited by *Pithecia* (Kinzey and Norconk, 1993; Norconk et al., 1998).

Despite processing a mechanically challenging diet, the molar morphology of *Chiropotes* suggests that after using the anterior teeth to breach a food's outer defenses, the food processed on the postcanine tooth row is relatively soft (Kinzey and Norconk, 1990, 1993; Martin et al., 2003). *Pithecia*, on the other hand, has thicker molar enamel than *Chiropotes* (Martin et al., 2003); additionally, *Pithecia* supplements its diet with leaves, a behavior not recorded for *Chiropotes* (Kinzey and Norconk, 1990, 1993). Considering all available dietary information, both *Pithecia* and *Chiropotes* belong in the "Resistant" food category. *Chiropotes* is predicted to have larger premolar roots and crowns than *Pithecia* due to the former's exploitation of very hard fruits inaccessible by the latter (Kinzey and Norconk, 1993; Norconk et al., 1998). However, due to its greater reliance on leaves and suggestions that its postcanine tooth row is more adapted to mechanically challenging foods (Martin et al., 2003), it is predicted that *Pithecia* will have higher values for molar root and crown surface area than *Chiropotes*.

Callicebus differs from the rest of the pitheciins in that they eat softer, fleshy fruits, supplemented with leaves (Sussman, 2000) and have adaptations of the anterior dentition to aid in fruit acquisition (Kinzey, 1992). *Callicebus* molar morphology is consistent with adaptation to frugivory, and there are no suggestions that it regularly eats mechanically resistant food items (Sussman, 2000). Consequently, *Callicebus* is placed in the "Soft" food category, and it is predicted that both *Pithecia* and *Chiropotes* will have larger tooth crowns and roots than *Callicebus* for all postcanine teeth.

Atelinae

The genera *Ateles* and *Alouatta* are included in Atelinae, both of which are among the largest-bodied and widest-ranging platyrrhine genera. *Alouatta* is one of the few New World monkeys that consumes large portions of leaves in its diet (Sussman, 2000; Teaford et al., 2006; Di Fiore and Campbell, 2007), which is reflected in the specialized morphology of its gut (Chivers and Hladik, 1984) and molars (Kay and Hylander, 1978). *Alouatta* supplements its diet with fruit and seeds (Di Fiore and Campbell, 2007), although the seeds are not destroyed as in the pitheciins, but rather pass through the intestinal tract intact (Sussman, 2000). In contrast to *Alouatta*, *Ateles* eats few leaves and instead consumes the bulk of its calories in fruit; in fact, *Ateles* is repeatedly identified in the literature as a ripe fruit specialist (Sussman, 2000; Di Fiore and Campbell, 2007; Felton et al., 2008). Based on the available data, *Alouatta* is put into the "Resistant" food category, and is predicted to have larger postcanine root and crown surface area than *Ateles*, which is in the "Soft" food category.

Catarrhines

The sample for this study is also composed of Old World monkeys and hominoids from the Colobinae, Cercopithicinae, and Homininae subfamilies.

Colobinae

This group is further subdivided into the Asian colobines (represented in this study by *Presbytis rubicunda, Presbytis hosei,* and *Trachypithecus cristata*) and the African colobines (*Colobus polykomos* and *Piliocolobus badius*). All colobines are known as "the leaf-eating monkeys", and have specialized stomachs that allow them to exploit this resource (Chivers 1994, Kay and Davies, 1994). However, there is a high degree of dietary variation among species such that some species of colobines consume a more mechanically challenging diet than others (Dasilva, 1994; Fashing, 2007).

Both *C. polykomos* and *P. badius* prefer to eat young leaves and buds and will supplement their diet with flowers, fruit, and seeds (Usongo and Amubode, 2001; Fashing, 2007). Additionally, both are described as seed predators, although *C. polykomos* has been documented harvesting seeds from thick, woody plants not utilized by *P. badius* (Dasilva, 1994*). C. polykomos* is also characterized by a molarized P4 (Swindler, 2002), a trait that has been linked with hard object feeding in extinct hominins (Robinson, 1954; Rak, 1983; Lucas et al., 2008) and in papionins (Fleagle and McGraw, 2002). Consequently, *C. polykomos* is classified in the "Resistant" diet category, while *P. badius* is classified in the "Soft" dietary category; it is predicted that *C. polykomos* will have larger postcanine tooth crowns and roots than *P. badius*. It should be

emphasized here that *P. badius* has a "Soft" food diet only in relation to *C. polykomos*, and is not considered to have a soft diet relative to primates as a whole.

Like African colobines, the diet of Asian colobines centers around folivory, supplemented variably with fruits and seeds (Kirkpatrick, 2007). Within this group, *P. rubicunda*'s diet, while largely folivorous, can include up to 80% seeds in some months (Davies, 1988). *P. hosei* appears to differ from *P. rubicunda* in that it has not been reported relying as heavily on seeds, and its focus is primarily on young leaves and flowers (Kirkpatrick, 2007).

Trachypithecus has been suggested to be better adapted to leaf-eating than *Presbytis* (Bennett and Davies, 1994; Yeager and Kool, 2000), evidenced by greater shearing crests on the molar teeth and larger forestomachs for processing chemically-defended plants (Chivers, 1994). *Trachypithecus* has also been observed to eat more mature leaves than *Presbytis*, which are more mechanically demanding than young leaves (Kirkpatrick, 2007). However, given that specializations for leaf-eating in *Trachypithecus* center on soft-tissue changes as well as tooth shape (but not size), there is no convincing *a priori* evidence that tooth size will differ among these taxa by dietary category.

Cercopithecinae

The cercopithecines make up a very large group that is further broken down into macaques, the baboons, mandrills, and mangabeys, and guenons.

Macaques

Macaques are represented by over 20 species that inhabit a wide variety of environments throughout the Old World. As a group, they are considered frugivorous, although this classification obscures the huge variety in habitat and resource availability among these monkeys (Menard, 2004; Thierry, 2007). The macaques included in this study are *Macaca fascicularis* (long-tailed macaque), *Macaca fuscata* (Japanese macaque), and *Macaca sylvanus* (Barbary macaque). All three species are examined in intraspecific analyses, but only *M. fascicularis* and *M. fuscata* were included in pair-wise comparisons due to an extremely low sample size for *M. sylvanus*.

M. fascicularis is considered among the most frugivorous of macaque species and spends up to 87% of its feeding time on fruit (Menard, 2004). They will supplement their diet with leaves, pith, seeds, and flowers when fruit is scarce (Yeager, 1996), but it has not been suggested that *M. fascicularis* is specially adapted to resistant food item consumption. *M. fuscata* lives in Japan, and its diet reflects its more temperate habitat. During the winter, *M. fuscata* diet is focused primarily on bark and seeds, in addition to twigs, roots, and grasses (Hill and Lucas, 1996), and it has been suggested that *M. fuscata's* craniofacial skeleton shows adaptation for consuming resistant food items (Constantino, 2007). In this study, *M. fuscata* is labeled as "Resistant" and is predicted to have larger postcanine tooth roots and crowns than *M. fascicularis*, a "Soft" food consumer.

African papionins: Baboons, Mandrills, and Mangabeys

Within baboons, mandrills, and mangabeys are two distinct lineages. *Lophocebus* (arboreal mangabeys), *Papio* (baboons), and *Theropithecus* (gelada baboons) make up one group, while *Cerocebus* (terrestrial mangabeys) and *Mandrillus* (mandrills and drills) form the other. These groupings are firmly supported by molecular (Distoell, 2000) and morphological (Fleagle and McGraw, 2002) evidence. On the whole, African papionins are all opportunistic omnivores with no major specializations of the digestive tract linking them to one specific food type, although what they actually consume is constrained both by habitat and competition for resources with other species (Jolly, 2007).

In the current study, the *Lophocebus-Papio-Theropithecus* group is represented by two species, *Lophocebus albigena* and *Papio anubis*. *L. albigena* feeds primarily in the tree canopy, and its diet is largely composed of figs and other fruits (Olupot et la., 1997); additionally, during times of fruit scarcity they rely very heavily on hard-shelled fruits and seeds (Lambert et al., 2004). *P. anubis* has a typical baboon diet, distinctive in that there is no distinguishable dietary specialization (Okecha and Newton-Fisher, 2006, Jolly, 2007). *P. anubis* has been recorded consuming leaves, fruits, seeds, stems, seedling, bark, roots, crops, and even garbage on a regular basis (Okecha et al., 2006). There is some indication that *P. anubis* dietary composition changes somewhat with season (Okecha et al., 2006), but it has not been suggested that *P. anubis* is especially adapted to resistant food items relative to other African papionins. Consequently, *L. albigena* is put in the "Resistant" food category and *P. anubis* in the "Soft"

category, with the expectation that *L. albigena* will have higher values for postcanine root and crown surface area than *P. anubis*.

The *Cercocebus-Mandrillus* group is characterized by adaptations to hard object feeding and strenuous foraging (Fleagle and McGraw, 2002). Both *Cercocebus* and *Mandrillus* forage on the forest floor, consuming fallen fruits, fungi, and invertebrates; additionally, *Mandrillus* will eat especially hard foods, including tough-shelled fruits, seeds, pith, and bark that are processed with the premolars (Hoshino, 1985; Harrison, 1988).

Although the diet of *Mandrillus* appears to focus more on hard object feeding than that of *Cercocebus*, both have molarized premolar crowns that are suggested to be adaptations to a mechanically resistant diet (Fleagle and McGraw, 2002). In this study, *Mandrillus* is classified as "Resistant" and *Cercocebus* as "Soft", but it must be emphasized that these categories apply only within the context of this specific pair-wise comparison. Relative to other cercopithecoids, both *Cercocebus* and *Mandrillus* feed on resistant foods.

Guenons

Guenons are cercopithecine (cheek-pouch) monkeys that live in a variety of habitats throughout sub-Saharan Africa. As a group, they are identifiable by adaptations to frugivory, including low, rounded molar cusps, simple stomachs, and cheek pouches (Enstam and Isbell, 2007). In the current study, the guenons are represented by the forest-dwelling *Cercopithecus mitis* and its close relation *Erythrocebus patas*, usually found in woodland-savanna environments (Enstam and Isbell, 2007; Isbell, 1998).

C. mitis has been recorded consuming large amounts of fruit, variably supplemented with young leaves, flowers, arthropods, and other invertebrates (Cords, 1986). The diet of *E. patas* is largely made up of colonially-living ants that are obtained by biting into the swollen thorns of *Acacia drepanolobium* trees (Isbell, 1998); patas monkeys supplement their diet with *A. drepanolobium* gum and a small proportion of fruit (Isbell, 1998; Enstam and Isbell, 2007).

Despite the fact that *C. mitis* and *E. patas* live in different environments with differing food resources, there is no indication that either species consumes more mechanically challenging food than the other. Both are labeled as "Soft" food eaters, and they are not considered in pair-wise comparisons since there is no prediction that one will have larger tooth roots and crowns than the other. They are, however, considered in the intraspecific analyses investigating patterns of tooth size and bite force along the tooth row.

Homininae

The hominoids are represented by *Pan troglodytes* (common chimpanzee), *Pan paniscus* (bonobo), and *Gorilla gorilla* (western lowland gorilla). Although *P. paniscus* is included in intraspecific analyses of patterns of crown size, root size, and bite force along the tooth row, it is not included in pair-wise comparisons of crown and root size since its diet largely overlaps with *P. troglodytes* (Stompf, 2007). Chimpanzees are highly frugivorous, even in times of food scarcity (Wrangham et al., 1998; Chapman et al., 2002; Stanford and Nkurununngi, 2003). In addition to fruit, chimps will supplement their diet with leaves and other low-quality foods during times of resource scarcity (Wrangham

et al., 1998; Chapman et al., 2002), however, they have no morphological adaptations associated with processing resistant food items.

Gorillas have long been considered a folivorous species, with morphological correlates to leaf-eating including a large body size, an enlarged hindgut, and long hindgut fermentation time (Watts, 1996). However, it has become evident that gorilla diet varies widely among species such that gorillas living in high-altitude environments with little-to-no access to fruits are almost entirely folivorous (e.g., *Gorilla berengei*, the mountain gorilla), while gorillas living at lower altitudes have more access to fruit and include significantly more fruit in their diet (e.g., *G. gorilla*, examined in this study) (Remis, 1997; Ganas et al., 2004; Robbins, 2007). In addition to fruit, *G. gorilla* will supplement its diet with leaves, pith, and bark during times of fruit scarcity (Remis, 1997; Oates et al., 2003).

Overall, the diets of chimpanzees and gorillas are similar, but during times of fruit scarcity their diets diverge, as chimpanzees continue pursuing fruit (Wrangham et al., 1998; Chapman et al., 2002) while gorillas greatly reduce their fruit intake and focus more on high fiber, low-quality plants to supply their daily calories (Remis, 1997; Oates et al., 2003; Robbins, 2007). In this study, *G. gorilla* is placed in the "Resistant" food category, and is expected to have larger postcanine tooth crowns and roots than *P. troglodytes*, which has a "Soft" food diet.

DATA COLLECTION

μCT scanning

All sample crania were scanned during using a micro-computed tomography (μCT) scanner located at the Center for Nanoscale Systems (CNS) at Harvard University. A μCT scan is much like a regular CT scan; a microfocus x-ray source is aimed at the object being scanned, and a planar x-ray detector collects the cross-sectional magnified projection images. Images are taken at each projection point within a 360-degree rotation. The number of projections can be changed depending on the needs of the researcher. In general, the more projections taken, the higher the resolution of the scan; however, increasing the number of projections also increases the time it takes to scan an object. A computer then synthesizes the stack of virtual cross-sections (commonly called slices), which results in the completed scan.

A μCT scan differs from a regular CT scan in that the resolution of the image is increased by decreasing the thickness of each slice from about 1mm to 10-50μm, increasing the total number of slices, and doubling the amount of pixels in each, which allows for the precise and accurate measurement of small structures (Peyrin et al., 1998; Ding et al., 1999; Laib et al., 2000), including tooth structures such as root surface area and enamel thickness (Olejniczak et al., 2008).

The scanner at CNS is a X-Tek HMXST225 μCT scanner (Figure 3.1) with an open source x-ray tube. The x-ray detector panel is a Perkin Elmer 1621, which provides a 2000 x 2000 pixel and 16 inch x 16 inch field of view with a 7.5 frames per second readout and a physical pixel size of 200 microns. The μCT

computer system consists of three individual 64-bit computers, each with its own function. The first is used for control and data acquisition, the second for three-dimensional (3D) reconstruction, and the third is a visualization station.

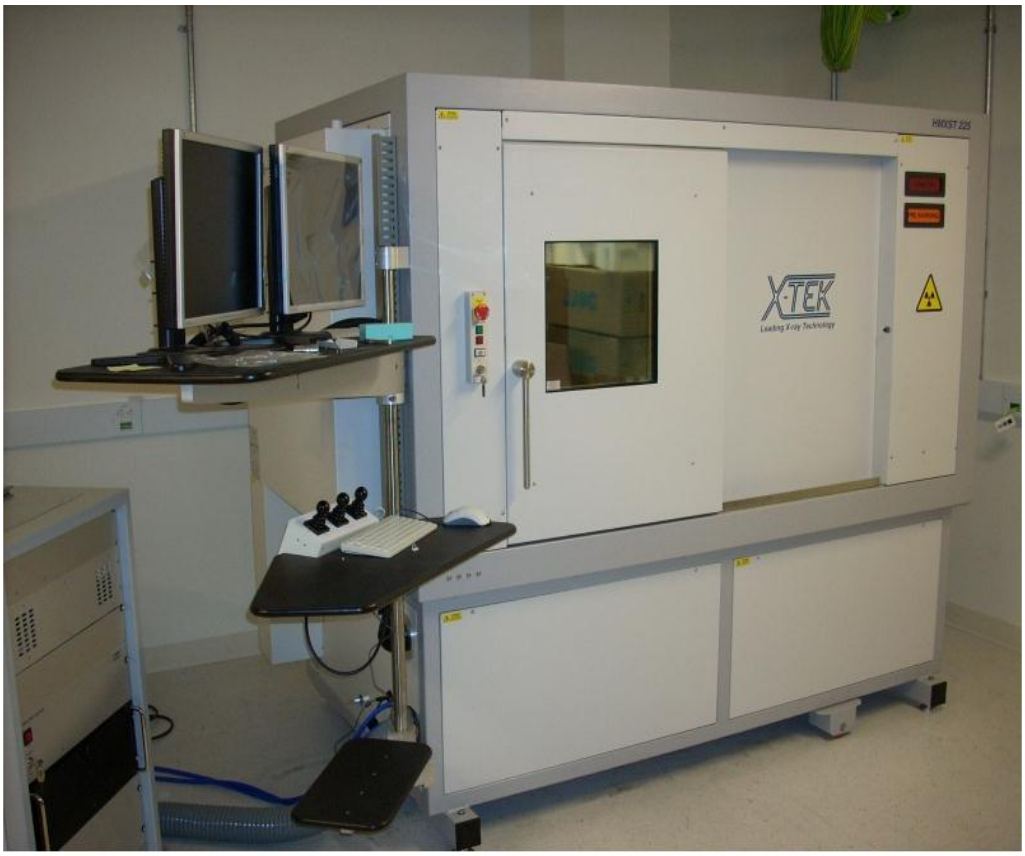

Fig. 3.1. µCT scanner at Harvard.

Each skull was placed in a Styrofoam holder that was then placed inside the scanner on a rotating platform. The Styrofoam held the skull in place while allowing the x-rays to fully penetrate the specimen without leaving visual artifacts. All crania in this study were scanned at parameters optimum for the highest possible resolution within the time available to capture all samples. Crania were placed in the scanner and then rotated 360°. Resolution was set as high as possible while keeping the entire specimen within the limits viewing window set by the scanner. All crania were scanned using 1000-1500 projections, scan time per specimen ranged from 18-60 minutes, and resolution ranged from 40 micrometers (in smaller species, e.g., *Callithrix*) to 125 micrometers for the largest species (e.g., *Gorilla*) (See Appendix A for all sample scanning parameters). Once each scan was complete, images were saved in DICOM format, a standard medical imaging format that is compatible with a wide range of biomedical software programs capable of viewing and measuring µCT scans.

Dental variable measurement

Completed scans were loaded into the Mimics 14.11 (Materialise, Inc.) software package, which is a program that enables the visualization of CT and µCT DICOM files with functions that allow for the production of 3D models from the scans. Each specimen's right-side maxillary postcanine teeth were isolated from the rest of the skull using thresholding and region growing tools.

By thresholding a scan, the skull is overlayed with a mask that contains only those pixels of the image with a value equal to or higher than the thresholding value (Figure 3.2). This mask is the basis for the 3D models of each

individual tooth. Once the threshold mask is laid down, the region growing tool allows for the mask to be split into several distinct objects once connecting pixels have been removed (Figure 3.3). In the current study, a threshold mask was laid over the entire skull and dentition for each specimen. Then, pixels that connected the right-side maxillary dentition to the alveolar bone and to each other were manually removed. Once each tooth was isolated, the region growing tool was used to create each tooth as a 3D model (Figure 3.4). Each model was saved and then exported as an ASCII STL file to be uploaded in the Geomagic (Raindrop, Inc.) software package for measurement. In specimens with a missing ride-side tooth, the corresponding left-side tooth was measured and used for analyses. Specimens missing the same tooth on both left and right side were used for analyses of individual teeth (e.g., scaling analyses), but were excluded from analyses examining patterns of tooth size along the tooth row.

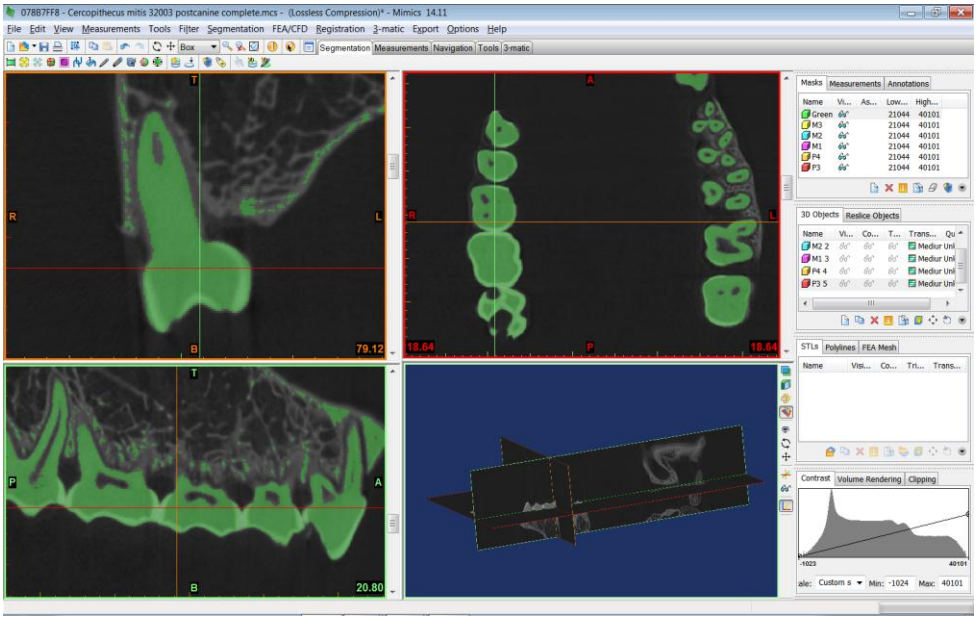

Fig. 3.2. *C. mitis* scan after thresholding.

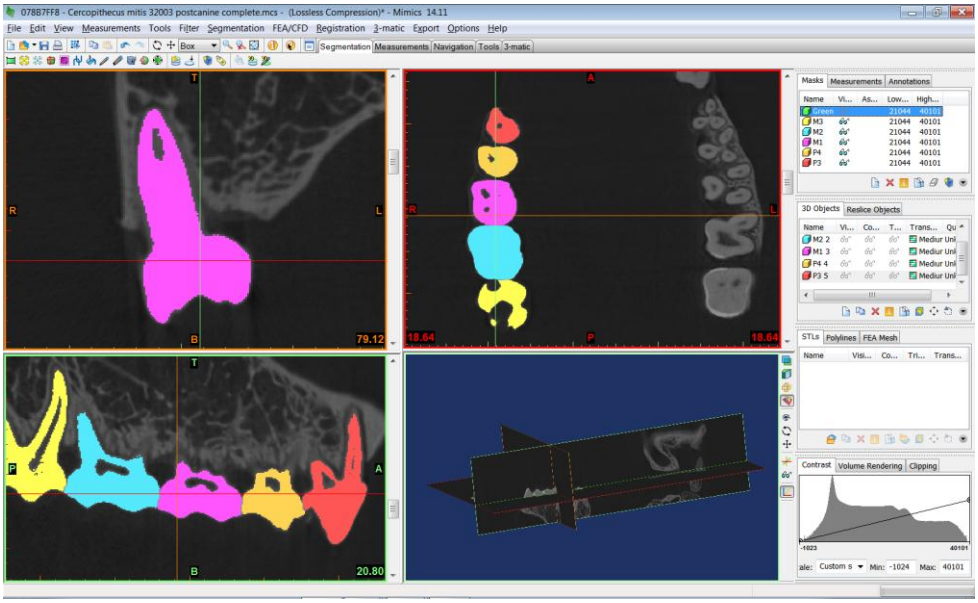

Fig. 3.3. *C. mitis* scan after region growing was used to separate individual teeth.

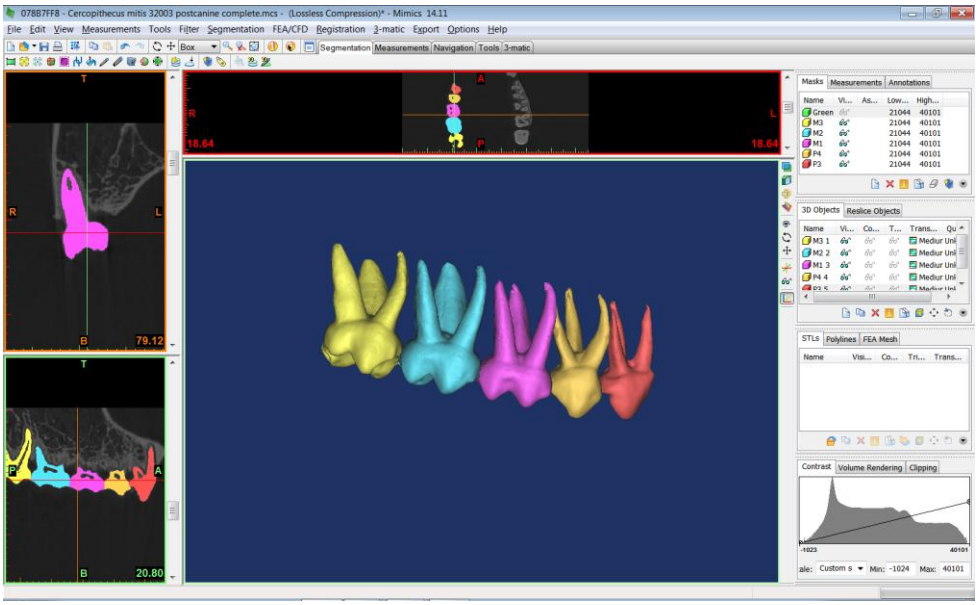

Fig. 3.4. 3D tooth models made from region growing masks.

Each tooth was measured for root surface area (RSA), crown surface area (CSA), and the area of a plane passed through the cervical margin (CMSA). The junction between tooth crown enamel and the tooth root is visually apparent in each scan. RSA was determined by selecting the portion of the tooth inferior to the enamel-root junction on all sides. CSA was determined by orienting the tooth in the occlusal view and measuring the total three-dimensional (3D) surface area of the visible crown (Figure 3.5).

Because the measurement for CSA may vary due to differences in enamel thickness and overall tooth wear, the two-dimensional (2D) area of the cervical margin (CMSA) was also measured as a functional proxy for crown size. Although CMSA is almot certainly an underestimation of crown size in most taxa, it is representative of the size of the area through which masticatory force must travel before reaching the tooth root. CMSA was calculated similarly to protocols

described in Kupzcik et al. (2009), who also used CMSA to help approximate crown size. Three points were placed on the inferior-most borders of the enamel root junction through which a plane was passed. Next, the portion of the tooth below the plane was removed, resulting in an isolated tooth crown. The bottom of the crown was closed off with a flat plane, and the 2D surface area of this plane was then measured as CMSA (Figure 3.6).

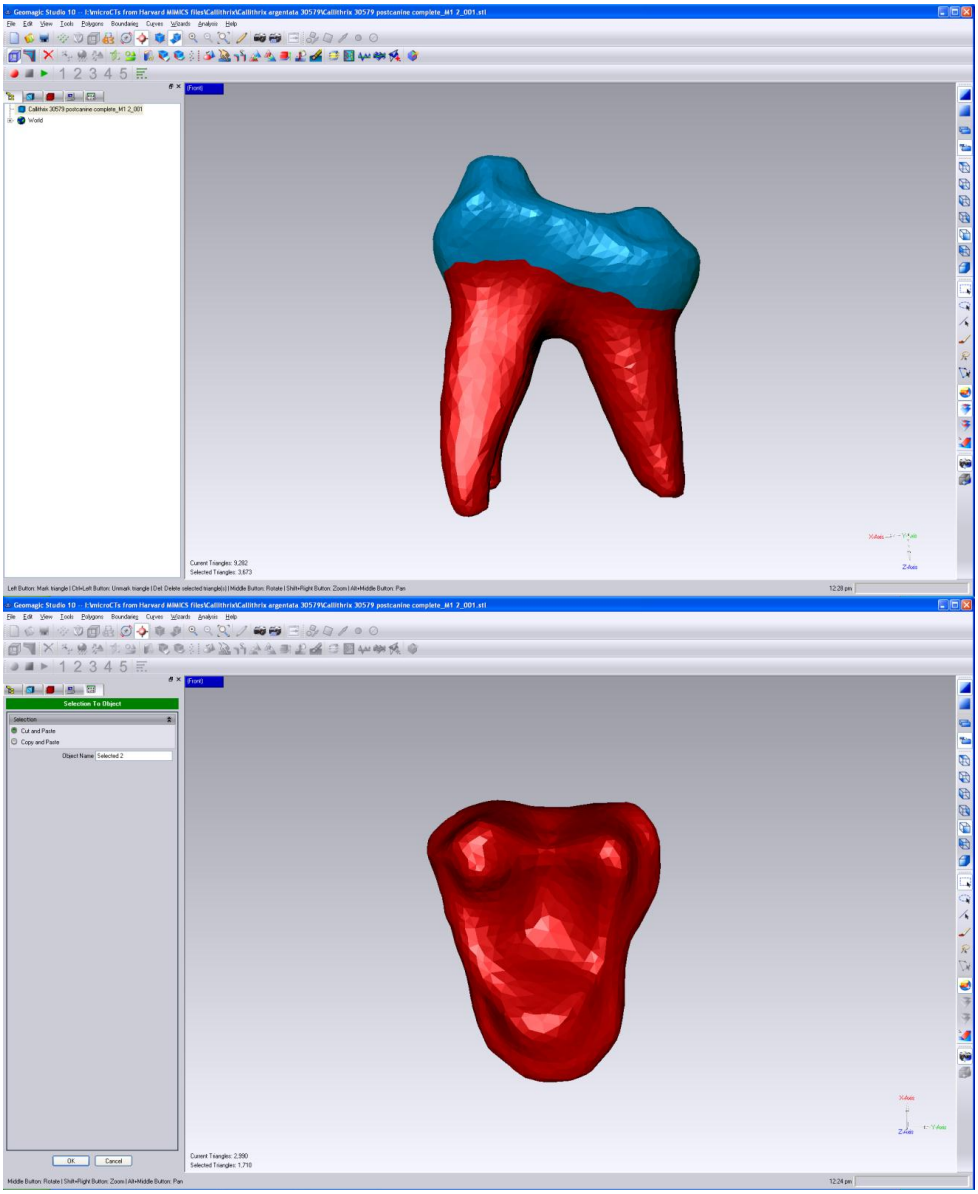

Fig. 3.5. Root surface area (RSA, in red) top; Crown surface area (CSA, in red), bottom. Both images of *Callithrix sp.* 30579.

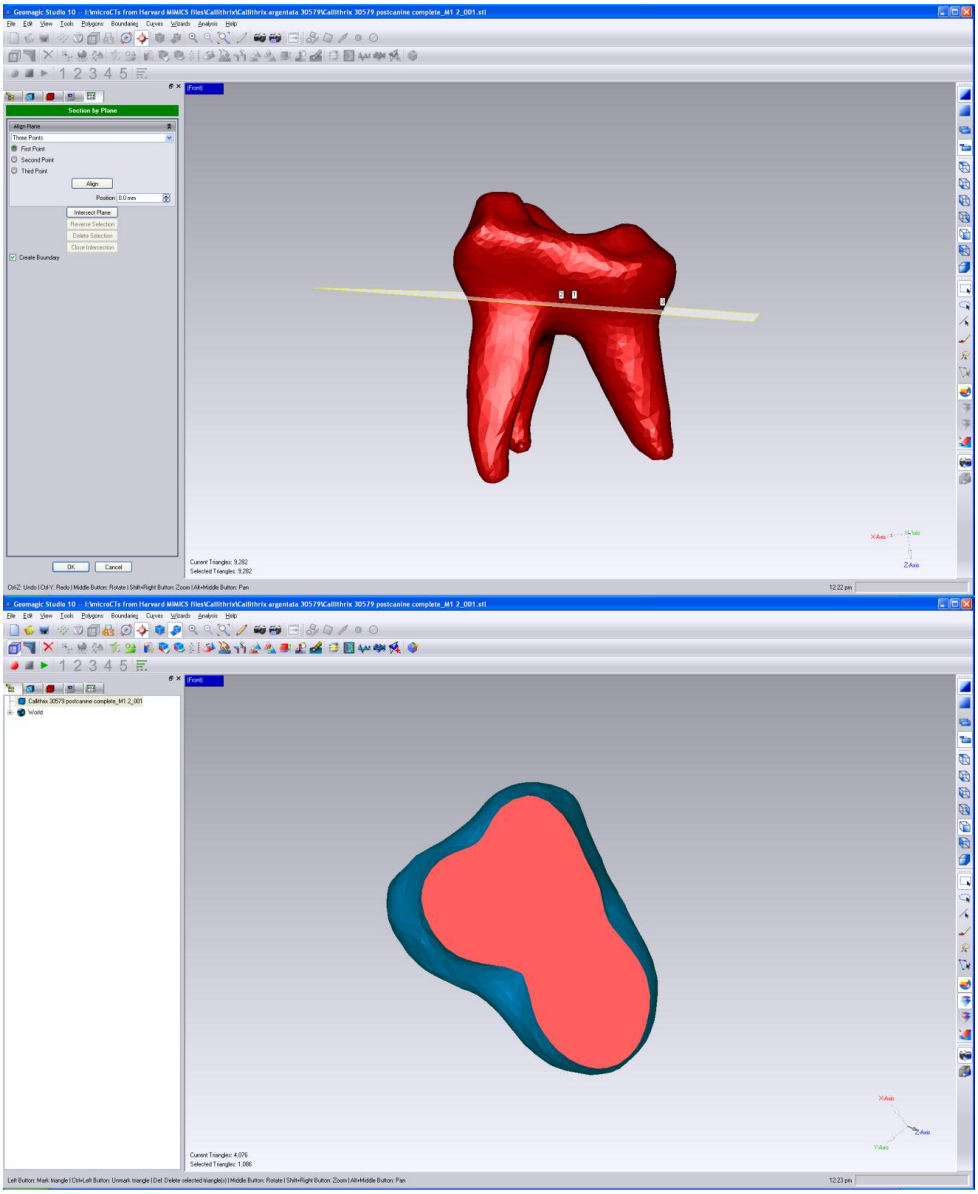

Fig. 3.6. Cervical margin surface area (CMSA) measurement. Plane being passed just inferior to the enamel-root junction, top. 2D cervical margin surface area, bottom.

BITE FORCE ESTIMATION

3D landmarks reflecting overall size and shape and masticatory parameters were collected for each specimen using a Microscribe G2X digitizer (Immersion Corp.) prior to scanning (See Figures 3.7, 3.8, and Table 3.3 for landmark descriptions). Landmarks used were based on those used in Spencer (1995) for capturing skull size and relative masticatory structure proportions. Skulls were placed on an elevated stand with the basicranium oriented superior to the neurocranium to facilitate landmark collection from every angle. Once all cranial landmarks were collected, the mandible of each cranium was carefully articulated so that the position of the cranium did not shift and landmarks at the centroids of masticatory muscle insertion sites were collected.

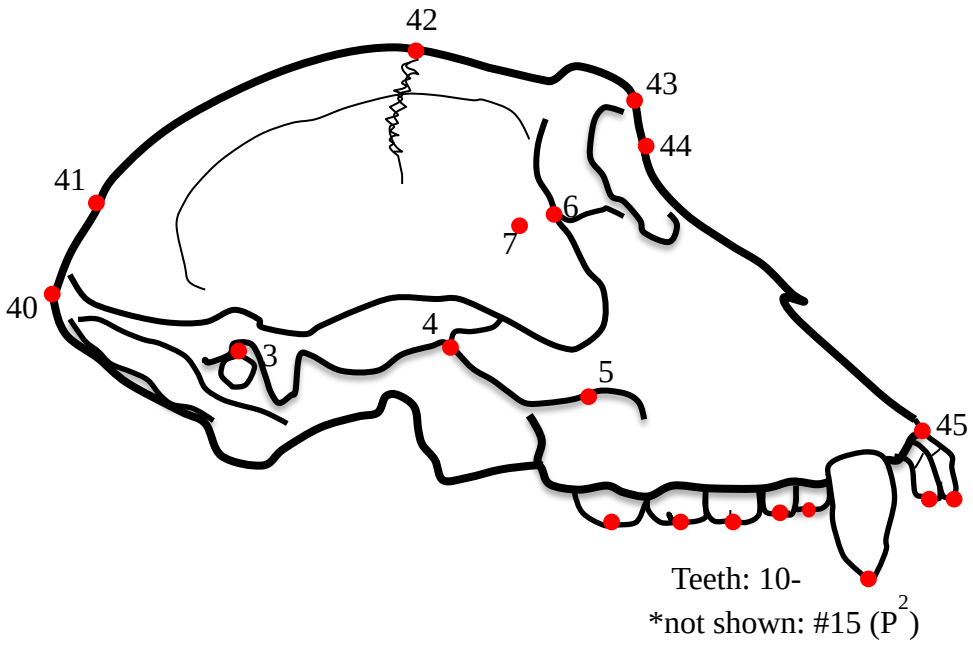

Fig. 3.7. Landmarks, lateral view. Note that skull pictured is a catarrhine and does not have P^2. Adapted after Spencer (1995).

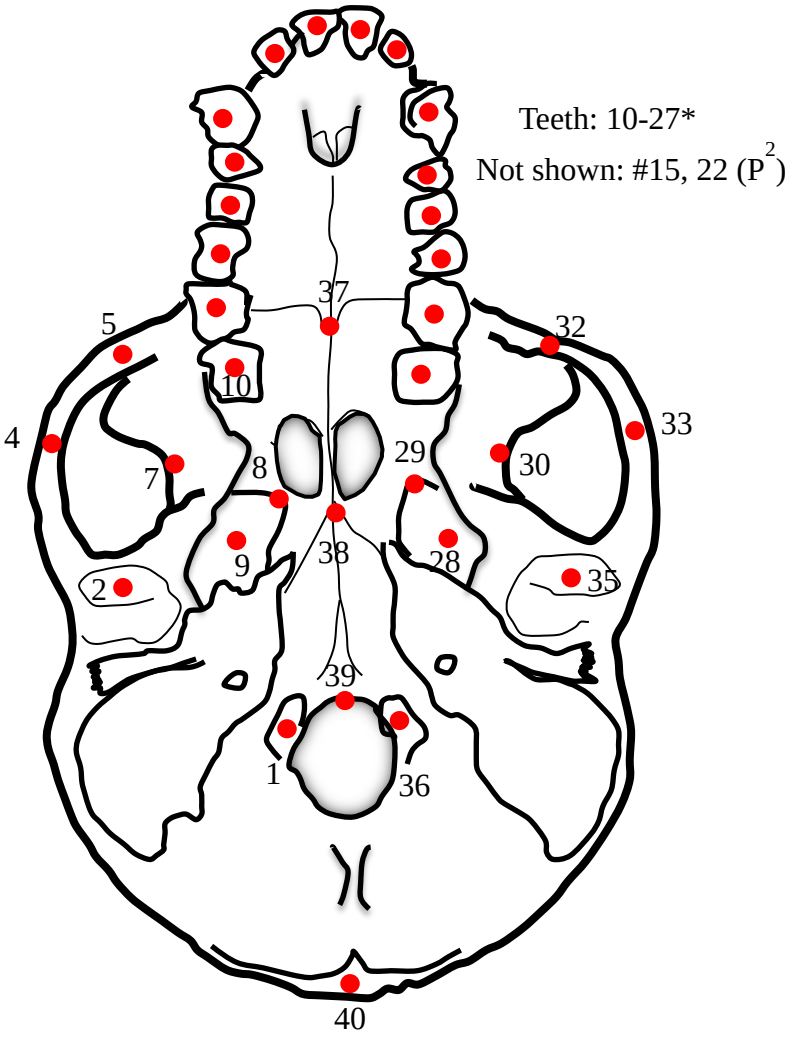

Fig. 3.8. Landmarks, inferior view. Note that the skull pictured is a catarrhine, and does not have P^2. Adapted after Spencer (1995).

TABLE 3.3. Digitized landmarks.

Landmark #	Description
1, 36	center of occipital condyles
2, 35	center of articular eminence
3, 34	porion
4, 33	inferior edge of zygomatic arch at the zygomaticotemporal suture
5, 32	inferior edge of zygomatic arch at the anteriormost point of origin of the superifical masseter
6, 31	intersection of temporal line and frontozygomatic suture
7, 30	most medial point in pterion region
8, 29	sphenopalatine suture at the intersection of the medial and lateral pterygoid plates
9, 28	center of medial surface of lateral pterygoid plate
10, 27	M^3
11, 26	M^2
12, 25	M^1
13, 24	P^4
14, 23	P^3
15, 22	P^{2a}
16, 21	C
17, 20	I^2
18, 19	I^1
37	intersection of intermaxillary and maxillopalatine sutures on ventral hard palate
38	most posterior midline point on vomer
39	most anterior midline point of foramen magnum
40	opisthocranion

[a]P^2 landmarks in Platyrrhines only *(cont)*

TABLE 3.3 (cont). Digitized landmarks.

Landmark #	Description
41	lambda
42	bregma
43	glabella
44	nasion
45	prosthion
46, 50	tip of coronoid process
47, 51	most anterior projection of ramus at the coronoid process
48, 52	centroid of insertion of superficial masseter on lateral ramus
49, 53	centroid of insertion of medial pterigoid on medial angle of mandible

Landmarks were chosen such that accurate measurement of masticatory parameters could be obtained and used to calculate bite force curves along the tooth row (discussed in detail below) for each individual in the sample. All calculations in the current study are based on Spencer's (1995) analysis of Greaves' (1978) model. After taking 3D landmarks, point clouds for each specimen were imported into MacMorph (Spencer and Spencer, 1993) software program for visualization and measurement.

Additionally, landmarks that captured overall size of the skull were collected so that variables could be size-corrected using a geometric mean of skull size prior to analysis. To calculate the geometric mean, six measurements were taken: cranial breadth, cranial height, and cranial length, in addition to facial breadth, facial height, and facial length. See Table 3.4 for details.

TABLE 3.4. MacMorph geometric mean measurements.

Variable	Measurement Type	Landmarks
Cranial breadth	distance	3, 34
Cranial height	distance	39, 42
Cranial length	distance	40, 43
Facial breadth	distance	4, 33
Facial height	distance	37, 43
Facial length	distance	37, 45

Masticatory system measurement

To estimate bite force curves along the tooth row, it was first necessary to collect measurements of basic masticatory system variables (Table 3.5). 3D landmark coordinates for each specimen were uploaded into MacMorph software and the appropriate measurements were collected. All measurements were defined and projected onto a specific plane (i.e., occlusal or sagittal) to facilitate the use of current models of feeding mechanics. Bicondylar breadth (BB) is the distance between articular eminence landmarks (2) and (35) projected onto occlusal plane. Palate breadth (PB) is the distance between M1 landmarks (12) and (25). Glenoid height (GH) is the distance of the articular eminence landmark (2) to the occlusal plane (landmarks 10, 13, and 24). The normal bite force moment arm length (the distance from the TMJ to the bite point in the sagittal plane) (b_N) and the horizontal distance from the TMJ to each bite point on the occlusal plane (b_H) were also measured, in addition to the lengths of the moment arms of the masticatory adductors (Table 3.5).

TABLE 3.5. MacMorph masticatory measurements

Measurement	Measurement type	Plane	Plane points	Landmarks
Bicondylar breadth	Projected line to plane	Occlusal	10 (27)[a], 13, 24	2, 35
Palate breadth	Projected line to plane	Occlusal	10 (27), 13, 24	12, 25
Glenoid height	Point to plane	Occlusal	10 (27), 13, 24	2 (35)
b_H	Projected line to plane	Occlusal	10 (27), 13, 24	2 to: 10, 11, 12, 13, 14, 15, 16, 17 , 18
b_N	Projected line to plane	Sagittal	40 (41), 42 (39), 44 (43)	2 to: 10, 11, 12, 13, 14, 15, 16, 17 , 18
Masseter moment arm	Projected line to plane	Occlusal	10 (27), 13, 24	4, 56
Temporalis moment arm	Projected line to plane	Occlusal	10 (27), 13, 24	7, 55
Medial pterygoid moment arm	Projected line to plane	Occlusal	10 (27), 13, 24	9, 57
Masseter moment arm	Projected line to plane	Sagittal	40 (41), 42 (39), 44 (43)	4, 56
Temporalis moment arm	Projected line to plane	Sagittal	40 (41), 42 (39), 44 (43)	7, 55
Medial pterygoid moment arm	Projected line to plane	Sagittal	40 (41), 42 (39), 44 (43)	9, 57

[a]Numbers in parentheses indicate alternate landmarks used to delineate a plane in the event that some landmarks are missing in a specimen.

Review of lever model and bite force calculation

Recall from Chapter 2 that the basic equation for bite force estimation is:

$$Bb + Jj + Mm = 0 \tag{1}$$

where B, J, and M are the bite force, joint reaction force, and muscles force respectively, and b, j, and m are their respective moment arms. By modeling the fulcrum at the TMJ (Figure 3.9), the joint reaction force moment arm becomes zero and the equation can be rewritten:

$$Bb - Mm = 0 \tag{4}$$

or

$$B = \frac{M * m}{b} \tag{5}$$

Furthermore, since the simple lever model only assesses forces that are normal (perpendicular) to the reference line, the equation can be further modified to express this assumption:

$$B_N = \frac{M_N * m_N}{b_N} \tag{6}$$

In this simple model, knowing the length of the muscle and bite force moment arms along with the magnitude of muscle force allows bite forces to be calculated for any bite point.

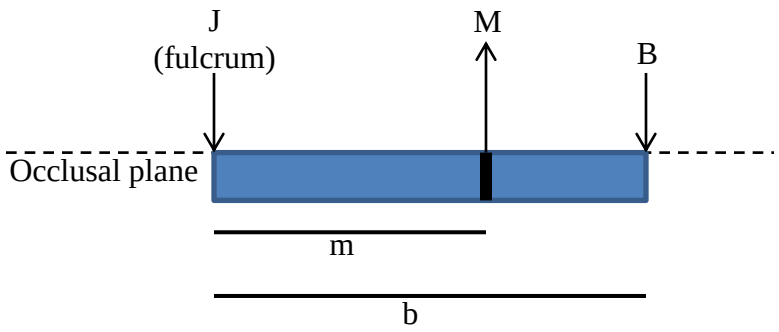

Fig. 3.9. Simple lever model review. J = joint reaction force, M = muscle resultant force, B = bite force, m = muscle resultant moment arm, b = bite force moment arm.

However this simple equation (6) does not accurately reflect all of the components that contribute to bite force. Information about muscle resultant inclination, TMJ height above the occlusal plane, and constraints that protect the lower jaw from dislocation must also be considered (Spencer, 1995, 1999). Determination and measurement of muscle force magnitude and inclination, muscle resultant moment arm length, and bite force moment arm length for this study are discussed in detail below.

Muscle resultant magnitude (M_N) and inclination

The most important factor in determining the maximum amount of force a muscle can produce, its physiological cross-sectional area (PCSA), has no known correlate in skeletal architecture. Therefore, in the current study, muscle resultant force, *M*, is set at a constant, maximum magnitude (until bite points in Region II, in which b-s muscle force decreases, discussed below). Setting *M* as a constant for all individuals precludes the estimation of absolute bite forces for each

specimen. However, the current study focuses on changes in the bite force magnitude along the tooth row within an individual, and does not compare bite force magnitudes among species. Thus, setting *M* as a constant does not impede our ability to examine predicted force patterns along the tooth row.

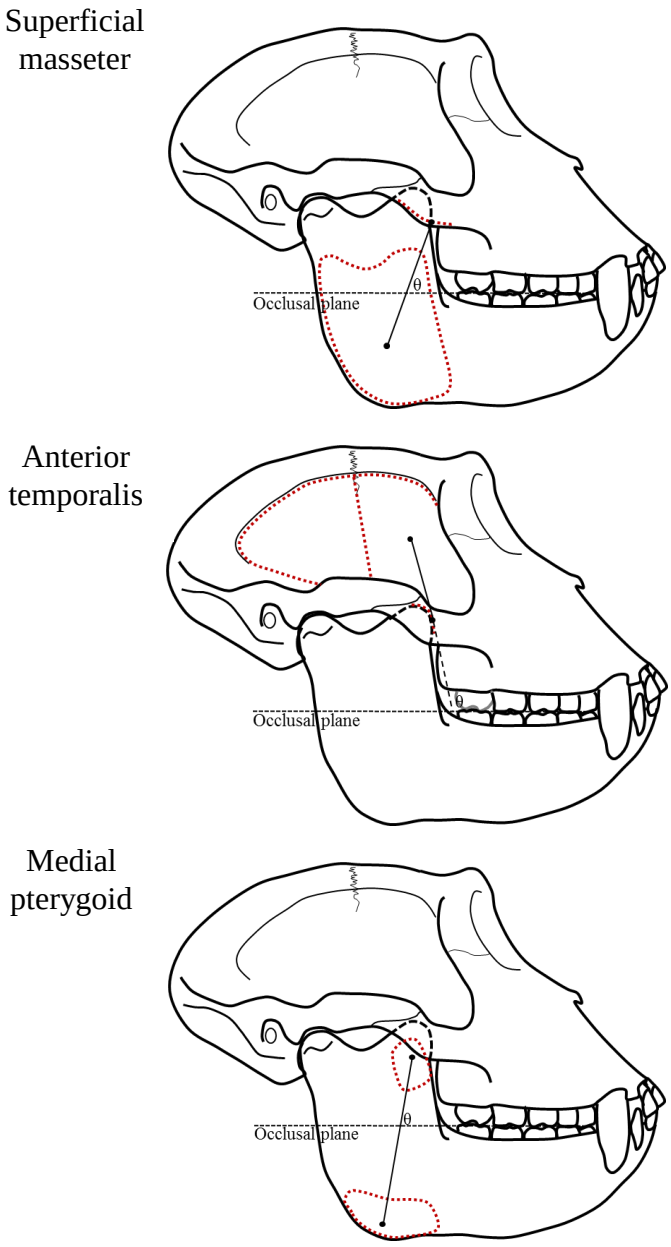

Fig. 3.10**.** Measurement of muscle resultant orientation. The red dotted lines indicate the muscle attachment areas for the masticatory adductors (top, superficial masseter; middle, anterior temporalis; bottom, medial pterygoid). Black circles indicate the estimated centroid of muscle attachment and insertion. A black line drawn between the two centroid points estimates muscle resultant force vector orientation. Additionally, the angle of each muscle resultant vector at the occlusal plane, Θ, was quantified. (Modified after Spencer, 1995).

To find the angle of the muscle resultant inclination at the occlusal plane (θ), first the angles of the anterior temporalis, superficial masseter, and medial pterygoid were measured (Figure 3.10). Muscle moment arm length was estimated in MacMorph by measuring the distance between the landmarks at the centroids of each muscle origin and insertion (see Table 3.3 for details). Muscle length was measured in both the sagittal and occlusal panes, creating a right triangle where muscle length in the sagittal plane ($M_{sagittal}$) is the hypotenuse and muscle length in the occlusal plane ($M_{occlusal}$) is the base (Figure 3.11).

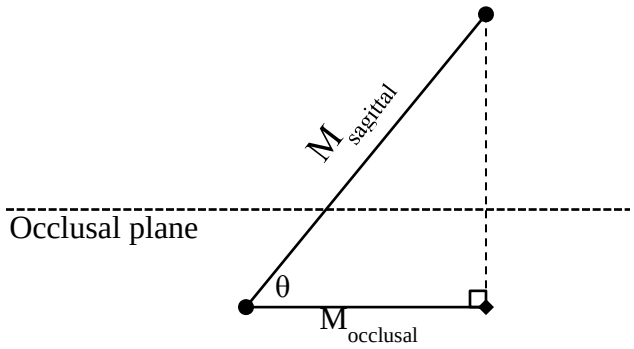

Fig. 3.11. Muscle resultant angle calculation. See text for details.

The angle at the occlusal plane can be found using a simple trigonometric formula:

$$\theta = \cos^{-1}\left(\frac{\overline{M_{occlusal}}}{\overline{M_{sagittal}}}\right) \quad (7)$$

The temporalis muscle is oriented differently than the superficial masseter and medial pterygoid muscles (Figure 3.10, middle). Instead of inclining anteriorly, the temporalis inclines more posteriorly due to the large portion of the muscle that extends posterior to its insertion on the mandible. To correctly calculate temporalis angle, the angle calculated in equation (7) must be subtracted from 180^{o}. To simplify calculations, the muscle angle at the occlusal plane was averaged to produced the angle of the masticatory muscle resultant at the occlusal plane, θ. While such simplifying assumptions are common in biomechanical analyses, it is important to emphasize that the extent to which each masticatory adductor contributes to total bite forces is not equal, so this estimate of muscle resultant angle includes some error.

Bite force moment arm (b_N)

Although Greaves (1978) modeled joint reaction force in line with the bite point (on the occlusal plane), in primates the TMJ is situated above the occlusal plane (discussed in Chapter 2). Consequently, the reference line changes for each bite point (Figure 2.5). In primates, with an anterosuperiorlly-oriented masticatory muscle resultant vector, the bite force moment arm (b_N) does not equal the horizontal distance from the TMJ to the bite point (b_H) (Figure 3.12),

because raising the TMJ makes b_N into the hypotenuse of a right triangle with one side measuring b_H and the other side measuring the height of the TMJ above the occlusal plane (glenoid height, GH). Thus,

$$b_N = \sqrt{b_H{}^2 + GH^2} \tag{8}$$

Glenoid height, b_H and b_N were measured in MacMorph based on landmark coordinates.

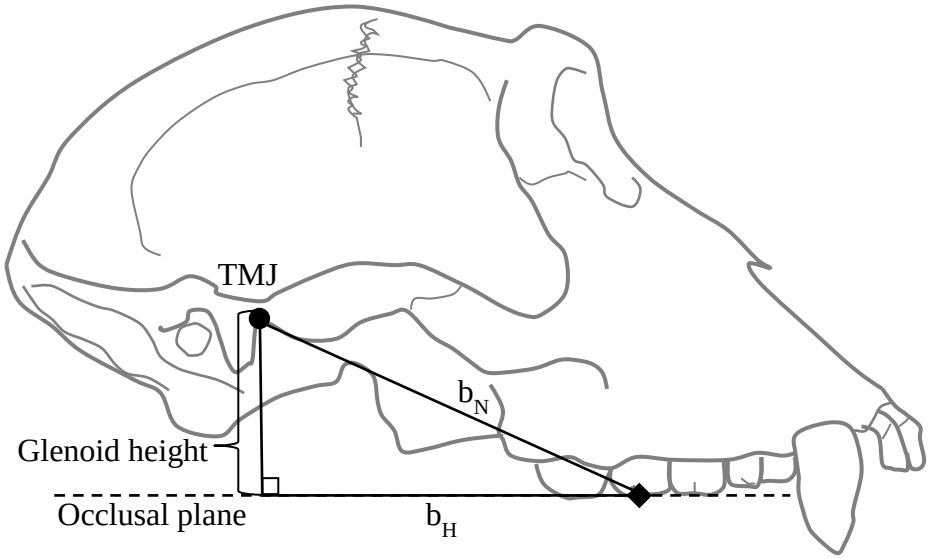

Fig. 3.12**.** Effect of raising the TMJ on b_N. See text for explanation.

Muscle resultant moment arm (m_N)

Greaves'(1978) model operates on the assumption that the muscle resultant is located directly posterior to the distal-most molars; however, measurements of muscle vectors (measured as lines connecting the centroids of the attachment and insertion sites for each muscle) suggest that the muscle resultant is actually more posteriorly located than indicated in Greaves' model (Spencer, 1995, 1999; Perry et al., 2011). Spencer (1995, 1999) suggests that although the muscle resultant is likely positioned more posteriorly than assumed by Greaves' model, the system *behaves* as though it is located more anteriorly due to the presence of a buffer zone around the triangle of support (discussed in Chapter 2).

Despite the fact that the muscle resultant is likely much more posterior than Greaves assumed, Spencer (1995, 1999) found that molar teeth across anthropoids are always located within Region II as calculated by Greaves. This supports the hypothesis that the triangle of support includes a buffer zone, and explains why the predictions of Greaves' (1978) model are supported by current studies, despite the discovery that the actual position of the muscle resultant differs from what was originally assumed. For this reason, rather than calculate estimated muscle resultant positions from muscular attachment and insertion landmarks, the a-p position of the muscle resultant for each individual was calculated as the horizontal distance from the TMJ to M3 in the occlusal plane (b_H *M3*).

As discussed previously, raising the TMJ above the occlusal plane changes the reference line at each bite point, which in turn changes the magnitude of b_N, normal bite force moment arm. Similarly, raising the TMJ also affects the muscle force resultant moment arm m_N. When the TMJ is raised, m_N no longer equals the horizontal distance from the TMJ to the muscle force vector in the occlusal plane, m_H. Additionally, if the muscle force vector is inclined, as in most primates, the reference line will change such that m_N will have a different value for every bite point along the tooth row (Figure 3.13).

Glenoid height, b_N, and b_H were measured in MacMorph, and θ was calculated in a previous section. Given these parameters (see Figure 3.14), it is possible to calculate m_N with the following equation

$$m_N = b_N - x \tag{9}$$

To calculate *x*, it is first necessary to find the value of *q*, which is the difference between m_H and b_H, and the angle β. To find β, it is first necessary to calculate α. The angle α is determined by the equation

$$\alpha = \sin^{-1}\left(\frac{GH}{b_N}\right) \tag{10}$$

The angle β is simply 180° - (α + θ). Now that *q* and β are known, it is possible to calculate *x* using the following equation

$$x = \sin\Theta \left(\frac{q}{\sin\beta}\right) \tag{11}$$

Calculating the muscle resultant moment arm highlights the effects of variation in glenoid (TMJ) height and muscle resultant inclination on calculations of bite force for any given bite point.

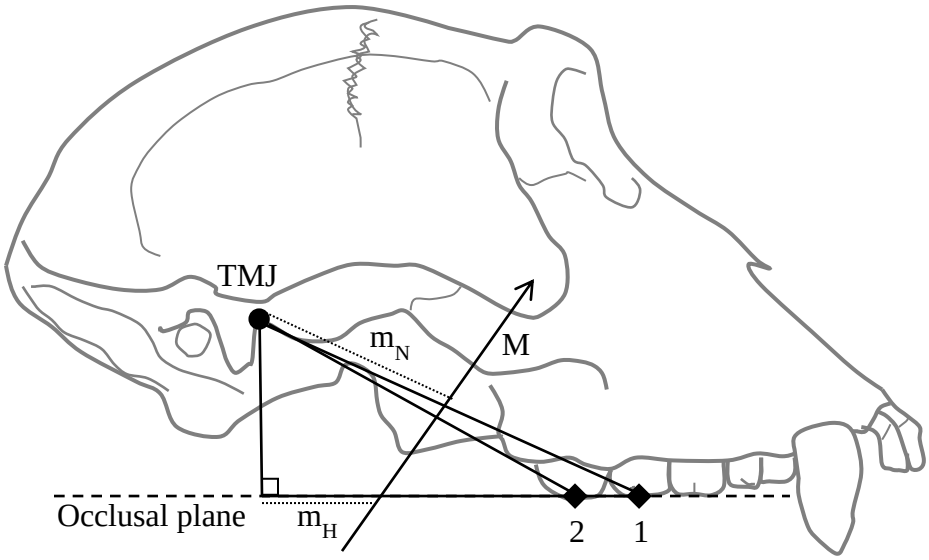

Fig. 3.13. Effect of raising the TMJ on m_N. Note that the reference line changes for bite points 1 and 2.

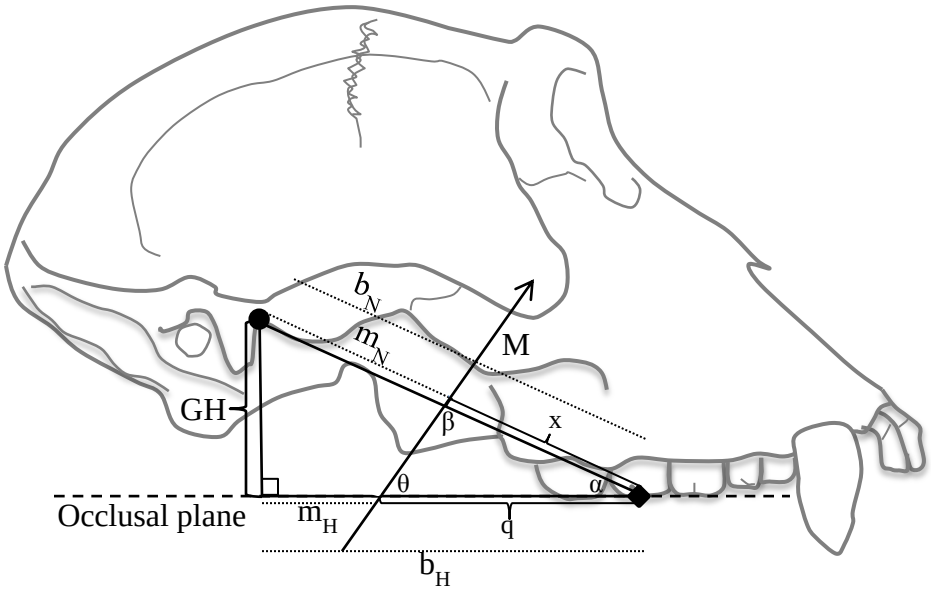

Fig. 3.14. Calculation of m_N. See text for details.

Calculating lateral muscle resultant movement in Region II

One major assumption of all lever models of feeding mechanics is that muscle force magnitude is always maximized. For bite points in Region I, this means that the muscle resultant falls on the midline, since both w-s and b-s muscles are firing equally. According to Greaves (1978), however, both sides only fire maximally in Region I; in Region II, the muscle resultant must move laterally to be accommodated within the triangle of support, which is accomplished by reducing muscle force on the balancing side.

To calculate bite forces along the tooth row, the lateral movement of the muscle resultant in Region II must also be calculated (Figure 3.15). To do this, it is necessary to know the distance between the w-s and b-s joint reaction forces

(bicondylar breadth, BB), the muscle resultant moment arm length in the sagittal plane (m_G), the angle of the b-s corner of the triangle of support (Σ), and the distance between the b-s and w-s muscle resultants (here, modeled as bicondylar breadth, BB). The distance the muscle resultant shifts towards the w-s in Region II is:

$$\overline{ML_M} = \left(\frac{m_G}{\tan \sum}\right) - \left(\frac{BB}{2}\right) \quad (12)$$

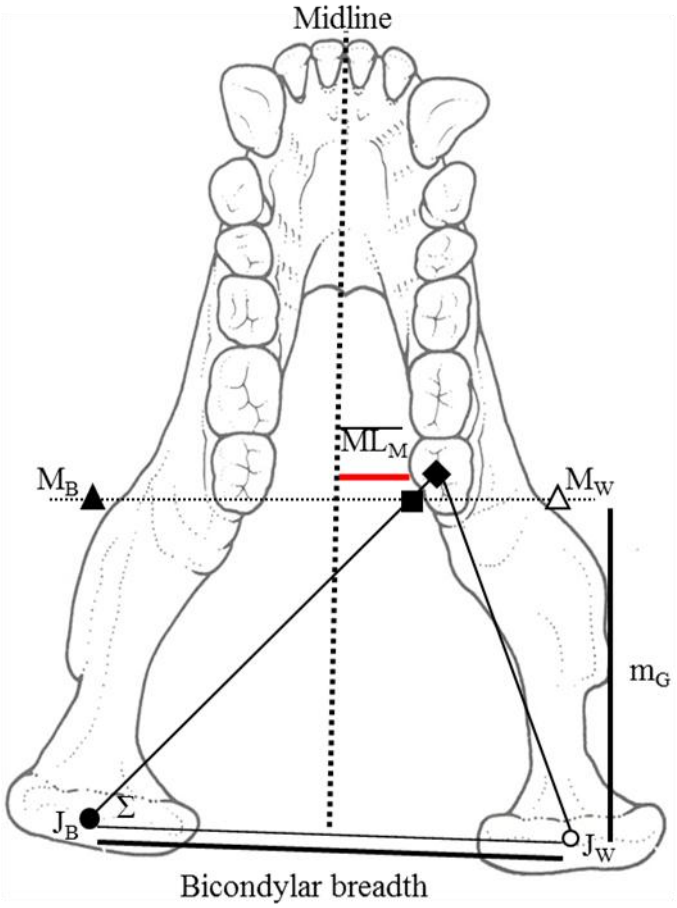

Fig. 3.15. Calculating muscle resultant shifts in Region II. J_B and J_W are the b-s and w-s joint reaction forces, respectively. M_B and M_W are the b-s and w-s muscle resultants (here, modeled as the same distance as bicondylar breadth, BB). Mandible illustration from Aiello and Dean (1992). Figure adapted from Spencer (1995).

The normal muscle resultant moment arm, m_N, calculated above, can help determine the muscle resultant moment arm in the sagittal plane, m_G (Figure 3.16) where

$$m_G = \sin\pi * m_N \tag{13}$$

The angle π is easily calculated since angle α is already known (discussed above).

Recall that the lateral shift in the muscle resultant is achieved by reducing the working side muscle force, resulting in a reduction of total muscle force (M_T). To calculate (M_T) we can apply a simple beam model, like that discussed in Chapter 2, such that the balancing side muscle force (which is unknown) is modeled at the fulcrum. Therefore,

$$M_W * BB = M_T * \left(\left(\frac{BB}{2}\right) + \overline{ML_M}\right) \tag{14}$$

which can be rewritten as

$$M_T = \frac{(M_W * BB)}{\left(\left(\frac{BB}{2}\right) + \overline{ML_M}\right)} \tag{15}$$

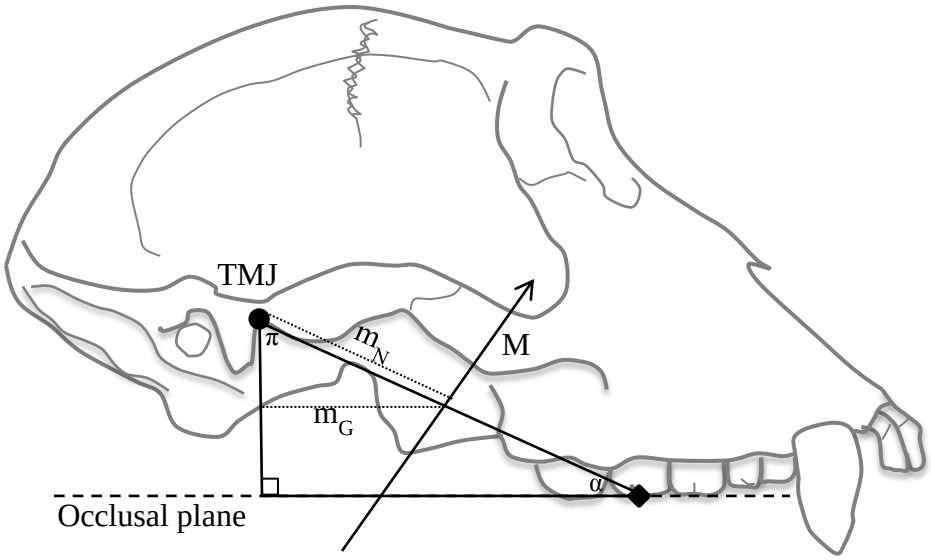

Fig. 3.16. Calculation of m_G. See text for details.

Summary of Calculations

Figure 3.17 shows the measurements, and Table 3.6 summarizes the equations used to calculate bite forces along the tooth row in the current study. As previously stated, all calculations in the current study are based on Spencer's (1995) lever model. Bite force curves were calculated for each individual in the study. Measurements of tooth root and crown surface area along the tooth row were compared with calculated bite force magnitudes to assess the hypothesis that dental variables covary with changes in bite force along the tooth row.

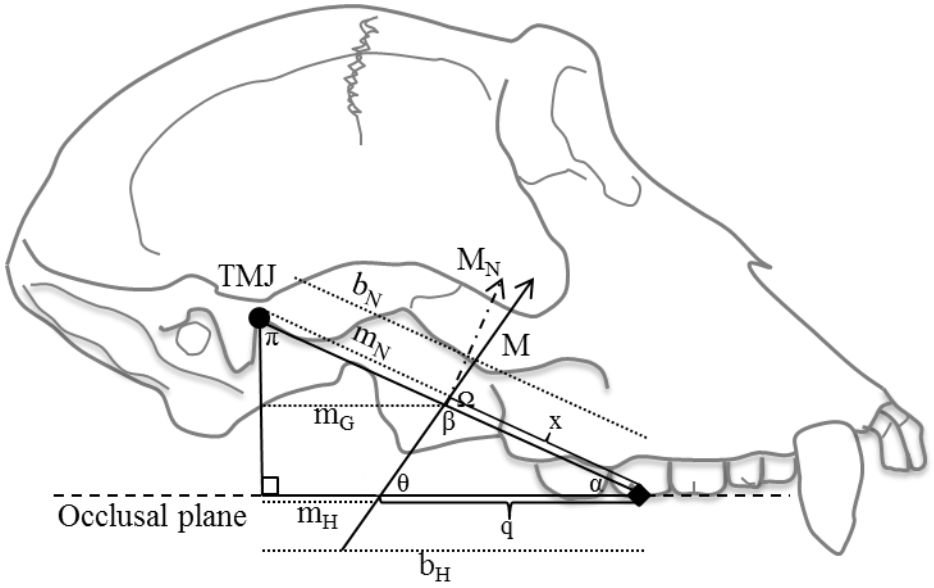

Fig. 3.17. Summary of measurements required for calculation of bite force.

TABLE 3.6. Equations required to calculate bite force.

	Basic Equation Variable	Required Components
Region I Equations	M_N	$M_N = M \sin \Omega$
		$\Omega = \Theta + \alpha$
		$\alpha = \sin^{-1}\left(\frac{GH}{b_N}\right)$
	m_N	$m_N = b_N - x$
		$x = \sin \Theta \left(\frac{q}{\sin \beta}\right)$
		$\beta = 180 - \Omega$
		$q = b_H - m_H$
Region II Equations	M_T	$M_T = \frac{(M_W * BB)}{\left(\left(\frac{BB}{2}\right) + \overline{ML_M}\right)}$
		$\overline{ML_M} = \left(\frac{m_G}{\tan \sum}\right) - \left(\frac{BB}{2}\right)$
		$\sum = \tan^{-1} \frac{b_H}{BB - \left(\frac{(BB - PB)}{2}\right)}$
	m_G	$m_G = \sin \pi * m_N$
		$\pi = 90 - \alpha$

ANALYTICAL METHODS

Size and scaling

The relationship between tooth size and body size has a long history of investigation in biological literature (Gould, 1975; Wood, 1979; Gingerich et al., 1985; Ungar, 1998; Yamashita, 1998; Vinyard and Hanna, 2005; Copes and Schwartz, 2010; and many more). However, repeated investigation suggests that, within Primates, teeth scale with body size variably among taxa (reviewed in Copes and Schwartz, 2010). Consequently, in the current study scaling relationships among variables were examined prior to statistical analyses designed for hypothesis testing. Rather than using body mass, which is typically not available for museum specimens like the ones used for this study, dental morphological features were examined in conjunction with skull size, which is calculated as a geometric mean of cranial vault and facial length, height, and breadth.

In scaling analyses, regression is used to determine whether or not the shape of a particular variable changes as overall size increases. The slope of the regression line indicates whether a variable increases (positive allometry), stays the same (isometry), or decreases (negative allometry) in relative size compared to overall size of an organism. Unless there is reason to believe that there is a shape change with size increase, isometry is the null hypothesis for scaling analyses. Isometry is geometric similarity; that is, a particular shape at any size has the same relative proportions (Schmidt-Nielsen, 1984). For example, a square

is isometric because its shape is the same at any size; all sides of a square are equal whether they are two or twenty millimeters. In the current study, root surface area (RSA) is examined along with the geometric mean of skull size (GMSkull). If RSA scales isometrically with GMSkull, it would indicate that the relative root size of a small primate and a large primate is the same. The slope of isometry will change depending on the dimension of the features being studied. For the current project, the slope of isometry is 2.0 because surface areas are compared to linear measurements.

There are two types of regression analyses that can be utilized in scaling analyses: Model I or Ordinary Least Squares (OLS) regression and Model II or Reduced Major Axis (RMA) regression. One central difference between OLS and RMA is their relationship with the correlation coefficient *r*. The slope of the OLS line is highly affected by *r*, because *r* is used in its calculation, whereas the slope of the RMA line is calculated independent of the correlation. This means that an RMA regression line has nothing to do with the presence or strength of a relationship (Ricker, 1984) and it is the same whether the data are highly correlated or not (Aiello, 1992). The only way to determine the presence of a relationship between data is to apply a test of significance, that is, the correlation coefficient *r*. Since they each have a different relationship with *r*, the OLS line and the RMA line can be very different for the same set of data; however, the higher the correlation coefficient, the closer the OLS line is to the RMA line (Aiello, 1992).

Another major difference between the OLS line and the RMA line is that OLS only minimizes the vertical difference between the data point and the line whereas RMA minimizes both the vertical and the horizontal distance between a data point and the line (Sokal and Rolf, 1981; Ricker, 1984; Aiello, 1992; Smith, 2009). OLS is therefore considered asymmetrical (Model I regression) since it assumes that all of the variability is located within one variable, whereas RMA recognizes variability in both variables, making it symmetrical (Model II regression) (Sokal and Rolf, 1981; Smith, 2009).

The issue of symmetry is important, because depending on the biological question being asked, one might expect variation to be partitioned symmetrically or asymmetrically. Smith (2009) states "If the biological question indicates that natural variation should be partitioned asymmetrically, use OLS; if symmetrically, the data should be modeled by RMA . . . ." (481). Put simply, in a symmetrical model (i.e. RMA), it does not matter which variable is plotted as x or y; they could be switched around with no effect on the outcome of the analysis. In an asymmetrical model (i.e. OLS), the x and y variables are fixed, and all of the variation is expected to be located within the y variable. The current study examines root and crown size versus skull size (which indicates an asymmetrical model) and also root versus crown size (which indicates a symmetrical model). Despite the fact OLS may have been preferred by some researchers for some analyses in the current study, RMA was used for each analysis because there is variation in all measurements examined, and because it is important to be able to compare results directly among analyses; furthermore, the correlation coefficients

(*r*) are very high for all relationships examined, indicating that the results of RMA and OLS analyses would be similar, if not the same, in this case (Aiello, 1992). Results from these analyses are discussed in Chapter 4.

The hypotheses tested in this study focus on the pattern of size change among different variables along the tooth row. Because the comparative sample for this study encompasses a broad body size range, even among some closely related species, it was necessary to size-adjust each variable prior to statistical analysis of pair-wise comparisons. There are several ways to mathematically adjust for size, but among the most common are the use of residuals from an OLS regression line and shape ratios (Jungers et al., 1995). Residuals are preferred by some researchers because they are completely size-free; that is, residuals are not correlated with x. Unfortunately, this means that residuals are also often shape-free, since some aspects of shape are correlated with size (Corrucini, 1987; Jungers et al., 1995).

In residual analysis, the regression line is assumed to represent functional equivalence, and residuals are evaluated using a criterion of subtraction (Pilbeam and Gould, 1974), meaning that residuals that fall above or below the line are interpreted as adaptations. However, the regression line may in fact represent an adaptive relationship; in other words, there is no reason to assume that a scaling relationship indicates functional equivalence (Corrucini, 1987; Jungers et al., 1995). Additionally, residuals are not intrinsically connected to living creatures; their distribution depends a great deal on the sample from which they are derived (Corrucini, 1987; Jungers et al., 1995).

Shape ratios, like residuals, are a measure of relative size; however, they differ from residuals in important ways. First, shape ratios are never completely size-free, because some aspects of shape are correlated with size. Second, shape ratios are made directly from variables of biological interest rather than calculated based on the scaling relationship within a specific sample. Shape ratios may give misleading or erroneous results when the relationship among variables is allometric; therefore it is important to use isometric variables when constructing shape ratios (Jungers et al., 1995). The current study uses shape ratios to size-adjust due to their direct relationship to pertinent biological variables and also because the variables under study were found to have an isometric relationship (discussed in Chapter 4). Each variable was divided by the geometric mean of skull size, and the resulting shape variables were used for subsequent comparative analyses.

Part 1: Dental relationships

Hypothesis 1a states that root and crown surface area should covary along the tooth row. Crown surface area as measured in the current study does not account for differences in occlusal form due to tooth wear. Consequently, cervical margin surface area (CMSA) was used as a proxy for crown surface area (CSA) for all analyses. To test Hypothesis 1a, the Kendall rank correlation coefficient (Kendall's tau [τ]) was used to determine the similarity of the order of ranked dental variables. In other words, the order of the smallest to largest tooth crown along the tooth row should match the order of smallest to largest tooth roots along the tooth row. The correlation coefficient indicates the magnitude and

direction of the correlation and can range from -1 (a perfect negative correlation, wherein one variable increases as the other decreases) to 1 (a perfect positive correlation, wherein both variables increase or decrease concurrently). Values near zero indicate that no relationship exists between the variables. Hypothesis 1a predicts that the correlation coefficient for root and crown size should be positive and close to 1.

Hypothesis 1b states that root surface area and crown size are functionally related, and primates with mechanically resistant diets will have relatively higher values for these characteristics than closely-related primates with soft diets. To test this hypothesis, closely-related primates of similar size but with diets of differing mechanical properties were examined in pair-wise comparisons (see Table 3.2 for the list of compared taxa). Primates were separated into dietary categories based on the mechanical properties of their diet (discussed in detail above). Primates whose diets are mechanically demanding (i.e., that are hard and/or tough, as discussed in Chapter 2) are in the "Resistant" category, while primates whose diets are not mechanically challenging are in the "Soft" food category. Nonparametric Mann-Whitney U-tests (for comparisons between two taxa) and Kruskall-Wallis tests (for comparisons between three or more taxa) were run to determine whether primates with a more resistant diet also had significantly larger tooth roots and crowns than those with soft diets as predicted by Hypothesis 1b.

Part II: Dental features and bite force patterns

Hypotheses 2 and 3 predict that bite force should covary with root size and crown size along the tooth row respectively. First, bite force curves were calculated for each specimen, as discussed above. Then, calculated bite forces were compared to measurements of root and crown size along the tooth row. As with Hypothesis 1a, Kendall's τ was used to assess the direction and magnitude of correlation among variables. Bite force magnitudes along the tooth row were ranked and compared with root (RSA) and crown size (CMSA) ranks. Hypotheses 2 and 3 predict that the correlation coefficients for bite force and dental variables be positive.

CHAPTER 4

SCALING RELATIONSHIPS AMONG DENTAL VARIABLES AND SKULL SIZE

Raw measurements of root surface area (RSA) and cervical margin surface area (CMSA) for platyrrhines and catarrhines are reported in Tables 4.1-4.4. Before testing Hypotheses 1-3, reduced major axis (RMA) regression (discussed in the previous chapter) was used to determine scaling relationships between root surface area and skull size, cervical margin surface area and skull size, and root and cervical margin surface area. Platyrrhines and catarrhines were examined separately from each other using species averages of measurements. Tables 4.5-4.8 report the log-transformed species averages for root size and cervical margin surface area for platyrrhines (Tables 4.5 [RSA] and 4.6 [CMSA]) and catarrhines (Tables 4.7 [RSA] and 4.8 [CMSA]).

TABLE 4.1. Root Surface Area (RSA) in mm^2: platyrrhines.

Species	Specimen	M3	M2	M1	P4	P3	P2
A. caraya	28095	166.34	234.53	187.53	136.43	125.20	97.63
A. caraya	28096		174.75	155.09	114.22	108.69	76.00
A. caraya	28654	176.88	265.92	227.70	157.94	140.02	109.02
A. caraya	28655	158.47	194.29	173.23	119.26	104.36	80.76
A. palliata	5323	108.39	159.72	138.01	107.61	110.12	94.69
A. palliata	5324	85.17	95.28	101.28	137.03	157.21	100.91
A. palliata	5325	83.16	102.24	104.95	131.60	157.22	99.76
A. palliata	5327	91.89	116.79	129.13	153.82	175.97	107.91
A. palliata	5328	88.80	105.47	123.24	162.09	183.68	106.30
A. palliata	5329	81.34	102.54	110.09	144.22	177.99	118.10
A. palliata	5331	105.06	117.00	120.88	115.11	190.56	151.12
A. palliata	6001	75.07	100.42	109.62	154.50	174.13	125.81
A. palliata	29609	111.97	125.25	131.52	179.89	206.83	135.71
A. palliata	29611	80.02	96.62	115.06	158.06	171.53	118.01
A. trivirgatus	8472	14.96	28.96	35.17	27.16	21.44	18.13
A. trivirgatus	19801	15.75	28.59	29.34	20.79	20.62	13.34
A. trivirgatus	19802	18.83	32.03	37.00	27.82	26.00	18.30
A. trivirgatus	19805	16.70	28.89	36.22	26.53	26.04	19.76
A. trivirgatus	27214	18.49	30.08	34.59	26.55	23.62	20.85
A. trivirgatus	30562	14.43	21.49	27.71	18.25	14.58	13.89
A. trivirgatus	39571	21.69	28.75	35.94	26.08	23.08	18.01
A. trivirgatus	52608	19.49	26.07	30.45	28.71	25.54	20.63
A. trivirgatus	B-8042	17.13	26.90	29.03	23.49	21.36	18.80
A. trivirgatus	B-8043	17.31	27.23	30.57	25.01	22.52	20.28
A. geoffroyi	5336		74.72	74.31	66.77	66.80	55.22
A. geoffroyi	5338	52.33	77.34	86.06	74.59	69.74	52.52
A. geoffroyi	5344	44.16	74.52	94.69	73.68	72.80	57.68
A. geoffroyi	5345	48.58	82.41	98.49	82.14	72.59	62.23
A. geoffroyi	5346	35.02	65.11	94.68	67.01	61.22	47.71
A. geoffroyi	5348	48.16	79.32	93.98	73.24	72.20	58.82
A. geoffroyi	5349	38.16	62.33	76.39	55.50	57.30	45.42
A. geoffroyi	5350	44.45	68.50	87.68	69.77	67.61	55.59
A. geoffroyi	5351	56.34	80.18	89.79	80.50	76.30	57.22
A. geoffroyi	5352	36.70	77.17	92.33	73.07	69.72	

(cont)

TABLE 4.1 (cont). Root Surface Area (RSA) in mm^2: platyrrhines.

Species	Specimen	M3	M2	M1	P4	P3	P2
A. geoffroyi	5353	46.89	81.71	84.58	67.10	61.66	48.54
A. geoffroyi	5354	37.39	66.60	74.33	60.66	62.25	52.85
A. geoffroyi	5355	59.53	93.93	111.02	93.18	80.59	62.61
A. geoffroyi	10138	40.75	75.42	101.51	77.33	81.84	66.05
A. geoffroyi	29626	36.66	73.18	89.36	71.11	63.94	50.96
A. geoffroyi	29628	26.10	55.09	73.06	58.39	58.31	40.72
A. geoffroyi	34322	41.06	66.22	73.45	65.57	66.52	54.49
C. moloch	20186	21.70	35.15	38.22	30.51	25.87	19.85
C. moloch	26922	31.63	52.43	57.96	42.08	34.72	27.54
C. moloch	30559	19.36	44.32	55.21	36.85	35.79	29.39
C. moloch	30566	18.82	34.91	37.01	32.30	28.64	21.88
C. moloch	32380	20.38	37.93	46.94	37.57	27.31	21.14
C. moloch	32383	21.86	34.71	41.72	32.11	27.56	23.71
C. moloch	37828	24.69	44.88	53.32	32.22	32.99	27.28
C. moloch	39073	20.53	36.61	44.07	34.52	28.54	24.96
C. moloch	39563	23.67	41.09	46.66	30.38	27.54	23.29
Callithrix sp.	30579	--	11.35	16.30	12.82	11.44	11.51
Callithrix sp.	30580	--	13.63	16.21	14.56	13.95	13.74
Callithrix sp.	30582	--	13.63	16.21	14.56	13.95	13.74
Callithrix sp.	32164	--	12.03	17.29	16.49	13.75	16.04
Callithrix sp.	32165	--	13.85	16.56	14.77	11.99	14.42
Callithrix sp.	34573	--	10.41	17.53	16.51	14.27	13.18
Callithrix sp.	30577	--	13.46	15.48	15.04	11.18	12.21
Callithrix sp.	30586	--	12.59	14.52	14.20	10.10	9.75
Callithrix sp.	30603	--	12.61	16.41	14.27	12.28	13.58
Callithrix sp.	37826	--	10.52	14.34	12.93	10.84	10.79
Callithrix sp.	440	--	16.43	22.88	18.74	18.16	16.69
Callithrix sp.	37823	--	15.60	21.28	15.73	14.41	12.64
Callithrix sp.	7165	--	13.89	19.99	14.51	13.74	14.29
C. apella	25811	42.73	90.32	109.76	106.48	111.42	111.41
C. apella	27097	27.21	53.36	92.66	80.27	84.64	82.94
C. apella	30724		53.50	76.82	83.46	87.10	91.33
C. apella	30726	25.31	55.45	71.46	70.31	73.17	75.59
C. apella	31062	30.26	59.58	85.63	80.71	83.34	79.20

(cont)

TABLE 4.1 (cont). Root Surface Area (RSA) in mm^2: platyrrhines.

Species	Specimen	M3	M2	M1	P4	P3	P2
C. apella	31064	25.16	60.02	82.75	85.85	90.73	83.06
C. apella	31066	26.94	47.03	68.10	74.23	78.03	82.05
C. apella	31072	22.79	55.55	68.04	80.31	80.75	78.70
C. apella	32049	24.77	52.79	79.25	82.97	90.79	85.30
C. apella	37831	30.45	59.93	78.51	87.82	86.15	97.53
C. apella	41090	22.14	51.81	91.12	79.54	85.73	94.18
C. apella	49635	33.02	67.78	84.96	96.84	104.87	107.25
C. apella	314062	30.00	58.77	85.54	79.49	83.35	79.34
C. capucinus	5332	44.83	58.78	71.55	70.17	76.60	78.09
C. capucinus	7317	39.96	58.19	75.35	75.78	75.97	75.71
C. capucinus	7322	35.48	54.30	65.95	66.25	69.85	61.54
C. capucinus	7323	36.98	59.99	68.09	62.66	68.92	68.41
C. capucinus	10135	35.24	52.49	61.05	63.75	65.46	56.94
C. capucinus	10136	34.22	50.27	52.93	60.78	61.54	57.93
C. capucinus	34323	34.44	53.58	54.20	60.42	63.34	62.77
C. capucinus	34326	61.63	45.45	55.63	58.43	60.64	55.52
C. capucinus	34353	44.75	64.57	77.94	73.61	76.04	68.81
Pithecia sp.	20266	28.79	38.11	43.83	40.04	46.33	34.60
Pithecia sp.	27124	28.41	35.17	45.08	40.43	42.22	30.38
Pithecia sp.	30720	23.03	29.80	31.24	33.02	35.35	27.79
Pithecia sp.	30718	27.30	36.14	37.34	32.42	33.10	31.08
Pithecia sp.	30719	36.05	46.94	54.60	47.10	45.54	41.50
Pithecia sp.	31061	26.32	37.82	45.38	40.41	42.17	38.88
Saguinus sp.	15324	--	13.81	22.32	22.08	20.13	19.93
Saguinus sp.	27331	--	10.39	15.84	14.67	14.39	15.07
Saguinus sp.	30597	--	11.99	20.71	19.64	18.39	20.91
Saguinus sp.	30601	--	11.63	19.09	21.97	21.15	20.52
Saguinus sp.	41567	--	12.15	21.73	17.78	17.10	16.41
Saguinus sp.	41568	--	14.98	20.83	18.01	18.46	17.50
Saguinus sp.	52557	--	7.78	17.19	16.41	16.84	15.90
Saguinus sp.	52615	--	11.75	19.62	17.91	16.25	15.12
Saguinus sp.	52616	--	15.97	24.65	20.03	20.45	18.66
Saguinus sp.	52658	--	14.22	20.50	18.20	16.46	15.66

(cont)

TABLE 4.1 (cont). Root Surface Area (RSA) in mm^2: platyrrhines.

Species	Specimen	M3	M2	M1	P4	P3	P2
Saimiri sp.	10131	11.74	20.15	25.95	26.02	29.49	33.80
Saimiri sp.	10134	11.27	23.19	26.12	27.34	28.05	34.76
Saimiri sp.	29488	13.36	23.56	29.31	27.79	31.39	35.36
Saimiri sp.	20187	16.38	25.10	33.19	27.00	29.30	33.86
Saimiri sp.	30568	11.25	18.99	26.90	23.60	22.24	21.54
Saimiri sp.	30569	13.74	24.43	32.68	26.26	28.60	34.25

TABLE 4.2. Cervical Margin Surface Area (CMSA) in mm^2: platyrrhines.

Species	Specimen	M3	M2	M1	P4	P3	P2
A. caraya	28095	28.16	37.76	31.98	17.53	15.55	13.38
A. caraya	28096	21.37	28.45	25.90	14.13	13.48	10.21
A. caraya	28654	31.39	42.67	35.97	19.79	18.03	16.74
A. caraya	28655	26.12	33.51	30.19	14.88	13.73	10.63
A. palliata	5323	22.42	34.51	32.08	17.66	16.86	15.76
A. palliata	5324	14.11	14.92	16.41	29.51	32.91	20.56
A. palliata	5325	14.31	16.63	17.31	28.60	32.84	22.52
A. palliata	5327	14.08	17.83	19.14	31.43	32.26	21.63
A. palliata	5328	14.11	17.84	17.81	30.24	34.63	20.88
A. palliata	5329	11.53	14.07	16.43	28.52	33.51	23.26
A. palliata	5331	14.29	18.25	18.81	28.78	34.47	24.82
A. palliata	6001	13.26	15.35	17.90	31.15	37.99	23.58
A. palliata	29609	15.80	17.25	19.58	31.46	33.77	24.53
A. palliata	29611	14.46	15.43	19.64	32.25	33.03	24.83
A. trivirgatus	8472	2.20	4.55	5.29	3.20	2.71	2.54
A. trivirgatus	19801	2.67	4.45	5.89	3.53	3.52	2.68
A. trivirgatus	19802	2.91	5.45	6.70	3.80	3.27	3.16
A. trivirgatus	19805	2.87	5.35	7.02	3.31	3.14	2.80
A. trivirgatus	27214	3.31	5.83	6.83	4.27	3.71	3.83
A. trivirgatus	30562	2.71	4.24	5.31	2.87	2.38	2.43
A. trivirgatus	39571	4.15	5.95	6.82	3.92	3.70	3.46
A. trivirgatus	52608	3.12	5.23	6.11	3.32	3.06	2.44
A. trivirgatus	B-8042	3.15	5.21	5.31	3.78	3.00	2.83
A. trivirgatus	B-8043	2.55	4.89	4.91	3.55	3.08	2.89
A. geoffroyi	5336		13.27	13.26	9.23	8.91	8.22
A. geoffroyi	5338	6.84	11.20	12.51	8.36	7.95	6.90
A. geoffroyi	5344	8.08	11.53	12.65	8.64	8.02	7.71
A. geoffroyi	5345	7.52	11.42	13.30	8.40	7.33	6.33
A. geoffroyi	5346	8.90	13.50	16.35	10.63	9.97	8.81
A. geoffroyi	5348	10.36	13.26	14.28	9.35	8.89	6.69
A. geoffroyi	5349	8.74	11.34	12.55	7.84	6.96	6.14
A. geoffroyi	5350	8.79	11.47	12.12	8.34	7.83	6.99
A. geoffroyi	5351	7.88	11.04	11.38	8.10	7.98	7.66
A. geoffroyi	5352	8.27	11.73	13.67	8.08	7.65	

(cont)

TABLE 4.2 (cont Cervical Margin Surface Area (CMSA) in mm^2: platyrrhines.

Species	Specimen	M3	M2	M1	P4	P3	P2
A. geoffroyi	5353	8.17	12.46	12.36	7.18	6.58	5.72
A. geoffroyi	5354	5.90	10.63	12.04	7.82	7.52	6.45
A. geoffroyi	5355	7.69	13.46	14.09	9.62	7.95	7.11
A. geoffroyi	10138	8.32	11.32	14.98	9.47	10.32	9.27
A. geoffroyi	29626	7.58	13.00	13.91	10.13	9.30	5.79
A. geoffroyi	29628	7.14	13.77	16.57	10.64	9.12	5.61
A. geoffroyi	34322	6.77	12.17	11.58	8.59	7.88	7.32
C. moloch	20186	3.45	5.47	6.72	3.67	3.17	2.65
C. moloch	26922	3.91	7.49	8.21	5.00	3.90	2.99
C. moloch	30559	2.89	7.72	9.44	4.26	3.75	3.19
C. moloch	30566	3.36	5.99	7.57	3.98	3.66	2.92
C. moloch	32380	3.54	7.10	8.08	4.81	4.06	3.15
C. moloch	32383	3.92	5.49	7.44	3.84	3.52	2.73
C. moloch	37828	3.12	6.01	7.70	3.83	3.34	2.79
C. moloch	39073	3.06	6.57	7.52	4.16	3.37	3.06
C. moloch	39563	3.42	6.73	8.22	4.42	3.86	2.99
Callithrix sp.	30579	--	1.67	2.98	1.91	1.42	1.34
Callithrix sp.	30580	--	2.14	2.96	2.08	1.81	1.81
Callithrix sp.	30582	--	2.14	2.96	2.08	1.81	1.81
Callithrix sp.	32164	--	2.24	3.27	2.35	1.95	2.02
Callithrix sp.	32165	--	2.15	3.16	2.16	1.83	1.78
Callithrix sp.	34573	--	1.84	3.04	2.00	1.86	1.57
Callithrix sp.	30577	--	2.14	3.31	2.32	1.74	1.43
Callithrix sp.	30586	--	2.46	3.13	2.18	1.78	1.46
Callithrix sp.	30603	--	2.25	3.25	2.08	1.69	1.77
Callithrix sp.	37826	--	1.90	2.82	2.04	1.75	1.46
Callithrix sp.	440	--	2.88	4.19	2.57	2.72	2.39
Callithrix sp.	37823	--	2.94	4.35	2.75	2.28	1.76
Callithrix sp.	7165	--	2.28	3.53	2.23	2.34	1.70
C. apella	25811	9.20	15.92	20.58	16.00	15.26	13.69
C. apella	27097	5.58	11.44	17.18	12.08	12.33	11.54
C. apella	30724		11.29	14.21	11.66	11.70	12.55
C. apella	30726	5.21	12.35	16.24	12.25	11.81	11.44
C. apella	31062	4.89	10.38	13.83	11.28	11.24	10.50

(cont)

TABLE 4.2 (cont). Cervical Margin Surface Area (CMSA) in mm^2: platyrrhines.

Species	Specimen	M3	M2	M1	P4	P3	P2
C. apella	31064	5.18	11.78	15.49	12.32	12.44	12.10
C. apella	31066	5.97	10.26	14.29	12.06	12.22	10.99
C. apella	31072	5.32	10.27	13.54	12.03	11.24	10.55
C. apella	32049	5.61	10.85	15.83	12.41	12.63	11.52
C. apella	37831	6.29	13.42	16.50	13.72	13.28	12.77
C. apella	41090	4.76	10.22	15.35	12.25	11.86	11.40
C. apella	49635	6.12	12.14	15.72	12.91	12.83	11.56
C. apella	314062	5.03	9.61	13.73	11.01	10.64	10.09
C. capucinus	5332	7.46	10.94	15.10	11.02	10.50	10.44
C. capucinus	7317	6.76	11.59	14.48	10.48	9.96	11.66
C. capucinus	7322	6.19	10.07	12.76	10.52	10.23	10.62
C. capucinus	7323	6.74	10.20	12.05	9.10	9.34	9.69
C. capucinus	10135	7.19	10.40	17.38	10.29	10.83	10.54
C. capucinus	10136	5.61	10.92	13.86	10.54	10.69	14.18
C. capucinus	34323	6.95	11.56	13.98	10.05	10.56	10.02
C. capucinus	34326	5.85	10.14	12.88	9.56	9.19	9.25
C. capucinus	34353	9.02	12.96	16.39	12.29	13.39	11.65
Pithecia sp.	20266	7.02	8.07	7.34	5.67	5.69	3.84
Pithecia sp.	27124	6.17	6.51	7.19	5.63	5.31	3.78
Pithecia sp.	30720	5.25	5.63	5.81	4.99	4.77	3.59
Pithecia sp.	30718	6.08	7.69	7.06	5.26	4.77	3.90
Pithecia sp.	30719	7.10	8.72	9.17	6.70	5.99	4.17
Pithecia sp.	31061	6.04	7.52	7.06	5.31	5.01	3.64
Saguinus sp.	15324	--	1.99	3.09	2.48	2.36	2.19
Saguinus sp.	27331	--	1.70	2.91	2.05	1.87	2.54
Saguinus sp.	30597	--	1.71	3.06	2.82	2.45	2.73
Saguinus sp.	30601	--	1.37	2.78	2.26	2.28	2.19
Saguinus sp.	41567	--	1.81	3.22	2.15	2.07	1.97
Saguinus sp.	41568	--	2.21	3.34	2.28	2.08	1.97
Saguinus sp.	52557	--	1.45	2.73	1.99	2.10	2.02
Saguinus sp.	52615	--	1.73	2.76	2.00	1.83	1.91
Saguinus sp.	52616	--	2.14	3.58	2.27	2.32	2.17
Saguinus sp.	52658	--	2.21	3.25	2.21	2.11	1.89

(cont)

TABLE 4.2 (cont). Cervical Margin Surface Area (CMSA) in mm^2: platyrrhines.

Species	Specimen	M3	M2	M1	P4	P3	P2
Saimiri sp.	10131	1.72	3.46	4.57	3.23	3.42	3.84
Saimiri sp.	10134	1.64	3.73	4.39	3.27	3.31	4.32
Saimiri sp.	29488	1.88	3.43	5.09	3.07	3.37	4.09
Saimiri sp.	20187	2.29	3.98	5.40	3.49	3.43	4.01
Saimiri sp.	30568	1.62	3.18	4.57	2.83	2.85	2.42
Saimiri sp.	30569	1.87	4.14	5.36	3.38	3.18	3.92

TABLE 4.3. Root Surface Area (RSA) in mm^2: catarrhines.

Species	Specimen	M3	M2	M1	P4	P3
C. mitis	7088	103.78	148.54	135.55	98.08	80.83
C. mitis	22734	85.56	107.13	98.99	68.35	50.84
C. mitis	25022	107.80	147.55	106.18	75.72	60.19
C. mitis	32003	117.91	134.79	107.86	65.36	50.46
C. mitis	39389	79.20	121.15	107.87	68.10	46.36
C. mitis	44264	79.39	131.14	104.78	50.33	43.38
C. mitis	44268	105.42	138.63	117.59	65.59	57.39
C. mitis	44274	138.90	176.93	132.53	84.27	65.99
C. polykomos	21151	163.68	229.98	196.75	121.58	101.10
C. polykomos	22356	185.50	241.78	241.39	164.02	136.23
C. polykomos	22624	189.39	242.14	241.81	164.09	137.83
C. polykomos	22626	199.66	238.07	215.31	169.39	145.89
C. polykomos	22850	201.20	238.88	215.57	167.06	146.26
C. polykomos	46368	197.89	240.46	243.69	175.30	126.09
C. torquatus	32625	307.51	328.78	248.15	193.26	160.70
C. torquatus	62638	289.82	298.97	232.36	190.70	155.09
C. torquatus	62639	265.52	361.89	295.16	234.83	185.49
E. patas	37280	199.27	225.94	160.98	131.35	101.88
E. patas	47015	163.68	207.82	159.64	104.54	87.80
E. patas	14016	200.00	204.75	145.93	110.37	91.58
E. patas	47018	142.61	144.44	142.31	88.87	69.99
G. gorilla	14750	568.33	938.90	920.52	713.56	706.26
G. gorilla	26850	605.78	867.23	857.61	641.86	776.11
G. gorilla	29047	959.32	1188.93	1067.93	870.93	962.45
G. gorilla	46325	596.16	917.98	884.65	737.91	728.12
L. albigena	18613	238.70	260.06	200.74	121.12	123.22
L. albigena	22737	121.36	184.87	162.74	120.58	84.65
L. albigena	23194	248.85	244.48	196.30	132.72	134.11
L. albigena	39395	173.02	203.56	170.18	121.48	123.33
L. albigena	39396	187.77	233.87	184.87	122.16	110.77
L. albigena	39402	189.72	238.81	190.89	112.88	104.73
M. fascicularis	12758	191.65	199.63	155.36	103.05	81.18
M. fascicularis	22277	175.94	187.21	131.78	115.49	86.54
M. fascicularis	35765	163.58	180.95	133.37	111.22	90.30

(cont)

TABLE 4.3 (cont). Root Surface Area (RSA) in mm^2: catarrhines.

Species	Specimen	M3	M2	M1	P4	P3
M. fascicularis	35937	126.33	140.71	103.84	98.99	80.97
M. fascicularis	35938	126.87	140.89	110.81	97.64	88.36
M. fascicularis	37781	167.14	174.63	129.05	111.09	90.68
M. fascicularis	41167	188.24	185.22	136.65	130.61	102.74
M. fuscata	37709	332.26	364.73	244.36	197.51	143.20
M. fuscata	61237	482.95	559.68	389.79	310.18	210.69
Mandrillus sp.	19986	600.49	587.45	372.58	281.90	236.90
Mandrillus sp.	20085	541.54	501.85	340.46	287.29	253.13
Mandrillus sp.	23168	509.76	506.93	336.46	302.90	263.98
Mandrillus sp.	23169	460.76	417.92	259.24	234.45	200.76
Mandrillus sp.	34089	709.45	713.53	533.10	396.94	293.32
Mandrillus sp.	34272	349.26	387.07	279.31	190.39	165.62
P. anubis	8304	601.32	612.92	368.68	267.49	218.13
P. anubis	21160	488.80	535.80	359.65	231.64	219.14
P. anubis	29787	349.99	382.73	276.21	176.37	142.62
P. anubis	31619	493.07	547.27	363.25	271.47	240.06
P. anubis	31949	595.75	668.03	436.32	319.55	266.71
P. badius	24080	208.34	232.00	203.27	176.78	129.81
P. badius	24775	150.64	146.90	125.01	109.97	97.54
P. badius	24793	181.98	184.21	143.63	125.03	89.07
P. badius	25627	147.87	156.61	143.09	101.85	87.95
P. badius	25631	166.76	192.24	170.05	105.76	138.68
P. badius	25810	180.89	199.50	198.83	140.50	100.82
P. badius	26552	165.93	169.98	144.33	136.54	100.46
P. badius	26553	202.77	229.35	209.99	166.14	121.58
P. badius	31939	131.06	143.51	139.88	84.62	74.49
P. hosei	35621	106.16	147.59	133.38	91.86	75.67
P. hosei	37370	82.24	101.89	103.39	90.84	78.34
P. hosei	37371	85.16	129.94	124.49	121.94	101.10
P. hosei	37772	89.40	119.57	121.01	113.58	97.09
P. hosei	37773	90.73	126.06	128.72	125.16	104.82
P. paniscus	38018	265.21	339.55	321.45	231.95	309.97
P. paniscus	38019	216.86	257.41	261.00	190.31	237.16
P. paniscus	38020	230.12	288.62	313.55	211.97	263.31

(cont)

TABLE 4.3 (cont). Root Surface Area (RSA) in mm^2: catarrhines.

Species	Specimen	M3	M2	M1	P4	P3
P. rubicunda	22276	110.86	128.88	129.42	108.36	106.48
P. rubicunda	35704	117.02	129.90	131.32	117.57	106.06
P. rubicunda	35705	111.27	127.13	129.52	98.93	95.81
P. rubicunda	35706	97.68	105.17	112.10	96.48	83.36
P. rubicunda	35712	93.39	110.71	103.55	93.71	81.71
P. rubicunda	37776	117.53	137.93	134.17	109.73	97.07
P. rubicunda	37778	116.38	148.51	140.90	150.89	126.88
P. rubicunda	37779	118.09	140.00	142.32	125.18	107.48
P. troglodytes	6244	262.09	333.85	336.35	267.11	341.12
P. troglodytes	9493	205.84	273.37	326.88	247.58	287.76
P. troglodytes	15312	252.23	364.82	388.54	273.70	324.25
P. troglodytes	17702	324.56	452.57	461.22	328.63	485.06
P. troglodytes	23167	363.48	577.12	600.69	394.04	518.77
P. troglodytes	N6960	252.77	389.23	481.48	383.34	455.81
P. troglodytes	N7261	332.31	414.99	444.61	345.18	339.37
P. troglodytes	46416	259.79	341.99	336.92	241.48	310.36
P. troglodytes	N6908	702.15	943.47	1005.03	765.92	985.96
P. troglodytes	N7265	235.15	317.57	346.64	298.56	316.31
T. cristata	35586	130.87	153.49	115.56	126.72	102.76
T. cristata	35603	108.56	136.16	127.94	108.35	82.10
T. cristata	35604	101.41	121.37	114.06	105.22	94.30
T. cristata	35610	125.85	133.80	131.54	115.51	85.82
T. cristata	35618	72.77	90.80	82.28	77.22	62.14
T. cristata	35636	69.45	81.96	78.21	75.46	58.21
T. cristata	35640	112.36	128.26	118.22	114.09	94.41
T. cristata	35663	104.19	118.65	121.11	103.11	79.35
T. cristata	35678	109.72	147.10	127.49	121.48	88.42
T. cristata	35682	124.53	137.49	128.95	109.55	82.22
T. cristata	35683	146.33	147.51	133.16	127.98	100.92
T. cristata	37387	132.51	160.91	141.29	119.03	91.69
T. cristata	35584	86.65	124.42	109.89	95.94	75.30

TABLE 4.4. Cervical margin surface area (CMSA) in mm^2: catarrhines.

Species	Specimen	M3	M2	M1	P4	P3
C. mitis	7088	17.88	23.32	20.28	11.96	9.30
C. mitis	22734	15.78	17.36	15.32	10.57	7.01
C. mitis	25022	13.23	19.19	13.90	8.70	7.07
C. mitis	32003	21.38	22.84	16.93	10.16	6.68
C. mitis	39389	15.44	19.65	17.49	10.37	7.20
C. mitis	44264	13.24	20.61	15.60	7.91	6.18
C. mitis	44268	17.76	21.70	17.09	10.53	8.34
C. mitis	44274	20.75	24.76	20.84	12.39	8.78
C. polykomos	21151	31.13	33.93	28.55	20.21	16.10
C. polykomos	22356	27.00	32.60	28.54	18.30	16.70
C. polykomos	22624	26.02	33.13	29.43	17.83	15.92
C. polykomos	22626	25.10	28.69	24.44	17.54	18.12
C. polykomos	22850	26.48	30.14	24.13	17.45	18.10
C. polykomos	46368	34.01	36.19	33.31	20.27	15.44
C. torquatus	32625	46.84	53.41	40.96	30.12	22.26
C. torquatus	62638	42.37	47.06	39.09	25.96	16.79
C. torquatus	62639	57.70	63.36	48.32	30.70	20.42
E. patas	37280	29.71	33.30	27.00	16.37	12.92
E. patas	47015	28.26	38.69	28.72	16.81	13.30
E. patas	14016	24.44	27.73	22.64	13.67	10.99
E. patas	47018	25.31	25.78	23.09	11.88	8.86
G. gorilla	14750	87.33	116.24	117.18	84.28	79.70
G. gorilla	26850	100.16	131.04	138.24	81.32	85.17
G. gorilla	29047	116.85	137.28	121.61	84.07	87.17
G. gorilla	46325	107.85	142.35	127.74	89.97	81.70
L. albigena	18613	32.02	36.62	28.78	14.38	12.22
L. albigena	22737	13.90	21.94	19.53	11.15	7.75
L. albigena	23194	32.06	40.79	30.18	17.77	14.44
L. albigena	39395	26.62	34.43	26.72	15.31	11.94
L. albigena	39396	27.97	38.90	28.45	17.92	14.10
L. albigena	39402	27.31	38.80	33.43	18.31	16.99
M. fascicularis	12758	42.90	42.60	33.88	16.88	12.95
M. fascicularis	22277	30.92	32.36	21.26	14.86	11.63
M. fascicularis	35765	23.60	24.81	18.95	13.54	11.03

(cont)

TABLE 4.4 (cont). Cervical margin surface area (CMSA) in mm^2: catarrhines.

Species	Specimen	M3	M2	M1	P4	P3
M. fascicularis	35937	21.53	23.87	17.89	12.16	9.31
M. fascicularis	35938	27.91	30.62	20.40	12.31	10.23
M. fascicularis	37781	28.41	30.84	20.96	14.53	11.50
M. fascicularis	41167	29.51	32.16	21.60	15.64	12.12
M. fuscata	37709	56.08	59.34	38.87	23.67	18.39
M. fuscata	61237	75.00	78.56	45.97	31.84	24.31
Mandrillus sp.	19986	103.52	101.73	63.94	40.88	31.52
Mandrillus sp.	20085	95.68	86.40	62.07	42.26	35.24
Mandrillus sp.	23168	94.91	95.47	75.05	53.49	36.06
Mandrillus sp.	23169	94.17	95.05	61.75	45.83	41.79
Mandrillus sp.	34089	100.66	102.19	80.90	44.49	33.70
Mandrillus sp.	34272	78.82	82.02	56.86	35.91	26.85
P. anubis	8304	112.58	117.56	68.47	42.32	35.58
P. anubis	21160	95.41	96.73	72.91	34.65	31.19
P. anubis	29787	71.72	71.15	53.96	30.40	21.73
P. anubis	31619	92.95	94.80	68.39	35.73	25.39
P. anubis	31949	100.19	95.58	67.18	38.44	31.54
P. badius	24080	27.87	31.64	26.58	17.23	13.72
P. badius	24775	25.32	26.63	22.73	14.16	13.27
P. badius	24793	28.66	26.76	23.21	17.34	13.52
P. badius	25627	23.00	22.88	20.73	11.58	11.52
P. badius	25631	21.78	26.74	25.76	11.93	15.37
P. badius	25810	22.39	26.19	26.33	14.65	11.86
P. badius	26552	22.40	22.70	18.97	11.29	9.26
P. badius	26553	23.98	26.86	23.76	14.24	12.39
P. badius	31939	21.04	21.46	19.35	12.00	10.96
P. hosei	35621	19.04	22.21	21.17	11.01	9.54
P. hosei	37370	12.75	14.59	12.70	7.89	7.21
P. hosei	37371	12.86	19.25	16.70	10.47	8.99
P. hosei	37772	13.10	17.98	15.66	10.55	9.86
P. hosei	37773	12.42	17.65	15.42	10.71	10.17
P. paniscus	38018	46.51	59.10	57.68	27.98	34.10
P. paniscus	38019	38.20	49.26	46.56	25.22	25.90
P. paniscus	38020	37.90	43.62	47.33	26.24	30.47

(cont)

TABLE 4.4 (cont). Cervical margin surface area (CMSA) in mm^2: catarrhines.

Species	Specimen	M3	M2	M1	P4	P3
P. rubicunda	22276	18.34	19.51	19.10	11.38	11.86
P. rubicunda	35704	16.59	18.82	18.00	10.90	10.29
P. rubicunda	35705	15.31	17.14	17.10	8.51	9.08
P. rubicunda	35706	12.67	15.71	14.90	9.41	8.69
P. rubicunda	35712	13.40	16.22	14.81	8.88	8.58
P. rubicunda	37776	18.11	19.65	19.11	11.20	10.67
P. rubicunda	37778	14.45	20.82	16.12	12.03	11.22
P. rubicunda	37779	19.51	21.72	20.39	13.24	12.60
P. troglodytes	6244	43.82	49.10	48.05	27.30	28.10
P. troglodytes	9493	42.32	53.61	69.79	32.82	34.60
P. troglodytes	15312	48.88	60.03	55.51	30.19	33.87
P. troglodytes	17702	53.89	68.60	65.16	35.92	42.50
P. troglodytes	23167	61.00	80.82	69.76	39.66	42.48
P. troglodytes	N6960	41.29	62.84	76.39	39.33	41.64
P. troglodytes	N7261	51.94	70.11	78.87	38.33	37.19
P. troglodytes	46416	51.44	60.81	70.35	33.89	36.78
P. troglodytes	N6908	122.95	141.77	149.15	84.45	96.11
P. troglodytes	N7265	40.33	52.50	61.28	35.52	36.36
T. cristata	35586	21.41	21.83	16.90	10.31	9.89
T. cristata	35603	14.24	17.67	17.20	9.46	8.87
T. cristata	35604	15.26	18.97	15.59	10.19	8.93
T. cristata	35610	18.42	19.56	17.42	10.99	8.51
T. cristata	35618	12.07	13.54	11.64	7.11	5.91
T. cristata	35636	10.76	11.88	10.96	6.21	6.46
T. cristata	35640	16.84	20.34	16.19	10.09	9.17
T. cristata	35663	17.24	22.01	17.54	11.44	10.45
T. cristata	35678	17.23	21.33	19.18	11.59	9.73
T. cristata	35682	17.73	20.96	17.25	11.24	9.54
T. cristata	35683	19.07	21.07	16.82	11.68	9.66
T. cristata	37387	18.68	23.27	18.65	11.89	9.72
T. cristata	35584	16.24	20.77	16.36	9.07	9.28

TABLE 4.5. Species averages for platyrrhines: Root surface area.

Species	N	lnGMSkull	lnM3	lnM2	lnM1	lnP4	lnP3	lnP2
Alouatta caraya	M = 1 F = 3	3.85	5.12	5.38	5.23	4.88	4.78	4.51
Alouatta palliata	M = 0 F = 10	3.84	4.76	5.17	4.99	4.75	4.67	4.50
Ateles geoffroyi	M = 0 F = 17	3.89	3.77	4.30	4.48	4.26	4.22	3.96
Aotus trivirgatus	M = 1 F = 8	3.37	2.86	3.33	3.48	3.22	3.11	2.90
Callicebus moloch	M = 10 F = 0	3.32	3.33	3.84	3.98	3.68	3.52	3.32
Callithrix sp.	M = 7 F = 7	3.07	n/a	2.56	2.84	2.70	2.56	2.58
Cebus apella	M = 5 F = 9	3.77	3.48	4.03	4.38	4.40	4.44	4.46
Cebus capucinus	M = 2 F = 8	3.79	3.71	4.02	4.18	4.19	4.23	4.18
Pithecia sp.	M = 4 F = 3	3.55	3.37	3.64	3.78	3.68	3.73	3.53
Saguinus sp.	M = 5 F = 5	3.09	n/a	2.52	3.01	2.93	2.89	2.87
Saimiri sp.	M = 7 F = 3	3.34	2.56	3.11	3.38	3.26	3.34	3.50
Chiropotes satanas	M = 0 F = 2	3.69	3.35	3.90	4.18	4.22	4.24	3.93

Total N: 109

TABLE 4.6. Species averages for platyrrhines: Cervical margin surface area

Species	N	lnGMSkull	lnM3	lnM2	lnM1	lnP4	lnP3	lnP2
Alouatta caraya	M = 1 F = 3	3.85	3.29	3.57	3.43	2.81	2.72	2.54
Alouatta palliata	M = 0 F = 10	3.84	3.13	3.53	3.41	2.89	2.80	2.65
Ateles geoffroyi	M = 0 F = 17	3.89	2.11	2.48	2.57	2.19	2.11	1.95
Aotus trivirgatus	M = 1 F = 8	3.37	1.09	1.63	1.79	1.27	1.15	1.07
Callicebus moloch	M = 10 F = 0	3.32	1.39	2.01	2.19	1.58	1.42	1.18
Callithrix sp.	M = 7 F = 7	3.07	n/a	0.82	1.18	0.79	0.65	0.54
Cebus apella	M = 5 F = 9	3.77	1.80	2.42	2.73	2.51	2.49	2.44
Cebus capucinus	M = 2 F = 8	3.79	1.93	2.39	2.67	2.35	2.35	2.37
Pithecia sp.	M = 4 F = 3	3.55	1.85	2.01	1.99	1.72	1.66	1.34
Saguinus sp.	M = 5 F = 5	3.09	n/a	0.61	1.12	0.81	0.76	0.77
Saimiri sp.	M = 7 F = 3	3.34	0.61	1.28	1.57	1.18	1.18	1.33
Chiropotes satanas	M = 0 F = 2	3.69	1.68	2.07	2.23	2.07	2.07	1.77

Total N: 109

TABLE 4.7. Species averages for catarrhines: Root surface area

Species	N	lnGMSkull	lnM3	lnM2	lnM1	lnP4	lnP3
Lophocebus albigena	M = 5 F = 3	4.05	5.26	5.44	5.22	4.85	4.79
Cercocebus torquatus	M = 2 F = 1	4.15	5.66	5.80	5.56	5.33	5.12
Cercopithecus mitis	M = 0 F = 12	3.88	4.66	4.92	4.73	4.24	4.00
Piliocolobus badius	M = 4 F = 5	3.93	5.14	5.21	5.10	4.85	4.65
Colobus polykomos	M = 1 F = 5	3.97	5.24	5.47	5.42	5.08	4.88
Erythrocebus patas	M = 3 F = 1	4.14	5.13	5.28	5.03	4.69	4.48
Macaca fascicularis	M = 1 F = 8	3.89	5.09	5.17	4.89	4.71	4.48
Macaca fuscata	M = 1 F = 1	4.19	6.01	6.14	5.76	5.54	5.18
Macaca sylvanus	M = 1 F = 0	4.15	5.79	5.76	5.30	5.21	5.10

(cont)

TABLE 4.7 (cont). Species averages for catarrhines: Root surface area

Species	N	lnGMSkull	lnM3	lnM2	lnM1	lnP4	lnP3
Mandrillus sp.	M = 5 F = 1	4.49	6.27	6.25	5.87	5.64	5.46
Pan paniscus	M = 0 F = 3	4.49	5.47	5.69	5.70	5.35	5.60
Pan troglodytes	M = 0 F = 13	4.50	5.88	6.15	6.14	5.94	6.14
Papio anubis	M = 4 F = 4	4.43	6.23	6.25	5.85	5.51	5.33
Presbytis hosei	M = 1 F = 4	3.83	4.51	4.83	4.81	4.69	4.52
Presbytis rubicunda	M = 4 F = 7	3.82	4.68	4.81	4.80	4.68	4.57
Trachypithecus cristata	M = 0 F = 14	3.80	4.70	4.86	4.76	4.67	4.43
Gorilla gorilla	M = 0 F = 5	4.69	6.47	6.86	6.84	6.57	6.64

Total N: 119

TABLE 4.8. Species averages for catarrhines: Cervical margin surface area

Species	N	lnGMSkull	lnM3	lnM2	lnM1	lnP4	lnP3
Lophocebus albigena	M = 5 F = 3	4.05	3.30	3.56	3.34	2.78	2.61
Cercocebus torquatus	M = 2 F = 1	4.15	3.89	4.00	3.76	3.36	2.99
Cercopithecus mitis	M = 0 F = 12	3.88	2.81	3.04	2.84	2.31	2.01
Piliocolobus badius	M = 4 F = 5	3.93	3.18	3.25	3.14	2.63	2.52
Colobus polykomos	M = 1 F = 5	3.97	3.34	3.48	3.33	2.92	2.82
Erythrocebus patas	M = 3 F = 1	4.14	3.29	3.45	3.23	2.69	2.44
Macaca fascicularis	M = 1 F = 8	3.89	3.35	3.42	3.09	2.64	2.40
Macaca fuscata	M = 1 F = 1	4.19	4.18	4.23	3.75	3.32	3.06
Macaca sylvanus	M = 1 F = 0	4.15	3.61	3.77	3.37	2.84	2.67

(cont)

TABLE 4.8 (cont). Species averages for catarrhines: Cervical margin surface area

Species	N	lnGMSkull	lnM3	lnM2	lnM1	lnP4	lnP3
Mandrillus sp.	M = 5 F = 1	4.49	4.55	4.54	4.20	3.78	3.53
Pan paniscus	M = 0 F = 3	4.49	3.71	3.93	3.92	3.28	3.41
Pan troglodytes	M = 0 F = 13	4.50	4.16	4.35	4.28	3.79	3.89
Papio anubis	M = 4 F = 4	4.43	4.50	4.54	4.18	3.59	3.34
Presbytis hosei	M = 1 F = 4	3.83	2.64	2.91	2.79	2.32	2.21
Presbytis rubicunda	M = 4 F = 7	3.82	2.79	2.90	2.85	2.34	2.31
Trachypithecus cristata	M = 0 F = 14	3.80	2.81	2.97	2.79	2.30	2.19
Gorilla gorilla	M = 0 F = 5	4.69	4.64	4.89	4.84	4.44	4.41
Total N:	119						

Platyrrhine RMA Results

Results for the platyrrhine RMA analyses are given in Table 4.9 including the slope of the RMA line, the ninety-five percent confidence interval (95% CI) for each line, the *r* value, which indicates the level of correlation between variables, and the r^2 value, which indicates how much of the variation contained in the sample is explained by the independent variable (i.e., skull size for the first two and root size for the last analysis). *Callithrix* and *Saguinus* were omitted from all analyses involving M3.

When root surface area (RSA) was compared to the geometric mean of skull size (GMSkull), the RMA slope was greater than 2 for all teeth. However, the 95% confidence intervals (95% CIs) encompass 2, which means that an isometric relationship between root size and skull size cannot be ruled out. Results also indicate that root and skull size are correlated, with *r* values ranging from 0.75 to 0.91 for all postcanine teeth. R^2 values are between 0.56 and 0.92 for all postcanine teeth.

TABLE 4.9. RMA results for platyrrhines

	Tooth	RMA slope	95% CI	r	r^2
[a]ln(GMSkull) vs. RSA	M3	3.42	1.58-5.27	0.75	0.56
	M2	2.94	1.95-3.93	0.88	0.77
	M1	2.44	1.74-3.15	0.91	0.83
	P4	2.36	1.82-2.90	0.95	0.90
	P3	2.42	1.93-2.91	0.96	0.92
	P2	2.24	1.66-2.82	0.93	0.87
[b]ln(GMSkull) vs. CMSA	M3	3.61	1.84-5.38	0.80	0.64
	M2	3.05	2.07-4.03	0.89	0.79
	M1	2.53	1.77-3.30	0.90	0.82
	P4	2.44	1.89-2.98	0.95	0.90
	P3	2.48	1.97-2.99	0.96	0.91
	P2	2.41	1.82-3.01	0.94	0.89
[c]RSA vs. CMSA	M3	1.05	0.91-1.20	0.99	0.97
	M2	1.03	0.96-1.12	0.99	0.99
	M1	1.03	0.91-1.17	0.98	0.97
	P4	1.03	0.93-1.14	0.99	0.98
	P3	1.03	0.92-1.13	0.99	0.98
	P2	1.08	0.94-1.21	0.98	0.97

[a]Analysis of skull geometric mean, ln(GMSkull), and root surface area, RSA.
[b]Analysis of skull geometric mean, ln(GMSkull), and cervical margin surface area, CMSA (used as a proxy for crown size).
[c]Analysis of root surface area, RSA, and cervical margin surface area, CMSA.

Comparing cervical margin surface area (CMSA) to GMSkull yielded similar results to the analysis on root surface area. RMA slopes were greater than 2 for all teeth, and the 95% CIs included 2 for all teeth except for M2, which has a 95% CI of 2.07-4.03. Thus, an isometric relationship between cervical margin surface area and skull size cannot be rejected, except in the case of M2 which suggests a slightly positively allometric relationship. In platyrrhines, M2 cervical margin surface area appears to increase at a faster rate than skull size such that a platyrrhine with a large skull has both an absolutely and relatively larger M2 cervical margin surface area than a platyrrhine with a small skull. CMSA and GMSkull are also correlated; the *r* value is lowest for M3 at 0.75 and ranges from 0.88 to 0.96 for M2 to P2. R^2 values are again lowest at M3 (0.64) and range from 0.79 to 0.91 for M2-P2.

Finally, root surface area and crown cervical margin area were compared. For this analysis, the expected slope of isometry is 1 rather than 2, since both RSA and CMSA are surface areas. The RMA slope is slightly higher than 1 for all teeth, and the 95% CIs include 1. Thus, isometry cannot be ruled out. Root size and cervical margin surface area are very highly correlated, with near-perfect *r* values of 0.98 to 0.99 for all postcanine teeth. R^2 values are between 0.97 and 0.99 for all postcanine teeth.

Catarrhine RMA Results

Results for catarrhines largely mirror those for platyrrhines and are shown in Table 4.10. Comparing RSA to GMSkull, the RMA slope is greater than 2 for all teeth, and the 95% CIs encompass 2. Root and skull size are correlated, with *r*

ranging from 0.89-0.94 in all postcanine teeth. R^2 is lowest for M3 (0.79), and falls between 0.82-0.88 for all other postcanine teeth. When CMSA is compared to skull size, RMA slopes are also greater than 2 for all teeth, and 95% CIs encompass 2 for all teeth except for P2, which has a 95% CI of 2.01-2.77. *R* values were high, ranging from 0.91-0.97 on postcanine teeth. R^2 was again lowest for M3 at 0.83, and ranged from 0.88-0.94 for the rest of the postcanine tooth row. Comparing root surface area to cervical margin surface area, the RMA slope is greater than 1 for all teeth except for P3, which has a slope of 0.97, and 95% CIs encompass 1 for all teeth. Correlation values were very high, ranging from 0.97 to 0.99, and r^2 ranges from 0.94-0.98 for all postcanine teeth.

TABLE 4.10. RMA results for catarrhines

	Tooth	RMA slope	95% CI	r	r^2
[a]ln(GMSkull) vs. RSA	M3	2.19	1.68-2.71	0.89	0.79
	M2	2.16	1.75-2.58	0.93	0.86
	M1	2.09	1.72-2.48	0.94	0.88
	P4	2.14	1.68-2.61	0.90	0.82
	P3	2.46	1.97-2.95	0.92	0.85
[b]ln(GMSkull) vs. CMSA	M3	2.29	1.81-2.78	0.91	0.83
	M2	2.21	1.83-2.60	0.94	0.88
	M1	2.14	1.88-2.41	0.97	0.94
	P4	2.24	1.88-2.61	0.95	0.90
	P3	2.39	2.01-2.77	0.95	0.90
[c]RSA vs. CMSA	M3	1.04	0.95-1.14	0.98	0.97
	M2	1.02	0.95-1.10	0.99	0.98
	M1	1.02	0.92-1.13	0.98	0.96
	P4	1.05	0.91-1.18	0.97	0.94
	P3	0.97	0.88-1.06	0.98	0.97

[a]Analysis of skull geometric mean, ln(GMSkull), and root surface area, RSA.

[b]Analysis of skull geometric mean, ln(GMSkull), and cervical margin surface area, CMSA (used as a proxy for crown size).

[c]Analysis of root surface area, RSA, and cervical margin surface area, CMSA.

Discussion of scaling analyses

The scaling analysis included in the current study does not directly address study hypotheses, but is crucial to establishing the extent to which variation in root and crown size is governed by overall skull size. Since the study hypotheses are primarily functional, it is important to establish the presence of variation in root and cervical margin surface area that cannot be explained by size alone. Results from scaling analyses indicate that almost all calculated RMA slopes are greater than the expected slope of isometry, however, the 95% CIs typically include a slope of isometry. Consequently, an isometric relationship between tooth size and skull size cannot be rejected. Furthermore, results indicate that root surface area and cervical margin surface area scale isometrically with one another.

Interestingly, there is variation in the degree of correlation between root and crown size and skull size. For all anthropoids, M3 root surface area and cervical margin surface area is noticeably less correlated with skull size than all other postcanine teeth. The relatively low correlation between M3 root and crown size and skull size is more pronounced in platyrrhines than in catarrhines, which may be due to the reduction in the size of M3 seen among cebids (the significance of which is discussed in more detail in Chapter 6).

The observed isometric relationship between tooth and skull size means that all primates are predicted to have the same relative tooth size regardless of skull size. Thus, any observed variation in tooth size is necessarily the result of non-size-related factors. One important consequence of this isometric relationship is that relative tooth root and crown size can be compared among taxa

using simple shape ratios, created by dividing the variable of interest (RSA or CMSA) by a measurement of overall size (GMSkull) (Jungers et al., 1995). Results from comparisons of shape variables are presented in Chapter 5. If variables are allometric (as opposed to isometric), all influences of size cannot be "removed" using a simple ratio because variables will still contain size-correlated shape differences. Allometric variables, therefore, are often examined by using residuals from a LS regression line (discussed in Chapter 3) using the LS slope as a measure of so-called functional equivalence (Pilbeam and Gould, 1974; Jungers et al., 1995). Using residuals, both size and size-correlated shape are removed from the variable of interest; however, this removal is achieved by assuming that a specific scaling relationship represents some functional standard, an assumption that in many cases may not be valid.

Results of the current scaling analysis differ from results reported in a similar analysis by Kupczik et al. (2009) in which the scaling relationship between root and crown size in some anthropoid taxa was assessed. Kupczik et al. (2009) report that root and crown volume scale isometrically with one another, but that root and crown surface area have an allometric relationship such that roots increase in size at a faster rate than crowns. It is unclear why results from the current study, which suggest an isometric relationship between root and crown size, do not match previous research since data were collected and measured using similar protocols. However, Kupczik et al. (2009) examined only mandibular M2s, while the current study examines maxillary postcanine teeth. This suggests that there may be differences in the relationship between root and

crown size between maxillary and mandibular teeth, a hypothesis that should be explored in future research.

The results of the scaling analyses provide the logical basis for the analyses of function discussed in upcoming chapters. Assessing the influence of skull size on tooth root and cervical margin surface area has revealed that factors other than overall size influence variation in tooth size. While this observation alone does not necessarily *support* a functional link between dental variation and force production, it is *consistent* with the predictions of the functional hypotheses examined in the current study. Furthermore, because root and crown size scale isometrically with skull size, variation in dental variables can be compared across taxa using shape ratios (see Chapter 5).

CHAPTER 5

PART I: DENTAL VARIABLES RESULTS AND DISCUSSION

In the previous chapter, it was shown that tooth root and crown size are highly correlated with skull size and one another across primates, and that some variation in root and crown size cannot be explained by skull size alone. The current chapter explores the correlation of root and crown size within species (Hypothesis 1a) and assesses whether variation in root and crown size can be attributed to variation in the functional demands of diet (Hypothesis 1b). As mentioned previously, cervical margin surface area (CMSA) is used as a proxy for crown size in the current study.

Hypothesis 1a: Results

Hypothesis 1a was tested using Kendall's τ (discussed in Chapter 3). Kendall's τ yields correlation coefficients that indicate the magnitude and direction of correlation between two sets of variables. Both root size (RSA) and cervical margin surface area (CMSA, a proxy for crown size) were quantified for all upper right-side postcanine teeth. Each variable was ranked largest to smallest and then rank order was compared between RSA and CMSA. A correlation coefficient near 1 indicates a strong positive correlation wherein both values increase or decrease concurrently. A value close to -1 indicates a strong negative correlation, wherein one value increases as the other decreases. Values near zero indicate that no correlation exists between variables. There was a significant, positive correlation between root and crown size for all taxa examined (See Table 5.1 for results).

TABLE 5.1. Kendall's τ correlation between root size (RSA) and crown size (CMSA as proxy).

Subfamily	Species	N	[a]correlation coefficient	[b]p-value
	Callithrix sp.	M = 7 F = 7	0.54	***
Callithrichinae	*Saguinus sp.*	M = 5 F = 5	0.72	***
	Aotus trivirgatus	M = 1 F = 7	0.82	***
	Cebus apella	M = 5 F = 9	0.41	***
	Cebus capucinus	M = 2 F = 7	0.32	**
Cebinae	*Saimiri sp.*	M = 4 F = 2	0.42	**
	Callicebus moloch	M = 10 F = 0	0.85	***
Pitheciinae	*Pithecia sp.*	M = 3 F = 3	0.27	*
	Alouatta caraya	M = 1 F = 3	1.00	***
	Alouatta palliata	M = 0 F = 10	0.83	***
Atelinae	*Ateles geoffroyi*	M = 0 F = 17	0.68	***
	Presbytis hosei	M = 1 F = 4	0.55	**
	Presbytis rubicunda	M = 4 F = 4	0.65	***
Colobinae	*Trachypithecus cristata*	M = 0 F = 14	0.77	***

(cont)

[a]Correlation coefficient. The sign of the number indicates a positive or negative correlation.

[b]p-values. *** = $p < 0.001$, ** = $p < 0.01$, * = $p < 0.05$, ns = not significant.

TABLE 5.1 (cont). Kendall's τ correlation between root size (RSA) and crown size (CMSA as proxy).

Subfamily	Species	N	[a]correlation coefficient	[b]p-value
	Colobus polykomos	M = 1 F = 5	0.76	***
Colobinae	*Piliocolobus badius*	M = 4 F = 5	0.88	***
	Macaca fascicularis	M = 1 F = 6	0.94	***
	Macaca fuscata	M = 1 F = 1	1.00	***
	Lophocebus albigena	M = 5 F = 1	0.81	***
	Cercocebus torquatus	M = 2 F = 1	0.93	***
	Papio anubis	M = 3 F = 2	0.91	***
	Mandrillus sp.	M = 5 F = 1	0.93	***
	Cercopithecus mitis	M = 0 F = 12	0.90	***
Cercopithecinae	*Erythrocebus patas*	M = 3 F = 1	0.95	***
	Pan paniscus	M = 0 F = 3	0.73	**
	Pan troglodytes	M = 0 F = 13	0.43	***
Hominidae	*Gorilla gorilla*	M = 0 F = 5	0.55	***
Total N:		216		

[a]Correlation coefficient. The sign of the number indicates a positive or negative correlation.

[b]p-values. *** = $p < 0.001$, ** = $p < 0.01$, * = $p < 0.05$, ns = not significant.

Hypothesis 1a: Discussion

Results indicate that root and crown size are significantly positively correlated in all anthropoid species. In other words, among primates the tooth with the largest root also has the largest crown, the tooth with the second-largest root has the second-largest crown, and so forth. Because sample size varies among species in the current study, correlation coefficients cannot be compared, so it is not possible to determine whether the correlation between root and crown size is stronger in one species than another. Results unequivocally support the prediction of Hypothesis 1a that root and crown size should covary along the tooth row.

Despite the fact that correlation coefficients cannot be directly compared among species, it is interesting to note the wide range of values reported above. All correlations between RSA and CMSA were statistically significant, however coefficients ranged in value from 0.27 in *Pithecia sp*. to 0.94 in *M. fascicularis*. Such a wide range of values is suggestive that while root and crown size are certainly significantly correlated with each other, there does not appear to be an inviolable structural relationship between the two. In other words, root size is not solely derived from crown size and vice versa.

These results are consistent with results from Kupczik et al. (2009), who also found that root and crown surface area were significantly positively correlated within *M. fascicularis* and *P. anubis* (but not in *H. sapiens*) mandibular M2s. However, Kupczik and colleagues also found that root and crown *volume* did *not* covary significantly within the same species, suggesting that the

relationship between root and crown size for mandibular M2s is not merely structural (Kupczik et al., 2009). As discussed in the previous chapter, a key difference between the current study and that of Kupczik et al. (2009) is the use of maxillary versus mandibular teeth, respectively. Consequently, results from Kupczik et al. (2009) may not be directly comparable to those from the current study; however, it is compelling that results from each study suggest that root and crown size may vary independently (see also Spencer, 2003).

In the previous chapter, results from interspecific scaling analyses showed that root and crown size vary in response to factors other than overall skull size. Here, results of intraspecific correlation analyses show that root and crown size covary along the tooth row, supporting the prediction of Hypothesis 1a. Furthermore, the total range of values of correlation coefficients across the sample suggests that covariation in root and crown size is not strictly a function of their structural connection. Hypothesis 1b, discussed below, assesses the hypothesis that root and crown size vary in response to diet; in other words, if tooth size is not related to overall skull size, and if root and crown size can vary independently, then it is possible that they covary along the tooth row due to functional demands.

Hypothesis 1b: Results

Hypothesis 1b states that crown and root size are related to tooth function; primates with a more mechanically resistant diet should have larger tooth roots and crowns than primates with a soft diet. To test this hypothesis, pair-wise

comparisons were conducted using Mann-Whitney U tests (for comparisons of two species) or Kruskall-Wallis tests (for comparisons among three species).

Results of the comparative analyses are summarized in Tables 5.2 (roots) and 5.3 (crowns) for platyrrhines, and Tables 5.4 (roots) and 5.5 (crowns) for catarrhines. Justification of each group of comparisons is discussed in detail in Chapter 3. Note that there are two comparisons that feature primates in the same dietary category, the *Aotus/Saimiri* comparison and the *Pithecia/Chiropotes* comparison. This is due to the fact that Cebinae (to which *Aotus*, *Saimiri*, and *Cebus* belong) and Pitheciinae (to which *Pithecia*, *Chiropotes* and *Callicebus* belong) are represented by more than two species in the current study. Therefore, Cebinae and Pitheciinae were analyzed using Kruskall-Wallis tests and multiple comparisons. Each comparison is discussed in detail below.

TABLE 5.2. Comparative results: Platyrrhine roots

Species	Diet Category	N	P2	P3	P4	M1	M2	M3
Alouatta palliata	Resistant	M = 0 F = 10						
Ateles geoffroyi	Soft	M = 0 F = 17	***	***	***	***	***	***
Cebus apella	Resistant	M = 7 F = 9						
Aotus trivirgatus	Soft	M = 4 F = 6	*	***	***	***	ns	*
Cebus apella	Resistant	M = 7 F = 9						
Saimiri sp.	Soft	M = 5 F = 5	***	***	***	***	***	**
Aotus trivirgatus	Soft	M = 4 F = 6						
Saimiri sp.	Soft	M = 5 F = 5	ns	ns	ns	ns	**	***
Cebus apella	Resistant	M = 7 F = 9						
Cebus capucinus	Soft	M = 2 F = 8	***	***	***	***	ns	**
Pithecia sp.	Resistant	M = 4 F = 3						
Callicebus moloch	Soft	M = 10 F = 0	ns	ns	ns	ns	ns	ns
Chiropotes satanas	Resistant	M = 0 F = 2						
Callicebus moloch	Soft	M = 10 F = 0	*	*	ns	ns	ns	ns
Pithecia sp.	Resistant	M = 4 F = 3						
Chiropotes satanas	Resistant	M = 0 F = 2	ns	ns	ns	ns	ns	ns

Asterisks (*) denote p-values. *** = p<.001, ** = p<.01, * = p<.05, ns = not significant.

TABLE 5.3. Comparative results: Platyrrhine crowns

Species	Diet Category	N	P2	P3	P4	M1	M2	M3
Alouatta palliata	Resistant	M = 0 F = 10						
Ateles geoffroyi	Soft	M = 0 F = 17	***	***	***	***	***	***
Cebus apella	Resistant	M = 7 F = 9						
Aotus trivirgatus	Soft	M = 4 F = 6	***	***	***	***	**	ns
Cebus apella	Resistant	M = 7 F = 9						
Saimiri sp.	Soft	M = 5 F = 5	***	***	***	***	***	***
Aotus trivirgatus	Soft	M = 4 F = 6						
Saimiri sp.	Soft	M = 5 F = 5	ns	ns	ns	ns	ns	**
Cebus apella	Resistant	M = 7 F = 9						
Cebus capucinus	Soft	M = 2 F = 8	*	***	***	*	ns	*
Pithecia sp.	Resistant	M = 4 F = 3						
Callicebus moloch	Soft	M = 10 F = 0	*	ns	ns	*	ns	**
Chiropotes satanas	Resistant	M = 0 F = 2						
Callicebus moloch	Soft	M = 10 F = 0	*	*	*	ns	ns	ns
Pithecia sp.	Resistant	M = 4 F = 3						
Chiropotes satanas	Resistant	M = 0 F = 2	ns	ns	ns	ns	ns	ns

Asterisks (*) denote p-values. *** = p<.001, ** = p<.01, * = p<.05, ns = not significant.

TABLE 5.4. Comparative results: Catarrhine roots

Species	Diet Category	N	P3	P4	M1	M2	M3
Colobus polykomos	Resistant	M = 1 F = 5					
Piliocolobus badius	Soft	M = 4 F = 5	ns	ns	*	*	ns
Mandrillus sp.	Resistant	M = 5 F = 1					
Cercocebus torquatus	Soft	M = 2 F = 1	*	ns	ns	ns	ns
Lophocebus albigena	Resistant	M = 5 F = 3					
Papio anubis	Soft	M = 4 F = 4	ns	**	*	**	**
Macaca fuscata	Resistant	M = 1 F = 1					
Macaca fascicularis	Soft	M = 1 F = 8	*	*	*	*	*
Gorilla gorilla	Resistant	M = 0 F = 5					
Pan troglodytes	Soft	M = 0 F = 13	ns	*	*	*	*

Asterisks (*) denote p-values. *** = p<.001, ** = p<.01, * = p<.05, ns = not significant.

TABLE 5.5. Comparative results: Catarrhine crowns

Species	Diet Category	N	P3	P4	M1	M2	M3
Colobus polykomos	Resistant	M = 1 F = 5					
Piliocolobus badius	Soft	M = 4 F = 5	***	*	*	*	*
Mandrillus sp.	Resistant	M = 5 F = 1					
Cercocebus torquatus	Soft	M = 2 F = 1	*	ns	ns	*	*
Lophocebus albigena	Resistant	M = 5 F = 3					
Papio anubis	Soft	M = 4 F = 4	***	***	***	***	***
Macaca fuscata	Resistant	M = 1 F = 1					
Macaca fascicularis	Soft	M = 1 F = 8	*	*	ns	*	*
Gorilla gorilla	Resistant	M = 0 F = 5					
Pan troglodytes	Soft	M = 0 F = 13	*	*	ns	*	*

Asterisks (*) denote p-values. *** = p<.001, ** = p<.01, * = p<.05, ns = not significant.

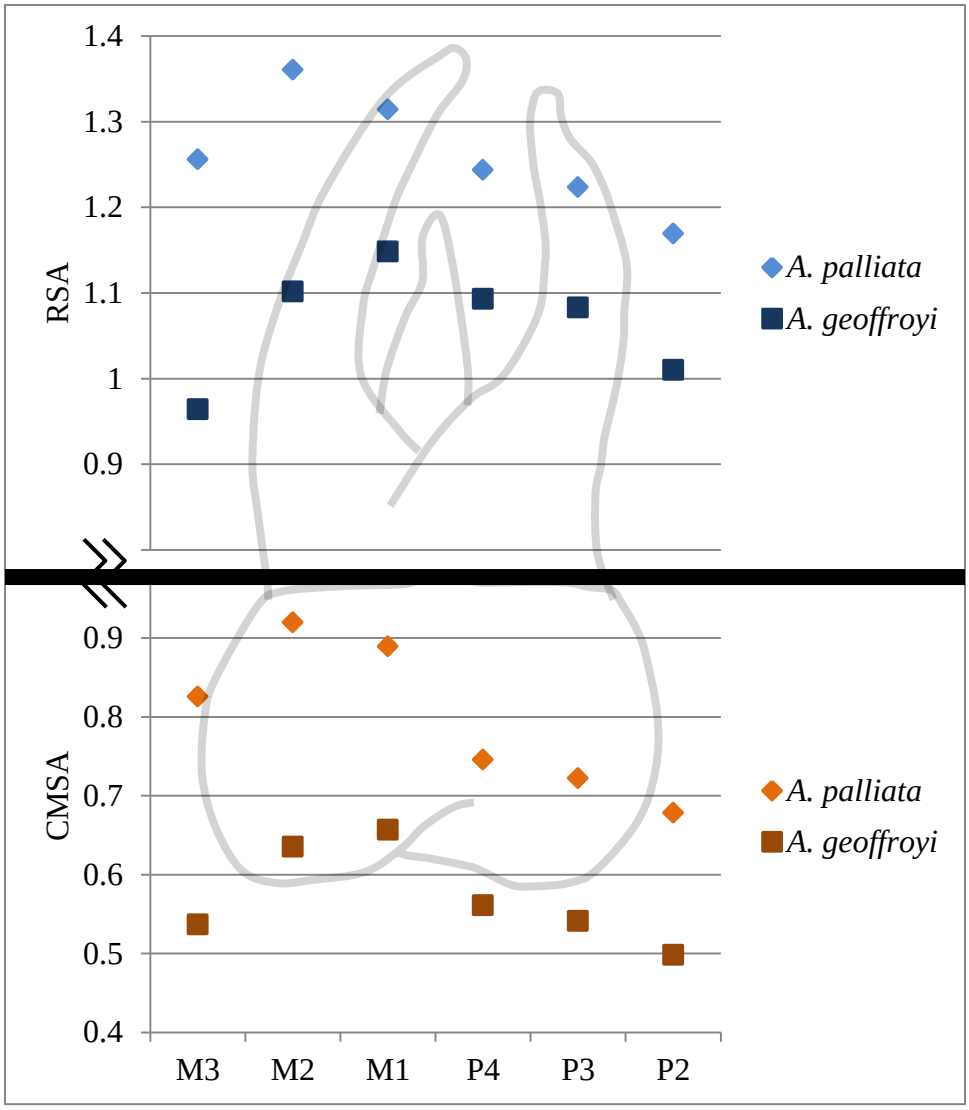

Fig. 5.1. *Alouatta/Ateles* MWU results. Tooth position is along the x-axis, and CMSA and RSA are on the bottom and top y-axes, respectively. Icons that are filled-in indicate significant differences between groups at $p < 0.05$. Icons that are not filled in indicate that there is no significant difference between groups for that variable.

Alouatta palliata, with a resistant diet, was compared to *Ateles geoffroyi*, with a soft diet (Figure 5.1). For all postcanine teeth, *Alouatta* RSA and CMSA are significantly larger than *Ateles*. This is consistent with past studies comparing molar size in *Alouatta* and *Ateles* (Kay, 1975; Anapol and Lee, 1994; Spencer, 1995), and matches the predictions of Hypothesis 1b.

Cebus apella, Saimiri sp., and *Aotus trivirgatus* were compared using a Kruskall-Wallis test (Figures 5.2a, b, and c). *C. apella* is in the resistant diet category and was predicted to have higher values for premolar RSA and CMSA than *Saimiri sp.* and *A. trivirgatus*. *Saimiri sp.* and *A. trivirgatus* were not expected to differ from each other since they are in the same dietary classification.

Cebus has larger roots and crowns than *Saimiri* for all teeth. *Cebus* has larger roots than *Aotus* for P3-M1, there is no significant difference between M2 root size, and *Aotus* has a significantly larger M3 root than *Cebus*. *Cebus* has significantly larger crowns than *Aotus* for all teeth except for M3, which is not significantly different in size than in *Aotus*. *Saimiri* and *Aotus* show no significant differences in RSA and CMSA for P2-M1. M2 roots, but not crowns, are significantly larger in *Aotus* than in *Saimiri,* and M3 roots and crowns are significantly larger in *Aotus* than *Saimiri*. Results indicate that both *Cebus* and *Saimiri* have smaller M3s than their relative, *Aotus,* a trait that has been observed in past studies (Kinzey, 1974; Rosenberger, 1992; Spencer, 1995). Furthermore, *C. apella* has significantly larger premolar roots and crowns than either *Saimiri* or *Aotus*, as predicted by Hypothesis 1b.

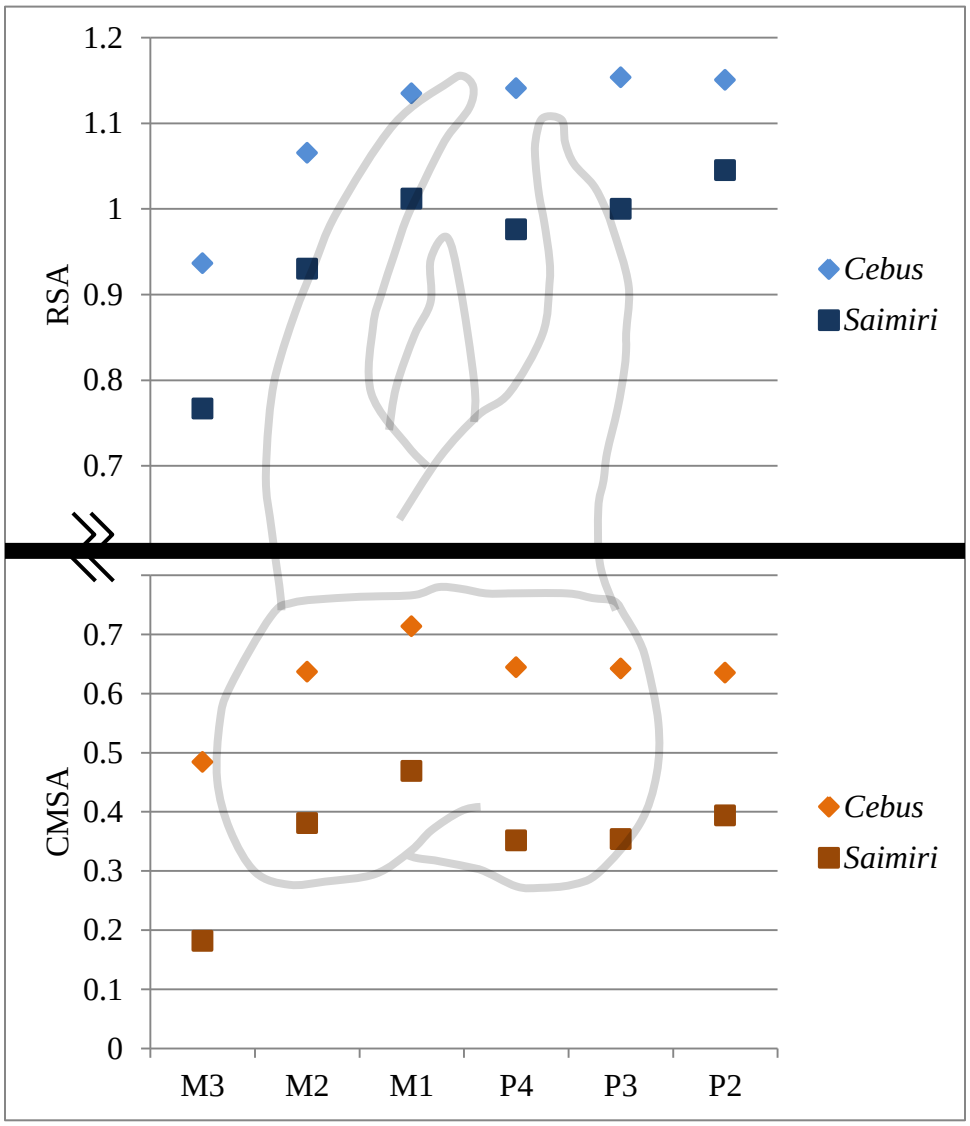

Fig. 5.2a. *Cebus/Saimiri* compared. See text for details.

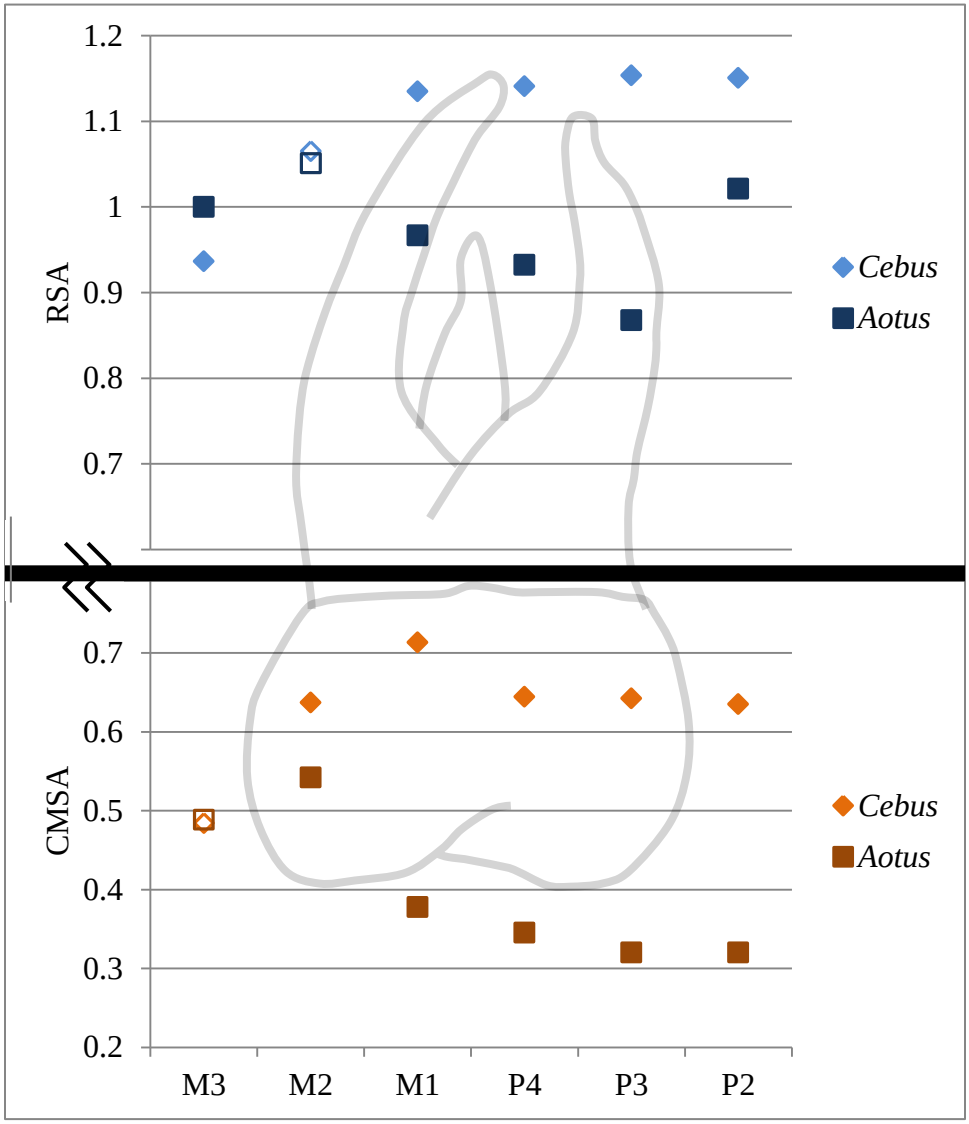

Fig. 5.2b. *Cebus*/*Aotus* compared. See text for details.

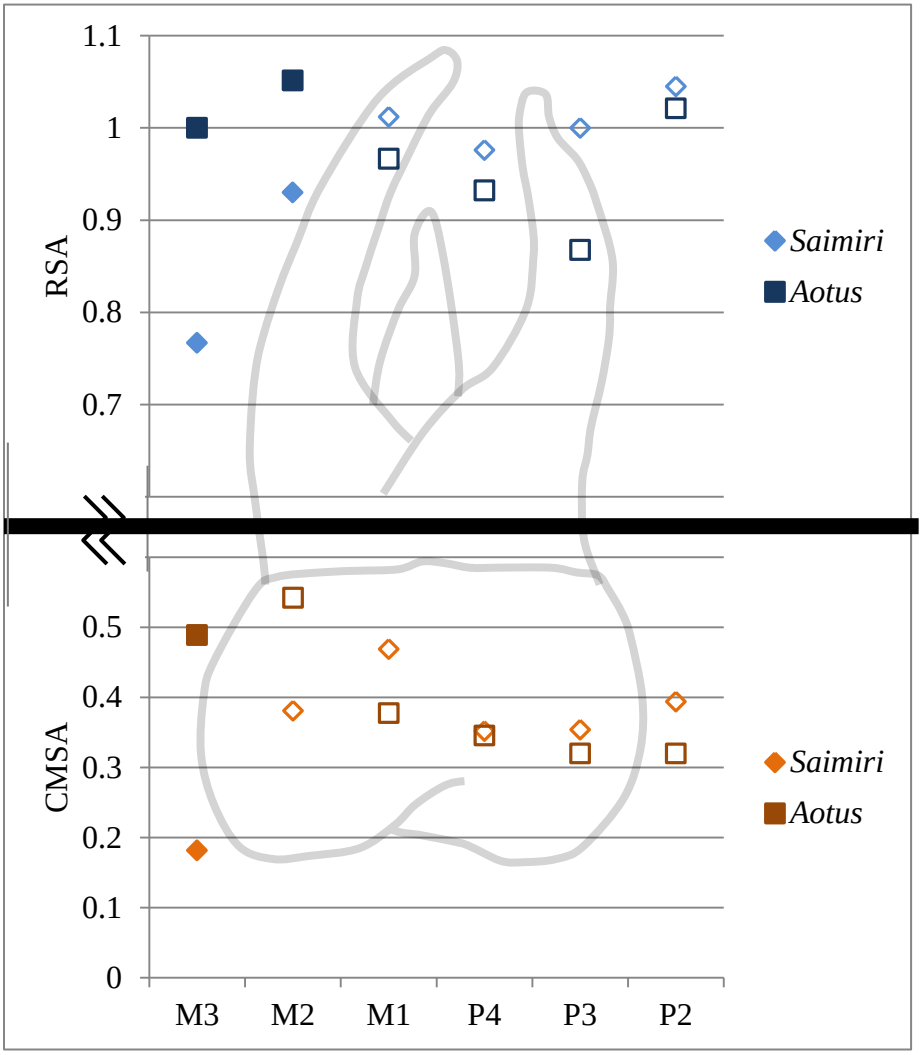

Fig. 5.2c. *Saimiri/Aotus* compared. See text for details.

Within the genus *Cebus*, *C. apella* and *C. capucinus* were compared using a Mann-Whitney U test (Figure 5.3). *C. apella* was predicted to have higher values for RSA and CMSA on premolar teeth relative to *C. capucinus*. *C. apella* has significantly larger root surface area and cervical margin surface area than *C. capucinus* for P2-M1, but *C. capucinus* M3 is significantly larger in both RSA and CMSA. M2 shows no differences in root or crown size between species.

Among pitheciins, *Callicebus moloch*, *Pithecia sp.* and *Chiropotes satanas* were compared (Figures 5.4a, b, and c). As discussed in Chapter 3, *C. moloch* is classified as having a soft food diet relative to both *Pithecia* and *Chiropotes* and was predicted to have smaller relative CMSA and RSA values for all postcanine teeth. *Pithecia* has larger crowns than *C. moloch* for P2-P4 and M3; *C. moloch* has a significantly larger M1 crown. There is no significant difference in root size between *C. moloch* and *Pithecia*. *Chiropotes* has significantly larger CMSA and RSA values than *C. moloch* for premolars, but there are no significant differences between the two species for M1-M3.

Both *Pithecia* and *Chiropotes* are categorized as resistant food eaters, but *Pithecia* was predicted to have higher values for molar root and crown size due to its increased reliance on processing tough leaves with its molar teeth relative to *Chiropotes*. Additionally, *Chiropotes* was predicted to have larger premolar RSA and CMSA than *Pithecia* due to its relative increase in reliance on hard foods that are processed with the canine and premolar teeth.

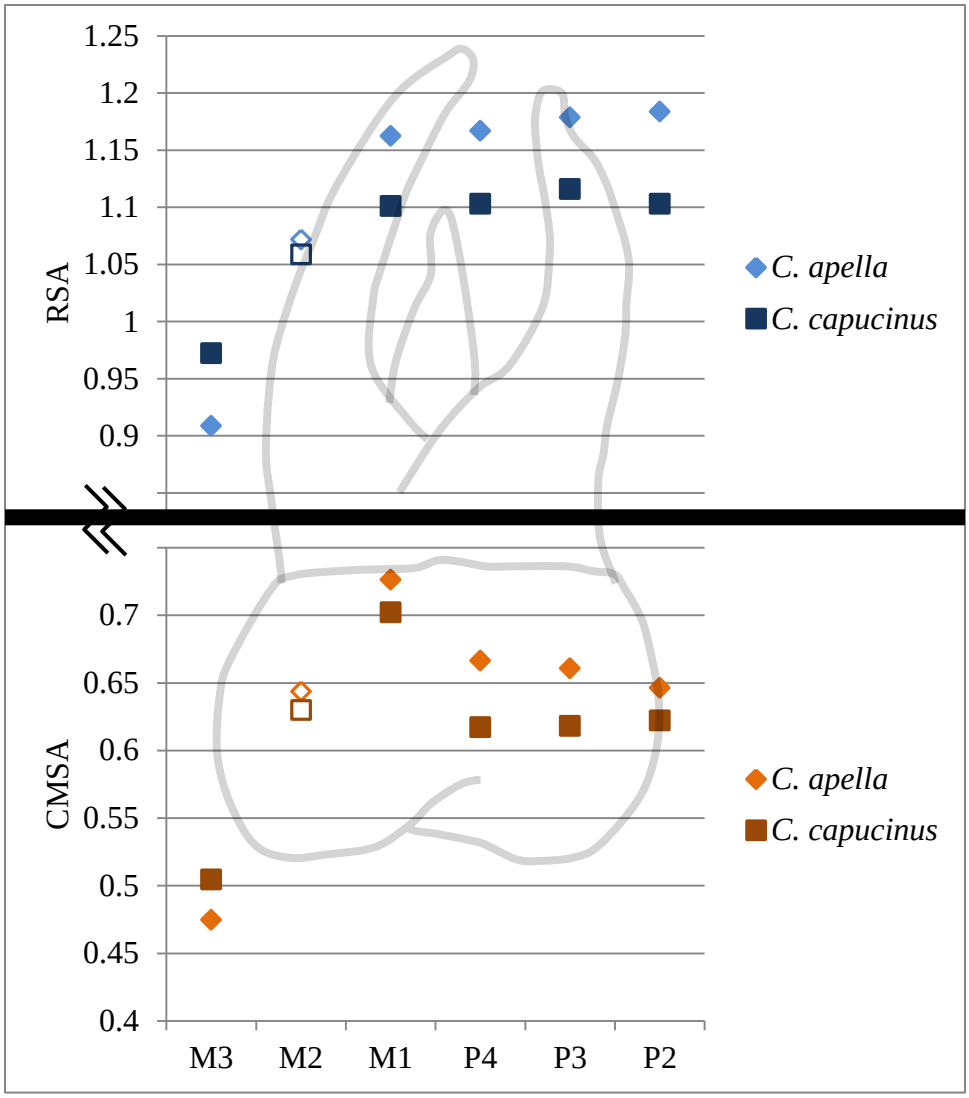

Fig. 5.3. *C. apella/C. capucinus* compared. See text for details.

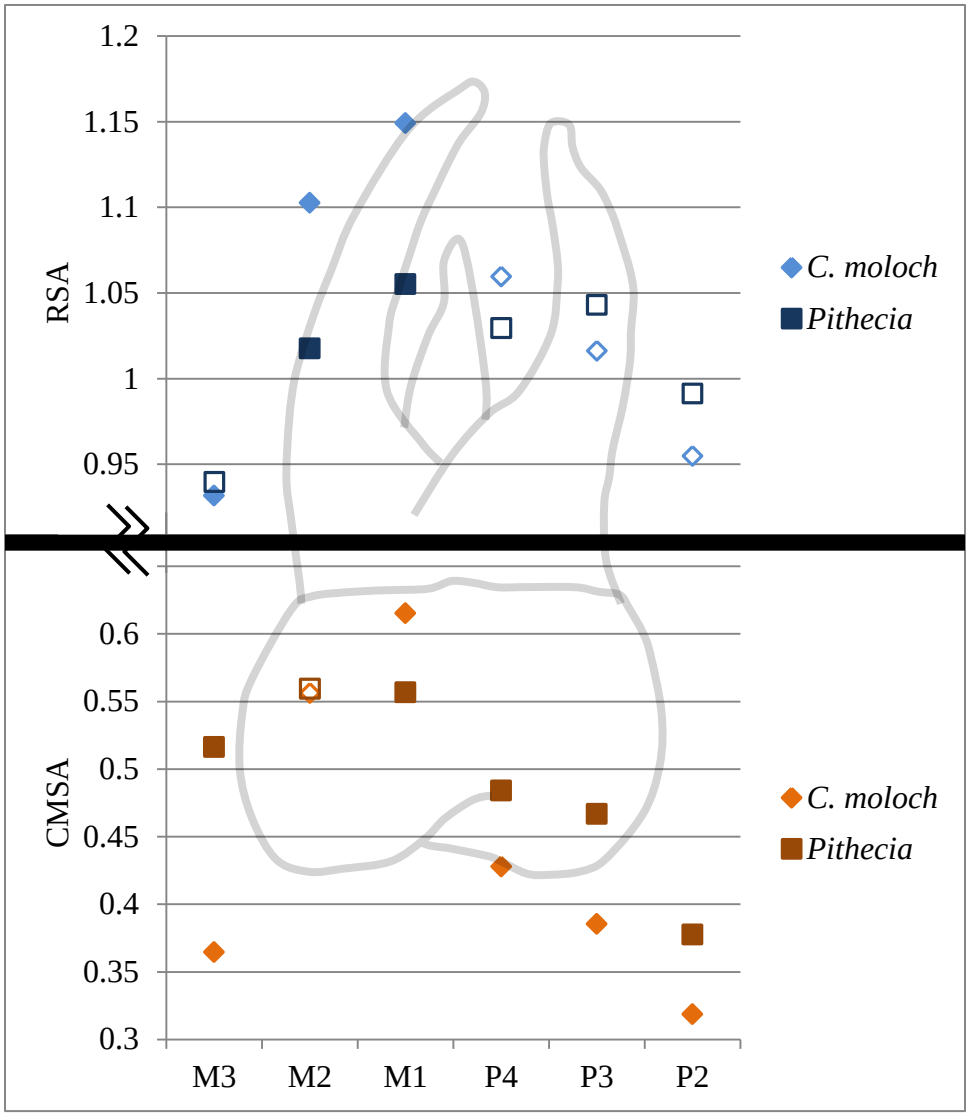

Fig. 5.4a. *C. moloch/Pithecia sp.* compared. See text for details.

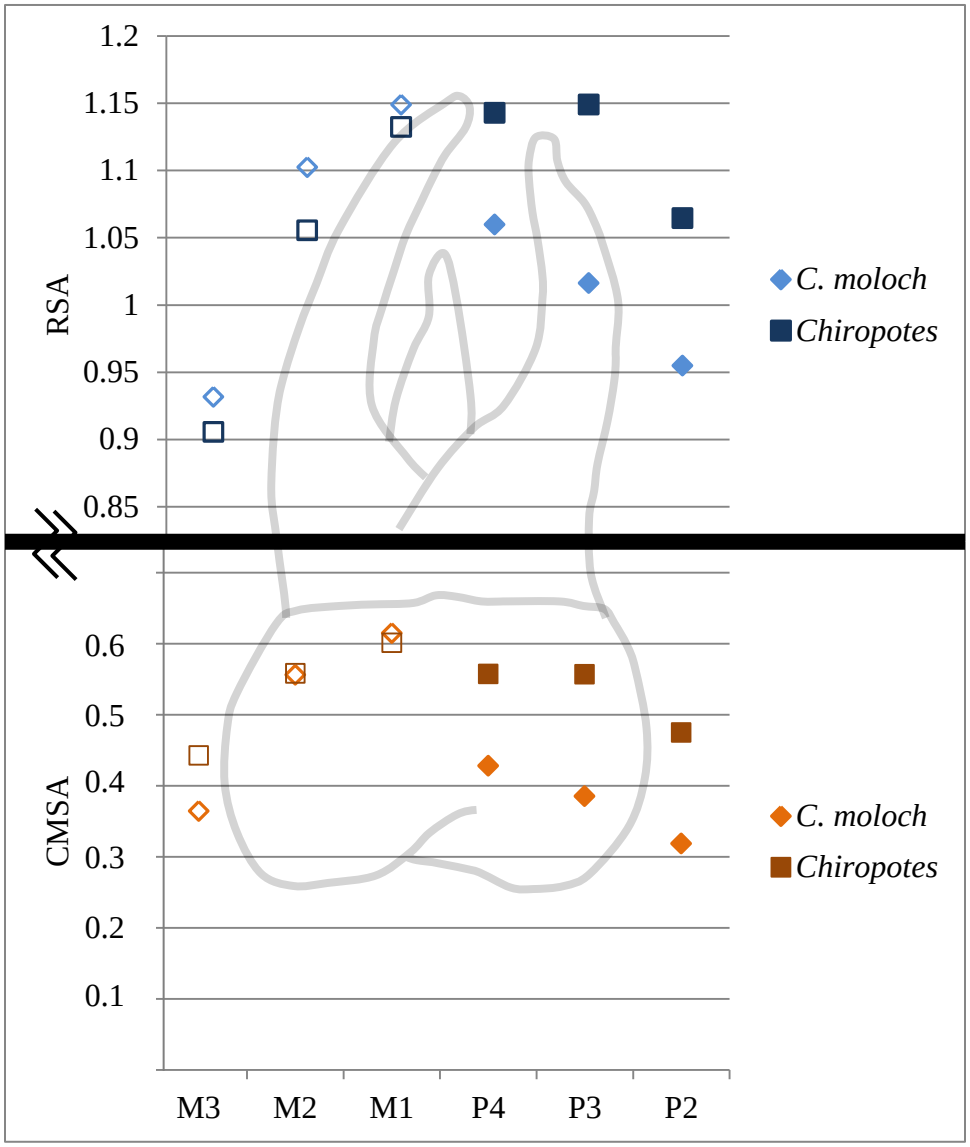

Fig. 5.4b. *C. moloch/Chiropotes* compared. See text for details.

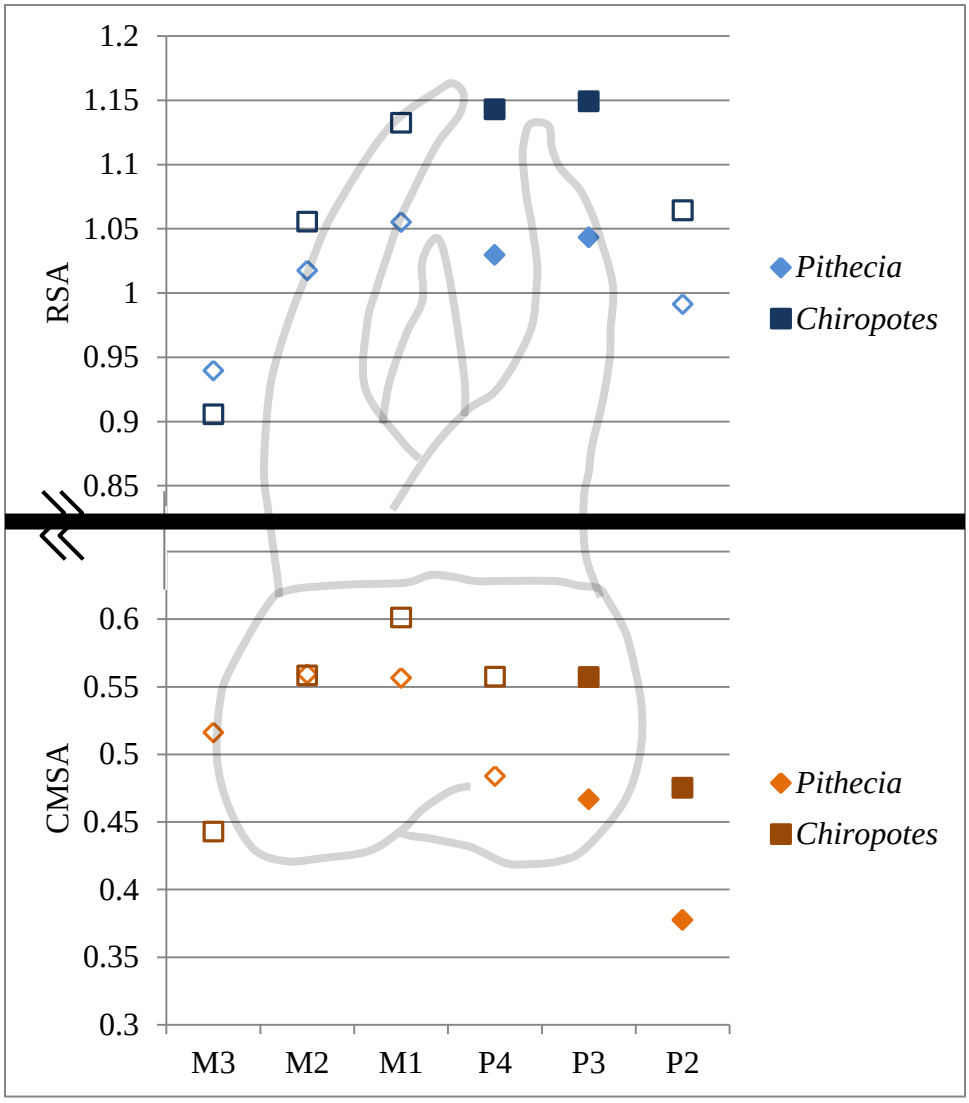

Fig. 5.4c. *Pithecia/Chiropotes* compared. See text for details.

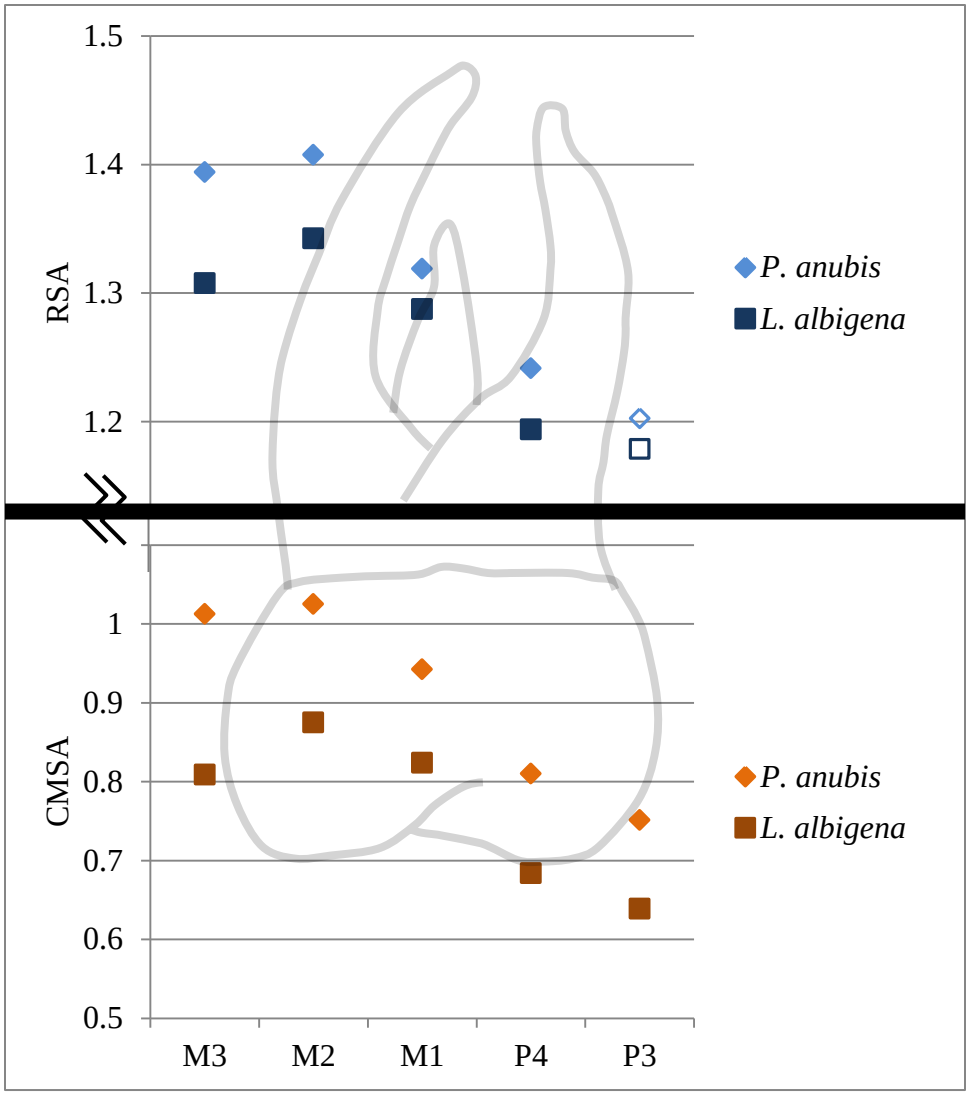

Fig. 5.5. *P. anubis/L. albigena* compared. See text for details.

CMSA was significantly larger in *Chiropotes* relative to *Pithecia* for P2 and P3, with no significant differences in crown size for the rest of the postcanine tooth row. RSA is significantly larger in *Chiropotes* relative to *Pithecia* for P3 and P4, with all other teeth showing no significant difference between the two species.

Papio anubis and *Lophocebus albigena* were compared (Figure 5.5) using a Mann-Whitney U test; it was predicted that *L. albigena* would have larger roots and crowns than *P. anubis*. However, results were opposite of what was predicted. For all teeth, *P. anubis* has significantly larger CMSA than *L. albigena*, and RSA is significantly larger in *P. anubis* for P4-M3. P3 RSA is not different between the two species.

Figure 5.6 depicts the results of the comparison between *Mandrillus sp.* and *Cercocebus torquatus*. *Mandrillus* was predicted to have higher values for tooth size than *C. torquatus*, and this prediction was upheld for CMSA on P3, M2, and M3. However, there was no difference between species in the CMSA of P4 and M1. Root size was not different between the two species, except for P3 in which RSA was significantly larger in *C. torquatus* than *Mandrillus*, contrary to predictions. In fact, while *Mandrillus* has larger postcanine tooth crowns than *C. torquatus*, *C. torquatus* roots are consistently larger than *Mandrillus* roots (although not at levels reaching statistical significance).

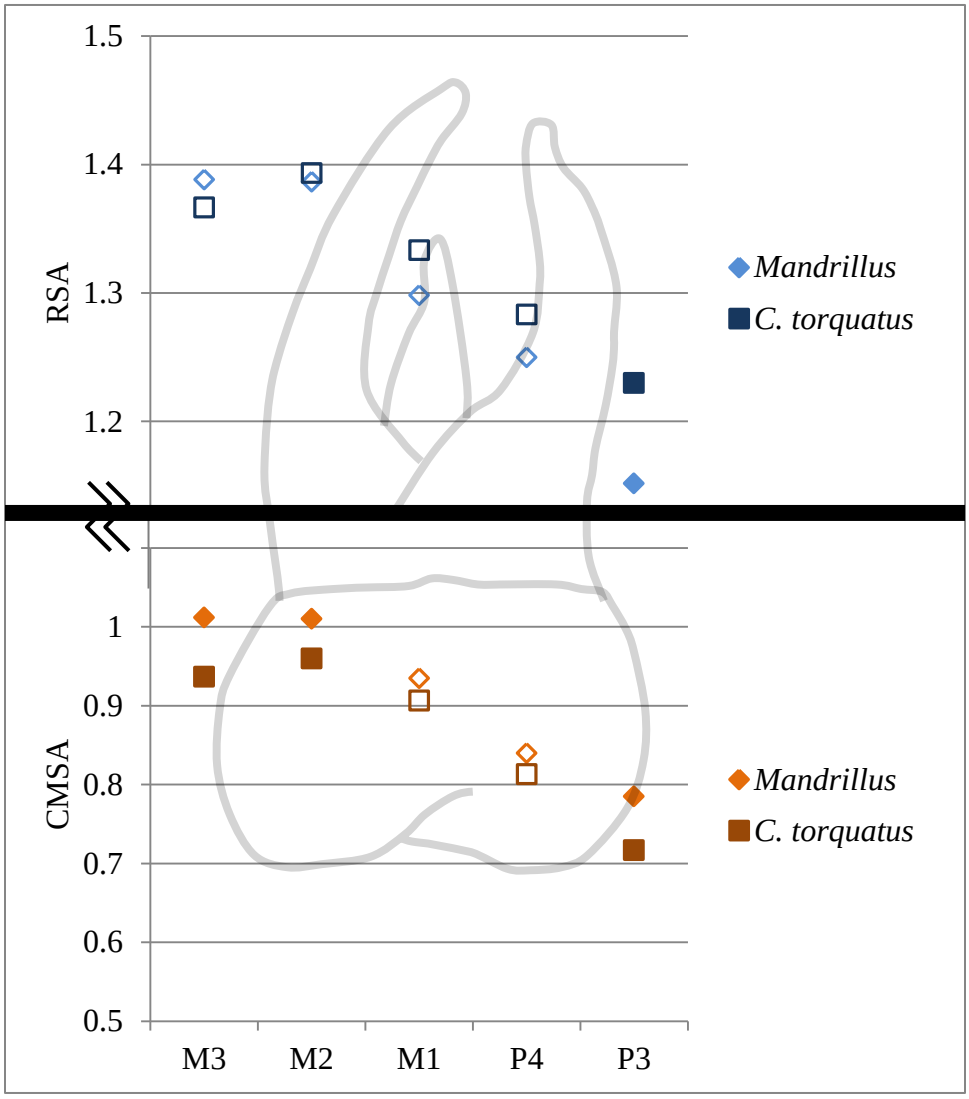

Fig. 5.6. *Mandrillus/C. torquatus* compared. See text for details.

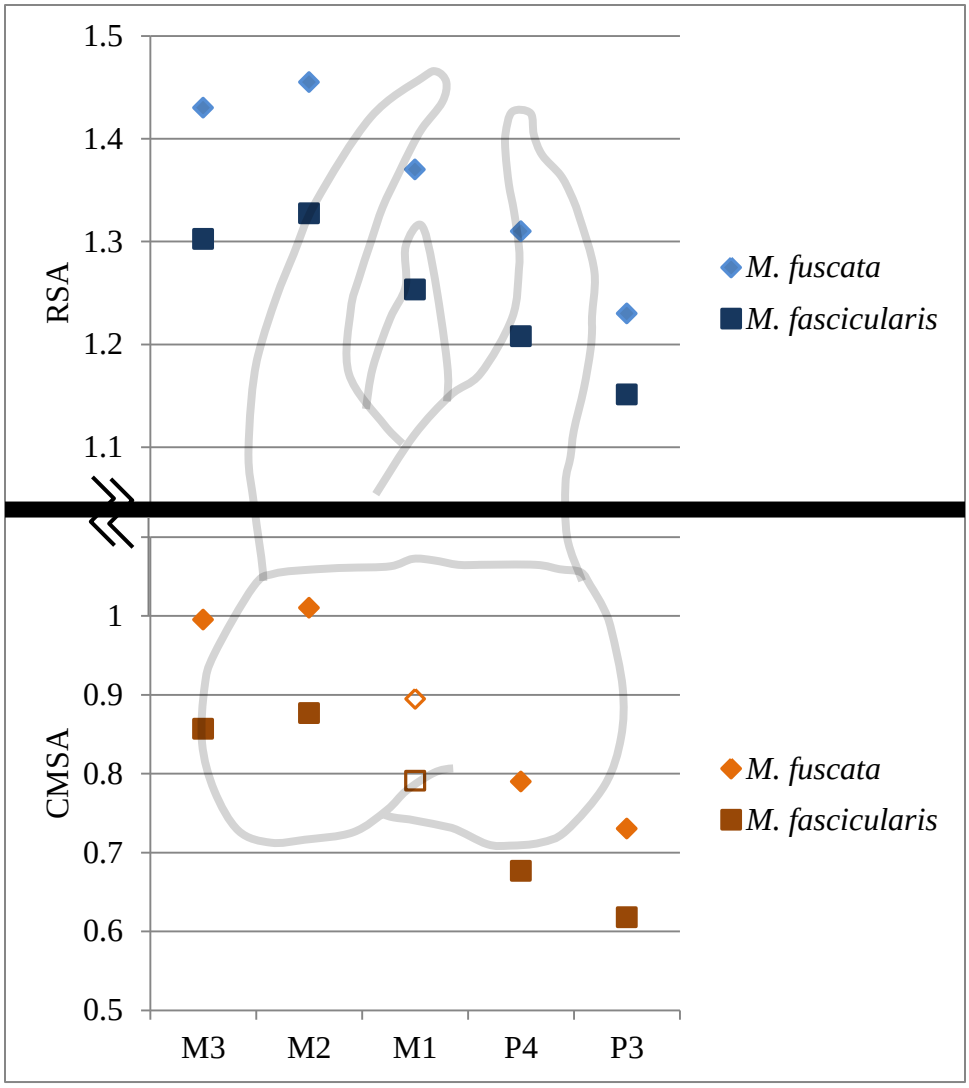

Fig. 5.7. *M. fuscata/M. fascicularis* compared. See text for details.

Macaca fuscata and *Macaca fascicularis* comparisons can be seen in Figure 5.7. *M. fuscata* has significantly larger CMSA values than *M. fascicularis* for all teeth except M1, which approaches, but does not reach, significance at p = 0.059. Root surface area is significantly larger in *M. fuscata* for all postcanine teeth, as predicted.

Colobus polykomos and *Piliocolobus badius* were compared (Figure 5.8), with *C. polykomos* predicted to have larger tooth roots and crowns than *P. badius*. *C. polykomos* has larger CMSA values than *P. badius* for all postcanine teeth. RSA was significantly larger in *C. polykomos* for M1 and M2, but no other teeth were significantly different for RSA between groups.

Within hominoids, *Gorilla gorilla* and *Pan troglodytes* were compared (Figure 5.9), with the expectation that RSA and CMSA values be higher in *Gorilla*. *Gorilla* values for CMSA were significantly larger than *Pan* with the exception of M1. RSA values for *Gorilla* were significantly larger than *Pan* for all teeth except for P3.

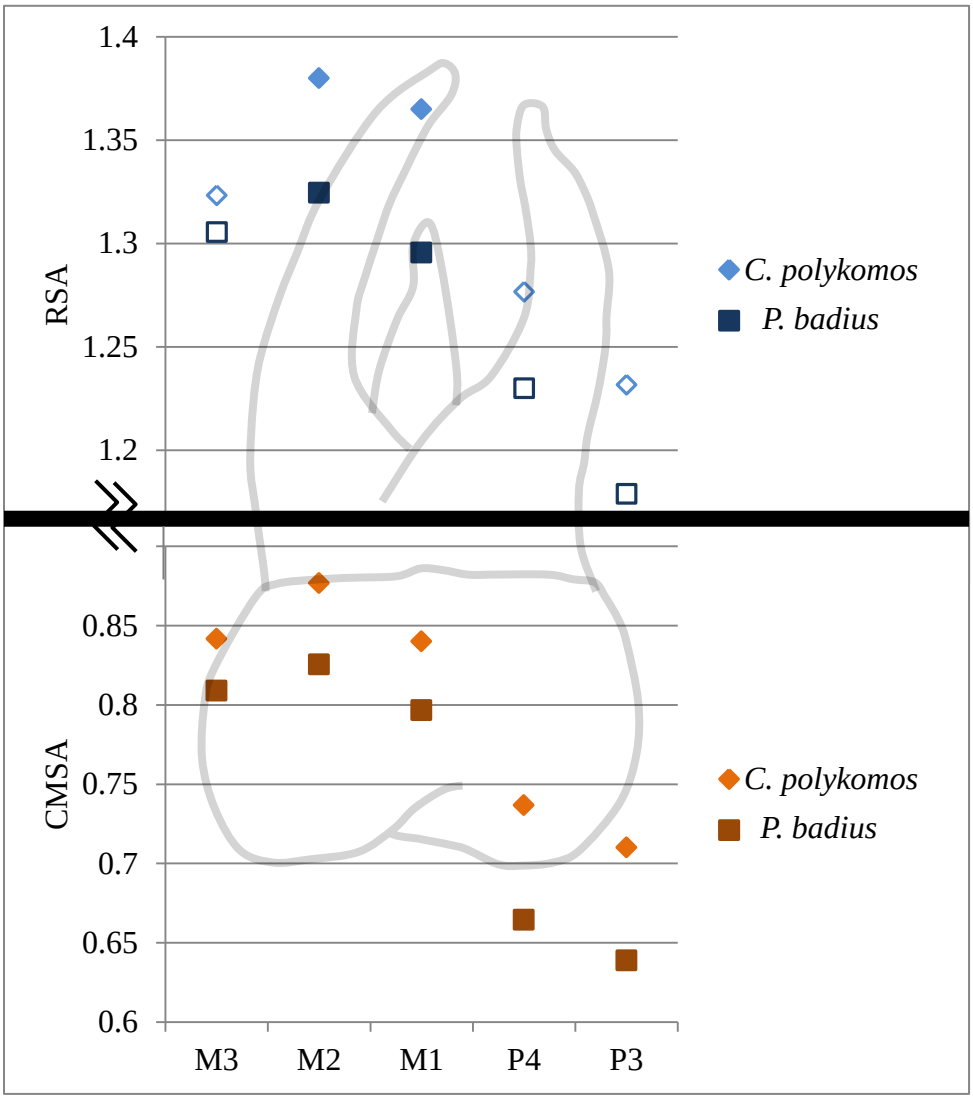

Fig. 5.8. *C. polykomos/P. badius* compared. See text from details.

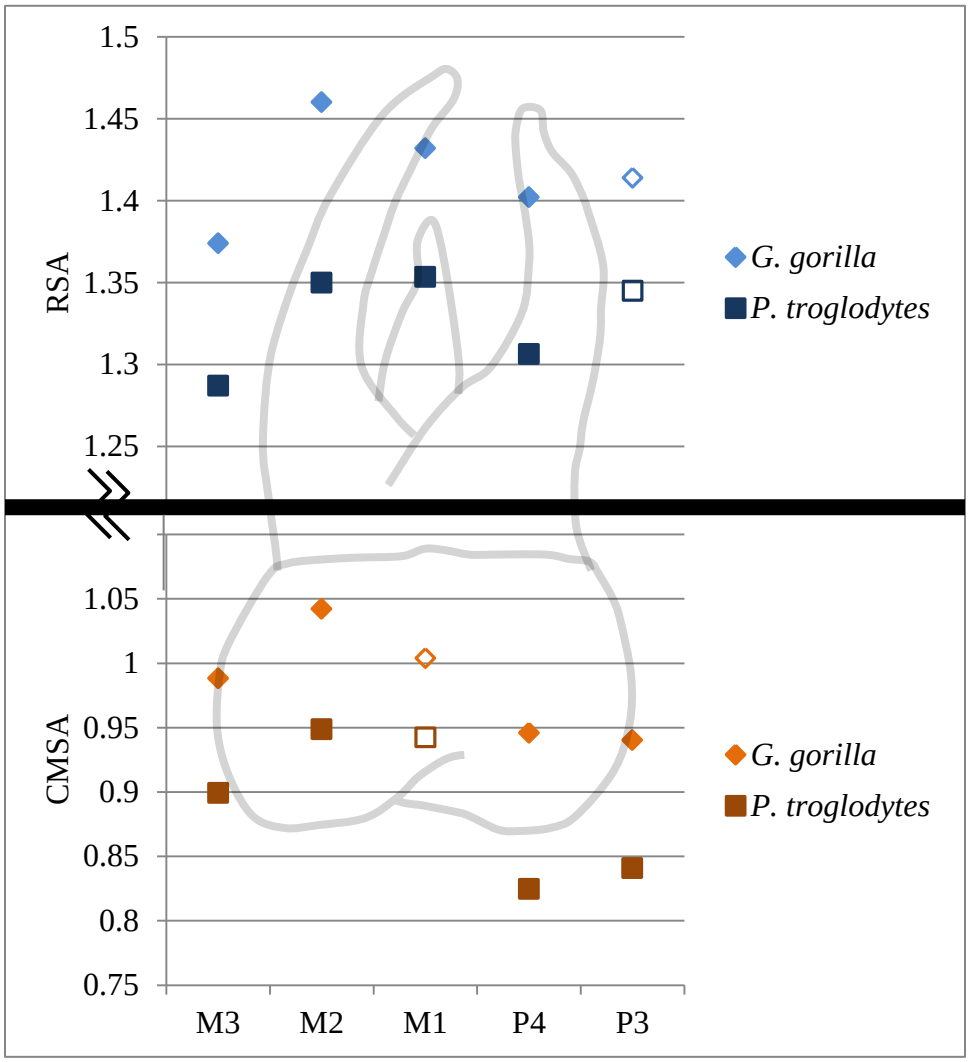

Fig. 5.9. *G. gorilla/P. troglodytes* compared. See text for details.

Hypothesis 1b: Discussion

Comparative analysis largely supports the predictions of Hypothesis 1b; primates with mechanically resistant diets tend to have larger tooth roots and crowns than close relatives with softer diets. However, results are not unequivocal. The pitheciins and the African papionins demonstrate notable deviations from predicted outcomes.

Results among pitheciins show a clear increase in premolar root and crown size in *Chiropotes sp.* relative to *C. moloch* and *Pithecia sp*., an observation that is consistent with the results of past research (Kinzey, 1992; Rosenberger, 1992; Spencer, 1995), and is likely a product of emphasizing the production of high bite forces at the anterior end of the postcanine tooth row. *Pithecia sp*., in contrast, shows no consistent difference in relative molar size compared to *Chiropotes sp*. or *C. moloch,* contrary to predictions. Spencer (1995) reported relatively small M3s in *Chiropotes* relative to *Pithecia sp*., a pattern that is apparent in the current study, but not statistically significant. Taken together, results from past and current analyses support Spencer's (1995) suggestion that selection for a targeted increase in force production on relatively anterior dentition in *Chiropotes sp*. may have resulted in an increase in premolar size at the cost of molar size.

Furthermore, the lack of differentiation in molar size between *Pithecia sp*. and *Chiropotes sp*. could be due to the fact that tooth size is predicted to increase when eating hard objects, like seeds (favored by *Chiropotes*), but not necessarily for tough objects, like leaves (favored by *Pithecia*) (Lucas et al., 1984; Lucas,

2004). Instead, food toughness is more closely related to tooth shape (e.g., the presence and size of shearing crests) (Kay, 1979, Lucas et al., 1984; Lucas, 2004). If this is the case, then comparing tooth size in an effort to distinguish the selection pressures of a tough food versus a hard food diet is inappropriate. Future work should measure both occlusal shape and size to determine the extent to which either is related to food hardness and toughness.

Among African papionins, *Mandrillus sp.* was predicted to have larger roots and crowns than *C. torquatus*. While this prediction was more or less upheld for crown size, *Mandrillus sp.* tooth roots are not significantly larger than *C. torquatus* roots. In fact, *C. torquatus* has larger average premolar root size than *Mandrillus*, although only the P3 root is significantly larger. Though *L. albigena* was predicted to have larger root and crown dimensions than *P. anubis*, *P. anubis* has significantly larger tooth roots and crowns than *L. albigena*. The failure of the predictions of Hypothesis 1b are apparent in the African papionins, where each species compared is known for having a mechanically resistant diet. Despite evidence that within African papionins there may be differences in diet related to food mechanical properties (discussed in Chapter 3), such differences, if they exist at all, are too small to be discerned by the current study protocols. Currently, there is no good way to distinguish "hard food eaters" from "harder food eaters" using dental data alone.

Results of the current comparative analyses suggest that food mechanical properties influence tooth size such that primates that consume a resistant diet typically have larger tooth roots and crowns than primates that consume a soft

diet. Furthermore, results support the suggestion that selection for concentrating high magnitude bite forces at the anterior end of the postcanine tooth row may result in the acquisition of enlarged premolars and small M3s like those seen in *Chiropotes* (Spencer, 1995).

CHAPTER 6

PART II: DENTAL FEATURES AND BITE FORCE PATTERNS

RESULTS AND DISCUSSION

In Chapter 4, it was shown that tooth root and crown size are highly correlated with skull size and one another across primates, and that some variation in root and crown size cannot be explained by skull size alone. In Chapter 5, it was shown that root and crown size are highly positively correlated along the tooth row in anthropoids. Furthermore, results from Chapter 5 support the hypothesis that root and crown size vary according to dietary category such that primates with a resistant diet have larger tooth roots and crowns than closely-related primates with a soft diet. Taken together, these results suggest that tooth root and crown surface area may be related to the production of masticatory force.

Part II of the current study focuses on determining the relationship between patterns of bite force and patterns of tooth root and crown size along the postcanine tooth row. Hypotheses 2 and 3 state that teeth that are habitually loaded with high magnitude forces will have larger roots and crowns, respectively, than teeth that experience lower magnitudes of force. Data on tooth root and crown size were collected from 3D models of teeth derived from μCT scans of primate skulls and compared with bite force curves calculated for each skull based on measurements taken from landmark data (discussed in detail in Chapter 3). Hypotheses 2 and 3 were tested using Kendall's τ to determine whether patterns of root size (RSA) and crown size (CMSA as a functional proxy) matched patterns of bite force (the bite force curve, BFC).

Bite force patterns: Results

Bite force curves were calculated based on measurements of masticatory parameters outlined in Chapter 3. Tables 6.1 - 6.6 show the measurements taken from landmark data on platyrrhines (6.1 – 6.3) and catarrhines (6.4 - 6.6), respectively. Measurements of basic masticatory parameters are located in Tables 6.1 (platyrrhines) and 6.4 (catarrhines). Recall that muscle resultant position in the current study is estimated by using the horizontal distance from the TMJ to M3 in the occlusal plane (b_H *M3)*, except in callitrichids in whom it is estimated using M2 (b_H *M2*). Both horizontal bite force moment arm (b_H) and normal bite force moment arm (b_N) were measured for platyrrines (Tables 6.2 and 6.3, respectively) and catarrhines (Tables 6.5 and 6.6, respectively). For discussion of equations used in bite force curve calculations, see Chapter 3.

TABLE 6.1. Platyrrhine masticatory system measurements (mm).

Species	Specimen	Bicondylar breadth	Palate breadth	Glenoid height	Muscle resultant position	Muscle resultant angle
A. caraya	25812	47.23	30.96	30.28	36.77	91.83
A. caraya	28095	49.09	31.10	21.21	36.84	87.78
A. caraya	28096	38.27	27.36	10.68	25.80	82.51
A. caraya	28655	43.29	27.84	19.46	27.44	84.78
A. caraya	28654	50.93	30.83	25.67		84.52
A. palliata	29609	40.52	27.12	16.01	24.34	80.08
A. palliata	29611	45.69	25.54	26.19	26.98	80.79
A. palliata	5323	46.56	29.23	22.97	29.67	80.12
A. palliata	5327	46.57	28.39	19.18	27.72	80.97
A. palliata	5328	45.50	26.21	18.23	29.63	107.36
A. palliata	5329	48.25	26.00	22.00	30.53	114.62
A. palliata	5331	44.38	29.06	17.91	30.63	80.09
A. palliata	5325	41.34	26.61	18.78		81.98
A. palliata	6001	42.40	26.77	14.51		76.00
A. palliata	5324	37.38	31.41	20.39	30.14	74.49
Aotus	19801	25.69	15.92	6.01	14.41	92.23
Aotus	19802	26.28	16.27	4.06	14.66	83.30
Aotus	19805	26.32	15.54	3.83	13.57	64.22
Aotus	27214	25.08	15.96	4.20	12.39	81.93
Aotus	30562	24.58	14.94	4.26	14.66	87.23
Aotus	39571	27.99	16.54	6.06	17.18	81.56
Aotus	52608	26.75	14.31	5.14	14.11	81.86
Aotus	8472	24.39	16.05	4.71	13.00	77.98
Aotus	B-8042	26.23	15.67	4.32	15.21	117.52
Aotus	B-8043	25.67	15.23	2.90	14.11	61.62
Ateles	10138	45.65	25.40	5.31	29.49	79.14
Ateles	29628	44.92	26.08	8.22	23.73	76.49
Ateles	34322	47.27	26.30	11.58	32.50	74.69
Ateles	5336	47.63	28.55	21.03	20.60	73.55
Ateles	5338	47.89	25.78	12.89	30.06	82.16
Ateles	5344	47.93	26.10	9.14	33.78	80.68
Ateles	5345	40.55	25.74	7.38	28.96	84.87

(cont)

TABLE 6.1 (cont). Platyrrhine masticatory system measurements (mm).

Species	Specimen	Bicondylar breadth	Palate breadth	Glenoid height	Muscle resultant position	Muscle resultant angle
Ateles	5346	42.65	26.78	8.35	29.71	79.16
Ateles	5350	47.01	27.10	10.69	29.07	78.09
Ateles	5351	46.25	28.25	7.74	32.58	106.82
Ateles	5352	41.37	26.06	8.02	27.25	81.45
Ateles	5353	43.98	25.64	8.63	29.35	78.28
Ateles	5354	44.80	24.04	10.02	28.64	78.34
Ateles	5355	42.30	27.35	9.57	28.71	78.47
C. apella	30162	41.95	24.39	11.14	24.38	81.70
C. apella	30166	40.47	24.26	8.50	21.34	86.51
C. apella	30724	42.32	25.01	6.78	23.23	87.39
C. apella	30726	38.10	22.47	5.08	19.37	79.92
C. apella	31064	40.82	24.83	8.21	22.55	77.05
C. apella	31072	40.69	22.76	8.95	21.27	79.40
C. apella	32049	38.92	24.75	5.26	20.72	80.99
C. apella	37831	43.26	24.09	8.93	25.06	80.50
C. apella	49635	42.58	23.74	6.60	26.79	112.94
C. apella	25811	45.59	27.15	8.04		84.00
C. apella	41090	43.16	23.36	8.18		72.25
C. capucinus	10135	40.07	24.24	6.22	20.24	74.23
C. capucinus	10136	42.58	24.31	3.86	23.03	76.69
C. capucinus	34323	39.07	24.06	6.81	24.01	75.95
C. capucinus	34326	44.52	24.72	5.92	23.92	69.16
C. capucinus	34353	43.84	24.63	9.55	22.73	73.10
C. capucinus	5332	44.25	24.98	6.47	25.07	79.68
C. capucinus	7317	42.99	23.67	3.41	26.40	75.58
C. capucinus	7322	39.98	23.28	5.79	21.22	77.05
C. capucinus	7323	40.82	23.21	4.25	22.97	78.11
Cacajao	27870	42.53	23.48	9.47		78.01
Callicebus	20186	27.57	15.73	5.11	16.59	86.21
Callicebus	20188	28.13	16.10	4.70	17.63	76.10
Callicebus	26922	29.95	16.40	7.62	17.87	70.43
Callicebus	30559	29.82	16.30	5.68	16.63	61.85

(cont)

TABLE 6.1 (cont). Platyrrhine masticatory system measurements (mm).

Species	Specimen	BB	Palate breadth	Glenoid height	Muscle resultant position	Muscle resultant angle
Callicebus	30564	26.91	15.39	5.04	15.99	82.37
Callicebus	30566	27.68	15.71	6.50	15.98	90.43
Callicebus	32380	30.11	16.91	5.85	19.18	84.18
Callicebus	32383	27.55	16.74	5.99	17.23	91.09
Callicebus	37828	28.09	16.52	7.20	16.64	93.34
Callicebus	39073	26.28	15.65	6.10	17.33	93.65
Callicebus	39563	27.71	15.95	6.63	16.67	90.74
Callithrix sp.	30580	19.07	11.85	2.65	12.16	80.51
Callithrix sp.	30582	19.42	11.74	1.70	12.31	70.94
Callithrix sp.	30583	20.10	12.26	1.38	14.44	73.18
Callithrix sp.	32164	18.66	12.32	2.53	13.30	70.92
Callithrix sp.	32165	18.93	11.92	2.52	12.00	73.20
Callithrix sp.	34573	19.31	12.34	1.23	12.56	74.08
Callithrix sp.	30577	17.94	12.08	2.64	11.05	69.79
Callithrix sp.	30586	19.22	11.46	2.29	13.16	71.79
Callithrix sp.	30603	20.85	12.04	2.94	13.19	72.82
Callithrix sp.	37826	19.36	12.98	1.20	13.35	72.71
Callithrix sp.	37823	19.90	12.28	1.86	13.35	72.66
Callithrix sp.	440	21.38	12.24	2.81	12.23	69.64
Callithrix sp.	7165	19.30	10.63	4.28	12.33	46.83
Chiropotes	31701	36.37	20.03	7.35	20.68	78.53
Chiropotes	6028	36.22	19.96	6.10	23.04	75.74
Pithecia sp.	27124	33.61	18.41	5.68	22.78	79.53
Pithecia sp.	30720	30.90	17.32	6.19	20.04	74.73
Pithecia sp.	20265	36.05	16.76	8.74		70.02
Pithecia sp.	30719	32.95	18.65	6.58	22.54	75.41
Pithecia sp.	31061	33.16	17.16	5.60	20.76	76.56
Saguinus sp.	15324	22.83	13.22	1.19	13.06	73.15
Saguinus sp.	27331	18.43	12.49	2.69	12.24	78.69
Saguinus sp.	30579	19.54	13.36	2.16	13.02	74.78
Saguinus sp.	30601	21.17	13.64	1.17	12.74	61.27
Saguinus sp.	41567	20.71	12.56	0.82	13.79	71.31

(cont)

TABLE 6.1 (cont). Platyrrhine masticatory system measurements (mm).

Species	Specimen	Bicondylar breadth	Palate breadth	Glenoid height	Muscle resultant position	Muscle resultant angle
Saguinus sp.	41568	19.43	13.55	1.12	12.62	72.34
Saguinus sp.	52557	20.70	12.91	0.38	13.30	81.31
Saguinus sp.	52558	21.11	13.41	2.45	14.23	67.60
Saguinus sp.	52616	21.42	12.83	2.96	13.65	71.83
Saimiri sp.	29488	27.41	14.97	1.97	14.22	74.93
Saimiri sp.	10131	24.49	15.01	4.77		71.74
Saimiri sp.	10134	26.54	14.88	4.37		75.24
Saimiri sp.	30568	22.73	14.67	3.43	10.50	68.35
Saimiri sp.	30569	24.48	14.59	5.26	13.69	64.64
Saimiri sp.	20187	26.87	15.84	3.03	15.50	58.63

TABLE 6.2. Platyrrhine b_H measurements (mm).

Species	Specimen	M3	M2	M1	P4	P3	P2
A. caraya	25812	36.77	44.25	50.94	55.65	60.72	66.33
A. caraya	28095	36.84	43.88	50.88	56.81	61.00	66.06
A. caraya	28096	25.80	32.52	38.62	43.02	48.11	52.52
A. caraya	28655	27.44	33.98	40.70	45.46	49.90	54.15
A. caraya	28654		47.31	55.31	60.40	65.43	70.52
A. palliata	29609	24.34	31.21	37.71	42.52	48.04	52.51
A. palliata	29611	26.98	32.85	39.99	45.38	50.22	54.40
A. palliata	5323	29.67	36.25	42.65	48.04	53.64	58.00
A. palliata	5327	27.72	34.10	41.21	46.28	51.52	56.22
A. palliata	5328	29.63	35.41	41.52	47.58	51.92	56.03
A. palliata	5329	30.53	36.59	43.87	48.22	52.47	57.01
A. palliata	5331	30.63	37.51	44.26	49.24	52.74	58.23
A. palliata	5325		28.26	35.52	41.43	45.37	49.82
A. palliata	6001		33.63	40.39	45.73	50.76	55.08
A. palliata	5324	30.14	36.66	43.11	48.02	53.47	63.95
Aotus	19801	14.41	17.27	20.21	22.49	24.45	26.95
Aotus	19802	14.66	17.63	20.73	22.97	25.14	27.15
Aotus	19805	13.57	16.19	19.22	21.24	23.77	25.60
Aotus	27214	12.39	15.01	17.96	20.73	22.71	24.85
Aotus	30562	14.66	16.95	19.52	22.24	23.71	26.02
Aotus	39571	17.18	19.91	22.93	24.81	26.89	28.66
Aotus	52608	14.11	17.04	20.07	22.27	24.21	26.37
Aotus	8472	13.00	15.64	18.57	20.47	22.66	24.56
Aotus	B-8042	15.21	17.57	20.51	22.21	24.13	26.56
Aotus	B-8043	14.11	16.80	19.30	21.86	23.82	25.27
Ateles	10138	29.49	34.19	38.63	42.95	45.65	48.36
Ateles	29628	23.73	28.45	33.50	37.05	40.31	43.78
Ateles	34322	32.50	36.90	41.25	44.59	48.13	51.60
Ateles	5336	20.60		35.54	40.25	43.71	48.50
Ateles	5338	30.06	34.75	38.40	42.19	45.36	
Ateles	5344	33.78	37.95	43.02	46.55	49.90	54.10
Ateles	5345	28.96	33.35	38.22	42.37	45.52	49.41

(cont)

TABLE 6.2 (cont). Platyrrhine b_H measurements (mm).

Species	Specimen	M3	M2	M1	P4	P3	P2
Ateles	5351	32.58	36.06	41.27	45.80	48.45	52.07
Ateles	5352	27.25	31.46	36.10	39.76	43.12	47.05
Ateles	5353	29.35	33.65	38.22	42.35	46.03	49.62
Ateles	5354	28.64	32.61	36.91	40.32	44.22	47.67
Ateles	5355	28.71	33.32	38.22	42.23	46.82	49.09
C. apella	30162	24.38	27.94	31.59	34.92	39.40	42.35
C. apella	30166	21.34	24.83	29.03	32.73	37.04	39.82
C. apella	30724	23.23	26.80	30.60	34.81	37.67	40.89
C. apella	30726	19.37	23.15	27.11	31.27	33.95	38.12
C. apella	31064	22.55	26.52	30.39	33.95	37.32	40.40
C. apella	31072	21.27	24.74	28.95	32.82	35.63	39.31
C. apella	32049	20.72	23.42	27.92	31.86	34.82	37.93
C. apella	37831	25.06	28.28	32.41	36.78	40.59	43.52
C. apella	49635	26.79	30.16	34.10	37.51	41.35	45.40
C. apella	25811		30.10	35.06	38.97	42.74	46.37
C. apella	41090		27.67	32.49	35.22	38.46	41.90
C. capucinus	10135	20.24	23.70	27.94	31.69	35.40	37.91
C. capucinus	10136	23.03	25.95	30.07	33.95	37.88	40.27
C. capucinus	34323	24.01	27.13	31.53	34.83	38.47	41.20
C. capucinus	34326	23.92	27.68	31.89	35.76	39.27	42.84
C. capucinus	34353	22.73	26.88	31.58	35.17	38.03	43.07
C. capucinus	5332	25.07	28.32	32.75	37.08	39.38	43.75
C. capucinus	7317	26.40	29.50	33.86	37.73	40.52	43.76
C. capucinus	7322	21.22	24.90	29.32	32.56	35.94	39.17
C. capucinus	7323	22.97	26.81	31.36	35.26	37.97	
Cacajao	27870		32.41	36.06	40.28	42.33	45.93
Callicebus	20186	16.59	19.79	22.84	25.28	27.52	29.03
Callicebus	20188	17.63	20.79	23.94	26.35	28.59	30.70
Callicebus	26922	17.87	20.69	24.13	26.67	28.86	31.20
Callicebus	30559	16.63	18.99	22.07	24.68	26.48	28.74
Callicebus	30564	15.99	18.43	22.01	24.57	27.33	29.28
Callicebus	30566	15.98	18.61	22.15	24.61	27.13	29.21
Callicebus	32380	19.18	21.83	24.92	27.77	30.37	32.20
Callicebus	32383	17.23	19.84	22.84	25.44	27.27	29.81

(cont)

TABLE 6.2 (cont). Platyrrhine b_H measurements (mm).

Species	Specimen	M3	M2	M1	P4	P3	P2
Callicebus	37828	16.64	19.18	22.49	25.20	27.60	30.36
Callicebus	39073	17.33	19.99	23.11	25.64	28.24	29.91
Callicebus	39563	16.67	19.55	22.64	25.73	27.78	
Callithrix sp.	30580		12.16	14.20	15.85	17.09	19.20
Callithrix sp.	30582		12.31	14.62	16.06	17.41	19.68
Callithrix sp.	30583		14.44	16.41	17.42	19.41	20.78
Callithrix sp.	32164		13.30	15.53	17.61	18.73	21.14
Callithrix sp.	32165		12.00	13.97	15.42	17.22	18.84
Callithrix sp.	34573		12.56	14.66	16.49	18.28	19.75
Callithrix sp.	30577		11.05	13.34	14.67	16.84	18.46
Callithrix sp.	30586		13.16	15.49	16.71	18.46	20.42
Callithrix sp.	30603		13.19	15.30	16.69	18.94	20.40
Callithrix sp.	37826		13.35	15.65	17.43	19.58	21.45
Callithrix sp.	37823		13.35	15.95	18.19	20.12	21.82
Callithrix sp.	440		12.23	14.96	16.51	18.29	20.09
Callithrix sp.	7165		12.33	14.28	15.56	17.58	18.90
Chiropotes	31701	20.68	23.34	26.51	29.78	32.91	36.00
Chiropotes	6028	23.04	25.46	28.74	31.96	34.00	36.80
Pithecia sp.	27124	22.78	25.15	28.48	31.29	33.80	36.26
Pithecia sp.	30720	20.04	22.48	25.91	28.05	30.96	33.07
Pithecia sp.	20265		25.52	28.81	31.02	32.81	
Pithecia sp.	30719	22.54	25.36	29.11	31.76	34.15	36.41
Pithecia sp.	31061	20.76	24.23	27.39	30.54	32.07	34.84
Saguinus sp.	15324		13.06	15.14	17.14	19.04	20.56
Saguinus sp.	27331		12.24	14.54	15.76	17.81	19.13
Saguinus sp.	30579		13.02	15.10	16.80	18.70	20.66
Saguinus sp.	30601		12.74	14.79	16.77	18.71	20.27
Saguinus sp.	41567		13.79	15.66	17.24	19.33	20.69
Saguinus sp.	41568		12.62	15.03	17.38	18.07	20.48
Saguinus sp.	52557		13.30	15.48	17.67	18.56	20.27
Saguinus sp.	52558		14.23	16.56	18.05	19.91	21.60
Saguinus sp.	52616		13.65	15.66	17.38	18.84	21.11
Saimiri sp.	29488	14.22	16.65	19.37	21.37	23.30	25.16
Saimiri sp.	10131		15.11	18.16	20.66	21.58	23.71

(cont)

TABLE 6.2 (cont). Platyrrhine b_H measurements (mm).

Species	Specimen	M3	M2	M1	P4	P3	P2
Saimiri sp.	10134		17.01	19.88	21.71	23.58	25.34
Saimiri sp.	30568	10.50	12.41	15.13	17.48	19.20	20.83
Saimiri sp.	30569	13.69	15.74	18.22	19.91	22.21	24.63
Saimiri sp.	20187	15.50	17.92	20.65	22.32	24.39	26.75

TABLE 6.3. Platyrrhine b_N measurements (mm).

Species	Specimen	M3	M2	M1	P4	P3	P2
A. caraya	25812	46.85	53.52	58.97	62.43	66.88	71.33
A. caraya	28095	41.77	48.41	54.42	59.49	62.96	67.08
A. caraya	28096	27.65	34.75	40.11	43.87	48.70	52.67
A. caraya	28655	33.55	39.40	45.06	48.72	52.49	56.22
A. caraya	28654		53.67	60.52	64.37	68.70	72.84
A. palliata	29609	28.00	34.99	40.64	44.21	48.81	52.60
A. palliata	29611	36.34	41.95	46.05	50.81	54.53	58.14
A. palliata	5323	36.95	43.02	48.54	52.58	57.47	61.03
A. palliata	5327	33.04	39.39	45.39	49.17	53.39	57.14
A. palliata	5328	34.47	40.04	44.59	50.44	53.45	57.06
A. palliata	5329	36.64	42.51	48.97	51.69	54.86	58.84
A. palliata	5331	34.91	41.75	47.57	51.67	53.80	58.76
A. palliata	5325		33.93	40.19	44.79	48.23	51.99
A. palliata	6001		37.21	43.35	47.90	52.31	56.01
A. palliata	5324	35.66	42.03	47.56	51.29	55.52	66.40
Aotus	19801	14.39	17.45	20.32	22.21	23.89	26.01
Aotus	19802	14.11	17.06	20.23	22.34	24.25	26.00
Aotus	19805	13.55	16.41	19.33	21.18	23.48	25.16
Aotus	27214	12.48	15.18	18.08	20.66	22.36	24.31
Aotus	30562	14.59	17.11	19.49	22.02	23.28	25.47
Aotus	39571	17.19	20.25	23.09	24.78	26.54	28.14
Aotus	52608	14.00	17.00	19.99	22.05	23.80	25.62
Aotus	8472	13.03	15.76	18.54	20.29	22.24	24.05
Aotus	B-8042	14.99	17.40	20.32	21.83	23.53	25.74
Aotus	B-8043	13.88	16.64	19.10	21.51	23.32	24.67
Ateles	10138	28.34	33.32	37.82	42.19	44.63	47.22
Ateles	29628	23.24	27.87	32.74	35.91	39.20	42.03
Ateles	34322	32.89	37.32	42.11	44.65	47.89	50.99
Ateles	5336	22.53		39.57	44.12	47.34	51.88
Ateles	5338	30.97	35.51	39.16	42.56	45.58	
Ateles	5344	33.84	38.05	42.99	46.34	49.47	53.56
Ateles	5345	28.97	33.45	38.21	42.20	45.13	48.77
Ateles	5346	29.66	33.70	38.92	42.56	46.24	50.34
Ateles	5350	29.76	33.94	39.07	42.19	45.38	48.60

(cont)

TABLE 6.3 (cont). Platyrrhine b_N measurements (mm).

Species	Specimen	M3	M2	M1	P4	P3	P2
Ateles	5351	33.16	36.92	41.53	46.15	48.43	51.85
Ateles	5352	27.69	31.92	36.47	39.98	43.12	46.88
Ateles	5353	29.62	33.95	38.37	42.34	45.82	49.14
Ateles	5354	28.75	32.79	36.86	39.96	43.82	46.97
Ateles	5355	29.57	34.31	39.00	42.84	47.04	48.98
C. apella	30162	25.05	28.70	32.24	35.19	39.20	41.88
C. apella	30166	21.66	25.32	29.59	32.93	36.93	39.43
C. apella	30724	21.58	25.57	29.74	33.59	36.26	39.22
C. apella	30726	18.59	22.73	26.65	30.72	33.27	37.14
C. apella	31064	22.31	26.35	30.59	33.76	36.77	39.45
C. apella	31072	20.96	24.64	28.83	32.33	34.83	38.08
C. apella	32049	19.21	22.45	27.34	31.03	33.86	36.70
C. apella	37831	24.45	28.18	32.51	36.57	40.03	42.60
C. apella	49635	25.46	29.67	33.54	36.99	40.58	44.37
C. apella	25811		29.57	34.53	38.18	41.77	45.19
C. apella	41090		26.15	31.11	33.75	36.94	40.39
C. capucinus	10135	19.86	23.64	27.92	31.49	34.95	37.34
C. capucinus	10136	21.35	24.49	29.07	32.82	36.56	38.81
C. capucinus	34323	23.59	26.99	31.47	34.72	38.06	40.55
C. capucinus	34326	22.88	26.94	31.36	35.06	38.44	41.74
C. capucinus	34353	22.88	27.21	31.79	35.34	38.03	42.68
C. capucinus	5332	24.24	27.79	32.43	36.56	38.82	42.87
C. capucinus	7317	24.36	28.25	32.80	36.59	39.30	42.41
C. capucinus	7322	19.95	24.00	28.53	31.67	35.03	37.58
C. capucinus	7323	22.08	26.14	30.64	34.55	37.18	
Cacajao	27870		32.65	36.41	40.30	42.19	45.67
Callicebus	20186	16.78	20.18	23.06	25.20	27.24	28.57
Callicebus	20188	17.63	20.90	24.04	26.18	28.22	30.20
Callicebus	26922	18.23	21.17	24.47	26.60	28.57	30.71
Callicebus	30559	16.10	18.82	21.68	24.11	25.63	27.74
Callicebus	30564	15.89	18.55	22.00	24.26	26.87	28.70
Callicebus	30566	16.33	18.98	22.46	24.66	26.93	28.64
Callicebus	32380	19.35	22.05	25.03	27.62	29.99	31.62
Callicebus	32383	17.88	20.55	23.37	25.74	27.37	29.60

(cont)

TABLE 6.3 (cont). Platyrrhine b_N measurements (mm).

Species	Specimen	M3	M2	M1	P4	P3	P2
Callicebus	37828	17.67	20.23	23.45	25.82	27.91	30.33
Callicebus	39073	17.45	20.27	23.31	25.62	27.99	29.42
Callicebus	39563	17.17	20.23	23.09	25.79	27.53	
Callithrix sp.	30580		12.11	14.25	15.78	16.92	19.14
Callithrix sp.	30582		12.05	14.52	15.90	17.17	19.37
Callithrix sp.	30583		14.06	16.16	17.05	18.95	20.34
Callithrix sp.	32164		13.19	15.50	17.49	18.48	20.89
Callithrix sp.	32165		12.00	14.02	15.40	17.07	18.72
Callithrix sp.	34573		12.47	14.60	16.38	18.11	19.57
Callithrix sp.	30577		11.20	13.51	14.74	16.76	18.66
Callithrix sp.	30586		12.91	15.27	16.44	18.03	20.13
Callithrix sp.	30603		12.96	15.07	16.38	18.56	19.96
Callithrix sp.	37826		13.08	15.51	17.20	19.34	21.20
Callithrix sp.	37823		12.97	15.66	17.77	19.65	21.33
Callithrix sp.	440		11.65	14.65	15.97	17.58	19.39
Callithrix sp.	7165		12.25	14.21	15.23	17.11	18.37
Chiropotes	31701	21.06	23.82	26.93	30.16	32.97	35.82
Chiropotes	6028	21.60	24.62	27.98	31.20	33.02	35.83
Pithecia sp.	27124	22.20	24.72	28.04	30.70	33.11	35.58
Pithecia sp.	30720	19.70	22.20	25.69	27.66	30.38	32.39
Pithecia sp.	20265		25.13	28.50	30.65	32.50	
Pithecia sp.	30719	23.00	25.97	29.61	32.14	34.34	36.48
Pithecia sp.	31061	20.02	23.52	26.75	29.76	31.19	34.32
Saguinus sp.	15324		12.29	14.56	16.44	18.28	19.82
Saguinus sp.	27331		12.25	14.65	15.67	17.60	18.85
Saguinus sp.	30579		12.76	14.92	16.47	18.23	20.19
Saguinus sp.	30601		12.47	14.49	16.38	18.19	19.76
Saguinus sp.	41567		13.20	15.23	16.64	18.66	19.98
Saguinus sp.	41568		12.36	14.87	17.09	17.66	20.14
Saguinus sp.	52557		12.81	15.08	17.18	18.03	19.79
Saguinus sp.	52558		14.02	16.39	17.79	19.49	21.20
Saguinus sp.	52616		13.45	15.54	17.13	18.45	20.81
Saimiri sp.	29488	13.31	15.99	18.58	20.44	22.26	24.17
Saimiri sp.	10131		15.40	18.36	20.53	21.27	23.39

(cont)

TABLE 6.3 (cont). Platyrrhine b_N measurements (mm).

Species	Specimen	M3	M2	M1	P4	P3	P2
Saimiri sp.	10134		17.12	19.85	21.37	23.16	24.83
Saimiri sp.	30568	10.30	12.48	15.12	17.29	18.83	20.39
Saimiri sp.	30569	13.87	16.11	18.52	19.95	22.02	24.58
Saimiri sp.	20187	14.91	17.59	20.20	21.65	23.63	26.07

(cont)

TABLE 6.4. Catarrhine masticatory system measurements (mm).

Species	#	Bicondylar breadth	Palate breadth	Glenoid height	Muscle resultant position	Muscle resultant angle
C. mitis	22734	40.30	23.78	6.54	16.39	74.53
C. mitis	25022	39.63	23.83	8.06	11.32	86.27
C. mitis	26832	44.15	26.55	8.66	19.65	78.14
C. mitis	32003	47.04	28.12	8.70	21.72	77.11
C. mitis	39389	40.38	24.16	5.43	19.17	77.49
C. mitis	39390	38.12	22.67	5.43	18.45	81.36
C. mitis	44264	46.97	27.31	11.24	19.30	80.06
C. mitis	44268	46.10	27.64	9.65	17.98	75.88
C. mitis	44274	43.82	28.45	12.65	17.15	82.68
C. mitis	7088	42.76	25.81	6.14	25.39	85.37
C. polykomos	21147	46.55	28.83	12.21	22.51	86.30
C. polykomos	21151	51.58	27.41	12.70	23.85	84.01
C. polykomos	21153	51.82	26.97	8.66	25.38	83.69
C. polykomos	22356	54.22	29.15	9.82	25.02	85.94
C. polykomos	22624	53.25	31.43	16.47	23.68	87.11
C. polykomos	22629	50.38	29.28	11.65	23.39	82.53
C. polykomos	22850	50.62	27.79	14.89	24.09	89.99
C. polykomos	46368	48.72	29.72	11.04	27.21	88.70
C. polykomos	47007	52.02	27.99	11.41	21.35	83.93
C. torquatus	18612	54.57	29.57	12.21	29.13	90.58
C. torquatus	19184	60.68	31.59	23.63	25.21	83.08
C. torquatus	19982	65.04	32.49	19.36	43.65	95.12
C. torquatus	21155	57.94	32.06	17.48	24.13	84.08
C. torquatus	23195	59.71	29.88	15.40	34.21	119.21
C. torquatus	25626	58.16	32.29	15.46	26.84	83.95
C. torquatus	25630	57.90	31.22	14.56	25.81	87.83
C. torquatus	32625	61.06	33.76	21.60	33.08	84.44
C. torquatus	62638	57.14	31.88	15.88	22.14	83.96
E. patas	37280	50.63	27.78	1.22	27.81	72.40
E. patas	47015	52.59	31.28	6.44	31.63	75.85
E. patas	47016	60.40	30.89	11.33	25.84	75.11
E. patas	47018	46.49	26.51	2.56	22.98	84.01

(cont)

TABLE 6.4 (cont). Catarrhine masticatory system measurements (mm).

Species	#	Bicondylar breadth	Palate breadth	Glenoid height	Muscle resultant position	Muscle resultant angle
G. gorilla	14750	91.34	53.04	47.62	39.70	79.36
G. gorilla	26850	93.30	49.38	54.36	39.14	81.10
G. gorilla	29047	94.72	51.05	60.96	27.29	74.70
G. gorilla	37264	91.76	53.38	48.23	39.31	79.87
G. gorilla	38326	90.28	51.79	54.45	30.49	79.71
G. gorilla	46325	92.66	52.69	51.28	45.11	79.12
L. albigena	18613	52.29	27.53	16.30	20.47	80.51
L. albigena	32194	55.71	28.67	18.72	18.85	77.30
L. albigena	39396	50.90	28.97	16.54	22.80	80.84
L. albigena	39402	49.50	29.63	18.90	22.29	83.20
L. albigena	6209	50.34	28.84	10.50	22.98	77.86
L. albigena	35937	42.79	23.92	12.57	14.46	82.26
M. fascicularis	22277	45.40	23.63	15.55	16.05	73.33
M. fascicularis	23812	47.04	22.97	11.79	20.30	82.91
M. fascicularis	35938	40.59	25.08	9.16	21.27	84.02
M. fascicularis	36030	42.87	26.58	7.98	18.70	78.50
M. fascicularis	37565	43.14	23.47	9.16	17.60	79.73
M. fascicularis	41167	33.83	26.29	14.64	23.20	67.15
M. fuscata	37709	60.83	33.17	15.26	30.51	84.78
M. fuscata	61273	61.54	37.43	19.30	30.46	87.27
M. sylvanus	7072	56.17	31.68	18.64	25.24	83.27
Mandrillus sp.	19986	68.16	42.53	21.01	46.62	88.66
Mandrillus sp.	20085	76.55	44.49	20.75	45.27	89.20
Mandrillus sp.	23168	77.20	46.73	21.77	45.74	86.98
Mandrillus sp.	23169	73.83	43.07	20.55	37.59	84.80
Mandrillus sp.	374089	77.29	46.58	15.90	60.77	88.21
Mandrillus sp.	34272	53.82	35.28	12.77	27.02	114.87
P. anubis	17342	69.45	39.99	12.57	44.15	83.06
P. anubis	17343	82.11	44.78	25.49	59.93	125.99
P. anubis	21160	83.05	40.89	19.13	45.37	85.43
P. anubis	21161	79.01	42.49	20.42	34.88	79.25
P. anubis	29786	77.30	45.11	20.19	40.58	82.13

(cont)

TABLE 6.4 (cont). Catarrhine masticatory system measurements (mm).

Species	#	Bicondylar breadth	Palate breadth	Glenoid height	Muscle resultant position	Muscle resultant angle
P. anubis	29787	66.63	36.15	11.81	32.55	84.30
P. anubis	29788	63.29	35.98	6.41	38.91	82.68
P. anubis	31619	70.24	37.21	14.88	46.08	101.95
P. anubis	8304	77.93	42.88	16.30	51.17	85.07
P. badius	24080	50.05	28.56	11.96	22.23	81.07
P. badius	24775	52.29	27.79	13.02	22.13	76.35
P. badius	24793	47.66	23.96	12.61	17.94	78.64
P. badius	25627	36.48	25.12	19.13	35.03	69.25
P. badius	25631	52.69	26.96	10.62	22.19	78.43
P. badius	25810	42.16	25.17	8.04	20.90	75.76
P. badius	26552	49.34	27.25	11.18	24.16	79.53
P. badius	26553	50.20	27.70	15.16	20.52	81.07
P. badius	27108	50.85	28.63	17.91	19.94	77.55
P. badius	31939	44.97	23.95	9.27	18.63	74.35
P. hosei	35621	46.60	24.24	6.02	21.13	81.01
P. hosei	37380	44.05	24.67	4.43	20.58	77.11
P. hosei	37371	47.13	24.37	6.47	18.62	75.49
P. paniscus	38019	81.40	41.98	26.42	29.67	90.27
P. paniscus	38020	77.33	46.45	27.31	33.27	77.21
P. rubicunda	22276	47.77	24.98	6.96	21.73	77.60
P. rubicunda	35704	42.31	22.81	9.04	14.23	76.36
P. rubicunda	35705	44.99	24.06	5.33	18.92	77.99
P. rubicunda	35706	42.16	21.59	7.59	15.37	75.36
P. rubicunda	35712	45.95	23.89	6.89	19.90	73.71
P. rubicunda	37666	43.65	22.22	6.44	23.01	80.00
P. troglodytes	15312	77.57	45.21	32.58	37.24	89.65
P. troglodytes	17702	77.92	48.94	33.20	35.10	77.98
P. troglodytes	23167	82.31	47.10	32.49	33.09	79.25
P. troglodytes	9493	80.08	47.32	35.30	26.36	79.82
P. troglodytes	N6960	81.22	44.36	29.99	34.57	74.41
P. troglodytes	N7261	77.08	50.42	34.28	32.76	72.35
P. troglodytes	N7265	75.09	46.07	28.95	31.82	78.90

(cont)

TABLE 6.4 (cont). Catarrhine masticatory system measurements (mm).

Species	#	Bicondylar breadth	Palate breadth	Glenoid height	Muscle resultant position	Muscle resultant angle
T. cristata	35567	47.23	24.34	7.81	18.92	80.82
T. cristata	35584	45.93	26.73	7.74	20.32	84.52
T. cristata	35586	33.79	25.71	5.55	22.09	79.61
T. cristata	35597	45.18	24.86	8.41	18.15	67.04
T. cristata	35603	48.66	24.50	7.52	22.24	83.56
T. cristata	35604	47.54	25.15	6.61	21.48	82.52
T. cristata	35605	49.46	26.59	6.94	22.98	86.27
T. cristata	35610	47.70	24.66	8.37	17.94	79.63
T. cristata	35618	49.37	26.11	8.27	24.68	86.88
T. cristata	35636	45.06	24.98	5.71	21.39	85.78
T. cristata	35640	44.09	23.99	7.15	17.38	80.27
T. cristata	35663	48.33	25.10	5.54	21.05	83.73
T. cristata	35678	46.87	26.10	8.15	22.96	87.37
T. cristata	35682	45.98	25.07	5.19	19.03	79.92
T. cristata	35696	48.34	23.46	6.19	23.71	87.00
T. cristata	35718	44.94	23.80	4.61	19.72	82.81
T. cristata	37387	45.86	24.87	9.16	19.38	86.97

TABLE 6.5. Catarrhine b_H measurements (mm).

Species	Specimen	M3	M2	M1	P4	P3
C. mitis	22734	21.05	26.29	31.02	34.82	37.71
C. mitis	25022	20.74	25.71	30.41	34.54	38.34
C. mitis	26832	26.85	32.81	39.43	43.95	48.12
C. mitis	32003	31.21	37.55	43.09	47.93	51.04
C. mitis	39389	24.46	29.86	35.07	38.91	42.89
C. mitis	39390	23.52	29.36	34.80	38.93	42.54
C. mitis	44264	26.98	32.61	38.97	43.90	47.89
C. mitis	44268	29.08	34.97	41.23	46.67	50.05
C. mitis	44274	25.68	32.00	38.40	43.73	47.99
C. mitis	7088	25.03	30.96	36.85	43.03	47.03
C. polykomos	21147	28.05	34.88	42.36	48.76	52.74
C. polykomos	21151	30.85	37.98	45.21	50.96	56.33
C. polykomos	21153	28.98	35.77	42.87	49.01	54.85
C. polykomos	22356	32.55	39.25	46.46	52.11	57.65
C. polykomos	22624	32.67	38.13	44.31	49.87	54.34
C. polykomos	22629	31.43	38.87	44.82	49.18	55.32
C. polykomos	22850	34.89	41.63	48.98	54.25	59.46
C. polykomos	46368	36.45	43.09	49.95	55.44	59.36
C. polykomos	47007	29.44	35.61	42.11	46.95	52.13
C. torquatus	18612	30.78	37.08	44.97	51.49	56.05
C. torquatus	19184	38.72	47.09	54.00	61.00	66.53
C. torquatus	19982	41.99	50.07	58.03	64.10	69.51
C. torquatus	21155	36.08	42.82	48.92	55.24	58.84
C. torquatus	23195	35.68	41.94	45.56	55.00	57.75
C. torquatus	25626	34.14	36.22	48.26	54.49	59.34
C. torquatus	25630	35.34	43.55	50.68	56.99	61.65
C. torquatus	32625	41.93	49.54	58.37	63.60	69.63
C. torquatus	62638	31.19	38.98	46.12	53.24	58.78
E. patas	37280	34.88	42.91	50.23	55.93	59.72
E. patas	47015	50.13	54.94	62.59	67.28	72.81
E. patas	47016	45.46	53.45	60.33	66.09	71.87
E. patas	47018	28.51	33.67	40.54	45.58	50.02

(cont)

TABLE 6.5 (cont). Catarrhine b_H measurements (mm).

Species	Specimen	M3	M2	M1	P4	P3
G. gorilla	14750	52.34	65.88	77.52	88.52	98.42
G. gorilla	26850	60.39	74.18	88.31	100.01	108.24
G. gorilla	29047	49.02	61.06	74.82	83.66	93.52
G. gorilla	37264	62.23	76.35	90.33	101.21	110.53
G. gorilla	38326	48.80	59.93	73.14	84.68	94.93
G. gorilla	46325	47.37	58.57	73.22	85.31	94.88
L. albigena	18613	28.37	34.36	40.93	46.84	51.27
L. albigena	32194	31.93	38.71	44.97	51.22	55.67
L. albigena	39396	32.12	38.30	44.96	50.24	55.31
L. albigena	39402	27.12	33.26	40.40	46.52	51.64
L. albigena	6209	33.63	40.01	45.33	50.85	55.27
L. albigena	35937	26.76	33.14	38.84	43.65	47.52
M. fascicularis	22277	27.39	33.92	40.21	45.04	49.14
M. fascicularis	23812	31.47	37.59	44.27	48.59	52.91
M. fascicularis	35938	24.56	30.28	36.85	41.44	46.06
M. fascicularis	36030	27.03	33.47	39.76	44.47	48.77
M. fascicularis	37565	25.06	30.64	37.74	41.54	45.76
M. fascicularis	41167	32.19	38.92	45.91	51.12	
M. fuscata	37709	37.50	45.73	54.06	61.05	65.99
M. fuscata	61273	41.02	50.74	59.72	66.88	72.49
M. sylvanus	7072	37.55	45.93	50.99	56.79	61.10
Mandrillus sp.	19986	59.88	70.60	82.18	93.08	100.25
Mandrillus sp.	20085	56.76	67.89	80.06	89.05	95.16
Mandrillus sp.	23168	62.22	71.88	82.59	91.36	98.43
Mandrillus sp.	23169	56.06	67.77	78.23	85.77	92.76
Mandrillus sp.	374089	77.62	89.54	101.70	112.40	121.43
Mandrillus sp.	34272	35.43	46.46	57.62	66.92	72.87
P. anubis	17342	56.07	69.96	80.27	89.42	95.95
P. anubis	17343	72.07	86.38	95.06	103.92	111.38
P. anubis	21160	60.11	72.05	84.80	92.53	99.97
P. anubis	21161	63.24	74.29	86.04	93.83	101.34
P. anubis	29786	63.86	75.52	87.76	95.34	104.60

(cont)

TABLE 6.5 (cont). Catarrhine b_H measurements (mm).

Species	Specimen	M3	M2	M1	P4	P3
P. anubis	29787	43.87	54.46	65.06	73.23	80.26
P. anubis	29788	47.31	59.25	69.41	68.87	83.28
P. anubis	31619	52.92	65.54	77.28	85.79	91.62
P. anubis	8304	64.49	77.67	89.41	97.41	106.04
P. badius	24080	28.75	35.01	41.37	46.45	50.66
P. badius	24775	30.97	37.25	42.24	47.39	50.99
P. badius	24793	25.95	30.75	37.20	42.55	47.70
P. badius	25627	40.78	47.45	51.62	56.68	61.69
P. badius	25631	29.20	34.93	40.97	45.69	50.17
P. badius	25810	24.48	31.00	37.50	42.87	47.26
P. badius	26552	28.13	34.25	40.84	45.22	49.51
P. badius	26553	28.38	34.62	41.13	45.63	50.36
P. badius	27108	32.62	39.19	45.46	50.70	55.24
P. badius	31939	26.05	31.77	36.85	42.63	46.02
P. hosei	35621	25.80	31.13	36.14	40.22	44.21
P. hosei	37380	28.35	33.05	38.01	43.02	44.92
P. hosei	37371	24.70	30.07	35.80	39.42	42.94
P. paniscus	38019	44.33	49.41	55.46	63.43	67.53
P. paniscus	38020	43.69	52.26	59.06	66.33	73.25
P. rubicunda	22276	26.92	31.71	37.18	41.62	46.17
P. rubicunda	35704	21.30	26.54	31.34	35.25	39.77
P. rubicunda	35705	24.56	29.71	33.75	37.75	41.54
P. rubicunda	35706	23.95	28.16	32.87	36.48	39.89
P. rubicunda	35712	27.13	31.62	35.82	39.69	42.88
P. rubicunda	37666	26.96	30.74	35.33	39.18	42.65
P. troglodytes	15312	52.71	60.11	70.94	79.29	84.77
P. troglodytes	17702	50.06	59.25	69.25	77.79	85.31
P. troglodytes	23167	50.47	60.08	70.73	77.79	85.62
P. troglodytes	9493	43.99	52.76	62.59	69.04	77.08
P. troglodytes	N6960	49.19	58.37	67.52	78.06	84.86
P. troglodytes	N7261	49.19	58.94	69.09	78.17	86.17
P. troglodytes	N7265	48.10	56.03	65.56	74.15	81.68

(cont)

TABLE 6.5 (cont). Catarrhine b_H measurements (mm).

Species	Specimen	M3	M2	M1	P4	P3
T. cristata	35567	26.72	31.11	37.02	41.17	45.29
T. cristata	35584	25.78	30.71	37.34	42.25	46.00
T. cristata	35586	25.93	31.85	37.51	41.63	45.83
T. cristata	35597	22.89	27.99	33.56	39.10	43.05
T. cristata	35603	28.68	33.37	38.78	43.44	46.95
T. cristata	35604	27.73	33.11	38.67	43.48	47.06
T. cristata	35605	27.98	33.61	40.54	46.10	49.48
T. cristata	35610	25.74	31.02	36.34	40.54	44.79
T. cristata	35618	27.49	33.24	38.37	42.74	46.88
T. cristata	35636	27.51	32.16	38.37	41.84	46.12
T. cristata	35640	25.15	30.19	35.93	40.40	45.52
T. cristata	35663	26.18	31.09	36.81	41.98	45.01
T. cristata	35678	27.38	32.43	37.90	42.79	46.10
T. cristata	35682	26.21	30.94	37.07	41.18	45.63
T. cristata	35696	25.97	30.97	37.21	41.41	46.26
T. cristata	35718	24.83	29.70	35.42	39.23	43.40
T. cristata	37387	25.18	30.19	35.75	40.59	44.21

TABLE 6.6. Catarrhine b_N measurements (mm).

Species	Specimen	M3	M2	M1	P4	P3
C. mitis	22734	20.52	26.29	31.04	34.25	37.10
C. mitis	25022	20.68	26.08	30.67	34.41	38.05
C. mitis	26832	26.83	33.17	39.65	43.79	47.66
C. mitis	32003	30.67	37.27	42.88	47.42	50.14
C. mitis	39389	23.04	28.93	34.27	37.63	41.30
C. mitis	39390	23.17	29.47	34.78	38.71	42.06
C. mitis	44264	26.77	32.72	39.05	43.38	46.98
C. mitis	44268	29.30	35.34	41.37	46.42	49.43
C. mitis	44274	27.64	33.97	40.10	44.87	48.63
C. mitis	7088	23.59	30.07	36.02	41.91	45.49
C. polykomos	21147	29.54	36.47	43.74	49.45	53.01
C. polykomos	21151	32.00	39.33	46.24	51.34	56.69
C. polykomos	21153	28.76	36.07	43.20	48.55	54.18
C. polykomos	22356	32.08	39.10	46.31	51.74	57.17
C. polykomos	22624	34.50	40.33	46.30	51.15	55.26
C. polykomos	22629	32.21	39.88	45.49	49.59	54.96
C. polykomos	22850	35.45	42.41	49.15	54.44	59.45
C. polykomos	46368	36.69	43.50	50.32	55.57	58.97
C. polykomos	47007	28.62	35.37	42.00	46.62	51.48
C. torquatus	18612	29.51	37.07	44.93	51.22	55.56
C. torquatus	19184	43.48	51.45	57.22	63.82	68.34
C. torquatus	19982	43.01	51.47	58.93	64.48	70.17
C. torquatus	21155	37.68	44.39	50.32	56.39	59.41
C. torquatus	23195	35.85	43.06	46.84	55.59	58.04
C. torquatus	25626	35.52	38.54	49.64	55.34	59.60
C. torquatus	25630	35.36	43.71	51.07	56.90	60.94
C. torquatus	32625	44.71	52.35	60.19	65.32	70.92
C. torquatus	62638	33.20	40.91	47.67	54.35	59.60
E. patas	37280	32.49	41.24	48.53	54.20	57.77
E. patas	47015	49.97	54.91	62.59	67.16	72.63
E. patas	47016	44.07	52.33	59.09	64.42	70.29
E. patas	47018	25.56	32.21	39.30	44.20	48.35

(cont)

TABLE 6.6 (cont). Catarrhine b_N measurements (mm).

Species	Specimen	M3	M2	M1	P4	P3
G. gorilla	14750	68.29	80.40	90.28	98.44	107.82
G. gorilla	26850	77.89	89.98	102.01	111.01	118.11
G. gorilla	29047	76.30	86.28	94.05	102.33	109.93
G. gorilla	37264	76.23	88.83	100.97	110.19	118.52
G. gorilla	38326	69.87	79.06	89.67	98.18	106.72
G. gorilla	46325	67.53	77.65	89.02	98.34	106.56
L. albigena	18613	30.62	36.69	42.88	48.11	52.64
L. albigena	32194	34.78	41.17	47.07	52.60	56.82
L. albigena	39396	34.01	40.24	46.69	51.43	56.12
L. albigena	39402	31.62	37.56	44.19	49.34	54.10
L. albigena	6209	33.09	40.27	45.58	50.60	54.86
L. albigena	35937	29.26	35.39	40.65	45.17	48.68
M. fascicularis	22277	29.38	35.88	41.70	45.84	49.54
M. fascicularis	23812	29.43	35.67	42.24	46.14	50.11
M. fascicularis	35938	24.88	30.92	37.38	41.59	45.85
M. fascicularis	36030	27.29	33.83	39.97	44.54	48.49
M. fascicularis	37565	24.94	30.81	37.71	41.40	45.32
M. fascicularis	41167	31.07	38.09	45.16	50.24	
M. fuscata	37709	38.09	46.79	55.06	61.56	65.98
M. fuscata	61273	43.90	53.38	61.79	68.95	73.72
M. sylvanus	7072	40.90	48.38	52.94	58.99	62.50
Mandrillus sp.	19986	62.83	73.14	84.61	95.16	102.45
Mandrillus sp.	20085	58.03	68.97	81.01	90.05	95.69
Mandrillus sp.	23168	63.79	73.35	84.16	93.07	99.92
Mandrillus sp.	23169	57.32	69.08	79.18	86.80	93.51
Mandrillus sp.	374089	75.37	87.61	100.39	111.11	120.01
Mandrillus sp.	34272	36.20	47.54	58.41	67.21	72.99
P. anubis	17342	55.47	69.58	79.75	88.25	95.29
P. anubis	17343	74.85	88.54	96.79	105.90	113.08
P. anubis	21160	61.06	73.15	85.73	93.09	100.56
P. anubis	21161	64.34	75.47	86.40	94.12	101.22
P. anubis	29786	64.45	76.56	88.56	95.98	105.56

(cont)

TABLE 6.6 (cont). Catarrhine b_N measurements (mm).

Species	Specimen	M3	M2	M1	P4	P3
P. anubis	29787	42.89	53.81	64.57	72.35	79.43
P. anubis	29788	45.12	57.99	68.80	67.97	82.13
P. anubis	31619	52.36	65.13	76.90	85.58	91.34
P. anubis	8304	64.80	77.85	89.68	97.53	105.85
P. badius	24080	28.99	35.90	42.25	46.46	50.25
P. badius	24775	30.48	37.59	42.28	47.23	50.16
P. badius	24793	25.58	31.20	37.53	42.30	47.02
P. badius	25627	39.37	46.04	50.00	54.79	63.81
P. badius	25631	28.37	34.54	40.74	45.33	50.26
P. badius	25810	23.57	30.70	37.32	42.24	46.28
P. badius	26552	28.21	34.75	41.32	45.28	49.24
P. badius	26553	29.80	36.10	42.20	45.99	50.42
P. badius	27108	36.08	42.47	48.29	53.00	56.86
P. badius	31939	26.10	32.41	37.69	42.39	45.68
P. hosei	35621	22.28	28.58	33.86	37.61	41.37
P. hosei	37380	26.66	31.96	37.01	41.84	43.51
P. hosei	37371	23.21	28.76	34.40	37.89	41.26
P. paniscus	38019	46.56	53.06	59.03	66.04	70.35
P. paniscus	38020	49.46	57.63	64.28	70.38	76.98
P. rubicunda	22276	24.81	30.19	35.86	40.19	44.66
P. rubicunda	35704	20.56	25.87	30.74	34.48	38.59
P. rubicunda	35705	21.67	27.40	31.52	35.17	38.85
P. rubicunda	35706	22.74	27.28	32.06	35.36	38.44
P. rubicunda	35712	25.21	30.10	34.65	38.28	41.26
P. rubicunda	37666	24.18	28.75	33.46	37.33	40.47
P. troglodytes	15312	60.39	67.72	77.78	84.84	90.28
P. troglodytes	17702	58.71	66.78	76.33	83.37	89.92
P. troglodytes	23167	58.82	68.18	77.54	83.67	90.47
P. troglodytes	9493	53.23	61.06	69.43	74.98	81.60
P. troglodytes	N6960	52.85	61.60	71.36	80.19	87.64
P. troglodytes	N7261	59.17	68.51	77.08	84.67	91.27
P. troglodytes	N7265	55.10	62.70	71.44	78.83	84.97

(cont)

TABLE 6.6 (cont). Catarrhine b_N measurements (mm).

Species	Specimen	M3	M2	M1	P4	P3
T. cristata	35567	25.77	31.08	36.90	40.58	44.41
T. cristata	35584	25.17	31.34	37.09	41.69	45.03
T. cristata	35586	24.28	30.58	36.36	39.96	43.89
T. cristata	35597	22.16	27.73	33.14	38.20	41.81
T. cristata	35603	26.63	31.69	37.16	41.56	44.66
T. cristata	35604	26.55	32.17	37.79	42.33	45.57
T. cristata	35605	26.59	32.52	39.78	44.87	47.89
T. cristata	35610	24.61	30.54	35.73	39.35	43.18
T. cristata	35618	26.68	32.83	37.70	41.63	45.75
T. cristata	35636	25.83	31.17	37.55	40.71	45.05
T. cristata	35640	24.38	29.83	35.57	39.78	44.29
T. cristata	35663	23.42	29.30	35.12	40.26	42.96
T. cristata	35678	26.20	32.03	37.61	42.10	44.99
T. cristata	35682	24.38	29.81	36.05	39.95	44.16
T. cristata	35696	23.50	29.14	35.28	39.04	43.78
T. cristata	35718	22.32	27.90	33.62	37.09	41.19
T. cristata	37387	24.50	30.30	35.97	40.06	43.43

TABLE 6.7. Platyrrhine postcanine bite force curves (N).

Species	Specimen	M3	M2	M1	P4	P3	P2
A. caraya	25812	94.82	99.88	104.36	107.69	105.52	96.94
A. caraya	28095	107.98	110.98	114.47	116.92	112.61	103.73
A. caraya	28096	108.82	109.14	112.29	114.36	106.14	97.07
A. caraya	28655	99.55	104.98	109.94	113.58	107.82	100.52
A. palliata	29609	104.15	106.87	111.17	109.42	97.39	89.07
A. palliata	29611	95.25	100.46	111.41	105.40	97.14	91.37
A. palliata	5323	98.66	103.53	107.96	112.26	105.80	98.59
A. palliata	5324	91.86	94.79	98.51	101.75	104.67	100.59
A. palliata	5325	129.49	101.34	107.54	112.55	114.46	116.60
A. palliata	5327	104.25	107.57	112.81	113.43	102.64	93.99
A. palliata	5328	109.08	112.23	118.16	105.49	93.93	86.08
A. palliata	5329	108.29	111.87	107.88	93.73	83.15	75.09
A. palliata	5331	106.04	108.59	112.45	115.18	111.17	101.51
A. palliata	6001	131.16	110.80	114.23	117.04	118.96	110.36
Aotus	19801	123.65	122.21	122.81	118.97	108.66	97.26
Aotus	19802	128.34	127.65	126.58	123.85	112.43	103.22
Aotus	19805	125.94	124.07	125.04	126.11	116.86	108.66
Aotus	27214	121.34	120.85	121.41	117.40	106.57	96.97
Aotus	30562	124.99	123.23	124.58	125.64	119.57	108.71
Aotus	39571	125.64	123.60	124.84	125.87	124.01	116.30
Aotus	52608	131.32	130.60	130.82	122.93	113.01	102.95
Aotus	8472	120.35	119.70	120.82	121.69	112.42	103.91
Aotus	B-8042	127.04	126.43	126.37	124.37	112.61	100.39
Aotus	B-8043	127.61	126.73	126.84	127.57	120.45	113.58
Ateles	10138	133.72	131.86	131.25	130.82	127.79	120.51
Ateles	29628	129.20	129.17	129.47	124.47	115.11	105.09
Ateles	34322	126.98	127.06	125.88	128.33	129.15	124.35
Ateles	5336	71.76		105.71	99.04	94.02	87.73
Ateles	5338	126.19	127.23	127.49	128.88	127.32	
Ateles	5344	129.26	129.15	129.58	130.07	130.61	123.29
Ateles	5345	122.30	121.98	122.37	122.83	123.40	114.97
Ateles	5346	123.06	122.60	122.98	123.87	124.64	113.94
Ateles	5350	123.92	124.73	125.66	126.65	125.15	116.18

(cont)

TABLE 6.7 (cont). Platyrrhine postcanine bite force curves (N).

Species	Specimen	M3	M2	M1	P4	P3	P2
Ateles	5351	121.99	121.27	123.38	123.22	124.21	118.99
Ateles	5352	120.76	120.94	121.46	122.03	122.71	114.73
Ateles	5353	125.19	125.23	125.85	126.37	126.40	117.34
Ateles	5354	129.66	129.44	130.33	131.33	126.88	117.86
Ateles	5355	117.93	117.96	119.04	119.73	120.90	116.18
C. apella	30162	123.09	123.12	123.92	125.50	118.30	110.30
C. apella	30166	123.20	122.62	122.68	124.28	110.81	102.81
C. apella	30724	135.32	131.76	129.34	127.58	117.51	107.65
C. apella	30726	131.08	128.13	127.98	122.02	112.35	99.57
C. apella	31064	125.69	125.16	123.54	125.06	118.63	109.35
C. apella	31072	130.16	128.78	128.79	124.39	114.74	103.75
C. apella	32049	131.87	127.54	124.85	125.53	116.32	106.25
C. apella	37831	131.67	128.92	128.07	129.20	120.23	111.89
C. apella	49635	135.12	130.53	130.55	130.21	120.20	108.19
C. capucinus	10135	127.00	124.93	124.70	125.41	114.27	106.87
C. capucinus	10136	137.33	134.90	131.69	131.70	119.64	112.22
C. capucinus	34323	125.98	124.42	124.01	124.17	124.10	115.84
C. capucinus	34326	134.44	132.13	130.77	131.16	122.22	112.01
C. capucinus	34353	127.22	126.50	127.21	127.44	119.01	105.83
C. capucinus	5332	132.21	130.27	129.10	129.65	125.68	112.92
C. capucinus	7317	139.78	134.69	133.15	133.00	128.96	119.15
C. capucinus	7322	134.45	131.14	129.90	127.95	116.32	105.39
C. capucinus	7323	132.64	130.77	130.50	129.15	119.91	
Cacajao	27870	93.06	122.92	112.32	101.08	96.28	89.13
Callicebus	20186	125.90	124.88	126.13	127.75	117.20	110.73
Callicebus	20188	127.20	126.53	126.67	128.02	122.65	114.26
Callicebus	26922	126.68	126.30	127.44	129.57	122.71	114.18
Callicebus	30559	133.57	130.48	131.64	132.37	126.50	117.24
Callicebus	30564	128.03	126.41	127.29	126.86	114.15	106.44
Callicebus	30566	124.85	125.10	125.83	122.79	111.12	102.23
Callicebus	32380	126.95	126.80	127.51	128.77	123.02	115.75
Callicebus	32383	119.88	120.11	121.59	122.96	121.47	110.53

(cont)

TABLE 6.7 (cont). Platyrrhine postcanine bite force curves (N).

Species	Specimen	M3	M2	M1	P4	P3	P2
Callicebus	37828	118.59	119.40	120.78	122.91	113.45	102.50
Callicebus	39073	124.49	123.62	124.28	125.45	116.11	108.96
Callicebus	39563	123.24	122.67	124.46	122.78	113.14	
Callithrix sp.	7165	n/a	129.81	129.60	131.76	132.51	132.69
Callithrix sp.	30580	n/a	123.86	122.92	123.90	124.59	123.74
Callithrix sp.	30582	n/a	127.34	125.51	125.90	126.39	125.38
Callithrix sp.	30583	n/a	127.58	126.15	126.92	127.24	126.91
Callithrix sp.	32164	n/a	121.47	120.70	121.29	122.09	121.91
Callithrix sp.	32165	n/a	122.72	122.29	122.88	123.80	123.51
Callithrix sp.	34573	n/a	122.90	122.52	122.84	123.17	123.14
Callithrix sp.	30577	n/a	117.92	118.02	118.95	120.09	118.24
Callithrix sp.	30586	n/a	127.72	127.10	127.35	128.28	127.10
Callithrix sp.	30603	n/a	129.04	128.72	129.19	129.38	128.75
Callithrix sp.	37826	n/a	122.20	120.81	121.33	121.21	121.14
Callithrix sp.	37823	n/a	127.30	125.97	126.60	126.64	121.93
Callithrix sp.	440	n/a	133.52	129.88	131.49	132.32	121.00
Chiropotes	31701	126.64	126.37	126.96	127.35	124.07	113.70
Chiropotes	6028	137.54	133.34	132.45	132.08	132.77	123.50
Pithecia sp.	27124	132.60	131.47	131.25	131.70	131.91	123.86
Pithecia sp.	30720	130.37	129.78	129.26	129.97	127.78	119.92
Pithecia sp.	30719	125.16	124.71	125.56	126.20	127.01	124.14
Pithecia sp.	31061	136.67	135.78	134.95	133.58	127.26	118.39
Saguinus	15324	n/a	134.59	131.70	132.05	131.92	125.31
Saguinus	27331	n/a	119.11	118.32	119.90	120.63	120.98
Saguinus	30579	n/a	121.20	120.22	121.16	121.85	121.55
Saguinus	30601	n/a	124.27	124.15	124.53	125.11	124.77
Saguinus	41567	n/a	130.06	128.01	128.99	128.97	128.92
Saguinus	41568	n/a	120.31	119.10	119.83	120.56	119.82
Saguinus	52557	n/a	127.89	126.44	126.69	126.80	126.17
Saguinus	52558	n/a	124.14	123.57	124.09	124.94	124.61
Saguinus	52616	n/a	126.94	126.05	126.91	127.72	126.88
Saimiri sp.	29488	138.20	134.69	134.85	130.89	119.54	110.76
Saimiri sp.	30568	123.91	120.87	121.63	121.29	110.58	102.25
Saimiri sp.	30569	123.69	122.44	123.28	125.06	124.91	114.72
Saimiri sp.	20187	130.80	128.19	128.63	129.72	128.60	118.09

TABLE 6.8. Catarrhine postcanine bite force curves (N).

Species	Specimen	M3	M2	M1	P4	P3
C. mitis	22734	129.03	125.78	125.70	120.02	111.30
C. mitis	26832	124.99	123.54	124.20	121.12	110.75
C. mitis	32003	127.38	126.11	125.79	126.52	120.93
C. mitis	39389	132.84	129.15	128.05	123.51	111.56
C. mitis	39390	127.31	124.95	125.49	120.08	109.64
C. mitis	44264	127.46	126.04	126.21	118.66	108.86
C. mitis	44268	124.10	123.72	124.61	123.69	115.35
C. mitis	44274	112.67	114.23	116.13	114.36	104.43
C. mitis	7088	132.33	128.41	127.59	112.96	102.50
C. polykomos	21153	132.55	130.45	130.53	115.90	103.61
C. polykomos	22356	131.98	130.57	130.49	121.78	110.29
C. polykomos	22624	119.10	118.91	120.36	122.62	113.70
C. polykomos	22629	123.42	123.28	124.62	125.01	110.92
C. polykomos	46368	123.41	123.05	123.31	123.93	119.10
C. polykomos	47007	133.76	130.92	130.37	120.76	108.96
C. torquatus	19184	117.13	120.38	124.13	119.19	109.76
C. torquatus	19982	130.21	129.75	131.34	120.20	111.73
C. torquatus	21155	123.29	124.20	125.17	124.42	116.90
C. torquatus	25626	123.61	120.86	125.03	120.69	110.93
C. torquatus	25630	129.86	129.46	128.94	118.00	108.66
C. torquatus	32625	120.78	121.88	124.90	124.59	114.74
C. torquatus	62638	120.60	122.32	124.20	112.67	102.82
E. patas	37280	138.64	134.37	133.67	122.82	114.53
E. patas	47015	125.81	125.48	125.41	125.63	125.72
E. patas	47016	136.50	135.16	135.10	135.74	125.37
E. patas	47018	142.07	133.14	131.39	122.89	111.24
G. gorilla	14750	96.98	103.68	108.64	108.45	101.19
G. gorilla	26850	101.40	107.82	113.22	108.77	102.62
G. gorilla	29047	83.49	91.97	103.39	104.36	97.95
G. gorilla	37264	103.22	108.68	113.12	114.73	107.19
G. gorilla	38326	88.77	96.34	103.66	101.22	93.97
G. gorilla	46325	89.44	96.17	104.87	101.60	94.66
L. albigena	18613	121.39	122.70	125.06	115.75	107.65
L. albigena	32194	121.23	124.16	126.15	119.35	111.36
L. albigena	39396	120.37	121.31	122.73	122.57	112.39

(cont)

TABLE 6.8 (cont). Catarrhine postcanine bite force curves (N).

Species	Specimen	M3	M2	M1	P4	P3
L. albigena	39402	107.31	110.79	114.38	109.81	100.61
L. albigena	6209	129.23	126.33	126.46	127.78	120.59
L. albigena	35937	117.33	120.13	122.57	120.15	110.91
M. fascicularis	22277	122.63	124.35	126.84	118.64	109.99
M. fascicularis	23812	143.70	141.61	133.56	121.51	111.31
M. fascicularis	35938	122.03	121.06	121.87	115.79	104.14
M. fascicularis	36030	122.28	122.14	122.81	121.25	110.55
M. fascicularis	37565	130.15	128.82	129.63	118.57	107.81
M. fascicularis	41167	116.60	114.99	114.41	114.51	
M. fuscata	37709	127.42	126.49	127.07	119.00	110.05
M. fuscata	61273	116.20	118.21	120.19	118.02	108.74
M. sylvanus	7072	117.40	121.40	123.17	123.11	118.22
Mandrillus sp.	19986	117.37	118.88	119.62	120.46	117.32
Mandrillus sp.	20085	123.72	124.51	125.00	123.14	115.23
Mandrillus sp.	23168	121.52	122.09	122.26	122.30	122.73
Mandrillus sp.	23169	123.54	123.92	124.80	124.81	118.19
Mandrillus sp.	374089	128.52	127.54	126.42	126.24	125.53
P. anubis	17342	128.29	127.61	127.75	123.68	115.88
P. anubis	17343	124.61	126.26	127.11	120.76	111.29
P. anubis	21160	131.93	132.00	132.56	127.23	118.28
P. anubis	21161	127.83	128.02	129.52	129.66	123.44
P. anubis	29786	125.14	124.58	125.16	125.45	121.14
P. anubis	29787	132.62	131.22	130.64	117.48	107.50
P. anubis	29788	133.70	130.28	128.64	129.20	112.67
P. anubis	31619	132.14	131.56	130.11	117.15	109.52
P. anubis	8304	128.40	128.71	128.62	128.85	120.15
P. badius	24080	126.28	124.18	124.69	120.13	110.28
P. badius	24775	132.69	129.41	130.47	127.25	118.21
P. badius	24793	135.02	131.17	131.92	117.05	105.06
P. badius	25627	122.68	122.07	122.28	122.53	114.51
P. badius	25631	136.17	133.80	133.05	125.10	115.57
P. badius	25810	130.07	126.46	125.84	113.35	102.73
P. badius	26552	128.48	126.99	127.35	121.72	111.52
P. badius	26553	122.74	123.60	125.62	117.71	107.67
P. badius	27108	115.69	118.07	120.46	122.40	115.69

(cont)

TABLE 6.8 (cont). Catarrhine postcanine bite force curves (N).

Species	Specimen	M3	M2	M1	P4	P3
P. badius	31939	130.25	127.92	127.59	121.55	113.20
P. hosei	35621	152.35	143.30	137.44	122.66	110.89
P. hosei	37380	136.33	132.57	131.67	130.42	124.54
P. hosei	37371	140.30	137.84	134.94	122.70	112.60
P. paniscus	38020	110.37	113.30	114.80	117.76	116.28
P. rubicunda	22276	142.50	137.94	136.16	126.55	114.24
P. rubicunda	35704	134.62	133.31	130.37	117.09	104.00
P. rubicunda	35705	147.69	141.30	139.53	125.05	113.20
P. rubicunda	35706	139.30	136.53	135.61	128.31	117.27
P. rubicunda	35712	141.61	138.23	136.03	134.44	124.45
P. rubicunda	37666	147.77	141.71	139.94	133.49	122.06
P. troglodytes	15312	110.29	112.16	115.24	118.09	115.66
P. troglodytes	17702	104.74	108.99	111.45	114.62	113.58
P. troglodytes	23167	109.15	112.10	116.04	118.27	114.24
P. troglodytes	9493	103.89	108.63	113.33	115.47	105.65
P. troglodytes	N6960	120.39	122.57	122.39	120.77	114.03
P. troglodytes	N7261	100.52	104.02	108.38	111.63	113.58
P. troglodytes	N7265	108.20	110.77	113.75	116.59	114.24
T. cristata	35567	136.85	132.11	132.41	127.23	115.60
T. cristata	35584	129.49	123.88	127.28	118.92	108.69
T. cristata	35586	121.30	118.30	117.17	118.33	109.78
T. cristata	35597	133.26	130.22	130.65	117.63	107.19
T. cristata	35603	143.26	140.08	138.82	127.11	116.87
T. cristata	35604	136.62	134.62	133.85	124.64	114.65
T. cristata	35605	136.87	134.43	132.56	117.64	108.95
T. cristata	35610	137.89	133.91	134.09	123.08	111.05
T. cristata	35618	134.79	132.45	133.14	123.55	112.78
T. cristata	35636	137.04	132.76	131.48	128.35	116.54
T. cristata	35640	133.61	131.09	130.83	122.40	107.90
T. cristata	35663	147.15	139.68	137.97	120.79	111.90
T. cristata	35678	134.25	130.07	129.45	123.67	114.17
T. cristata	35682	139.15	134.34	133.09	125.07	112.47
T. cristata	35696	148.80	143.11	133.77	119.03	105.99
T. cristata	35718	145.46	139.19	136.19	122.01	109.84
T. cristata	37387	133.28	129.21	128.88	118.71	108.86

Bite force curves were calculated based on Spencer's (1995) lever model. The constrained lever model predicts that bite forces will increase in Region I, the anterior portion of the mouth, but will plateau and remain constant throughout Region II, located just posterior to Region I. The leveling-out of bite forces in Region II is due to a constraint within the masticatory system that protects the TMJ from dislocation due to tensile loading. Furthermore, Spencer (1995) observed that raising the TMJ above the occlusal plane (the configuration shared by anthropoid primates) will affect the bite force curve such that forces in Region II may *decrease* distally (model predictions summarized in Table 6.9). Thus, bite force curves in this study were expected to increase in Region I, then flatten or decrease in Region II. While bite forces were calculated for every bite point along the tooth row, only postcanine tooth data were used in the current analysis (see Tables 6.7 and 6.8 [above] for playtrrhine and catarrhine bite force curves, respectively).

Calculated bite force patterns are variable both within and among species. Because bite forces were calculated using an arbitrary constant for muscle force (see discussion in Chapter 3), it is not appropriate to compare force values between specimens or species. However, the pattern of force distribution can be compared. To more clearly see the pattern of force along the tooth row, a representative specimen from each species was graphed along with representatives of closely-related species (Figures 6.1 to 6.4, below).

TABLE 6.9. Lever model predictions for Regions I and II.

	Region I		Region II	
	Bite force magnitude	Why?	Bite force magnitude	Why?
Simple lever model	increase	Reduction in *b*, bite force moment arm length	increase	Reduction in *b*, bite force moment arm length
Constrained lever model	increase	Reduction in *b*, bite force moment arm length	plateau	Reduction in *M*, muscle force
Spencer model	increase	Reduction in *b*, bite force moment arm length	plateau or decrease	Reduction in *M*, muscle force and a raised TMJ

Across anthropoids, there are three typical patterns of bite force on the postcanine tooth row. First, bite forces increase on the premolars and then level-off on the molars (as in *P. anubis*, Figure 6.4). Alternately, bite forces may increase on the premolars and then decrease on the molars (as in *A. caraya*, Figure 6.1). Finally, bite forces increase on the premolars, and then continue to increase throughout the molar row at a slower relative rate (as in *P. rubicunda*, Figure 6.3). In addition to the three patterns just described, two specimens have bite force curves that show a sharp increase in bite force on M3 (as in *A. palliata* 5325, Figures 6.5 and 6.6). While bite force patterns within a species are generally similar, some species, particularly *A. palliata* (see Figure 6.5), contain a variety of bite force curve patterns, underscoring the effect of individual variation on the ability of the masticatory system to produce high-magnitude bite forces along the tooth row.

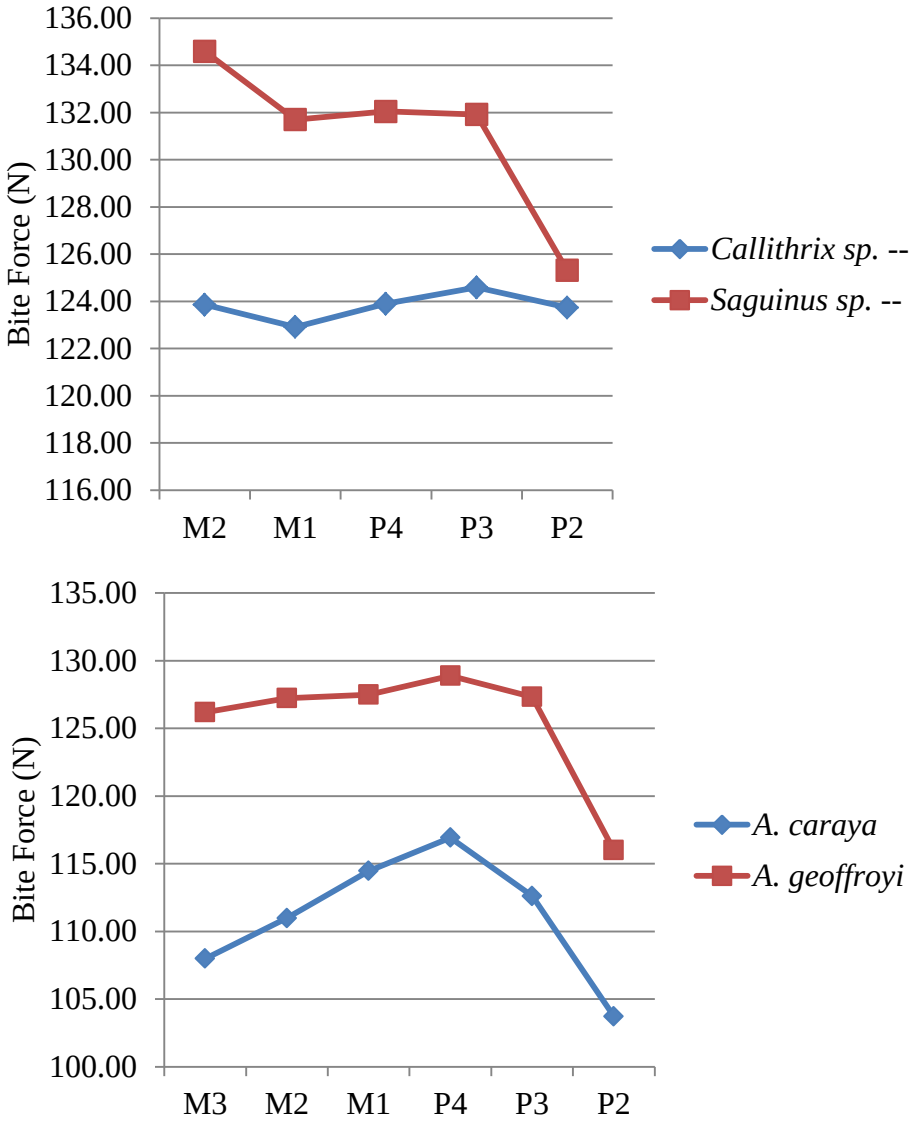

Fig. 6.1. Bite force curves for *Callithrix* and *Saguinus* (top) and for *A. caraya* and *A. geoffroyi* (bottom).

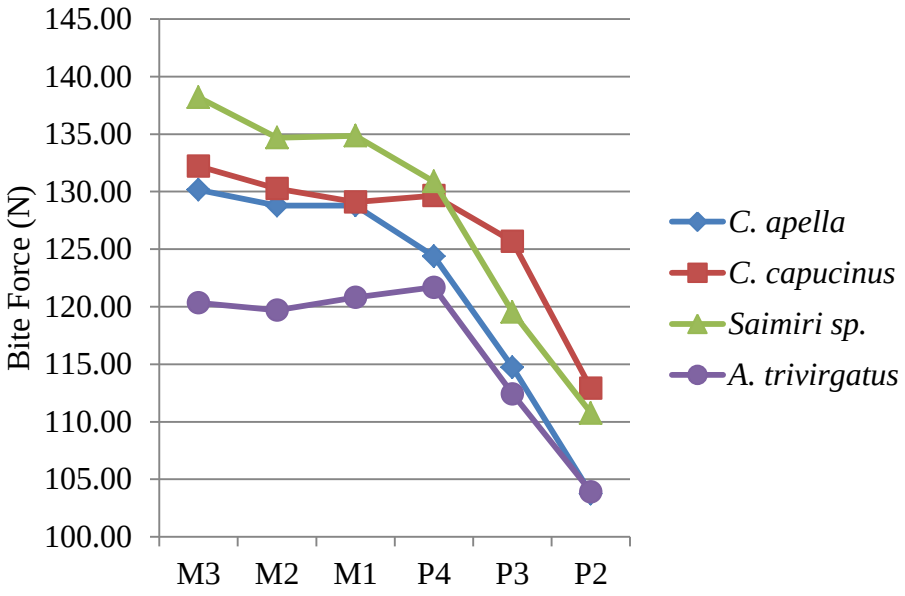

Fig. 6.2. Bite force curves for the subfamily Cebinae.

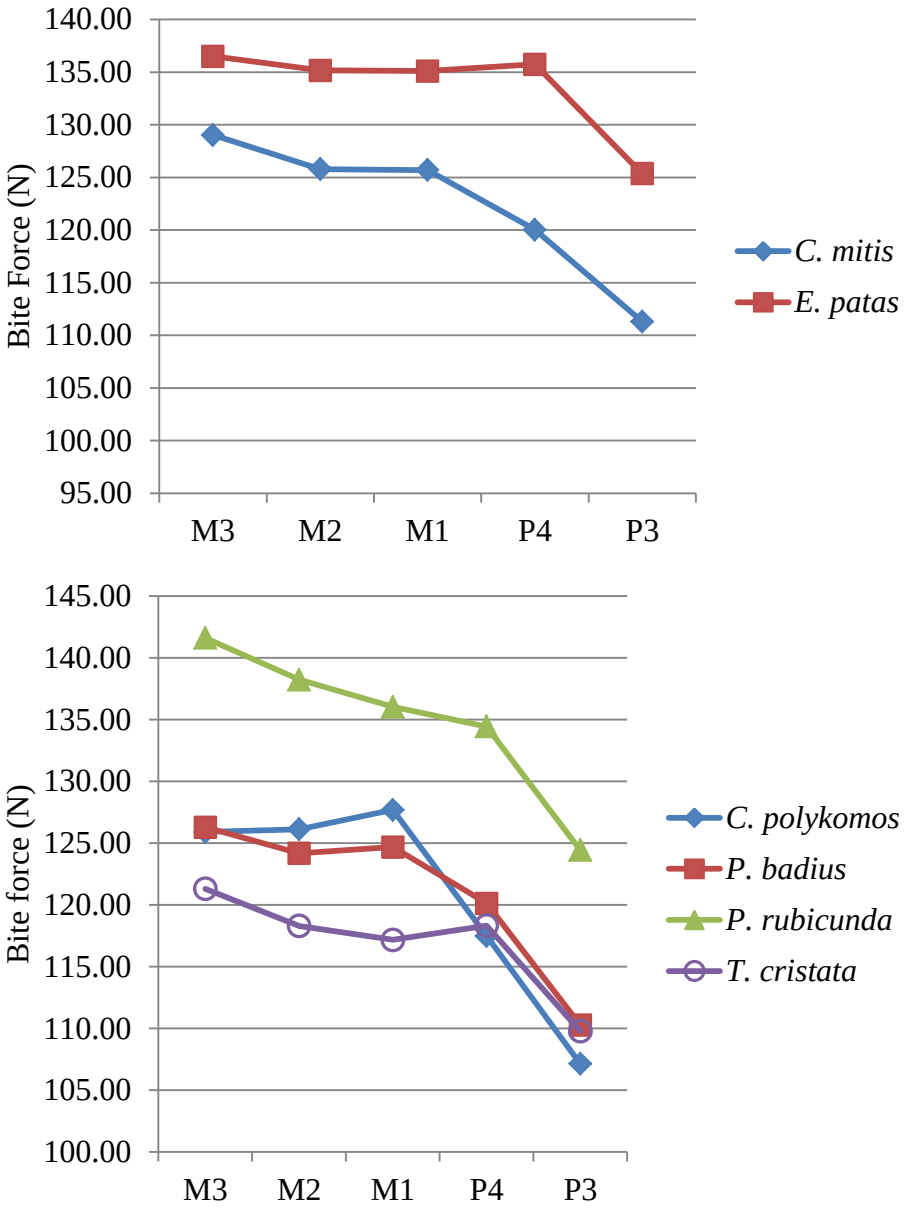

Fig. 6.3. Bite force curves for *C. mitis* and *E. patas* (top) and for colobine monkeys (bottom).

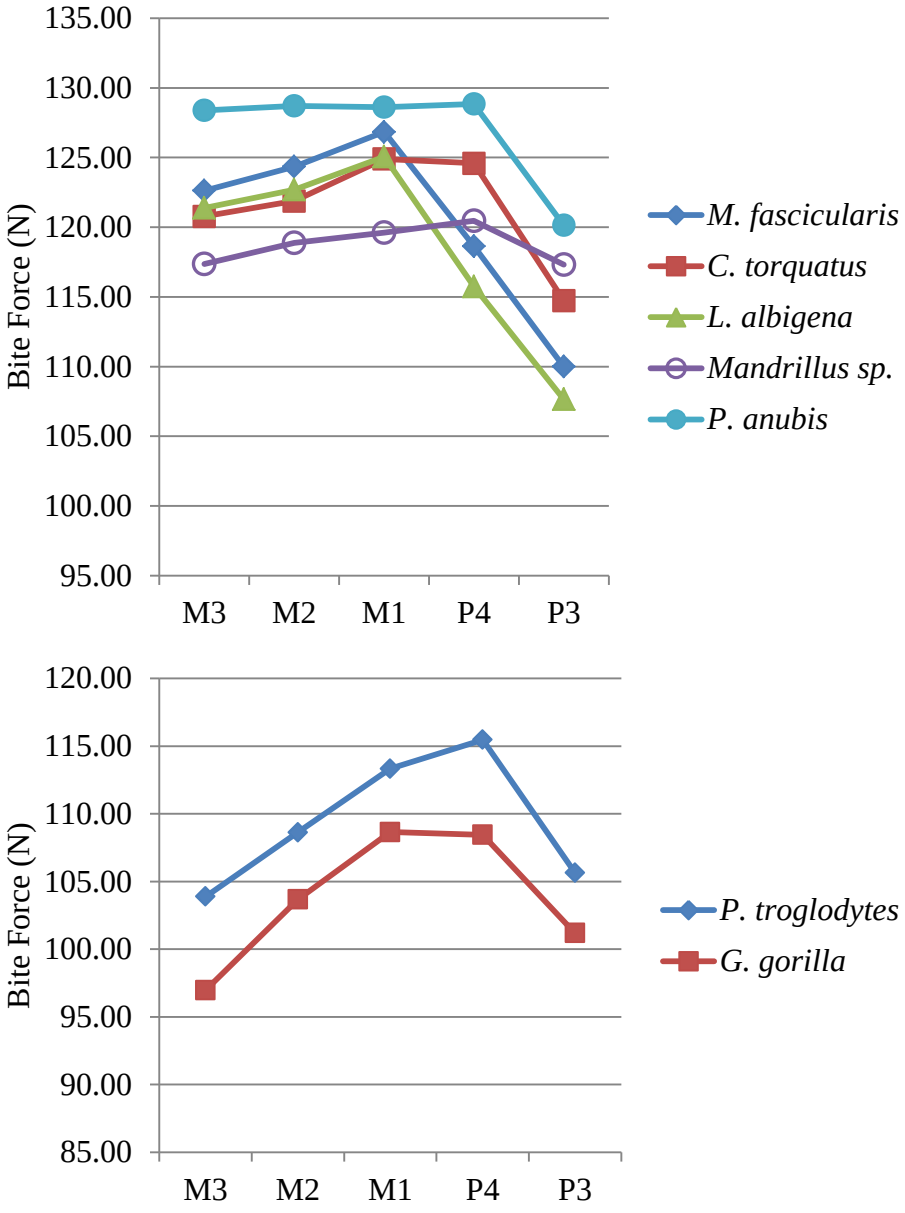

Fig. 6.4. Bite force curves for African papionins (top) and hominoids (bottom).

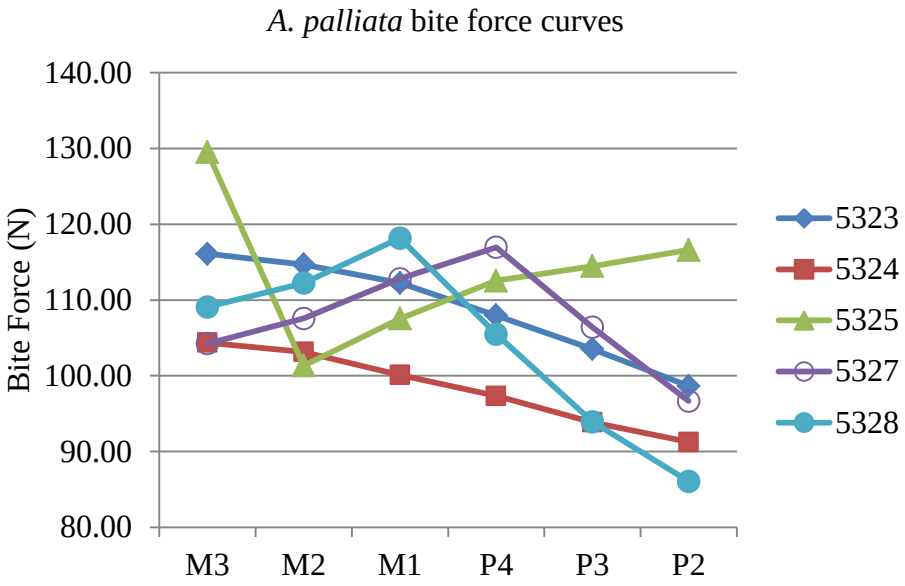

Fig. 6.5. Bite force curves for five *A. palliata* individuals.

Bite force patterns: Discussion

While many bite force curves calculated for the current study reflect steady or decreasing bite forces in Region II, many also indicate that bite forces continually increase as the bite point moves distally, even when considering the constraints in Region II that protect the TMJ from dislocation (Tables 6.7 and 6.8; Figures 6.1-6.5). While some patterns fell outside of specified model predictions, all patterns are consistent with Spencer's (1995) model in that changes in TMJ height, muscle resultant inclination, and muscle force production along the tooth row are incorporated into bite force curve estimations. The varying patterns of bite force curves seen in the current study are a result of the incredible amount of craniofacial variation seen among anthropoid primates.

Recall from equation (5) that the major variables affecting bite force are muscle resultant force, *M*, muscle resultant moment arm, *m*, and bite force moment arm, *b*. For all models of feeding mechanics discussed in the current study, *M* is predicted to be at a constant, maximum magnitude throughout Region I. Consequently, the predicted increase in bite force in Region I is a result of a decrease in *b* relative to *m*. In other words, the continual decrease of the bite force moment arm as the bite point moves posteriorly along the tooth row is the driving factor behind the increases in bite force typical of Region I.

In Region II, bite force moment arm continues to decrease, but balancing-side muscle force also decreases to shift the muscle resultant laterally and protect the TMJ from dislocation. If the decrease in muscle force cannot counteract the effect of the increasing muscle resultant moment arm (caused by an

anterosuperiorly inclined muscle resultant, discussed in Chapter 2) and decreasing bite force moment arm, both of which are changing in ways that result in increasing bite force, maximum bite force magnitude will continue to increase throughout Region II, albeit at a slower rate than in Region I, producing a bite force curve like the ones seen in the examples from *C. mitis* and *P. rubicunda* in Figure 6.3.

As mentioned above, the bite force curve of *A. palliata* 5325 (Figure 6.6) differs from the more typical patterns observed in the current study. Bite force increases posteriorly in Region I, a pattern shared among all primates included in the current study and predicted by all models of feeding mechanics. For *A. palliata* 5325, Region II begins with P2 and shows a decline in bite forces until M2, which is due to the decrease in the b-s muscle force required to keep joint integrity in this region.

However, bite force on M3 is dramatically increased relative to M2 (or indeed any tooth), counter to model predictions. Examination of the calculations involved in estimating bite force reveals that the increase in bite force on M3 in *A. palliata* 5325 is due to a calculated increase in b-s muscle force on this bite point. The increase in b-s muscle force is due to a large decrease in muscle resultant moment arm at M3 that in turn affects the calculation of the amount of lateral shifting necessary to maintain the muscle resultant within the triangle of support (Equation 12, discussed in Chapter 3). In essence, the decrease in *m* mimics a posteriorly-positioned muscle resultant that requires relatively less lateral shifting

to remain inside the triangle of support, resulting in a calculated increase in bite force on M3.

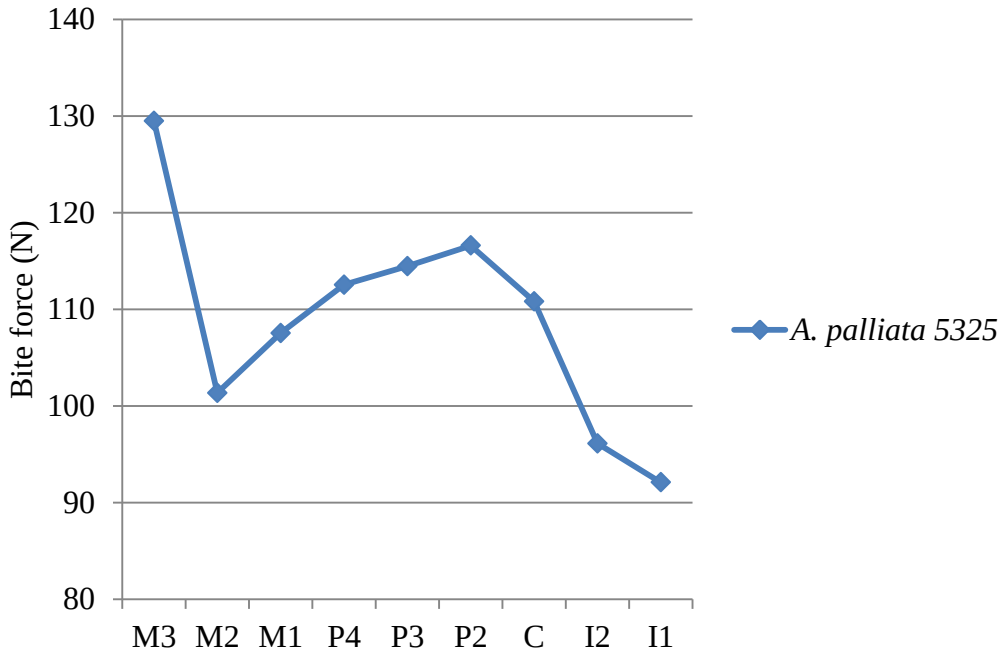

Fig. 6.6. *A. palliata* 5325 bite force curve. See text for details.

It is unlikely, however, that this calculated increase in distal-most bite force reflects an actual ability to produce more force posteriorly. Rather, the dramatic increase in bite force on M3 in *A. palliata* 5325) is a result of slight variations within variables in a ratio (the muscle force moment arm / the bite force moment arm) that approaches zero that has downstream effects, including increasing balancing-side muscle force at the distal-most bite point. Rather than increasing dramatically at M3, as indicated by calculation, it is more likely that

muscle force is actually decreasing posteriorly due to the safety considerations proposed by Greaves (1978) and Spencer (1995), and that the high bite force calculated for M3 in this instance is the result of mathematical idiosyncrasy.

One way to combat the effect of the disjunct between the model of feeding mechanics and actual loading parameters is to refine how muscle force is approximated. In Greaves' (1978) model, b-s muscle force decreases to shift the muscle resultant laterally while w-s muscles continue firing at maximum magnitudes. However, experimental studies using EMG show that muscle recruitment patterns during mastication in primates is extremely complex. Working- and balancing-side muscles fire asynchronously throughout mastication, and even muscles on the same side vary in when and at what magnitude they fire (Hylander et al., 1992, 2005; Hylander and Johnson, 1994; Spencer, 1995). Furthermore, research has shown that muscle recruitment patterns are different for humans, macaques and baboons, owl monkeys, ring-tailed lemurs, and fat-tailed galagos (Hylander et al., 1994, 2005), suggesting that an evolutionary change in muscular recruitment pattern during mastication has occurred in these species in addition to changes in craniofacial form over time.

Experimental studies have shown that both working- and balancing-side muscles vary in activity throughout mastication (Hylander et al., 1987), suggesting that the simple decrease in balancing- to working-side force ratio suggested by Greaves obscures the complexity of actual masticatory muscle force output patterns. Since physiological cross-sectional area (PCSA) is an indicator of the magnitude of force a muscle can produce (discussed in Chapter 3), knowing

the PCSA of the anterior temporalis, superficial masseter, and medial pterygoid muscles for a species would allow each muscle to be weighted in terms of how much it can contribute to total muscle force. Currently, these data are sparse and confined to a limited number of primate species; research on PCSA in a variety of primate species is necessary to supply to data required to estimate actual muscle forces during primate mastication (cf. Perry et al., 2011).

Calculated bite force curves for primates in this study display a variety of patterns, especially at distal bite points. Bite force increases throughout Region I for all species, but force patterns in Region II vary both within and among species. In Region II, calculated bite forces may increase, plateau, or decrease, without violating the constraints of Spencer's (1995) model, depending on the exact spatial configuration of the masticatory muscles, TMJs, the gnathic skeleton and the teeth.

Muscle resultant position revisited

As discussed in Chapter 3, the horizontal distance from the TMJs to M3 in the occlusal plane (b_H *M3*) is used in the current study as a proxy for muscle resultant position (m_H) despite the fact that its actual position is likely more posterior in the mouth. To assess whether data in the current study support a more anterior muscle resultant position (as assumed by Greaves) or a more posterior muscle resultant position (as found by comparative analyses, Spencer, 1995; Perry et al., 2011), muscle resultant position was estimated for each specimen in the sample using data from landmark coordinates in conjunction with MacMorph software (Spencer and Spencer, 1993) and compared to b_H *M3*.

To calculate muscle resultant position, the angle of each masticatory adductor (superficial masseter, anterior temporalis, and medial pterygoid) was calculated as described in Chapter 3. Next, the horizontal distance from the TMJ to the muscle insertion centroid in the occlusal plane (h_{MI}) was calculated from measurements taken in MacMorph (Figure 6.7). Then, the distance from the muscle insertion centroid to the occlusal plane (v_{MI}) was measured. Using the muscle resultant angle at the occlusal plane (θ, calculated in Chapter 3), it is possible to determine the distance between the muscle insertion centroid and the intersection of the muscle vector and the occlusal plane (z) using the equation

$$z = \frac{v_{MI}}{\tan \theta} \tag{16}$$

To find m_H for each muscle, z is added to h_{MI}, and the values for each muscle are averaged for a single muscle resultant position. Finally, m_H was divided by b_H *M3*, and the resulting ratios were compared.

Results indicate that the calculated muscle resultant in anthropoids is positioned significantly posterior to M3 ($p < 0.001$; MWU-test), as has been suggested by other studies (Spencer, 1995; Perry et al., 2011). Additionally, the m_H/b_H *M3* ratio for platyrrhines is significantly larger than in catarrhines ($p < 0.001$; MWU-test). In other words, the muscle resultant position in platyrrhines is more anterior relative to catarrhines, which indicates that Region II is shifted anteriorly (or that the buffer zone is smaller) in the former relative to the latter. An anterior shift of Region II requires b-s muscle force to be reduced at more

anterior bite points, suppressing maximum bite force magnitudes while protecting the TMJ; in addition, an anterior movement of Region II would result in the concentration of the highest achievable bite forces at its anterior end. The reduction in the distance between the distal-most tooth and the muscle resultant in platyrrhines may be a result of the facial orthagnathy characteristic of cebids and callitrichids.

Shifting the tooth row posteriorly relative to the TMJ has been interpreted as an adaptation for increasing bite force throughout primate evolution, because this configurational shift reduces the length of the bite force moment arm relative to the muscle resultant moment arm. An anterio-posteriorly shortened face has been observed in many extant primate species that consume hard and/or tough foods (i.e., *C. apella*), and is a distinguishing feature of the extinct paranthropines, who are typically reconstructed consuming a mechanically resistant diet. However, when accounting for *all* of the parameters that influence bite force, including raising the TMJ above the occlusal plane and inclining the muscle resultant, it becomes apparent that a-p shortening of the face (and thus shortening the bite force moment arm) will also impact how and where muscle force is distributed along the tooth row such that muscle force begins to decrease at relatively anterior bite points to protect TMJ integrity. It is suggested that there is a limit to the extent to which bite forces can be increased with facial shortening in primates due to the safety features in place to protect the TMJ from dislocation.

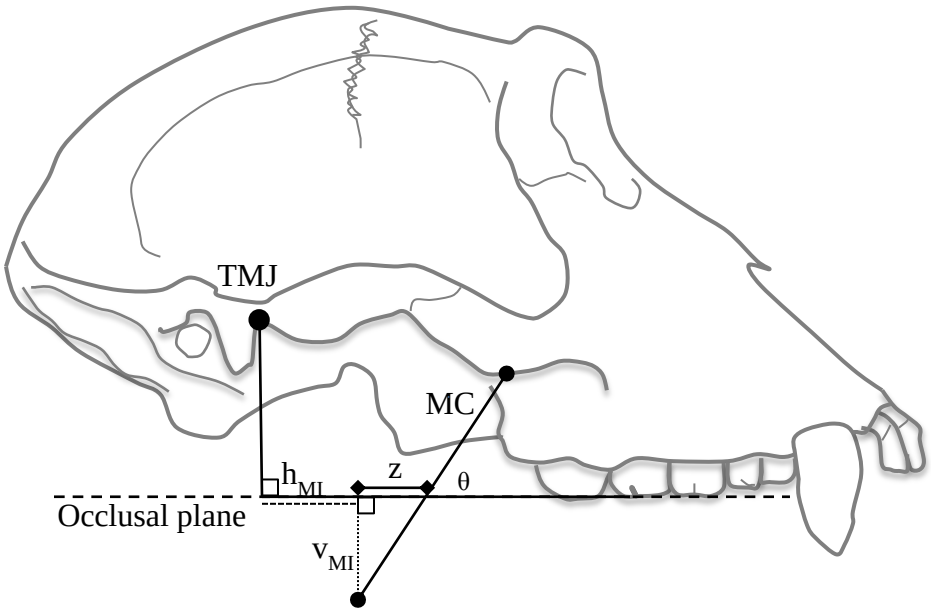

Fig. 6.7. Finding m_H. MC = the length between the muscle origin and insertion centroids. v_{MI} = the vertical distance from the muscle insertion centroid to the occlusal plane. h_{MI} = the horizontal distance from the TMJ to the muscle insertion centroid in the occlusal plane. z = the distance from the muscle insertion centroid to the muscle vector/occlusal plane intersection in the occlusal plane. θ = the angle of the muscle resultant force vector at the occlusal plane (calculated in Chapter 3).

Hypotheses 2 and 3: Results

Results indicate that among anthropoids, estimated bite force curves have a variety of shapes; estimated force increases in Region I for all taxa, but estimated forces in Region II are more diverse (either increasing, staying the same, or decreasing). Hypotheses 2 and 3 predict that, regardless of the shape of the bite force curve, root surface area and cervical margin surface area should correlate significantly with predicted force along the tooth row. Root surface area (RSA), cervical margin surface area (CMSA), and bite force magnitudes (BFC)

were ranked highest to lowest along the tooth row for all postcanine teeth. RSA and CMSA were each compared to BFC separately. Results are summarized in Tables 6.10 (RSA) and 6.11 (CMSA). For each species there is a correlation coefficient, which indicates the magnitude and direction of the correlation between bite force and root size or bite force and crown size. It was expected that the tooth with the largest RSA (Hypothesis 2) and the largest CMSA (Hypothesis 3) should also have the highest calculated bite force (BFC) relative to other postcanine teeth.

TABLE 6.10. Kendall's τ results, Part II: Root size and bite force

Subfamily	Species	N	[a]correlation coefficient	[b]p-value
Callithrichidae	*Callithrix sp.*	M = 7 F = 7	-0.40	***
	Saguinus sp.	M = 5 F = 5	-0.13	ns
Cebinae	*Aotus trivirgatus*	M = 1 F = 7	0.27	**
	Cebus apella	M = 5 F = 9	-0.50	***
	Cebus capucinus	M = 2 F = 7	-0.46	***
	Saimiri sp.	M = 4 F = 2	-0.43	***
Pitheciinae	*Callicebus moloch*	M = 10 F = 0	0.38	***
	Pithecia sp.	M = 3 F = 3	-0.10	ns
Atelinae	*Alouatta caraya*	M = 1 F = 3	0.19	ns
	Alouatta palliata	M = 0 F = 10	0.24	**
	Ateles geoffroyi	M = 0 F = 17	0.22	**
Colobinae	*Presbytis hosei*	M = 1 F = 4	0.32	ns
	Presbytis rubicunda	M = 4 F = 4	0.36	*
	Trachypithecus cristata	M = 0 F = 14	0.42	***

(cont)

[a]Correlation coefficient. The sign of the number indicates a positive or negative correlation.

[b]p-values. *** = $p < 0.001$, ** = $p < 0.01$, * = $p < 0.05$, ns = not significant.

TABLE 6.10 (cont). Kendall's τ results, Part II: Root size and bite force

Subfamily	Species	N	[a]correlation coefficient	[b]p-value
Colobinae	*Colobus polykomos*	M = 1 F = 5	0.40	**
	Piliocolobus badius	M = 4 F = 5	0.57	***
Cercopithecinae	*Macaca fascicularis*	M = 1 F = 6	0.64	***
	Macaca fuscata	M = 1 F = 1	0.50	ns
	Lophocebus albigena	M = 5 F = 1	0.39	*
	Cercocebus torquatus	M = 2 F = 1	0.38	ns
	Papio anubis	M = 3 F = 2	0.67	**
	Mandrillus sp.	M = 5 F = 1	0.18	ns
	Cercopithecus mitis	M = 0 F = 12	0.48	***
	Erythrocebus patas	M = 3 F = 1	0.41	*
Homininae	*Pan paniscus*	M = 0 F = 3	-0.23	ns
	Pan troglodytes	M = 0 F = 13	0.12	ns
	Gorilla gorilla	M = 0 F = 5	0.33	ns
Total N:		216		

[a]Correlation coefficient. The sign of the number indicates a positive or negative correlation.

[b]p-values. *** = $p < 0.001$, ** = $p < 0.01$, * = $p < 0.05$, ns = not significant.

The pattern of correlation between bite force and root size among platyrrhines is complex. *A. palliata, A. trivirgatus, A. geoffroyi,* and *C. moloch* all show a moderate, statistically significant positive correlation between bite force and root size, as predicted by Hypothesis 2. However, *Callithrix sp., C. apella, C. capucinus*, and *Saimiri sp.* all show strong significant *negative* correlations between bite force and root size. In other words, for these four taxa, an increase in bite force magnitude correlates with a decrease in tooth root size. There is no significant relationship between RSA and BFC in *A. caraya, Pithecia sp.*, and *Saguinus sp*.

Among catarrhines, *L. albigena, C. mitis, P. badius, C. polykomos, E. patas, M. fascicularis, P. anubis, P. rubicunda,* and *T. cristata* all show a significant positive correlation between bite force and root size, as predicted by Hypothesis 2. However, for *C. torquatus, G. gorilla, M. fuscata, Mandrillus, P. paniscus, P. troglodytes,* and *P. hosei* there is no significant correlation between bite force and root size.

TABLE 6.11. Kendall's τ results, Part II: Cervical margin surface area and bite force

Subfamily	Species	N	[a]correlation coefficient	[b]p-value
Callithrichidae	*Callithrix sp.*	M = 7 F = 7	-0.29	**
	Saguinus sp.	M = 5 F = 5	-0.29	*
Cebinae	*Aotus trivirgatus*	M = 1 F = 7	0.30	**
	Cebus apella	M = 5 F = 9	-0.09	ns
	Cebus capucinus	M = 2 F = 7	-0.26	*
	Saimiri sp.	M = 4 F = 2	-0.26	ns
Pitheciinae	*Callicebus moloch*	M = 10 F = 0	0.46	***
	Pithecia sp.	M = 3 F = 3	0.26	ns
Atelinae	*Alouatta caraya*	M = 1 F = 3	0.16	ns
	Alouatta palliata	M = 0 F = 10	0.32	**
	Ateles geoffroyi	M = 0 F = 17	0.25	**
Colobinae	*Presbytis hosei*	M = 1 F = 4	0.67	**
	Presbytis rubicunda	M = 4 F = 4	0.52	**
	Trachypithecus cristata	M = 0 F = 14	0.58	***

(cont)

[a]Correlation coefficient. The sign of the number indicates a positive or negative correlation.

[b]p-values. *** = $p < 0.001$, ** = $p < 0.01$, * = $p < 0.05$, ns = not significant.

TABLE 6.11 (cont). Kendall's τ results, Part II: Cervical margin surface area and bite force

Subfamily	Species	N	[a]correlation coefficient	[b]p-value
	Colobus polykomos	M = 1 F = 5	0.30	ns
Colobinae	*Piliocolobus badius*	M = 4 F = 5	0.60	***
	Macaca fascicularis	M = 1 F = 6	0.61	***
	Macaca fuscata	M = 1 F = 1	0.50	ns
	Lophocebus albigena	M = 5 F = 1	0.39	*
	Cercocebus torquatus	M = 2 F = 1	0.38	ns
	Papio anubis	M = 3 F = 2	0.67	**
	Mandrillus sp.	M = 5 F = 1	0.21	ns
	Cercopithecus mitis	M = 0 F = 12	0.51	***
Cercopithecinae	*Erythrocebus patas*	M = 3 F = 1	0.41	*
	Pan paniscus	M = 0 F = 3	-0.28	ns
	Pan troglodytes	M = 0 F = 13	-0.28	*
Homininae	*Gorilla gorilla*	M = 0 F = 5	0.10	ns
Total N:		216		

[a]Correlation coefficient. The sign of the number indicates a positive or negative correlation.

[b]p-values. *** = $p < 0.001$, ** = $p < 0.01$, * = $p < 0.05$, ns = not significant.

When comparing bite force to crown size among platyrrhines, the patterns are similar to comparisons with root size, though not the magnitude of the correlation. Among *A. palliata, A. trivirgatus, A. geoffroyi* and *C. moloch*, there was a moderate, statistically significant positive correlation between bite force and crown size as predicted by Hypothesis 3. Furthermore, for *A. palliata, A. trivirgatus, A. geoffroyi* and *C. moloch*, the correlation coefficient is higher for analyses of crown size relative to analyses of root size, indicating a slightly stronger tie between bite force and crown size than bite force and root size for these species. *Callithrix sp., C. capucinus*, and *Saguinus sp.* all have significant, negative correlations between bite force and crown size. Interestingly, the correlation coefficients show a much weaker relationship between bite force and crown size than bite force and root size in *Callithrix sp., C. capucinus*, and *Saguinus sp.*

When BFC is compared to CMSA in catarrhines, overall patterns are similar to comparisons with RSA. *L. albigena, C. mitis, P. badius, M. fascicularis, P. anubis, P. hosei, P. rubicunda,* and *T. cristata* all showed significant positive correlations between BFC and CMSA as predicted by Hypothesis 3, and in all cases except for *M. fascicularis*, the correlation coefficient increased relative to the comparison between BFC and RSA. *C. torquatus, C. polykomos*, *E. patas, G. gorilla, M. fuscata, Mandrillus*, and *P. paniscus* all show no significant correlation between BFC and CMSA. *P. troglodytes* has a statistically significant, weak negative correlation between BFC and CMSA.

Hypotheses 2 and 3: Discussion

The purpose of Part II of the current study was to determine the extent to which tooth size (root and crown size) correlates with bite force magnitude along the tooth row. Although tooth root and crown size are assessed in separate analyses, results are similar for both; consequently, the discussion and figures for this section will feature analyses of root surface area with the understanding that conclusions are the same for both root and crown size unless otherwise indicated. Among platyrrhines, four species show a significant, positive correlation between root size and bite force magnitude, four species show a significant, negative correlation between root size and bite force magnitude, and three species show no significant relationship between bite force magnitude and root size. Among catarrhines, nine species show significant, positive correlations between root size and bite force magnitude, and seven show no significant relationship between the two. Additionally, *P. troglodytes* has a significant, negative correlation between CMSA and BFC.

About one half (13 of 27) of the anthropoid species examined in the current study show a significant, positive correlation between root/crown size and BFC as predicted by Hypotheses 2 and 3. Ten species show no significant relationship between root/crown size and BFC, although restricted sample sizes may account for the failure of some species to achieve significance even when their correlation coefficients are positive and relatively high (e.g., *M. fuscata*). Furthermore, four species of platyrrhine show significant, negative correlations between RSA and BFC, opposite predictions.

The negative correlation seen among callitrichids and cebids is due to slight variation in estimted molar bite forces combined with molars that dramatically decrease in size distally. Because data were analyzed using rank correlations, the magnitude of the difference in calculated force had no effect on the outcome. Consequently, if M1 has a calculated bite force of 125.02 N and M2 has a calculated bite force of 125.15 N, then M2 bite force is ranked more highly than M1 bite force, despite the fact that the slight calculated difference in force may not translate to an actual, functional difference. Thus, slight differences in the variables of interest can potentially affect correlation analyses, especially if those differences result in a change in rank assignment.

P. troglodytes also has a significant, negative correlation between CMSA and BFC (Figure 6.8). Closer examination reveals that bite forces for chimpanzees were typically estimated to be highest on P4 and then decrease along the rest of the molar row. However, for many specimens, P4 was the smallest tooth. While the patterns of bite force and tooth size along the molar row appear consistent with Hypotheses 2 and 3, the fact that the premolars decrease in size from P3 to P4 causes the negative correlations seen among chimpanzees.

Although the correlation between tooth size and bite force magnitude was not significant for ten of the twenty-seven species examined, correlation coefficients indicate a positive correlation between the two for most species. Although results from correlation analyses examining the relationship between bite force and tooth size are equivocal, the fact that 63% of the time root size and crown size correlate significantly is important and compelling. To achieve a

significant result, tooth size must correlate with bite force in one, specific way; that is, the largest teeth are located where the highest bite forces are produced. Non-significance may result from any number of factors, including there being no relationship between tooth size and bite force, but also slight variations in tooth size or bite force estimate along the dental arcade that result in differences in rank assignment. That the majority of taxa show significant, positifve relationships between tooth size and estimated bite forces, especially considering the large amount of individual variation affecting the patterns of each of these variables, suggests a true functional link between them.

Despite the multitude of different postcanine bite force patterns seen across taxa and within species (i.e., *A. palliata*), there is a significant correlation between bite force magnitudes and root and crown surface area on postcanine teeth across anthropoid taxa that are diverse in size, geographical location, phylogenetic history, and dietary category. Although tooth size along the dental arcade cannot be predicted from estimated bite forces in many sample taxa, results provide compelling evidence that information on specific dimensions of craniofacial form related to masticatory function can predict relative tooth size along the dental arcade among a broad array of anthropoid taxa. Future studies that incorporate more detailed information on relative muscle force contribution (discussed above) into calculations of bite force may increase the utility of using the lever model in this way by accommodating a broader range of craniofacial variability than the current analysis.

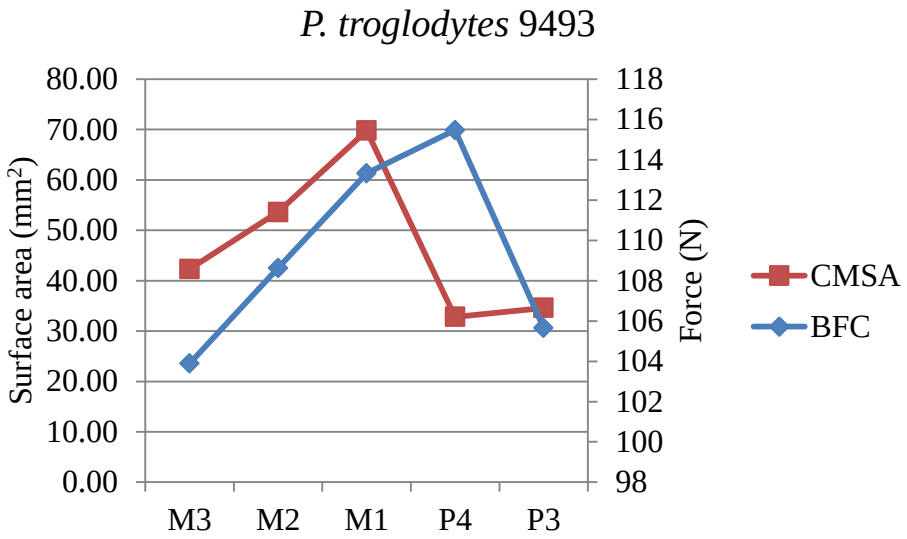

Fig. 6.8. Comparison of CMSA and BFC curves in P. troglodytes 9493. Note the decrease in CMSA from P3 to P4 while BFC is increasing between these teeth.

CHAPTER 7

CONCLUSIONS

The goal of the current study was to determine whether tooth root and crown size varies in response to selection for masticatory force production. In other words, are teeth with big roots and crowns also the teeth that withstand the highest bite forces? To assess the relationships among tooth root size, crown size, bite force patterns, and skull size, it was necessary to procure data on craniofacial spatial relationships and on tooth root and crown size from the same individual. Because root size cannot be measured with the tooth *in situ* without destroying samples, and to increase image resolution, µCT scanning of samples was necessary to collect the root surface area data integral to this project. Consequently, data for this project comprise the largest and taxonomically broadest sample of primate root surface area currently available.

In Chapter 4, the general scaling pattern of root, crown, and skull size was examined across anthropoids. Root and crown size were plotted against the geometric mean of skull size to determine the extent to which dental size correlates with overall size. RMA analyses suggest that root and crown size are isometric relative to skull size, and that there is a high correlation between both root and crown size and skull size across anthropoids, although the strength of this relationship is variable along the tooth row. Results suggest that body size alone does not account for all of the variation present in primate tooth root and crown size.

Chapter 5 reveals the results of Part I of the current study, in which Hypotheses 1a and 1b were tested. Hypothesis 1a simply states that root surface area and crown sizes will covary along the tooth row, and is supported by research that suggests that root surface area (Spencer, 2003; Kupzcik, 2003) and crown size (Demes and Creel, 1988; Spencer, 2003; Lucas, 2004) should be greatest where bite forces are highest. Scaling analyses clearly indicate that root and crown surface area can vary in relative size, a conclusion that is supported by results from other studies (Spencer, 2003; Kupczik et al., 2009), which suggests that their covaration along the tooth row may be the result of a shared functional pressure. Hypothesis 1a is supported by the results of the current study. An analysis using Kendall's τ shows that root and crown size are very tightly correlated along the tooth row in anthropoid primates. Covariation in root and crown size along the tooth row by itself is not indicative of shared function; big crowns may just grow big roots. However, when considered in conjunction with the results of other analyses both from this study and from past research, it is suggestive that tooth root and crown size vary in response to masticatory force.

Hypothesis 1b states that root surface area and crown size are functionally related, and primates with mechanically resistant diets will have relatively higher values for these characteristics than closely-related primates with soft diets. Pair-wise comparisons between primates with resistant versus soft diets support the predictions of Hypothesis 1b overall; generally, the primates processing a resistant diet had larger tooth roots and crowns than those processing soft diets.

There are two groups, however, in which Hypothesis 1b was not supported: the pitheciins and the African papionins.

Among pitheciins, it was predicted that *Chiropotes* would have larger premolar roots and crowns than either *Callicebus* or *Pithecia*, and that *Pithecia* would have larger molar roots and crowns than either *Chiropotes* or *Callicebus*. Although the predictions regarding *Chiropotes* were supported, those regarding *Pithecia* were not. Both *Pithecia* and *Chiropotes* are categorized as having a resistant diet, however, the mechanical properties of diet differ between these taxa. While *Chiropotes* is an acknowledged hard object feeder and seed predator, *Pithecia* is more folivorous, incorporating more tough plants into its diet (Kinzey and Norconk, 1990, 1992). Although the properties "hard" and "tough" are both considered "Resistant" for the purposes of the current study, the mechanical properties of a hard food are very different than those of a tough food (discussed in detail in Chapter 2). It has been suggested by Lucas (1984; 2004) that, while tooth size will correlate with food hardness, it is tooth shape that correlates with food toughness. As the current study only measures tooth root and crown size, and does not quantify shape, dental morphological differences between taxa that are related to adaptation for tough food may be overlooked.

The African papionins, who are as a group classified as durophagous (Jolly, 2007), also deviate from hypothesized predictions. The pair-wise comparisons in African papionins paired *Lophocebus* and *Papio*, and *Cercocebus* and *Mandrillus*. While one of each of these pairs is labeled as a "Soft" food consumer for the purposes of the current study, all taxa in this group are eating

mechanically resistant items; the differences between a hard food processer and a harder food processor are likely too subtle to detect using the data from the current study. Overall, hypotheses in Part I of the current study are upheld. Tooth root and crown surface area covary along the tooth row, and are relatively larger in primates that process a resistant diet.

Crown size and root surface area covary along the tooth row; past research suggests they may be related to bite force. Bite force magnitude is known to change with bite point (Mansour and Reynick, 1975; Pruim et al., 1980; van Eijden et al., 1988; van Eijden, 1991; Oyen and Tsay, 1991; Iwase, 1998; Spencer, 1998; Throckmorton and Ellis, 2001; Dumont and Herrell, 2003; Ferrario et al., 2004), and comparative studies suggest that teeth with bigger roots withstand larger masticatory forces (Spencer, 2003). Furthermore, previous research has suggested that crown size should be largest where bite forces are highest (Hylander, 1985; Demes and Creel, 1988; Spencer, 2003; Lucas, 2004). In Chapter 6 (Part II of the current study) correlation analyses were performed to determine whether root (Hypothesis 2) and crown (Hypothesis 3) size increase on teeth that typically withstand high-magnitude loading.

Bite force curves calculated based on the Spencer (1995) model show that there are a variety of patterns of bite force along the tooth row among primates. While members of the same taxon tended to have similarly-shaped force curves, even within a species patterns of maximum force distribution differed. This suggests that even the relatively minor variances present among individuals of the

same species can have an enormous impact on the magnitude and patterns of force produced along the tooth row.

Analysis of muscle resultant position as estimated from muscle landmarks compared to setting the muscle resultant directly behind M3 (as in Greaves, 1978), discussed in Chapter 6, reveals that, as a group, platyrrhines have a more anteriorly-placed muscle resultant than catarrhines. Moving the muscle resultant anteriorly effectively shifts Region II anteriorly, allowing high bite forces on relatively anterior teeth, but results in decreasing b-s muscle force as the bite point moves distally, which typically decreases bite force. In species in which the tooth row is located far in front of the TMJ (e.g., *Papio*), such an anterior shift in muscle resultant would not necessarily result in a decrease in distal bite forces because when teeth are placed relatively anteriorly to the TMJ there is little danger of the muscle resultant falling outside of the triangle of support, even at distal bite points. However, moving the muscle resultant anteriorly in a species with an orthognathic face (or reducing facial prognathism in a species with an anteriorly-placed muscle resultant) will result in a decrease in bite force at distal bite points because anterior movement of the muscle resultant places it and the tooth row very close together, increasing the chance of loading the TMJ in tension, thus requiring a decrease in b-s muscle force to protect joint integrity.

An orthognathic face has traditionally been interpreted as a general adaptation to produce high bite forces (DuBrul, 1977; Hylander, 1979a, Ravosa, 1990; Antón, 1994); however, current results suggest that a-p facial shortening (on its own) may be most advantageous in species that concentrate relatively high

bite forces on relatively anterior teeth for food processing (i.e., *C. apella*, *Chiropotes*).

When bite force curves were compared with patterns of root and crown size along the tooth row, results were equivocal. Bite force and tooth size were expected to be significantly, positively correlated, and slightly more than half of the examined taxa show the predicted relationship. In some cases, correlation coefficients between tooth size and bite force magnitude were high and positive but not significant due to small sample size (i.e., *M. fuscata*). Cebids and callitrichids demonstrate a significant, negative correlation between tooth size patterns and bite force distribution along the tooth row; it is suggested that this may be due to slight variations in estimated bite forces on molar teeth that may have been impacted by how rank was assigned in some individuals (discussed in Chapter 6). Though correlation results may seem underwhelming, it is important to remember that in this case a significant result (found in the majority of analyses) is much stronger evidence for supporting the hypothesis than a non-significant result is for rejecting it (discussed in Chapter 6).

Taken together, results of the current study indicate that primate teeth vary in size depending on the amount of masticatory force production required to process food. Not only do primates with mechanically resistant diets typically have larger roots and crowns than close relatives with soft diets, but in many taxa, individuals the largest teeth are typically situated where the highest bite forces can be produced along the tooth row.

Results from the current study potentially impact the interpretation of fossil materials. Among extinct hominins, members of the genus *Paranthropus* are characterized by a specialized facial form that is hypothesized to be related to producing high magnitude bite forces. These characteristics include the anterior migration of the masticatory adductors, increased height of the TMJ above the occlusal plane and pronounced orthognathy, as well as the presence of molarized premolars and hypermegadont molars (Robinson, 1956; Walker, 1981; Rak, 1986; Demes and Creel, 1988; Constantino and Wood, 2007).

However, while it has been shown that each of the cranial features mentioned above can, individually, favor an increase in bite forces, it is also true that some combinations of these features may limit bite force production at distal bite points. Specifically, it is suggested here that an increase in facial orthognathy combined with anteriorly-placed masticatory muscles will only increase bite forces at anterior bite points, not for the whole dental arcade. This is supported by the fact that some exant species examined in the current study that combine an anteriorly-positioned muscle resultant and facial orthognathy also have relatively small M3s (as in cebids, or no M3s, in the case of callitrichids), and this phenomenon has also been observed for *Chiropotes* by Spencer (1995).

Based on current comparative evidence, the presence of an a-p short face and forward-positioned muscles in *Paranthropus* should not be accompanied by large distal molars. Molarized premolars are linked to the production of high bite forces on premolars (Rak, 1986; Kinzey, 1992; Scott and McGraw, 2001), which may compromise bite force production on the molars. However, the presence of

megadont molars in *Paranthropus* clearly indicates the need to generate high forces at more distal bite points. To increase both anterior and posterior bite force, an anteriorly-placed muscle resultant should accompany the anterior movement of the dental arcade to circumvent injury to the TMJ (Spencer and Demes, 1993; Spencer, 1995). However, paranthropine orthognathy suggests that the teeth were positioned relatively posteriorly (i.e., closer to the TMJ), which increases the probability that the muscle resultant will fall outside of the triangle of support at posterior bite points. To maintain high bite forces on distal teeth in this configuration, a narrow palate would be expected, since such a configurational change would allow the b-s muscles to exert maximum force at more posterior bite points before having to decrease force output to protect the TMJ.

Paranthropines, however, have wide palates, similar to other hominins (Kimbel et al., 2004). A relatively wide palate allows a greater portion of the dental arcade to be included in Region II, in which the highest bite forces are located relatively anteriorly along the tooth row (Spencer, 1995), but it does not counteract the effect of the decrease in b-s muscle force that characterizes Region II. Therefore, although a wide palate allows more teeth to be included in Region II, it does not convey higher bite forces at more posterior bites (Spencer, 1995).

Why, then, does *Paranthropus* have big molars? In the past, it has been suggested that *Paranthropus* could exert bite forces over a large occlusal area, but that the magnitude of that force was not exceptional when scaled against crown size (Demes and Creel, 1988). Consequently, it has been suggested that

Paranthropus morphology is more suited to producing low magnitude, repetitive like those required for breaking down tough foods (e.g., leaves) rather than hard foods (Demes and Creel, 1988), a suggestion that has found support in recent studies of isotope and microwear analyses (Sponheimer et al., 2006; Ungar et al., 2008; Ungar and Sponheimer, 2011).

However, in Demes and Creel (1988), the bite force equivalent at maxillary M2 was plotted against the occlusal surface area of the entire postcanine tooth row. The current study shows that estimated bite forces can change dramatically over the length of the dental arcade, and that individual facial configuration can produce variable bite force curves within taxa. Thus, Demes and Creel's (1988) assessment of *Paranthropus* bite force capability excludes important information about the pattern of force distribution along the tooth row.

In an analysis of Neandertal and modern human facial biomechanics, Spencer and Demes (1993), suggest that the flattening of anterior dentition against the postcanine dentition seen in Neandertals is a way to increase the mechanical advantage for anterior bite points without sacrificing molar occlusal area. *Paranthropus* exhibits a similar configuration, in which the anterior teeth are greatly reduced in size and the anterior dental arcade appears flattened relative to other australopiths (Grine, 1981), and is suggestive that they, too, had to be able to produce high anterior (in this case, premolar) bite forces while maintaining a large molar surface area.

Recent research using stable isotope analysis suggests that most hominins have an isotopic signature that is indicative of a varied diet that includes plants

using both C_3 (e.g., fruits) and C_4 (e.g., grasses, sedges) photosynthetic pathways (Sponheimer and Lee-Thorp, 1999; Sponheimer et al., 2006; Ungar and Sponheimer, 2011). Interestingly, *P. boisei* does not fit the pattern of other hominins; rather than having a mixed bag of C_3/C_4 foods, *P. boisei* had a high level of C_4 foods incorporated into its diet, indicating to some researchers that grasses and/or sedges may have been an important food resource (Cerling et al., 2011; Ungar and Sponheimer, 2011).

Furthermore, recent microwear analyses suggest that *P. boisei* and the (presumably) closely-related *P. robustus* have different patterns of wear on their molar teeth (Ungar et al., 2008). While *P. robustus* molars have a high incidence of pitting and surface complexity, indicators of a hard food diet, *P. boisei* molars show little pitting and low levels of surface complexity, suggesting its diet may not have consisted of high amounts of hard foods (Ungar et al., 2008).

The results of these separate lines of inquiry are potentially far-reaching as they suggest that *P. boisei* and *P. robustus* not only ate different foods, but that they ate foods that differed in their mechanical properties (Ungar and Sponheimer, 2011). However, given the certainty that some aspects of craniofacial form evolve in response to food mechanical properties, one must ask "If they ate foods that differed in mechanical properties, why do their faces look the same?"

The difficulty in teasing out the differences between adaptation for hard foods and adaptation for tough foods has been discussed previously (see Chapter 2). However, results from the current study suggest that the specific combination

of having anteriorly-placed chewing muscles and an orthognathic face (traits shared by the paranthropines) confers the ability to concentrate higher magnitudes of bite force on premolar teeth, but not on molar teeth. In extant primates, this configuration is seen among *Chiropotes sp*. and *C. apella*, which use their canine/premolar teeth to puncture the hard, outer shells of seeds, nuts, and some fruits. Because the premolars are preferentially loaded with hard objects in these taxa, it has been suggested that premolar microwear (rather than molar microwear) may give a more accurate assessment of whether or not hard objects were consumed by an extinct species (Strait et al., 2009). Recently, Daegling et al. (2011), examined both premolar and molar microwear in the extant hard-object feeder *Cercocebus atys* (the sooty mangabey), and found no significant differences in signal between the two, supporting the validity of conclusions based on molar microwear analysis.

The extent to which *P. boisei* and *P. robustus* differ in dietary proclivites is unknown, but current isotope and microwear data suggest that *P. robustus* ate a relatively larger variety of foods, including hard objects, while *P. boisei* focused more completely on C_4 grasses and/or sedges and did not consume hard objects (Ungar and Sponheimer, 2011). Such a conclusion is at odds with the current biomechanical analyses that conclude that the paranthropine face looks the way it does due to a similar dietary specialization that included hard object feeding. Results from the current study imply that paranthropines may be adapted to producing high bite forces on premolars while maintaining a large molar occlusal area. Considering the extremely large estimated size of paranthropine masticatory

adductors, it seems likely that both members of the genus *Paranthropus* could produce high bite forces throughout Region II. However, it is possible that the extent to which anterior (premolar) force production is emphasized differs between *P. boisei* and *P. robustus*. Data on craniofacial configuration can help to reconstruct bite force ability; however, these data are limited for fossil taxa in which large portions of the skull may be distorted or missing. Comparing even a few individuals, though, may help to determine the extent to which *P. boisei* and *P. robustus* differ in specific features, like positions of the tooth row and the muscle resultant relative to the TMJ.

The current study highlights the fact that all craniofacial features related to bite forces are not equal. Adaptations for increasing bite force on anterior teeth may result in a sacrifice in distal occlusal surface area to protect the TMJ from injury, while configurations favoring high distal bite forces do so at the expense of biting hard on anterior teeth. It is important to distinguish not *that* a taxon is capable of producing high bite forces, but *where* on the tooth row such forces are produced to understand how changes in craniofacial form relate to diet.

Future research on the relationship between bite force production and dental form should also include analysis of relative enamel thickness along the tooth row. Masticatory stress on the tooth crown is resisted by enamel (Thresher and Saito, 1973; Yettram et al., 1976; Kaewsuriyathumrong and Soma, 1993) (note: some models have suggested that dentin may also resist significant masticatory stresses [Spears et al., 1993]). As variation in enamel thickness necessarily affects the way stress is distributed through the tooth, multiple

functional hypotheses link enamel thickness to masticatory force production via dietary selection pressures. Species eating an abrasive diet are subject to a relatively high rate of dental wear; therefore, it has been proposed that thick enamel increases the life of the teeth in these species by increasing the amount of wear required to expose the dentin (Molnar and Gantt, 1977; Teaford et al., 1996; Schwartz, 2000a). Alternately, thick enamel has been proposed as an adaptation to resist fracture when biting on hard objects (Kay, 1981; Lucas et al., 2008 a,b; Vogel et al., 2008). These hypotheses are not mutually exclusive, and both associate thick enamel with a resistant diet.

Enamel thickness varies along the tooth row (in humans, Macho and Berner, 1993; Grine, 2002; in pitheciins, Martin et al., 2003; in hominoids, Schwartz et al., 2000a; Smith et al., 2005; across primates, Shellis et al., 1998). Studies in humans have detected a trend towards an increase in enamel thickness at more posterior tooth positions (Macho and Berner, 1993; Spears and Macho, 1995, 1998; Macho and Spears, 1999; Schwartz, 2000b; Grine, 2002), and some researchers link this increase in thickness to a proposed increase in bite force on posterior teeth as predicted by the simple lever model (Macho and Berner, 1993, 1994; Spears and Macho, 1995, 1998; Macho and Spears, 1999; but see Grine et al., 2005 for an alternate interpretation). However, studies on non-human primates do not agree as to whether enamel thickness increases posteriorly (in hominoids, Smith et al., 2005) or whether no specific trend exists (across primates, Shellis et al., 1998; *Papio ursinus*, Grine et al., 2005).

Confounding adaptive hypotheses of enamel morphology is the fact that enamel thickness is highly positively correlated with the size of the tooth crown and body size (Shellis et al., 1998; Schwartz, 2000a; Grine et al., 2005) (although it is possible that this correlation is due, at least in part, to the fact that enamel thickness contributes to crown size). Despite a general correlation between enamel structure and crown and body size (Shellis et al., 1998), many studies suggest that dietary pressure has been a major determinant of enamel variation. Animals that process hard diets have thicker enamel (primates and bats, Dumont, 1995, 1999; primates, Shellis et al., 1998; hominoids, Smith et al., 2005, Vogel et al., 2008) and more decussation (Maas and Dumont, 1999; Schwartz, 2000a; Macho et al., 2003; Martin et al., 2003) than their close relatives who process soft diets.

In the current study, the relationship among tooth root and crown size and bite force production is explored among a broad sample of primates. Taken together, results indicate that tooth root and crown size vary in response to the magnitude of occlusal loads. By linking root size with bite force production, it is possible to evalutate hypotheses of force production in extinct species for which adequate fossil data on craniofacial form and crown size may be unavailable. Results of the current study also suggest that the relationship between tooth roots and crowns in maxillary teeth may differ from the relationship between tooth roots and crowns in the mandibular teeth (Kupczik et al., 2009). This may have important implications for understanding how masticatory force is distributed in the maxilla relative to the mandible, and should be the subject of future research.

REFERENCES

Abbot SA. 1984. A comparative study of tooth root morphology in the great apes, modern man and early homininds. PhD dissertation. University of London.

Aiello L. 1992. Allometry and the analysis of size and shape in human evolution. J Hum Evol 22:127-147.

Aiello L, Dean C. 2002. An Introduction to Human Evolutionary Anatomy. Elsevier Academic Press, London.

Akiyoshi M, Inoue M. 1963. On the functional structure of cementum. Bul Tok Med Dent Univ 10:41-59.

Anderson RA, Macbrayer LD, Herrel A. 2008. Bite force in vertebrates: Opportunities and caveats for use of a nonpareil whole animal performance measure. Biol J Linn Soc 93:709-720.

Antón SC. 1994. Masticatory muscle architecture and bone morphology in primates. Ph.D. dissertation, University of California, Berkely.

Asundi A, Kishen A. 2000. A strain gauge and photoelastic analysis of in vivo strain and in vitro stress distribution in human dental supporting structures. Arch Oral Bio 45:543-550.

Bennett EL, Davies AG. 1994. The ecology of Asian colobines. In: Davies AG, Oates JF, editors. Colobine Monkeys: Their Ecology, Behavior, and Evolution. Cambridge University Press, Cambridge. 129-172.

Binder WJ, Van Valkenburgh B. 2000. Development of bite strength and feeding behavior in juvenile spotted hyenas (*Crocuta crocuta*). J Zool Lond 252:273-283.

Bouvier M. 1986a. A biomechanical analysis of mandibular scaling in Old World monkeys. Am J Phys Anthropol 69:473-482.

Bouvier M. 1986b. Biomechanical scaling of mandibular dimensions in New World monkeys. Int J Primatol 7:551-567.

Brin I, Koyoumdijsky-Kaye E. 1981. The influence of premature extractions of primary molars on the ultimate root length of their permanent predecessors. J Dent Res 65:962-965.

Brin I, Ben Bassat Y, Einy S, Koyoumdjisky-Kaye E. 1991. Premature extractions of primary molars and the crown/root ratio of their permanent successors. ASDC J Dent Child 58:409-412.

Cerling TE, Mbua E, Kirera FM, Manthi FK, Grine FE, Leakey MG, Sponheimer M, Uno KT. 2011. Diet of *Paranthropus boisei* in the early Pleistocene of east Africa. PNAS 108:9337-9341.

Chai H, James J, Lee W, Constantino PJ, Lucas PL, Lawn BR. 2009. Remarkable resilience of teeth. PNAS 106:7289-7293.

Chapman CA, Chapman LJ, Cords M, Gathua JM, Gautier-Hion A, Lambert JE, Rode K, Tutin, CEG, White LJT. 2002. Variation in the diets of *Cercopithecus* species: Differences within forests, among forests, and across species. In: Glenn ME, editor. Guenons: Diversity and Adaptation in African Monkeys. Kluwer Academic/Plenum Publishers, New York. 325-350.

Chen J, Xu L. 1994. A finite element analysis of the human temporomandibular joint. J Biomech Engineering 116:401-407.

Chiba M, Yamane A, Oshima S, Komatsu K. 1990. In vitro measurement of regional differences in the mechanical properties of the periodontal ligament in the rat mandibular incisor. Archs Oral Biol 35:153-161.

Chivers DS. 1994. Functional anatomy of the gastrointestinal tract. In: Davies AG, Oates JF, editors. Colobine Monkeys: Their Ecology, Behavior and Evolution. Cambridge University Press, Cambridge. 205-227.

Chivers DS, Hladik CM. 1984. Diet and gut morphology in primates. In: Food Acquisition and Processing in Primates. Chivers DJ, Wood BA, Bilsborough A, editors. Plenum Press, New York. 213-230.

Cochard LR. 1987. Postcanine tooth size in female primates. Am J Phys Anthropol 74:47-54.

Constantino P. 2007. Primate masticatory adaptations to fracture-resistant foods. Ph.D. dissertation, George Washington University.

Copes LE, Schwartz GT. 2010. The scale of it all: postcanine tooth size, the taxon-level effect, and the universality of Gould's scaling law. Paleobiol 36:188-203.

Cords M. 1986. Interspecific and intraspecific variation in diet of two forest guenons, *Cercopithecus ascanius* and *C. mitis*. J Anim Ecol 55:811-827.

Corruccini RS. 1987. Shape in morphometrics: comparative analyses. Am J Phys Anthropol 73:289‑303.

Cuozzo FP, Sauther ML. 2006. Temporal change in tooth size among ring-tailed lemurs (*Lemur catta*) at the Beza Mahafaly Special Reserve, Madagascar: effects of an environmental fluctuation. In: Jolly A., Sussman RW, Koyama N, Rasamimanana H, editors. Ring-Tailed Lemur Biology. Springer, New York. 343-366.

Daegling DJ. 1990. Geometry and biomechanics of hominoid mandibles. Ph.D. dissertation, State University of New York at Stony Brook.

Daegling DJ. 1993. The relationship of in vivo bone strain to mandibular corpus morphology in *Macaca fasicularis*. J Hum Evol 25:247-269.

Daegling DJ. 2007. Morphometric estimation of torsional stiffness and strength in primate mandibles. Am J Phys Anthropol 132:261-266.

Daegling DJ, Hylander WL. 1997. Occlusal forces and and mandibular bone strain: Is the primate jaw "overdesigned"? J Hum Evol 33:705-717.

Daegling DJ, McGraw WS. 2001. Feeding, diet and jaw form in West African *Colobus* and *Procolobus.* Int J Primatol 22:1033-1055.

Dasilva GL. 1994. Diet of *Colobus polykomos* on Tiwai Island: Selection of food in relation to its seasonal abundance and nutritional quality. Int J Primatol 15:655-680.

Davies AG, Bennett EL, Waterman PG. 1988. Food selection by two South-east Asian colobine monkeys (*Presbytis rubicunda* and *Presbytis melalophos*) in relation to plant chemistry. Biol J Linn Soc 34:33-56.

Deines DN, Eick JD, Cobb CM, Bowles CQ, Johnson CM. 1993. Photoelastic stress analysis of natural teeth and three osseo-integrated implant designs. Int J Periodontics Restorative Dent 13:540-549.

Dellow PG, Lund JP. 1971. Evidence for central timing of rhythmical mastication. J Physiol (Lond) 214:1-13.

Demes B, Creel N, Preuschoft H. 1986. Functional significance of allometric trends in the hominoid masticatory apparatus. In: Else JG., Lee PC, editors. Primate Evolution. Cambridge: Cambridge University Press. 229-237.

Demes B, Creel N. 1988. Bite force, diet and cranial morphology of fossil hominids. J Hum Evol.17:657–670.

Dessem D, Iyadurai OD, Taylor A. 1988. The role of periodontal receptors in the jaw-opening reflex in the cat. J Physiol (Lond) 406:315-330.

Di Fiore A, Campbell CJ. 2007. The Atelines: Variation in ecology, behavior, and social organization. In: Campbell CJ, Fuentes A, MacKinnon KC, Panger M, Bearder SK, editors. Primates in Perspective. Oxford University Press, Oxford. 155-185.

Digby LJ, Ferrari SF, Saltzman W. 2007. Callitrichines: The role of competition in cooperatively breeding species. In: Campbell CJ, Fuentes A, MacKinnon KC, Panger M, Bearder SK, editors. Primates in Perspective. Oxford University Press, Oxford. 85-106.

Dirks W. 2003. Effect of diet on dental development of four species of catarrine primates. Am J Primatol 61:29-40.

Disotell TR. 2000. Molecular systematics of the Cercopithecidae. In: Whitehead PF, Jolly CJ, editors. Old World Monkeys. Cambridge University Press, Cambridge. 29-56.

Dorow C, Krstin N, Sander FG. 2002. Experiments to determine the material properties of the periodontal ligament. J Orofac Orthop 63:94-104.

Dorow C, Krstin N, Sander FG. 2003. Determination of the mechanical properties of the periodontal ligament in a uniaxial tensional experiment. J Orofac Orthop 64:100-107.

Dumont ER. 1995. Enamel thickness and dietary adaptation among extant primates and chiropterans. J Mamm 76:1127-1136.

Dumont ER. 1997. Cranial shape in fruit, nectar and exudate feeding mammals: Implications for interpreting the fossil record. Am J Phys Anthropol 102:187-202.

Dumont ER.1999. The effect of food hardness on feeding behaviour in frugivorous bats (Phyllostomidae): an experimental study. J Zool Lond 248:219–229.

Dumont ER, Herrel A. 2003. The effects of gape angle and bite point on bite force in bats. J Exp Biol 206:2117-2123.

Elgart-Berry A. 2004. Fracture toughness of mountain gorilla (*Gorilla gorilla berengei*) food plants. Am J Primatol 60:275-285.

Endo B. 1966. Experimental studies on the mechanical significance of the form of the human facial skeleton. J Fac Sci Univ Tok 3:1-106.

Enstam KL, Isbell LA. 2007. The guenons (Genus Cercopithecus) and their allies. In: Campbell CJ, Fuentes A, MacKinnon KC, Panger M, Bearder SK, editors. Primates in Perspective. Oxford University Press, Oxford. 252-274.

Embery G. 1990. An update on the biochemistry of the periodontal ligament. Euro J Orthodon 12:77-80.

Fashing PJ. 2007. African colobine monkeys: Patterns of between-group interaction. In: Campbell CJ, Fuentes A, MacKinnon KC, Panger M, Bearder SK, editors. Primates in Perspective. Oxford University Press, Oxford. 201-224.

Felton AM, Felton A, Wood JT, Lindenmayer DB. 2008. Diet and feeding ecology of *Ateles chamek* in a Bolivian semihumid forest: The importance of *Ficus* as a staple food resource. Int J Primatol 19:379-403.

Fernandez-Duque E. Aotinae: Social monogamy in the only nocturnal haplorhines. In: Campbell CJ, Fuentes A, MacKinnon KC, Panger M, Bearder SK, editors. Primates in Perspective. Oxford University Press, Oxford. 139-154.

Ferrari SF, Martins ES. 1992. Gummivory and gut morphology in two sympatric callithrichids (*Callithrix emiliae* and *Saguinus fuscicollis weddelli*) from western Brazilian Amazonia. Am J Phys Anthropol 88:97-103.

Ferrario VF, Sforza C, Serrao G, Dellavia C, Tartaglia GM. 2004. Single tooth bite forces in healthy young adults. J Oral Rehab 31:18-22.

Fill TS, Carey JP, Toogood RW, Major PW. 2011. Experimentally determined mechanical properties of, and models for, the periodontal ligament: Critical review of current literature. J Dent Biomech 2011:1-10. http://dbm.sagepub.com/content/early/2011/08/31/2011.312980

Fleagle JG, McGraw WS. 2002. Skeletal and dental morphology of African papionins: unmasking a cryptic clade. J Hum Evol 42:267-292.

Foster KD, Woda A, Peyron MA. 2006. Effect of texture of plastic and elastic food models on the parameters of mastication. J Neurophysiol 95:3469-3479.

Ganas J, Robbins MM, Nkurunungi JB, Kaplin BA, McNeilage A. 2004. Dietary variability of mountain gorillas in Bwindi Impenetrable National Park, Uganda. Int J Primatol 25:1043-1072.

Garber PA, Rosenberger AL, Norconk MA. 1996. Marmoset misconceptions. In: Norconk MA, Rosenberger AL, Garber PA, editors. Adaptive Radiations of Neotropical Primates. Plenum Press, New York.

Gathercole LJ, Keller A. 1982. Biophysical aspects of the fibres of the periodontal ligament. In: Berkovitz BKB, Moxham BJ, Newman HN, editors. The Periodontal Ligament in Health and Disease. Pergamon Press, Oxford. 103-118.

Gimenez M, Fernandez-Duque E. 2003. Summer and winter diet of night monkeys in the gallery and throne forests of the Argentinean Chaco Rev Etol 5:164.

Gingerich PD. 1974. Size variability of the teeth in living mammals and the diagnosis of closely related sympatric fossil species. J Paleontol 48:895-903.

Gingerich PD, Smith BH. 1985. Allometric scaling in the dentition of primates and insectivores. In: Jungers WL, editor. Size and Scaling in Primate Biology. New York: Plenum Press. 257-272.

Gould SJ. 1966. Allometry and size in ontogeny and phylogeny. Biol Rev 41:587-640.

Gould SJ. 1975. On the scaling of tooth size in Mammals. Amer Zool 15:353-362.

Greaves WS. 1978. The jaw lever system in ungulates: a new model. J Zool Lond 184:271–285.

Grine FE. 1986. Dental evidence for dietary differences in *Australopithecus* and *Paranthropus*: A quantitative analsysis of permanent molar microwear. J Hum Evol 15:783-822.

Grine FE. 2002. Scaling of tooth enamel thickness and molar crown size reduction in modern humans. S Af J Sci 98:503-509.

Grine FE, Spencer MA, Demes B, Smith HF, Strait DS, Constant DA. 2005. Molar enamel thickness in the Chacma baboon, *Papio ursinus* (Kerr 1792). Am J Phys Anthropol 128:812-822.

Gysi S. 1921. Studies on the leverage problem of the mandible. Dental Digest. 27:74-84, 144-150, 203-308.

Hannam, AG. 1982. The innervation of the periodontal ligament. In: Berkovitz BKB, Moxham BJ, Newman HN, editors. The Periodontal Ligament in Health and Disease. Pergamon, Oxford. 173.

Haraldson T. 1983. Comparisons of chewing patterns in patients with bridges supported on osseointegrated implants and subjects with natural dentitions. Acta Odontol Scand 41:203-208.

Harrison MJ. 1988. The mandrill in Gabon's rain forest – Ecology, distribution and status. Oryx 22:218-228.

Hidaka O, Morimoto T, Masuda Y, Kato T, Matsuo R, Inoue T, Kobayashi M, Takada K. 1997. Regulation of masticatory force during cortically induced rhythmic jaw movements in anesthetized rabbit. J Neurophysiol 77:3168-3179.

Hill DA, Lucas PW. 1996. Toughness and fiber content of major leaf foods of Japanese macaques (*Macaca fuscata yakui*) in Yakushima. Am J Primatol 38:221-231.

Hillson S. 1986, 2005. Teeth: Second Edition. Cambridge University Press, Cambridge.

Hlusko LJ, Lease LR, Mahaney MC. 2006. Evolution of genetically correlated traits: Tooth size and body size in baboons. Am J Phys Anthropol 131:420-427.

Hoshino J. 1985. Feeding ecology of mandrills (*Mandrillus sphinx*) in Campo Animal Reserve, Cameroon. Primates 26:248-273.

Hylander WL. 1975. Incisor size and diet with special reference to Cercopithecidae. Science 189:1095-1098.

Hylander WL. 1981. Patterns of stress and strain in the macaque mandible. In: Carlson CS, editor. Craniofacial biology. Monograph #10, Craniofacial Growth Series, Center for Human Growth and Development. University of Michigan: Ann Arbor. 1–37.

Hylander WL. 1984. Stress and strain in the mandibular symphysis of primates: A test of competing hypotheses. Am J Phys Anthrop 64:1–46.

Hylander WL. 1985. Mandibular function and biomechanical stress and scaling. Am Zool 25:315–330.

Hylander WL. 1988. Implications of in vivo experiments for interpreting the functional significance of "robust" australopithecine jaws. In: Grine F, editor. Evolutionary History of the "Robust" Australopithecines. Aldine De Gruyter: New York. 55–83.

Hylander WL, Johnson KR, Crompton AW. 1987. Loading patterns and jaw movements during mastication in Macaca fascicularis: A bone-strain, electromyographic, and cineradiographic analysis. Am J Phys Anthropol 72:287-314.

Hylander WL, Johnson KR, Crompton AW. 1992. Muscle force recruitment and biomechanical modeling: An analysis of masseter muscle function during mastication in *Macaca fascicularis*. Am J Phys Anthropol 88:365-387.

Hylander WL, Johnson KR. 1994. Jaw muscle function and wishboning of the mandible during mastication in macaques and baboons. Am J Phys Anthropol 94:523-547.

Hylander WL, Wall CE, Vinyard CJ, Ross C, Ravosa MR, Williams SH, Johnson KR. 2005. Temporalis function in anthropoids and strepsirrhines: An EMG study. Am J Phys Anthropol 128:35-56.

Imbeni V, Kruzic JJ, Marshall GW, Marshall SJ, Ritchie RO. 2005. The dentin–enamel junction and the fracture of human teeth. Nature Mat 4:229–232.

Isbell LA. 1998. Diet for a small primate: Insectivory and gummivory in the (large) patas monkey (Erythrocebus patas pyrrhonotus). Am J Primatol 45:381-398.

Iwase M, Sugimori M, Karachi Y, Nagumo M. 1998. Changes in bite force and occlusal contacts in patients treated for mandibular prognathism by orthognathic surgery. J Oral Maxillo Fac Surg 56:850-855.

Izawa K. 1979. Foods and feeding behavior of wild black-capped capuchin (*Cebus apella*). Primates 20:57-76.

Janis CM, Fortelius M. 1988. On the means whereby mammals achieve increased functional durability of their dentitions, with special reference to limiting factors. Biol Rev Cambridge Philos Soc 63:197–230.

Janson CH, Boinski S. 1992. Morphological and behavioral adaptations for foraging in generalist primates: the case of the Cebines. Am J Phys Anthropol 88:483-498.

Jernvall J, Jung H. 2000. Genotype, phenotype, and developmental biology of molar tooth characters. Yrbk Phys Anthropol 48:171-190.

Jernvall J, Thesleff I. 2000. Reiterative signaling and patterning during mammalian tooth morphogenesis. Mech Devel 92:19-29.

Johnsen SE, Trulsson M. 2003. Receptive field properties of human periodontal afferents responding to loading of premolar and molar teeth. J Neurophysiol 89:1478-1487.

Johnsen SE, Trulsson M. 2005. Encoding of amplitude and rate of tooth loads by human periodontal afferents from premolar and molar teeth. J Neurophysiol 93:1889-1897.

Jolly CJ. 2007. Baboons, mandrills and mangabeys: Afro-papionin socioecology in a phylogenetic perspective. In: Campbell CJ, Fuentes A, MacKinnon KC, Panger M, Bearder SK, editors. Primates in Perspective. Oxford University Press, Oxford. 240-251.

Jungers WL, Falsetti AB, Wall CE. 1995. Shape, relative size, and size-adjustments in morphometrics. Yrbk Phys Anthropol 21:137‑161.

Kaewsuriyathumrong C, Soma K. 1993. Stress of tooth and PDL structure created by bite force. Bull Tokyo Med Dent Univ 40:217-232.

Kangas AT, Evans AR, Thesleff I, Jernvall J. 2004. Nonindependence of mammalian dental characters. Nature 432:211-214.

Kavanaugh KD, Evans AR, Jernvall J. 2007. Predicting evolutionary patterns of mammalian teeth from development. Nature.449:427-433.

Kay RF. 1975. The functional adaptations of primate molar teeth. Am J Phys Anthropol 42:327-352.

Kay RF. 1978. Molar structure and diet in extant Cercopithecoidea. In: Butler PM, Joysey K, editors. Development, function and evolution of teeth. London, Academic Press. 309-339.

Kay RF. 1981. The nut-crackers: a new theory of the adaptations of the ramapithecines. Am J Phys Anthropol 55:141-151.

Kay RF, Hylander WL. 1978. The dental structure of mammalian folivores with special reference to primates and phalangeroidea (Marsupalia). In: Ecology of Arboreal Folivores. Montgomery GG, editor. Cambridge University Press, Cambridge. 173-191.

Kay RNB, Davies AG. 1994. Digestive physiology. In: Davies AG, Oates JF, editors. Colobine Monkeys: Their Ecology, Behavior and Evolution. Cambridge University Press, Cambridge. 229-249.

Kimbel WH, Rak Y, Johanson DC. 2004. The skull of Australopithecus afarensis. Oxford University Press, Oxford.

Kinzey WG. 1974. Ceboid models for the evolution of hominoid dentition. J Hum Evol 3:193-203.

Kinzey WG, Norconk MA. 1990. Hardness as a basis of fruit choice in two sympatric primates. Am J Phys Anthropol 81:5-15.

Kinzey WG, Norconk MA. 1993. Physical and chemical properties of fruit and seeds eaten by *Pithecia* and *Chiropotes* in Surinam and Venezuela. Int J Primatol 4:207-227.

Kirkpatrick RC. 2007. The Asian colobines: Diversity among leaf-eating monkeys. In: Campbell CJ, Fuentes A, MacKinnon KC, Panger M, Bearder SK, editors. Primates in Perspective. Oxford University Press, Oxford. 186-200.

Komatsu K. 2010. Mechanical strength and viscoelastic response of the periodontal ligament in relation to structure. J Dent Biomech 2010:1-18. http://dbm.sagepub.com/content/1/1/502318

Komatsu K, Yamazaki Y, Yamaguchi S, Chiba M. 1998. Comparison of biomechanical properties of the incisor periodontal ligament among different species. Anat Rec 250:408-417.

Koyabu DB, Endo H. 2009. Craniofacial variation and dietary adaptations of African colobines. J Hum Evol 56:525-536.

Kupzcik K. 2003. Tooth root morphology in primates and carnivores. PhD. Dissertation. University College London.

Kupzcik K, Olejniczak AJ, Skinner MM, Hublin J. 2009. Molar crown and root size relationship in anthropoid primates. In: Koppe T, Meyer G, Alt KW, editors. Comparative Dental Morphology. Front Oral Biol 13:16–22.

Lambert JE, Champan CA, Wrangham RW, Conklin-Brittain NL. 2004. Hardness of cercopithecine foods: Implications for the critical function of enamel thickness in exploiting fallback foods. Am J Phys Anthropol 125:363-368.

Lavigne G, Kim JS, Valiquette C, Lund JP. 1987. Evidence that periodontal pressoreceptors provide positive feedback to jaw closing muscles during mastication. J Neurophysiol 58:342-358.

Linden RWA. 1990. Periodontal mechanoreceptors and their functions. In: Taylor A, editor. Neurophysiology of jaws and teeth. London: Macmillan Press. 52-95.

Lucas PW. 2004. Dental functional morphology: How teeth work. Cambridge University Press: New York.

Lucas PW, Corlett RT, Luke DA. 1986a. Sexual dimorphism of tooth size in anthropoids. Hum Evol 1:23-39.

Lucas PW, Corlett RT, Luke DA. 1986b. Postcanine tooth size and diet in anthropoid primates. Z Morph Anthrop 76:253-276.

Lucas PW, Constantino PJ, Wood BA. 2008. Inferences regarding the diet of extinct hominins: Structural and functional trends in dental and mandibular morphology. J Anat 212:486-500.

Luke D. 1998. The structure and function of the dentogingival junction and periodontal ligament. In: Harris M, Edgar M, Meghji S, editors. Clinical Oral Science. Reed Educational and Professional Publishing Ltd, Oxford. 134-140.

Lund JP, Kolta A. 2006. Adaptation of the central masticatory pattern to the biomechanical properties of food. Quintessence International Congress Series 1284:11-20.

Lund JP, Lamarre Y. 1973. The importance of positive feedback from periodontal pressoreceptors during voluntary isometric contraction of jaw closing muscles in man. J Biol Buccale 1:345-351.

Maas MC. 1991. Enamel structure and microwear: An experimental study of the response of enamel to shearing force. Am J Phys Anthropol 85:31-49.

Maas MC, Dumont ER. 1999. Built to last: The structure, function, and evolution of primate dental enamel. Evol Anthropol 8:133-150.

Maas MC, OLeary M. 1996. Evolution of molar enamel microstructure in North American Notharctidae (primates). J Hum Evol 31:293-310.

Macho GA, Berner ME. 1993. Enamel thickness of human maxillary molars reconsidered. Am J Phys Anthropol 92:189-200.

Macho GA, Berner ME. 1994. Enamel thickness and the helicoidal occlusal plane. Am J Phys Anthropol 94:327-337.

Macho GA, Spears IR. 1999. Effects of loading on the biomechanical behavior of molars of *Homo, Pan* and *Pongo*. Am J Phys Anthropol 109:211-227.

Macho GA, Jiang Y, Spears IR. 2003. Enamel microstructure; a truly three-dimensional structure. J Hum Evol 45:81-90.

Mandel U, Dalgaard P, Viidik A. 1986. A biomechanical study of the human periodontal ligament. J Biomechanics 19:637-645.

Mansour RM, Reynick RJ. 1975. *In vivo* occlusal forces and moments, I: Forces measured in terminal hinge position and associated moments. J Dent Res 54:114-120.

Martin LB, Olejniczak AJ, Maas MC. 2003. Enamel thickness and microstructure in pitheciin primates, with comments on dietary adaptations of the middle Miocene hominoid, *Kenyapithecus*. J Hum Evol 45:351-367.

Masterson TJ, Hartwig WC. 1998. Degrees of sexual dimorphism in *Cebus* and other New World monkeys. Am J Phys Anthropol 107:243–256.

Maynard Smith J, Savage RJG. 1959. The mechanics of mammalian jaws. School Sci Rev 141:289–301.

Menard N. 2004. Do ecological factors explain variation in social organization? In: Thierry B, Singh M, Kaumanns W, editors. Macaque Societies: A Model for the Study of Social Organization. Cambridge University Press, Cambridge. 106-131.

Meyers MA, Chawla KK. 2009. Mechanical Behavior of Materials (2nd Edition). Cambridge University Press, Cambridge.

Mistry S, Hamdy S. 2008. Neural control of feeding and swallowing. Phys Med Rehabil Clin N Am 19:709-728.

Molnar S, Gantt DG. 1977. Functional implications of primate enamel thickness. Am J Phys Anthropol 46:447-454.

Morimoto T, Inoue T, Masuda Y, Nagashima T. 1979. Sensory components facilitating jaw-closing muscle activities in the rabbit. Exp Brain Res 76:424-440.

Natali AN, Pavan PG, Carniel EL, Dorow C. 2004. Viscoelastic response of the periodontal ligament: An experimental-numerical analysis. Connective Tissue Research 45:222-230.

Norconk MA, Grafton BW, Conklin-Brittain NL. 1998. Seed dispersal by neotropical seed predators. Am J Primatol 45:103-126.

O'Higgins PO, Chadfield P, Jones N. 2001. Facial growth and the ontogeny of morphological variation within and between the primates *Cebus apella* and *Cercocebus torquatus.* J Zool Lond 254:337–357.

Oates JF, McFarland KL, Groves JL, Bergl RA, Linder JM, Disotell TR. 2003. The Cross River gorilla; natural history and status of a neglected and critically endangered subspecies. In: Taylor AB, Goldsmith ML, editors. Gorilla Biology: A Multidisciplinary Perspective. Cambridge University Press, Cambridge. 472-497.

Okecha AA, Newton-Fisher NE. 2006. The diet of olive baboons (*Papio anubis*) in the Budongo Forest Reserve, Uganda. In: Newton-Fisher NE, Notman H, Paterson JD, Reynolds V, editors. Primates of Western Uganda. Springer, New York. 61-73.

Olupot W, Chapman CA, Waser PM, Isabirye-Basuta G. 1997. Mangabey (*Cercocebus albigena*) ranging patterns in relation to fruit availability and the risk of parasite infection in Kibale National Park, Uganda. Am J Primatol 43:65-78.

Orchardson R, MacFarland SH. 1980. The effect of local periodontal anaesthesia on the maximum biting force achieved by human subjects. Arch Oral Biol 25:799-804.

Oxnard CE. 1985. Hominids and hominoids, lineages and radiations. In: Tobias PV, editor. Hominid Evolution: Past, Present and Future. Alan R. Liss, New York. 271-278.

Oyen OJ. Tsay TP. 1991. A biomechancial analysis of craniofacial form and bite force. Am J Dentofac Orthop 99:298-309.

Panagiotopoulou O, Kupczik K, Cobb SN. 2011. The mechanical function of the periodontal ligament in the macaque mandible: a validation and sensitivity study using finite element analysis. J Anat 218:75-86.

Park J, Herr Y, Kim H, Gronostajski RM, Cho M. 2007. Nfic gene disruption inhibits differentiation of ondontoblasts responsible for root formation and results in formation of short and abnormal roots in mice. J Periodontol 78:1795-1802.

Pearson CH. 1982. The ground substance of the periodontal ligament. In: Berkovitz BKB, Moxham BJ, Newman HN, editors. The Periodontal Ligament in Health and Disease. Pergamon Press, Oxford. 119-149.

Perelman P, Johnson WE, Roos C, Seuanex HN, Horvath JE, Moreira MAM, Kessing B, Pontius J, Roelke M, Rumpler Y, Schneider MPC, Silva A, O'Brien SJ, Decon-Slattery J. 2011. A molecular phylogeny of living primates. PLoS Genet 7: e1001342.

Perry JMG, Hartstone-Rose A, Logan RL. 2011. The jaw adductor resultant and estimated bite force in primates. Anatomy Research International 2011: Article ID 929848, 11 pp.

Pilbeam DR, Gould SJ. 1974. Size and scaling in human evolution. Science 186:892-901.

Plavcan JM. 2002. Taxonomic variation in the patterns of craniofacial dimorphism in primates. J Hum Evol 42:579-608.

Porter CA, Page SL, Czelusniak J, Schneider H, Schneider MPC, Sampaio I, Goodman M. 1997. Phylogeny and evolution of selected primates as determined by sequences of the e-globin locus and 5' flanking regions. Int J Primatol 18:261-295.

Proeschel PA, Morneburg T. 2002. Task-dependence of activity/bite force relations and its impact on estimation of chewing force from EMG. J Dent Res 81:464-468.

Pruim GJ, de Jongh HJ, ten Bosch JJ. 1980. Forces acting on the mandible during bilateral static bite at different bite force levels. J Biomech 13:755-763.

Rak Y. 1983. The australopithecine face. Academic Press: New York.

Ray DA, Xing J, Hedges DJ, Hall MA, Laborde ME, Anders BA, White BR, Stoilova N, Fowlkes JD, Landry KE, Chemnick LG, Ryder OA, Batzer MA. 2005. *Alu* insertion loci and platyrrhine primate phylogeny. Mol Phylo Evol 35:117-126.

Ravosa MJ. 1990. Functional assessment of subfamily variation in maxillomandibular morphology among Old World monkeys. Am J Phys Anthropol 82:199-212.

Ravosa MJ. 1991. Stuctural allometry of the mandibular corpus and symphysis in prosimian primates. J Hum Evol 20:3-20.

Remis MJ. 1997. Western lowland gorillas (*Gorilla gorilla gorilla*) as seasonal frugivores: Use of variable resources. Am J Primatol 43:87-109.

Rensberger JM. 1997. Mechanical adaptation in enamel. In: von Koenigswald W, Sander PM, editors. Tooth Enamel Microstructure. Balkema, Rotterdam. 237–257.

Rensberger JM. 2000. Pathways to functional differentiation in mammalian enamel. In: Teaford ME, Smith MM, Furgerson MWJ, editors. Development, function and evolution of teeth. Cambridge University Press, Cambridge. 252–269.

Ricker WE. 1984. Computation and uses of central trend lines. Can J Zool 62:1897-1905.

Robbins MM. 2007. Gorillas: Diversity in ecology and behavior. In: Campbell CJ, Ruentes A, MacKinnon KC, Panger M, Bearder SK, editors. Primates in Perspective. Oxford University Press, Oxford. 305-321.

Robinson JT. 1954. Prehominid dentition and hominid evolution. Evolution 8:324-334.

Rosenberger AL. 1992. Evolution of feeding niches in New World monkeys. Am J Phys Anthropol 88:525-562.

Schneider H, Rosengberger AL. 1996. Molecules, morphology, and platyrrhine systematics. In: Norconk MA, Rosenberger AL, Garber PA, editors. Adaptive Radiations of Neotropical Primates. Plenum Press, New York. 3-19.

Schroeder, HE. 1991. Oral Structural Biology: Embryology, structure, and function of normal hard and soft tissues of the oral cavity and temporomandibular joints. Thieme Medical Publishers, Inc., New York.

Schwartz GT. 2000a. Taxonomic and functional aspects of the patterning of enamel thickness distribution in extant large bodied hominoids. Am J Phys Anthropol 111:221-244.

Schwartz GT. 2000b. Enamel thickness and the helicoidal wear plane in modern human mandibular molars. Arch Oral Biol 45:401-409.

Scott JE. 2011. Folivory, frugivory, and postcanine size in the Cercopithecoidea revisited. Am J Phys Anthropol. 146:20-27.

Scott RS, Ungar PS, Bergstrom TS, Brown CA, Grine FE. 2005. Dental microwear texture analysis reflects diets of living primates and fossil hominins. Nature 436:693-695.

Shellis RP, Beynon AD, Reid DJ. 1998. Variations in molar enamel thickness among primates. J Hum Evol 35:507-522.

Sloan P. 1982. Structural organization of the fibres of the periodontal ligament. In: Berkovitz BKB, Moxham BJ, Newman HN, editors. The Periodontal Ligament in Health and Disease. Pergamon Press, Oxford. 51-72.

Smith RJ. 2009. Use and misuse of the reduced major axis for line-fitting. Am J Phys Anthropol 140:476‑486.

Sofaer JA. 1977. Co-ordinated growth of successively initiated tooth germs in the mouse. Arch Oral Biol 22:71-72.

Sokal RR, Rolf FJ. 1981. Biometry. New York: Freeman.

Smith RJ 1978. Mandibular biomechanics and temporomandibular joint function in primates. Am J Phys Anthropol 49:341-350.

Smith TM, Olejniczak AJ, Martin LB, Reid DJ. 2005. Variation in hominoid molar enamel thickness. J Hum Evol 48:575-592.

Spencer MA. 1995. Masticatory system configuration and diet in anthropoid primates. Ph.D. dissertation, State University of New York at Stonybrook.

Spencer MA. 1998. Force production in the primate masticatory system: electromyographic tests of biomechanical hypotheses. J Hum Evol 34:25–54.

Spencer MA. 1999. Constraints on masticatory system evolution in anthropoid primates. Am J Phys Anthrop 108:450–483.

Spencer MA. 2003. Tooth-root form and function in platyrrhine seed-eaters. Am J Phys Anthropol 122:325-335.

Spencer MA, Demes B. 1993. Biomechanical analysis of masticatory function: configuration in Neandertals and Inuits. Am J Phys Anthropol 91:1–20.

Sponheimer M, Lee-Thorp J. 1999. Isotopic evidence for the diet of an early hominid, *Australopithecus afrianus*. Science 283:368-370.

Sponheimer M, Lee-Thorp J, de Ruiter D, Codron D, Codron J, Baugh AT, Thackeray F. 2005. Hominins, sedges, and termites: new carbon isotope data from the Sterkfonetin valley and Kruger National Park. J Hum Evol 48:301-312.

Stanford CB, Nkurununngi JB. 2003. Behavioral ecology of sympatric chimpanzees and gorillas in Bwindi Impenetrable National Park, Uganda: diet. Int J Primatol 24:901-918.

Steele-Perkins G, Butz KG, Lyons GE, Zeichner-David M, Kim H, Cho M, Gronostajski RM. 2003. Essential role for NFI-C/CTF transcription-replication factor in tooth root development. Mol Cel Biol 23:1075-1084.

Stompf R. 2007. Chimpanzees and bonobos: Diversity within and between species. In: Campbell CJ, Ruentes A, MacKinnon KC, Panger M, Bearder SK, editors. Primates in Perspective. Oxford University Press, Oxford. 321-344.

Strait SG, Vincent JFV. 1998. Primate faunivores: physical properties of prey items. Int J Primatol 19:867-878.

Swindler DR. 2002. The Dentition of Living Primates. Academic Press, New York.

Taylor AB, Vogel ER, Dominy NJ. 2008. Food material properties and mandibular load resistance abilities in large-bodied hominoids. J Hum Evol 55:604-616.

Teaford MF, Maas MC, Simons EL. 1996. Dental microwear and microstructure in Early Oligocene primates from the Fayum, Egypt: Implications for diet. Am J Phys Anthropol 101:527-543.

Teaford MF, Lucas PW, Ungar PS, Glander KE. 2006. Mechanical defenses in leaves eaten by Costa Rican howling monkeys (*Alouatta palliata*). Am J Phys Anthropol 129:99-104.

Thierry B. 2007. The macaques: A double-layered social organization. In: Campbell CJ, Ruentes A, MacKinnon KC, Panger M, Bearder SK, editors. Primates in Perspective. Oxford University Press, Oxford. 224-239.

Thompson EN, Biknevicius AR, German RZ. 2003. Ontogeny of feeding function in the gray short tailed opossum Monodelphis domestica: Empirical support for the constrained model of jaw biomechanics. J Exp Biol 206:923-932.

Thresher RW, Saito GE. 1973. The stress analysis of human teeth. J Biomechanics 6:443-449.

Throckmorton GS, Ellis E. 2001. The relationship between surgical changes in dentofacial morphology and changes in maximum bite force. J Oral Maxillo Surg 59:620-627.

Trulsson M, Gunne HSJ. 1998. Food-holding and –biting behavior in human subjects lacking periodontal receptors. J Dent Res 77:574-582.

Türker TS. 2002. Reflex control of human jaw muscles. Crit Rev Oral Biol Med 13:85-104.

Türker TS, Jenkins M. 2000. Reflex responses induced by tooth unloading. J Neurophysiol 84:1088-1092.

Uchida A. 1998. Variation in tooth morphology of *Gorilla gorilla*. J Hum Evol 34:55-70.

Ungar PS. 1998. Dental allometry, morphology, and wear as evidence for diet in fossil primates. Evol Anthropol 6:205-217.

Ungar PS, Grine FE, Teaford MF. 2008. Dental microwear and diet of the Plio-Pleistocene hominin *Paranthropus boisei*. PLoS ONE 3:e2044. doi:10.1371/journal.pone.0002044.

Ungar PS, Sponheimer M. 2011. The diets of early hominins. Science 334:190-193.

Usongo LI, Amubode RO. 2001. Nutritional ecology of Prewss's red colobus monkey (*Colobus badius preussi* Rahm 1970) in Korup National Park, Cameroon. Afr J Ecol. 39:121-125.

van Driel WD, van Leeuwn EJ, Von den Hoff JW, Maltha JC, Kuijpers-Jagtman AM. 2000. Time-dependent mechanical behavior of the periodontal ligament. Proc Instn Mech Engrs H 214:497-504.

van Eijden TMGJ. 1991. Three-dimensional analyses of human bite-force magnitude and moment. Archs. Oral Biol 36:535-539.

van Eijden, TMGJ, Klok EM, WeijsWA, Koolstra JH. 1988. Mechanical capabilities of the human jaw muscles studied with a mathematical model. Arch Oral Biol 33:819-826.

Vinyard CJ, Wall CE, Williams SH, Hylander WL. 2003. Comparative function of skull morphology of tree-gouging primates. Am J Phys Anthropol 120:153-170.

Vinyard CJ, Hanna J. 2005. Molar scaling in strepsirrhine primates. J Hum Evol 49:241-269.

Vogel ER, vanWoerden JT, Lucas PL, Atomoko SSU, van Schaik CP, Dominy NJ. 2008. Functional ecology and evolution of hominoid molar enamel thickness: *Pan troglodytes schweinfurthii* and *Pongo pygmaeus wurmbii*. J Hum Evol 55:60-74.

Ward SC, Molnar S. 1980. Experimental stress analysis of topographic diversity in early hominid gnathic morphology. Am J Phys Anthropol 53:383–395.

Watts DP. 1996. Comparative socioecology of gorillas. In : McGrew WC, Marchant LF, Nishida T, editors. Great Ape Societies. Cambridge University Press, Cambridge. 16-28.

Wood BA. 1979. An analysis of tooth and body size relationships in five primate taxa. Folia Primatol 31:187-211.

Wood BA, Abbott SA, Uytterschaut H. 1988. Analysis of the dental morphology of Plio-Pleistocene hominids IV. Mandibular postcanine root morphology. J Anat 156:107-139.

Wood BA, Li Y, Willoughby C. 1991. Intraspecific variation and sexual dimorphism in cranial and dental variables among higher primates and their bearing on the hominid fossil record. J Anat 174:5–205.

Wrangham RW, Conklin-Brittain NL, Hunt KD. 1998. Dietary response of chimpanzees and cercopithecines to seasonal variation in fruit abundance. I. Antifeedants. Int J Primatol 19:949-970.

Wright BW. 2005. Craniodental biomechanics and dietary toughness in the genus *Cebus*. J Hum Evol 48:473-492.

Yamashita N. 1998. Molar morphology and variation in two Malagasy lemur families (Lemuridae and Indriidae). J Hum Evol 35:137-162.

Yamashita N. 2003. Food procurement and tooth use in two sympatric lemur species. Am J Phys Anthropol 121:125-133.

Yamazaki Y, Komatsu K, Arai T, Chiba M. 2001. The effects of a high-carbohydrate diet on the stress-strain behavior of the periodontal ligament of the distal root of the mandibular first molar in hamsters. J Periodont Res 36:301-308.

Yeager CP. 1996. Feeding ecology of the long-tailed macaque (Macaca fascicularis) in Kalimantan Tengah, Indonesia. Int J Primatol 17:51-62.

Yeager CP, Kool K. 2000. The behavioral ecology of Asian colobines. In Whitehead PF, Jolly CJ, editors. Old World Monkeys. Cambridge University Press, Cambridge. 496-521.

Yettram AL, Wright KWJ, Pickard HM. 1976. Finite element stress analysis of the crowns of normal and restored teeth. J Dent Res 55:1004-1011.

APPENDIX A

μCT SCANNING PARAMETERS

Species	Museum #	kV	uA	W	Projections	Voxel size	Magnification	Volume size
Alouatta caraya	28095	80	125	10.0	1500	0.11	1.83	967x1093x1293
Alouatta caraya	28096	80	125	10.0	1100	0.08	2.50	828x1193x1231
Alouatta caraya	28654	80	125	10.0	1500	0.11	1.83	806x1055x1319
Alouatta caraya	28655	85	125	10.6	1100	0.08	2.50	967x1382x1476
Alouatta palliata	5323	85	125	10.6	1100	0.08	2.50	1083x1514x1590
Alouatta palliata	5324	85	125	10.6	1100	0.08	2.50	966x1374x1475
Alouatta palliata	5325	85	125	10.6	1100	0.08	2.50	957x1328x1345
Alouatta palliata	5327	85	125	10.6	1100	0.08	2.50	933x1320x1344
Alouatta palliata	5328	85	125	10.6	1100	0.08	2.50	964x1357x1460
Alouatta palliata	5329	85	125	10.6	1100	0.08	2.50	979x1331x1498
Alouatta palliata	5331	85	125	10.6	1100	0.08	2.50	950x1311x1457
Alouatta palliata	6001	85	125	10.6	1100	0.08	2.50	913x1278x1394
Alouatta palliata	29609	85	125	10.6	1000	0.08	2.50	891x1312x1296
Alouatta palliata	29611	85	125	10.6	1100	0.08	2.50	1208x1369x1410
Aotus trivirgatus	8472	80	125	10.0	1000	0.04	4.91	1267x1126x1492
Aotus trivirgatus	19801	80	125	10.0	1000	0.04	4.91	1171x1190x1486
Aotus trivirgatus	19802	80	125	10.0	1000	0.04	4.91	1208x1158x1428
Aotus trivirgatus	19805	80	125	10.0	1000	0.04	4.91	1252x1145x1487
Aotus trivirgatus	27214	80	125	10.0	1000	0.04	4.91	1209x1120x1422
Aotus trivirgatus	30562	80	125	10.0	1000	0.04	4.91	1225x1134x1447
Aotus trivirgatus	39571	75	115	8.6	1000	0.04	4.91	1123x1457x1504
Aotus trivirgatus	52608	80	125	10.0	1000	0.04	4.91	1265x1146x1501

(cont)

Species	Museum #	kV	uA	W	Projections	Voxel size	Magnification	Volume size
Aotus trivirgatus	B-8042	80	125	10.0	1000	0.04	4.91	1266x1097x1460
Aotus trivirgatus	B-8043	80	125	10.0	1000	0.04	4.91	1038x1287x1458
Ateles geoffroyi	5336	80	110	8.8	1100	0.08	2.50	945x1431x1482
Ateles geoffroyi	5338	90	120	10.8	1100	0.06	3.15	1256x1661x1672
Ateles geoffroyi	5344	80	110	8.8	1100	0.08	2.50	857x1357x1492
Ateles geoffroyi	5345	80	110	8.8	1100	0.08	2.50	850x1271x1373
Ateles geoffroyi	5346	80	110	8.8	1100	0.08	2.50	891x1328x1428
Ateles geoffroyi	5348	80	110	8.8	1100	0.08	2.50	949x1357x1455
Ateles geoffroyi	5349	90	120	10.8	1100	0.06	3.15	1271x1699x1715
Ateles geoffroyi	5350	80	110	8.8	1100	0.08	2.50	903x1287x1438
Ateles geoffroyi	5351	90	120	10.8	1100	0.06	3.15	1271x1687x1724
Ateles geoffroyi	5352	80	110	8.8	1100	0.08	2.50	840x1280x1397
Ateles geoffroyi	5353	80	110	8.8	1100	0.08	2.50	850x1177x1319
Ateles geoffroyi	5354	80	110	8.8	1100	0.08	2.50	930x1231x1394
Ateles geoffroyi	5355	80	110	8.8	1100	0.08	2.50	897x1320x1428
Ateles geoffroyi	10138	90	120	10.8	1100	0.06	3.15	1221x1674x1744
Ateles geoffroyi	29626	90	120	10.8	1100	0.06	3.28	1155x1615x1740
Ateles geoffroyi	29628	90	120	10.8	1100	0.06	3.15	1209x1646x1639
Ateles geoffroyi	34322	90	120	10.8	1100	0.06	3.15	1366x1530x1816
Callicebus moloch	20186	80	120	9.6	1050	0.05	4.25	894x1318x1284
Callicebus moloch	20188	80	120	9.6	1050	0.05	4.25	1054x1297x1313
Callicebus moloch	26922	80	120	9.6	1050	0.05	4.25	1089x1347x1353

(cont)

Species	Museum #	kV	uA	W	Projections	Voxel size	Magnification	Volume size
Callicebus moloch	30559	80	120	9.6	1050	0.05	4.25	932x1309x1196
Callicebus moloch	30564	80	120	9.6	1050	0.05	4.25	1061x1234x1344
Callicebus moloch	30566	80	120	9.6	1050	0.05	4.25	869x1338x1307
Callicebus moloch	32380	80	120	9.6	1050	0.05	4.25	926x1436x1227
Callicebus moloch	32383	80	120	9.6	1050	0.05	4.25	901x1306x1061
Callicebus moloch	37828	80	120	9.6	1050	0.05	4.25	907x1381x1271
Callicebus moloch	39073	80	120	9.6	1050	0.05	4.25	1108x1243x1092
Callicebus moloch	39563	80	120	9.6	1050	0.05	4.25	1077x1294x1347
Callithrix sp.	30579	80	125	10.0	1000	0.04	4.91	970x854x1145
Callithrix sp.	30580	80	125	10.0	1000	0.04	4.91	831x843x1086
Callithrix sp.	30582	80	125	10.0	1000	0.04	4.91	919x787x1133
Callithrix sp.	30583	80	125	10.0	1000	0.04	4.91	936x907x1140
Callithrix sp.	32164	80	125	10.0	1000	0.04	4.91	960x750x1190
Callithrix sp.	32165	80	125	10.0	1000	0.04	4.91	891x817x1136
Callithrix sp.	34573	80	125	10.0	1000	0.04	4.91	991x821x1183
Callithrix sp.	30577	80	125	10.0	1000	0.04	4.91	980x803x1177
Callithrix sp.	30586	80	125	10.0	1000	0.04	4.91	960x750x1190
Callithrix sp.	30603	80	125	10.0	1000	0.04	4.91	960x751x1162
Callithrix sp.	37826	80	125	10.0	1000	0.04	4.91	894x860x1152
Callithrix sp.	440	80	125	10.0	1000	0.04	4.91	894x860x1153
Callithrix sp.	37823	80	125	10.0	1000	0.04	4.91	954x907x1244

(cont)

Species	Museum #	kV	uA	W	Projections	Voxel size	Magnification	Volume size
Callithrix sp.	7165	80	125	10.0	1000	0.04	4.91	895x835x1139
Cebus apella	25811	90	120	10.8	1100	0.06	3.35	1234x1648x1645
Cebus apella	27097	80	115	9.2	1100	0.06	3.40	1055x1599x1548
Cebus apella	27891	90	120	10.8	1100	0.06	3.35	1142x1558x1567
Cebus apella	28679	80	115	9.2	1100	0.07	2.78	989x1234x1334
Cebus apella	30724	80	115	9.2	1100	0.07	2.98	920x1341x1256
Cebus apella	30726	80	115	9.2	1100	0.07	2.78	796x1146x1183
Cebus apella	31062	80	115	9.2	1100	0.08	2.50	791x1061x1201
Cebus apella	31064	80	115	9.2	1100	0.07	2.78	894x1215x1295
Cebus apella	31066	80	115	9.2	1100	0.07	2.78	834x1146x1259
Cebus apella	31072	80	115	9.2	1100	0.07	2.98	938x1312x1337
Cebus apella	32049	80	115	9.2	1100	0.07	2.98	913x1294x1297
Cebus apella	37831	80	115	9.2	1100	0.07	2.78	942x1300x1294
Cebus apella	37833	90	120	10.8	1100	0.06	3.35	1287x1724x1702
Cebus apella	41090	90	120	10.8	1100	0.05	4.11	1686x1388x1876
Cebus apella	49635	90	120	10.8	1100	0.06	3.35	1124x1451x1617
Cebus capucinus	5332	80	115	9.2	1100	0.08	2.50	860x1017x1223
Cebus capucinus	7317	80	115	9.2	1100	0.08	2.50	828x1155x1199
Cebus capucinus	7322	80	115	9.2	1100	0.08	2.50	762x998x1099
Cebus capucinus	7323	80	115	9.2	1100	0.08	2.50	775x1053x1172
Cebus capucinus	10135	80	115	9.2	1100	0.08	2.50	749x1026x1149
Cebus capucinus	10136	80	115	9.2	1100	0.08	2.50	787x1023x1136

(cont)

Species	Museum #	kV	uA	W	Projections	Voxel size	Magnification	Volume size
Cebus capucinus	34323	80	115	9.2	1100	0.08	2.50	777x1071x1143
Cebus capucinus	34326	80	115	9.2	1100	0.08	2.50	828x1051x1202
Cebus capucinus	34353	80	115	9.2	1100	0.08	2.50	828x1061x1206
Cebus capucinus	73218	80	115	9.2	1100	0.08	2.50	756x1024x1124
Cercocebus torquatus	32625	85	125	10.6	1100	0.09	2.20	1076x1356x1579
Cercocebus torquatus	62638	85	125	10.6	1100	0.09	2.20	932x1339x1435
Cercocebus torquatus	62639	85	125	10.6	1100	0.09	2.20	850x1313x1356
Cercopithecus mitis	7088	80	125	10.0	1100	0.08	2.50	884x1137x1317
Cercopithecus mitis	22734	80	125	10.0	1100	0.08	2.50	797x1038x1152
Cercopithecus mitis	25022	80	125	10.0	1100	0.08	2.50	813x1064x11914
Cercopithecus mitis	26832	80	125	10.0	1100	0.08	2.50	831x1101x1332
Cercopithecus mitis	31986	80	125	10.0	1100	0.08	2.50	861x1043x1166
Cercopithecus mitis	32003	80	125	10.0	1100	0.08	2.50	941x1225x1391
Cercopithecus mitis	39375	80	125	10.0	1100	0.08	2.50	834x1036x1183
Cercopithecus mitis	39389	80	125	10.0	1100	0.08	2.50	948x1138x1317
Cercopithecus mitis	39390	80	125	10.0	1100	0.08	2.50	772x1075x1238
Cercopithecus mitis	44264	80	125	10.0	1100	0.08	2.50	863x1133x1250
Cercopithecus mitis	44268	80	125	10.0	1100	0.08	2.50	875x1182x1363
Cercopithecus mitis	44274	80	125	10.0	1100	0.08	2.50	861x964x1369
Chiropotes satanas	31701	80	115	9.2	1100	0.05	3.80	1079x1529x1705
Chiropotes satanas	6028	80	115	9.2	1100	0.05	3.80	1095x1595x1647
Colobus polykomos	21151	70	110	7.7	1050	0.08	2.63	1300x1098x1608

(cont)

Species	Museum #	kV	uA	W	Projections	Voxel size	Magnification	Volume size
Colobus polykomos	22356	70	110	7.7	1050	0.08	2.63	1193x1136x1708
Colobus polykomos	22624	85	125	10.6	1050	0.08	2.63	1255x1130x1637
Colobus polykomos	22626	85	125	10.6	1050	0.08	2.63	1262x1130x1680
Colobus polykomos	22850	80	105	8.4	1050	0.08	2.63	1225x1054x1803
Colobus polykomos	46368	70	110	7.7	1050	0.08	2.63	1328x1206x1809
Erythrocebus patas	37280	80	125	10.0	1100	0.08	2.42	998x1265x1636
Erythrocebus patas	47015	80	125	10.0	1100	0.08	2.42	1215x1332x1847
Erythrocebus patas	47016	80	125	10.0	1100	0.08	2.42	1357x1145x1856
Erythrocebus patas	47018	80	125	10.0	1100	0.08	2.42	876x1156x1580
Gorilla gorilla	14750	85	90	7.7	1500	0.13	1.59	1086x1117x1938
Gorilla gorilla	17684	85	90	7.7	1500	0.13	1.59	1095x1221x1905
Gorilla gorilla	20089	85	90	7.7	1500	0.12	1.68	1240x998x1427
Gorilla gorilla	26850	85	90	7.7	1500	0.12	1.62	1055x1202x1935
Gorilla gorilla	29047	85	90	7.7	1500	0.12	1.65	1068x1152x1911
Gorilla gorilla	37265	85	90	7.7	1500	0.12	1.72	1156x1155x1925
Gorilla gorilla	37266	85	90	7.7	1500	0.12	1.65	1133x1180x1954
Gorilla gorilla	38326	85	90	7.7	1500	0.12	1.65	1152x1139x1929
Gorilla gorilla	46325	85	90	7.7	1500	0.13	1.59	1079x1212x1963
Lophocebus albigena	6209	80	125	10.0	1100	0.09	2.23	1067x1111x1492
Lophocebus albigena	18613	80	125	10.0	1100	0.09	2.23	1111x878x1482
Lophocebus albigena	22737	80	125	10.0	1100	0.09	2.23	972x1107x1514
Lophocebus albigena	23194	80	125	10.0	1100	0.09	2.23	1030x1240x1534

(cont)

Species	Museum #	kV	uA	W	Projections	Voxel size	Magnification	Volume size
Lophocebus albigena	39388	80	125	10.0	1100	0.09	2.23	910x1092x1394
Lophocebus albigena	39395	80	125	10.0	1100	0.09	2.23	1161x1265x1547
Lophocebus albigena	39396	80	125	10.0	1100	0.09	2.23	1030x1226x1511
Lophocebus albigena	39402	80	125	10.0	1100	0.09	2.23	1221x1228x1460
Macaca fascicularis	8461	80	125	10.0	1050	0.06	3.25	1193x1473x1856
Macaca fascicularis	12758	80	125	10.0	1050	0.06	3.25	1202x1445x1895
Macaca fascicularis	22277	80	125	10.0	1050	0.06	3.25	1196x1421x1722
Macaca fascicularis	23812	80	125	10.0	1050	0.06	3.25	1092x1389x1658
Macaca fascicularis	35765	80	125	10.0	1050	0.06	3.25	1250x1105x1645
Macaca fascicularis	35937	80	125	10.0	1050	0.06	3.25	1020x1309x1520
Macaca fascicularis	35938	80	125	10.0	1050	0.06	3.25	1101x1288x1497
Macaca fascicularis	36030	80	125	10.0	1050	0.06	3.25	1536x1159x1690
Macaca fascicularis	37781	80	125	10.0	1050	0.06	3.25	1369x1045x1693
Macaca fascicularis	41167	75	120	9.0	1050	0.09	2.20	1155x1256x1494
Macaca fuscata	37709	80	110	8.8	1050	0.09	2.20	1004x1426x1492
Macaca fuscata	61273	80	110	8.8	1050	0.09	2.20	1102x1661x1718
Macaca sylvanus	7072	80	110	8.8	1100	0.09	2.20	1114x1274x1476
Mandrillus sphinx	19986	85	125	10.0	1100	0.11	1.80	954x1070x1931
Mandrillus sphinx	20085	85	125	10.0	1100	0.11	1.80	869x1092x1901
Mandrillus sphinx	23168	85	125	10.0	1100	0.11	1.50	999x1218x1971
Mandrillus sphinx	23169	85	125	10.0	1100	0.11	1.80	929x1165x1853
Mandrillus sphinx	34089	85	125	10.0	1100	0.13	1.59	916x1054x1958

(cont)

Species	Museum #	kV	uA	W	Projections	Voxel size	Magnification	Volume size
Mandrillus sphinx	34177	85	125	10.0	1100	0.09	2.20	1045x960x1809
Mandrillus sphinx	34272	85	125	10.0	1100	0.09	2.20	1102x994x1869
Mandrillus sphinx	34273	85	125	10.0	1100	0.07	2.74	1190x916x1595
Pan paniscus	38018	80	120	9.6	1500	0.09	2.13	1307x1269x1924
Pan paniscus	38019	80	120	9.6	1500	0.09	2.18	1268x1249x1894
Pan paniscus	38020	80	120	9.6	1500	0.10	2.02	1290x1256x1923
Pan troglodytes	6244	80	120	9.6	1000	0.08	2.44	1199x859x1561
Pan troglodytes	6244	80	120	9.6	1500	0.11	1.88	1256x1344x1931
Pan troglodytes	9493	80	120	9.6	1500	0.11	1.82	1202x1322x1914
Pan troglodytes	15312	80	120	9.6	1500	0.11	1.90	1359x1391x1913
Pan troglodytes	17702	80	120	9.6	1000	0.08	2.59	1334x1045x1750
Pan troglodytes	17702	80	120	9.6	1500	0.10	1.95	1205x1117x1954
Pan troglodytes	23167	80	120	9.6	1500	0.11	1.89	1159x1212x1941
Pan troglodytes	26847	80	120	9.6	1500	0.10	2.00	1290x1470x1922
Pan troglodytes	26849	80	120	9.6	1500	0.11	1.89	1159x1309x1932
Pan troglodytes	37260	80	120	9.6	1500	0.10	2.00	1297x1124x1844
Pan troglodytes	46414	80	120	9.6	1300	0.08	2.43	1281x1388x1916
Pan troglodytes	46415	80	120	9.6	1300	0.09	2.32	1375x1259x1926
Pan troglodytes	46416	80	120	9.6	1500	0.10	2.00	1346x1256x1884
Pan troglodytes	N6908	80	95	7.6	1500	0.11	1.85	1310x1155x1887
Pan troglodytes	N6911	80	95	7.6	1500	0.11	1.85	1234x1191x1810
Papio anubis	8304	85	125	10.0	1100	0.12	1.70	1020x1033x1919

(cont

Species	Museum #	kV	uA	W	Projections	Voxel size	Magnification	Volume size
Papio anubis	8466	85	125	10.0	1100	0.08	2.50	922x897x1441
Papio anubis	17342	85	125	10.0	1100	0.11	1.86	998x944x1911
Papio anubis	17343	90	125	11.3	1100	0.13	1.59	913x1008x1957
Papio anubis	21160	85	125	10.0	1100	0.12	1.70	1082x1209x1885
Papio anubis	21161	90	125	11.3	1100	0.12	1.70	979x1057x1919
Papio anubis	26473	85	125	10.0	1100	0.10	2.00	1162x1078x1796
Papio anubis	29786	80	125	10.0	1100	0.12	1.70	1101x840x1891
Papio anubis	29787	85	125	10.0	1100	0.10	2.00	1161x1055x1818
Papio anubis	29788	85	125	10.0	1100	0.10	2.00	1187x1101x1775
Papio anubis	31619	85	125	10.0	1100	0.11	1.86	1218x1104x1859
Papio anubis	31949	90	125	11.3	1100	0.11	1.82	1149x1023x1860
Piliocolobus badius	24080	80	125	10.0	1100	0.08	2.50	1023x1249x1361
Piliocolobus badius	24775	80	125	10.0	1100	0.09	2.23	1149x960x1369
Piliocolobus badius	24793	80	125	10.0	1100	0.08	2.50	1002x1315x1284
Piliocolobus badius	25627	80	125	10.0	1100	0.08	2.50	960x1225x1230
Piliocolobus badius	25631	80	125	10.0	1100	0.09	2.23	1133x1263x1362
Piliocolobus badius	25810	80	125	10.0	1100	0.08	2.50	935x1158x1249
Piliocolobus badius	26552	80	125	10.0	1100	0.08	2.50	992x1288x1262
Piliocolobus badius	26553	80	125	10.0	1100	0.09	2.23	1007x1075x1476
Piliocolobus badius	27108	80	125	10.0	1100	0.08	2.50	1001x1389x1473
Piliocolobus badius	31939	80	125	10.0	1100	0.08	2.50	920x1177x1206
Pithecia sp.	5057	80	115	9.2	1050	0.05	3.99	1010x1290x1551

(cont)

Species	Museum #	kV	uA	W	Projections	Voxel size	Magnification	Volume size
Pithecia sp.	20265	80	115	9.2	1050	0.05	3.99	1052x1347x1492
Pithecia sp.	20266	80	115	9.2	1050	0.05	3.99	1029x1438x1514
Pithecia sp.	27124	80	115	9.2	1050	0.05	3.99	1051x1401x1589
Pithecia sp.	30720	80	115	9.2	1050	0.05	3.99	946x1296x1488
Pithecia sp.	30718	80	115	9.2	1050	0.05	3.99	1085x965x1567
Pithecia sp.	30719	80	115	9.2	1050	0.05	3.99	998x1445x1652
Pithecia sp.	31061	80	115	9.2	1050	0.05	3.99	4064x1356x1438
Presbytis hosei	35621	80	125	10.0	1100	0.08	2.50	863x1171x1174
Presbytis hosei	37370	80	125	10.0	1100	0.08	2.50	879x1172x1175
Presbytis hosei	37371	80	125	10.0	1100	0.08	2.50	913x1185x1176
Presbytis hosei	37372	80	125	10.0	1100	0.08	2.50	781x982x978
Presbytis hosei	37772	80	120	9.6	1100	0.08	2.50	957x1252x1259
Presbytis hosei	37773	80	120	9.6	1100	0.08	2.50	958x1253x1206
Presbytis rubicunda	22276	80	120	9.6	1100	0.08	2.50	894x1221x1245
Presbytis rubicunda	35704	80	125	10.0	1100	0.08	2.50	908x1202x1171
Presbytis rubicunda	35704	90	125	11.3	800	0.11	1.90	511x476x1904
Presbytis rubicunda	35705	80	125	10.0	1100	0.08	2.50	894x1192x1107
Presbytis rubicunda	35705	90	125	11.3	800	0.11		485x470x1894
Presbytis rubicunda	35706	80	125	10.0	1100	0.08	2.50	869x1168x1036
Presbytis rubicunda	35712	80	125	10.0	1100	0.08	2.50	891x1189x1216
Presbytis rubicunda	36820	80	120	9.6	1100	0.08	2.50	904X1119X1083
Presbytis rubicunda	37666	80	125	10.0	1100	0.08	2.50	907x1055x1171

(cont)

Species	Museum #	kV	uA	W	Projections	Voxel size	Magnification	Volume size
Presbytis rubicunda	37666	90	125	11.3	800	0.10	2.00	372x538x1941
Presbytis rubicunda	37776	80	120	9.6	1100	0.08	2.50	1208X948X1240
Presbytis rubicunda	37777	80	120	9.6	1100	0.08	2.50	825x1104x1181
Presbytis rubicunda	37778	80	120	9.6	1100	0.08	2.50	903X1253X1114
Presbytis rubicunda	37779	80	120	9.6	1100	0.08	2.50	908x1237x1259
Saguinus sp.	15324	80	125	10.0	1000	0.04	4.91	998x951x1224
Saguinus sp.	27331	80	125	10.0	1000	0.04	4.91	906X737X1149
Saguinus sp.	27332	80	125	10.0	1000	0.04	4.91	873x852x1108
Saguinus sp.	30597	80	125	10.0	1000	0.04	4.91	791x1045x1259
Saguinus sp.	30601	80	125	10.0	1000	0.04	4.91	879x1014x1237
Saguinus sp.	41567	80	125	10.0	1000	0.04	4.91	879x1014x1238
Saguinus sp.	41568	80	125	10.0	1000	0.04	4.91	957x927x1259
Saguinus sp.	52557	80	125	10.0	1000	0.04	4.91	947x803x1184
Saguinus sp.	52615	80	125	10.0	1000	0.04	4.91	938x904x1209
Saguinus sp.	52616	80	125	10.0	1000	0.04	4.91	844x1051x1206
Saguinus sp.	52658	80	125	10.0	1000	0.04	4.91	942x900x1215
Saimiri sp.	10131	80	120	9.6	1050	0.05	4.25	891x1404x1045
Saimiri sp.	10132	80	120	9.6	1050	0.05	4.25	864x1438x1054
Saimiri sp.	10133	80	120	9.6	1050	0.05	4.25	838x1158x1382
Saimiri sp.	10134	80	120	9.6	1050	0.05	4.25	832x1161x1350
Saimiri sp.	29488	80	120	9.6	1050	0.05	4.25	865x1130x1341
Saimiri sp.	20187	80	120	9.6	1050	0.05	4.25	952x1212x1400

(cont)

Species	Museum #	kV	uA	W	Projections	Voxel size	Magnification	Volume size
Saimiri sp.	27197	80	120	9.6	1050	0.05	4.25	907x1096x1419
Saimiri sp.	30568	80	120	9.6	1050	0.05	4.25	806x982x1228
Saimiri sp.	30569	80	120	9.6	1050	0.05	4.25	878x1202x1231
Saimiri sp.	30572	80	120	9.6	1050	0.05	4.25	1144x882x1296
Saimiri sp.	43484	80	120	9.6	1050	0.05	4.25	981x1082x1334
Trachypithecus cristata	12729	90	125	11.3	800	0.10	2.06	535x618x1844
Trachypithecus cristata	35567	90	120	10.8	1000	0.05	3.99	1592x1434x1765
Trachypithecus cristata	35584	90	120	10.8	1000	0.05	3.92	1558x1467x1901
Trachypithecus cristata	35586	90	120	10.8	1000	0.05	3.99	1687x1517x1789
Trachypithecus cristata	35597	90	120	10.8	1000	0.05	3.99	1423x1491x1749
Trachypithecus cristata	35603	90	120	10.8	1000	0.05	3.99	1573x1435x1902
Trachypithecus cristata	35604	90	120	10.8	1000	0.05	3.99	1624x1433x1869
Trachypithecus cristata	35605	90	120	10.8	1000	0.05	3.99	1681x1479x1750
Trachypithecus cristata	35610	90	120	10.8	1000	0.05	3.99	1639x1391x1683
Trachypithecus cristata	35615	80	110	8.8	1000	0.05	3.99	1335x1464x1759
Trachypithecus cristata	35618	80	110	8.8	1000	0.06	3.39	1299x1497x1615
Trachypithecus cristata	35636	80	110	8.8	1000	0.06	3.10	1391x1234x1502
Trachypithecus cristata	35640	80	110	8.8	1000	0.06	3.59	1244x1529x1686
Trachypithecus cristata	35645	80	110	8.8	1000	0.05	3.99	1429x1272x1570
Trachypithecus cristata	35663	80	110	8.8	1000	0.06	3.59	1221x1375x1652
Trachypithecus cristata	35678	85	120	10.2	1050	0.06	3.40	1208x1451x1667
Trachypithecus cristata	35682	80	110	8.8	1100	0.07	3.04	1306x1240x1485

(cont)

Species	Museum #	kV	uA	W	Projections	Voxel size	Magnification	Volume size
Trachypithecus cristata	35683	80	110	8.8	1000	0.06	3.59	1265x1539x1718
Trachypithecus cristata	35696	80	110	8.8	1000	0.06	3.19	1379x1162x1614
Trachypithecus cristata	35718	80	110	8.8	1000	0.06	3.59	1475x1163x1614
Trachypithecus cristata	37387	80	110	8.8	1000	0.06	3.59	1245x1483x1687